Dissertation

submitted to the

Combined Faculty of Natural Sciences and Mathematics

of the Ruperto Carola University Heidelberg, Germany

for the degree of

Doctor of Natural Sciences

presented by

M.Sc. Valentina Volpin

born in: Milan, Italy

Oral examination:

.....

A screening for novel immune-checkpoints identifies CAMK1D as a kinase responsible for immune resistance in multiple myeloma

Referees:

Prof. Dr. Philipp Beckhove

Prof. Dr. Stefan Wiemann

The work described in this thesis was performed from 2014 to 2015 in the Department of Translational Immunology at the National Center for Tumor Diseases – NCT of the German Cancer Research Center - DKFZ in Heidelberg, Germany and from 2016 to 2018 in the Department of Interventional Immunology at the Regensburg Center for Interventional Immunology – RCI in Regensburg under the supervision of Prof. Dr. Philipp Beckhove.

Declaration

I herewith declare that I have completed this thesis single-handedly without any unauthorized help of a second party. Any help that I have received in my research work or in the preparation of this thesis has been duly acknowledged.
Heidelberg, 26.03.2018

_____
Valentina Volpin

Acknowledgements

Most likely the majority of people to whom I will hand over this thesis, after admiring the cover and weight of this “book”, will instinctively look at the acknowledgments, perhaps the most understandable chapter for many. It is indeed with the “conclusion” of a great PhD experience, that undoubted enriched my life and in which each of you contributed in some way that I would like to “start” by thanking you one by one.
(Besides, afterwards, you can also continue to enjoy reading this thesis from page 1).

In the end of this long but somehow quickly-passed life journey I would like to start by thanking Prof. Philipp Beckhove. Philipp gave me the opportunity to perform my PhD in a valorous lab, where I could work on an important and very interesting project. From my very first day in the lab he gave me both guidance and freedom to explore, which made this project and me grow. His constant support and motivation made this PhD an absolute learning experience.
A special thanks goes also to my TAC members Prof. Stefan Wiemann and Prof. Karsten Mahnke for their supervision and valuable comments. Their fruitful inputs during the TAC meetings helped shaping this project.
Moreover, I would like to spend a word of gratitude to all the Beckhove lab-members. This experience would not have been the same without those who turned out to be more than just colleagues. Everyone contributed to the motivating and friendly milieu in which I worked. Therefore I would like to thank Till for his constant help over the years, especially with bioinformatics analyses. I truly appreciated your precious suggestions and support. Next, I would like to thank Antonio. Besides being the one who made the whole lab laugh on a daily basis I am grateful for your precious scientific advices. A special thanks goes also to Slava for her inputs on scientific questions, for organizing amusing evenings outside the lab and for always providing chocolate during long working days. I would like to express my gratitude to my PhD partners Chih-Yeh and Ayse with whom I have shared long lab and office hours. You made this time fly with a smile on my face. I also thank all the Master- and Bachelor-students I have supervised during these years starting from Ralph to Maja and Madlen who contributed to the project. I would like to thank Heiko for his humor, Maria, Anchana and Kathy for their suggestions and mature advises. I am grateful also to Nisit for preparing the soil of the HTP-screen and for the productive discussions at iOmx. A special thanks goes to

our brilliant technicians Birgitta and Karin, Jasmin, Janine and Eva who brought a joyful atmosphere in the lab.
My gratitude goes also to Sabine T., Sabine R. and Mattea for their efficient and professional administrative help at RCI.
The international environment at DKFZ allowed me to meet amazing people from different countries with whom I have shared unforgettable experiences.
Thanks to my former colleagues of D015, Hans-Henning, Noemi, Lora, Christina, Simone, Ludmila, Mariana, Sabrina, Giovanni as well as Miriam and Irmi for their technical and administrative support.

I cannot forget to mention all my friends, scientists and non, on whom I can always rely on. A special thanks goes to my oldest best-friends Sara and Matteo, who have been proven as always real friends to turn to for advice. Thanks also to Pietro, Reidar, Fabio, Ludo…and all the others.

Finally, I've reserved these last lines, to the people who made me what I am today: my Family! In particular I owe my parents a lot. You taught me important principles since I was born and although being physically distant during these years you have showed me all the affection one could ever wish and you have always supported and encouraged my choices. Grazie Mami, grazie Papi!
In line, I would like to thank my four beloved grandparents for having been great examples of kindness and strength and for their unconditional love.
Moreover, I would like to thank a person who deserves a deep gratitude: my sister, Monica. The one with whom I've shared most of my life, the best sister one could ever wish. Thank you for always prompting me to reach the highest peak. You have transmitted me your scientific passion and thanks to your great fighting spirit I was able to achieve also this challenge.
An exclusive expression of gratitude goes to Victor. Thank you for always being there for me. Your presence and support has been fundamental during this journey and if I reached this goal it is also thanks to you.
I would like to conclude these acknowledgements by remembering the person who for me was of fundamental importance, the one that always told me how proud she was of me and to whom I dedicate this thesis: my grandmother Omi.

“Nothing in life is to be feared, it is only to be understood.
Now is the time to understand more, so that we may fear less”

Marie Curie

To my grandmother, Omi

Summary

Despite tremendous progresses in cancer immunotherapy, a plethora of tumor patients is still refractory to current immunotherapeutic strategies. Unresponsiveness to therapy is ascribed to the ability of cancer cells to elude the immunosurveillance. Indeed, by taking advantage of different immune-checkpoint molecules tumor cells can either dampen immune cell functionality or promote tumor cell resistance towards immune attack.

The current study aimed at identifying novel tumor-associated immune-checkpoint molecules by developing a RNAi high-throughput (HTP) screening and successively corroborate candidate genes whose blockade increases anti-tumor immune response.

Hence, I generated stable luciferase expressing multiple myeloma cells, transfected them with a siRNA library targeting 2887 genes (enriched for kinases and surface-associated molecules) and co-cultured them with HLA-A2-matched patient-derived marrow-infiltrating lymphocytes (MILs). T cell-mediated killing of tumor cells was assessed by measuring the remaining luciferase activity of knocked down tumor cells. The HTP screening revealed 128 genes whose knockdown increased T cell-mediated tumor cell death more efficiently than the positive control CCR9.

To validate the results, candidate genes were re-tested in a secondary screening that allowed to distinguish between genes altering tumor susceptibility towards MIL-mediated killing and those impairing MIL activity.

Among the candidate immune-checkpoints the serine/threonine protein kinase CAMK1D was selected for extensive validation. Knockdown of CAMK1D resulted in increased tumor susceptibility towards MIL-mediated killing. In particular, CAMK1D was shown to support intrinsic tumor resistance towards T cell attack by interfering with the apoptotic signaling cascade. By directly interacting with effector caspases, CAMK1D inhibits caspases activation and activity via phosphorylation. In line, CAMK1D depletion sensitizes tumor cells to FasL-induced apoptosis by MILs. These results obtained in the hematological malignancy were further confirmed in uveal melanoma emphasizing the relevant role of CAMK1D in different tumor entities.

Taken together, this study describes the establishment of a HTP-discovery platform to unravel the arsenal of immune-checkpoint molecules used by cancer cells to escape the immune system. The molecular pathway of CAMK1D is described highlighting the importance of discovering immune-checkpoints that mediate resistance towards T cell attack.

Zusammenfassung

Trotz enormer Fortschritte in der Krebsimmuntherapie ist eine Vielzahl von Tumoren immer noch gegen aktuelle immuntherapeutische Strategien resistent. Die Unempfindlichkeit gegenüber einer Therapie wird der Fähigkeit von Krebszellen zugeschrieben, sich der Immunüberwachung zu entziehen. In der Tat können Tumorzellen, indem sie verschiedene Immun-Checkpoint-Moleküle ausnutzen, entweder die Immunzellfunktionalität reduzieren oder die Tumorzellresistenz gegen einen Immunangriff fördern.

Die aktuelle Studie zielte darauf ab, neue tumorassoziierte Immun-Checkpoint-Moleküle zu identifizieren. Hierzu wird ein RNAi-Hochdurchsatz (HTP) -Screening entwickelt und Kandidatengene, deren Blockade die antitumorale Immunantwort verstärkt, werden anschließend validiert.

Daher generierte ich stabile Luciferase-exprimierende multiple Myelomzellen, transfizierte sie mit einer siRNA-Bibliothek von 2887 Genen (angereichert an Kinasen und oberflächenassoziierten Molekülen) und ko-kultivierte sie mit HLA-A2-übereinstimmenden aus Patienten gewonnen Knochenmark-infiltrierenden Lymphozyten (MILs). T-Zell-vermittelte Tötung von Tumorzellen wurde durch Messung der verbleibenden Luciferase-Aktivität von überlebenden Tumorzellen bewertet. Das HTP-Screening identifizierte 128 Gene, deren Knockdown T-Zell-vermittelten Tumorzelltod effizienter erhöhte als die positive Kontrolle CCR9.

Um die Ergebnisse zu validieren, wurden Kandidatengene in einem sekundären Screening erneut getestet. Das Screening ermöglichte es zwischen solchen Genen zu unterscheiden, welche die Anfälligkeit der Tumorzellen gegenüber MIL-vermittelter Tötung reduzieren, und solchen, welche die MIL-Aktivität beeinträchtigen. Unter den Kandidaten wurde die Serin/Threonin-Proteinkinase CAMK1D zur extensiven Validierung ausgewählt. Der Knockdown von CAMK1D führte zu einer erhöhten Anfälligkeit des Tumors für MIL-vermittelte Tötung. Insbesondere wurde gezeigt, dass CAMK1D die intrinsische Tumorresistenz gegenüber dem T-Zell-Angriff durch Störung der apoptotischen Signalkaskade unterstützt. Durch direkte Interaktion mit Effektorcaspasen hemmt CAMK1D die Aktivierung und Aktivität von Caspasen durch Phosphorylierung. Ebenso sensibilisiert die Depletion von CAMK1D Tumorzellen gegen die FasL-induzierte Apoptose durch MILs. Diese Ergebnisse, die bei der hämatologischen Malignität erhalten wurden, wurden im Uvea-

Melanom weiter bestätigt. Dies unterstreicht die relevante Rolle von CAMK1D in verschiedenen Tumorentitäten.

Zusammengefasst beschreibt diese Studie die Etablierung einer HTP-Plattform, um das Arsenal an Immun-Checkpoint-Molekülen zu entschlüsseln, die von Krebszellen verwendet werden, um dem Immunsystem zu entkommen. Der molekulare Signalweg von CAMK1D zeigt die Wichtigkeit der Entdeckung von Immun-Checkpoint-Molekülen, die Resistenz gegen T-Zell-Angriff vermitteln.

Table of Contents

1 Introduction

1.1 Hallmarks of cancer

The term "cancer" defines a cluster of diseases characterized by the uncontrolled growth and spread of abnormal cells, eventually leading to death. With around 8 million cancer-related deaths per year and approximately 14 million new cases, cancer represents one of the leading causes of mortality worldwide [1]. According to the World Health Organization (WHO), by 2030 this global burden is estimated to grow to around 21 million new cancer cases and 13 million cancer-related deaths. The transformation of normal cells into a malignant state can arise from a genetic predisposition and/or from the exposure to risk factors. Cancer cells are capable of propagating throughout the body, obstructing the function of healthy organs and thereby threatening the host's survival. The transformation of a normal cell to a tumor cell is a multistage process: it is initiated by genetic alterations leading to abnormal proliferation, escalating to tumor promotion that includes the outgrowth of tumor cells and finally culminating in tumor progression and dissemination. In the year 2000, Hanahan D. and Weinberg R.A., outlined the multistage process of tumorigenesis and summarized the major hallmarks of cancer into six biological competences acquired during this process [2], namely:

1. *Sustaining proliferative signaling*: tumor cells can either activate molecular regulators of the cell cycle or induce paracrine secretion of growth factors thereby supporting their own proliferation [3, 4].
2. *Evading growth suppressors*: tumor cells can become resistant to anti-growth signals by dysregulating tumor suppressors such as p53 and retinoblastoma-associated proteins (Rb) [5, 6]. Alternatively, cancer cells can become insensitive to cell contact inhibition, consequently outgrowing uncontrollably [7].
3. *Resisting cell death*: tumor cells acquire mechanisms to evade programmed cell death (apoptosis) by downregulating pro-apoptotic molecules while upregulating anti-apoptotic proteins [8].

4. *Inducing Angiogenesis*: in order to increase access to nutrients required for their growth during tumor progression the generation of new blood vessels into the tumor is stimulated [9].
5. *Enabling replicative immortality*: tumor cells can acquire limitless replicative potential by the expression of a telomerase that sustains telomeres elongation, thereby preventing cell senescence [10].
6. *Activating invasion and metastasis:* tumor cells can gain the capacity to invade local and distant sites by loss of E-cadherin expression responsible for cell adhesion [11].

A decade of research further demonstrated that tumor cells do not only acquire the above-mentioned hallmarks but also interact with benign stromal cells of the tumor microenvironment (TME) [12]. Hence, additional hallmarks of cancer cells associated with the TME were published in 2011 [13]. These hallmarks postulated that:

- Inflammation generated by immune cells in the TME can support tumor progression.
- Tumor cells and the associated TME avoid immune destruction. Although tumor cells are frequently recognized and eliminated by immune cells, these malignant cells develop different mechanisms to evade immune recognition [12].
- Genetic instability and mutations provide cancer cells with tumor promoting alterations, boosting tumor progression.
- Tumor cells deregulate cellular energetic circuits. By reprogramming the energetic metabolism from aerobic to anaerobic (glycolysis), tumor cells can subsist the hypoxic conditions that operate within tumors [14] while supporting the neoplastic proliferation.

Significant progresses have been accomplished in the last two decades in exploring these hallmarks, facilitating the development of therapies targeting different tumor entities. Importantly, understanding the role of the immune system in cancer progression and the mechanisms employed by tumor cells to avoid immune-mediated eradication provide a significant outline of the complex interplay between tumor cells and the immune cells, culminating in cancer progression and metastasis.

1.2 The cancer immunity cycle

In the beginning of the 20th century, Paul Ehrlich proposed the idea that transformed cells are recognized by the immune system, which constantly tries to eliminate the altered cells before they are manifested clinically. In the mid 20th century, this notion found experimental evidence and gave rise to the immunosurveillance theory further developed by Burnet and Thomas. This theory postulated that the host immune system is capable of recognizing and destroying transformed cells in an early stage of tumor development [15]. Only by the end of 1900, this theory found acceptance, when experimental animal models using knockout mice confirmed the existence of cancer immunosurveillance with both the innate and adaptive arms of the immune system playing a role in controlling tumor outgrowth. Indeed, the presence of tumor antigen-specific T cells in the tumor microenvironment is associated with improved survival and can thus be used as a predictive biomarker. The generation of an anti-tumor immunity reaction is a complex multi-step process that is described by the "cancer immunity cycle" (Figure I) [16] outlined in the following 7 steps:

1. To initiate an effective anti-tumor immunity, neo-antigens created during tumor development have to be released and captured by professional antigen presenting cells (APC) such as dendritic cells (DCs). Importantly, tumor cells have to be discriminated from healthy cells. This can be achieved by the recognition of different tumor associated antigens (TAA) by immune cells.
   TAAs can derive from:
   i) self-antigens overexpressed in tumors (e.g. Survivin and EpCAM)
   ii) mutated self-antigens (e.g. p53)
   iii) chromosomal breakpoint antigens (e.g. BCR-ABL)
   iv) products of tissue differentiation (e.g. MART1)
   v) oncogenic-viruses (E6 and E7 encoded by HPV-16)
   vi) products of genes expressed during development but silenced in normal tissue (Cancer testis antigens e.g. MAGE and NY-ESO)

   Chemotherapy and radiation therapy have been proven to support the release of TAA, thus facilitating TAA uptake by immune cells inducing tumor cell death [17].

2. Upon TAAs uptake, DCs undergo maturation by additionally receiving stimulatory signals from pro-inflammatory cytokines (such as tumor necrosis factor (TNF) and interferon-α (IFN-α)) and co-signaling receptors (CD40/CD40L interaction). This maturation ensures DCs to process and present tumor-derived antigens on the cell surface through their major histocompatibility complex, MHC-I or MHC-II.

3. In the lymph node, mature DCs present the MHC-bound peptide to naïve T cells. If the cancer specific antigen is recognized as foreign the antigen-presentation induces the priming and activation of effector T cell responses inducing anti-tumor immunity. If the antigen is viewed as self and innocuous, immune tolerance is mediated by regulatory T cells.

4. After the priming phase in the lymph nodes, cytotoxic CD8 T cells migrate to the tumor site. Driven by chemokines that interact with chemokine receptors (such as CXCL9 and CXCL10 ligands for CXCR3) [18], T cells can reach the tumor tissue.

5. In order to infiltrate the tumor tissue, T cells need to cross the endothelial barrier. To do so, it is necessary that the immune cells express adhesion molecules such as L-selectin or integrins like LFA1 (lymphocyte function-associated antigen 1) that binds to ICAM1 (intracellular adhesion molecule 1) on endothelial cells, allowing a successful infiltration of the immune cells in the tumor site.

6. Once in the tumor microenvironment, effector T cells have to recognize through their specific T cell receptors (TCR) their cognate tumor associated antigens presented on MHC-I molecules expressed on the surface of tumor cells.

7. Ultimately, the recognition and binding process induces activation of downstream TCR signaling pathways in the cytotoxic T cells. This results in the release of effector cytokines (e.g. IFN-γ, or IL-2 (interleukin-2)) and cytolytic vesicles containing granzyme B and perforin. Altogether, these effector mechanisms lead to tumor cell lysis, which consequently release TAAs, allowing the uptake by surrounding APCs and re-starting the cancer immunity cycle.

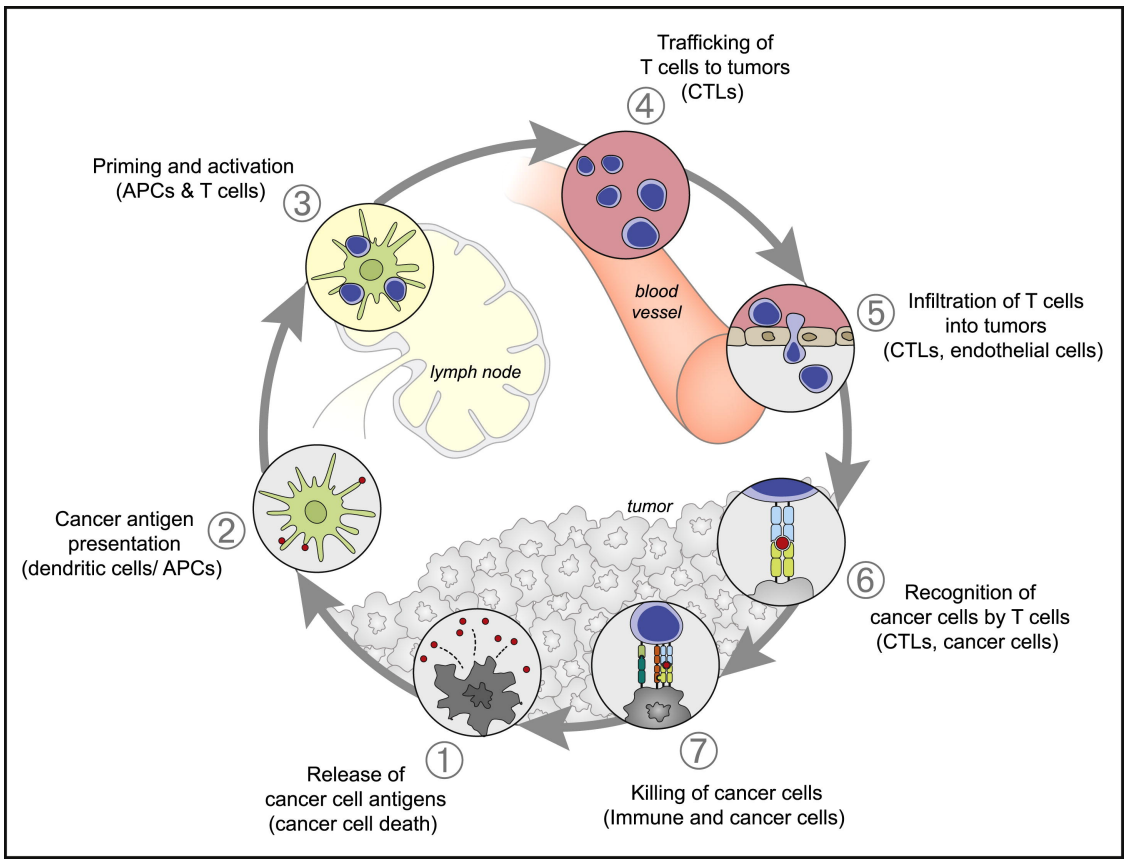

Figure I. The cancer immunity cycle. Seven steps of immune cells involved in the generation of an anti-tumor immune response. Adapted from Chen *et al.,* Immunity, 2013 [16].

1.3 Cancer immunoediting

Despite the immunosurveillance theory explained in section 1.2, which postulates that immune cells are able to build up an efficient anti-tumor response [19], the immune system may also be responsible for tumor progression. The latter occurs when tumor cells that display the fitness to survive in an immunocompetent host are selected over immunogenic tumor cells or when certain conditions within the tumor microenvironment are established, facilitating tumor outgrowth. The adverse role of the immune system favoring tumor-mediated immune evasion arises from cancer immunoediting. The principle of immunoediting, responsible for tumor progression, comprises 3E-phases: elimination, equilibrium and escape.

1.3.1 Elimination

In the elimination phase, also known as immunosurveillance, abnormal cells are recognized and eliminated by the immune system. Two cell subsets are mainly involved: natural killer (NK) cells and CD8 T cells, also called cytotoxic T lymphocytes (CTLs). NK cells can recognize altered tumor cells lacking the expression of MHC-I molecules and eliminate them via secretion of cytotoxic granules such as perforin and granzyme or via the engagement of tumor necrosis factor (TNF) receptor superfamily (TNFRSF) members, such as TNFR-I, Fas and TRAIL receptors on tumor cells [20, 21]. On the contrary, CD8 T cells are able to elicit a tumor-specific immune response. By recognizing a plethora of TAAs presented on the MHC-I complex, CTLs eliminate the transformed cells, thereby maintaining cellular homeostasis. However, in most cancer patients the immune system is unable to completely perform tumor eradication, leading to cancer immune equilibrium and eventually escape.

1.3.2 Equilibrium

In the equilibrium stage, the aberrant tumor cells and immune cells reach a steady state [22]. During this phase, tumor cells are in a dormant stage [23] because of hostile conditions from the tumor microenvironment. These quiescent cells are able to persist for decades in the body, eventually causing the phenomenon of tumor relapse. In the equilibrium phase, the elimination of tumor cells and the growth of immune-selected tumor cell variants are in balance [24].

1.3.3 Escape

If the immune-resistant malignant cell variants succeed to shift the equilibrium in their favor, immune escape occurs. Malignant clones, selected by the immune pressure and harboring molecular abnormalities elude both the innate and the adaptive anti-tumor immune responses [25], resulting in uncontrolled tumor proliferation, ultimately manifested as a clinically apparent disease [26].

1.4 Immune escape mechanisms

Being a critical regulator of tumor biology, the immune system is capable of controlling tumor development. Nevertheless, due to cancer immunoediting, cancer cell clones can evolve and escape the immune-mediated elimination. Indeed, tumor cells have developed different strategies to interfere with the ability of the immune system to develop effective immunological responses. These different mechanisms of immune inhibition can be categorized in i) mechanisms impairing effector immune cell functionality and ii) mechanisms conferring tumor cell resistance towards immune attack. Besides these mechanisms, the tumor microenvironment plays a pivotal role in creating an immune-suppressive environment at the tumor site, thus contributing to immune escape mechanisms.

1.4.1 Immune-checkpoints: molecules impairing immune cell functionality

It is now clear that the process of T cell activation requires an antigen-specific signal through the TCR as well as an additional antigen non-specific signal, recognized as the co-stimulatory signal. Over the past years, an extended array of co-stimulatory – as well as co-inhibitory - pathways have been discovered and characterized, emerging as important players in the immune system to fine tune the effector function of T cells. By the end of the 20th century, the concept that lymphocytes are negatively regulated by what are now called inhibitory immune-checkpoints was proposed. Indeed, during immune evasion, tumor cells can reduce the functionality of immune cells by taking advantage of inhibitory immune-checkpoint molecules normally employed to induce peripheral immune tolerance and limit autoimmunity by dampening T cell response [27].

Immune-checkpoint molecules are a plethora of receptors and ligands normally expressed on the surface of T cells and APCs [28]. They can either transduce positive (co-stimulatory immune-checkpoints) or negative (co-inhibitory immune-checkpoints) signals upon TCR activation [29]. Known immune-checkpoint molecules can be broadly classified into two families based on their molecular structure, the CD28 immunoglobulin (Ig) superfamily and the tumor necrosis factor receptor (TNFR) family. The former comprises CD28 and the inducible co-stimulator (ICOS) molecules that exert positive signals, and cytotoxic T-lymphocyte antigen 4 (CTLA-4), programmed cell death (PD-1), programmed death ligand 1 (PD-L1), B and T lymphocyte attenuator (BTLA), lymphocyte activation gene 3 (LAG-3),

T cell immunoglobulin mucin 3 (TIM-3), T cell immunoreceptor with Ig and ITIM domains (TIGIT), V-domain Ig suppressor of T cell activation (VISTA), carcinoembryonic antigen related cell adhesion molecule 6 (CEACAM6) which instead induce co-inhibitory signals [29]. The TNFR family includes CD27, OX40 (or CD134), 4-1BB (or CD137), HVEM (Herpes virus entry mediator), CD30, GITR (glucocorticoid-induced tumor necrosis factor receptor) and CD40, all mediating positive co-stimulatory signals.

The members of the CD28 family are characterized by a variable Ig-like extracellular domain and a short cytoplasmic tail, while members of the TNFR superfamily are type I transmembrane proteins presenting extracellular domains rich in six cysteine repeats that form disulphide bridges.

The identification of several inhibitory immune-checkpoints and their critical function in dampening T cell responses has brought immune-checkpoints to the forefront of immunologic research. Among them, CTLA-4/CD80 and PD-1/PD-L1 pathways have been most actively studied in the context of clinical therapy.

1.4.1.1 The functional role of CTLA-4

CTLA-4 (also known as CD152), a member of the immunoglobulin superfamily, is inducibly expressed on the surface of T cells, with maximal expression occurring two to three days following T cell activation [30, 31]. In resting T cells, CTLA-4 resides mostly intracellularly and only a small amount is expressed on the surface [32]. CTLA-4, structurally homologous to CD28, was shown to bind to CD80 (B7.1) and CD86 (B7.2) expressed on APCs with an approximately 10–20-fold higher affinity than CD28 [33]. The role of CTLA-4 as a major negative regulator of T cell activation was established with CTLA-4$^{-/-}$ mice in 1995 [34]. CTLA-4 deficient mice succumbed from massive lymphoproliferation within the spleen and lymph nodes and end-organ infiltration by activated lymphocytes at three to four weeks of age [35]. Previous studies reported that the cytoplasmatic domain of CTLA-4 containing an immunoreceptor tyrosine-based inhibitory motif (ITIM) was responsible to interact with the tyrosine phosphatase SHP-2 [36] and the serine/threonine phosphatase PP2A [37], thereby reversing the TCR activation-induced phosphorylation and limiting the T cell response. Surprisingly, different studies showed that only the extracellular domain of CTLA-4 is sufficient to exert its inhibitory function. Indeed, Tai et al. demonstrated that CTLA-4$^{-/-}$ mice transgenically expressing only the membrane-anchored extracellular domain of CTLA-4

were able to induce immune suppression as competently as the wild type CTLA-4 [38]. Thus, CTLA-4 inhibitory potential may predominantly be due to ligand competition. By binding to CD80/86 it reduces the access of CD28 to their shared ligands thus depriving the T cell of the costimulatory signal (Figure II). Beside its role on activated T cells, CTLA-4 fosters the activation of Tregs, thus promoting the immunosuppressive role of the tumor microenvironment [39, 40]. As CTLA-4 expressed on T cells, also CTLA-4 positive Tregs can outcompete CD28 binding to its ligands. Furthermore, it has been shown that Tregs are able to remove CD80/86 expressed on APCs, thereby limiting CD28-CD80/86 engagement [41]. Therefore, targeting CTLA-4 using antibody therapy may lower the threshold of T cell activation, promoting T cell expansion and positively impacting on clinical immune responses.

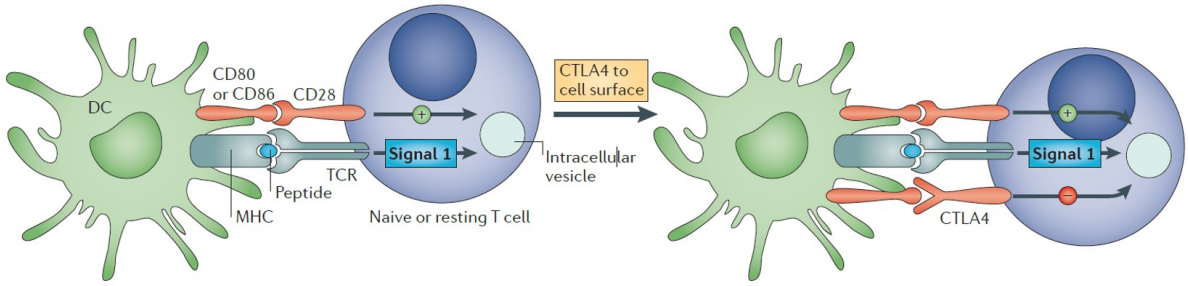

Figure II. Cytotoxic T lymphocyte-associated antigen-4 (CTLA-4) suppresses T cell activation. Upon antigen presentation through the MHC-TCR interaction, CTLA-4 molecules, that reside in intracellular vesicles, are upregulated on the surface of T cells. By binding to CD80 or CD86 on DCs, CTLA-4 induces an inhibitory signaling, which dampens the T cell response. Adapted from Pardoll *et al.,* Nat Rev Cancer, 2012 [28].

1.4.1.2 The functional role of PD-1

Similarly to CTLA-4, another crucial co-inhibitory receptor is PD-1 (CD279), also a member of the CD28 Ig-superfamily and expressed on activated T cells, B cells, natural killer T cells, monocytes and DCs [42]. Upon binding to its ligands PD-L1 (CD274) or PD-L2 (CD273) expressed on APCs or induced on epithelial and endothelial cells upon inflammation, PD-1 translocates to the central supra-molecular activation complex (cSMAC) of the immunological synapse [43]. There it co-localizes with the TCR microclusters, where the immunoreceptor tyrosine-based switch motif (ITSM) domain of PD-1 is phosphorylated, subsequently recruiting the tyrosine phosphatase SHP2 responsible for the dephosphorylation

of the TCR-associated kinases (e.g. ZAP70) and consequently abrogating TCR signaling [44-46].

As a result, T cells reduce the production of cytokines such as, IFN-γ, IL-2 and TNF-α, T cell proliferation is inhibited ultimately leading to exhaustion of effector T cells. In particular, in a model defined as "cancer innate immune resistance", genomic instable cancer cells, that harbor altered molecular pathways, are able to induce the expression of inhibitory immune-checkpoints such as PD-L1 (Figure III A). Moreover, when tumor cells interact with effector T cells, the interaction between the TCR and the MHC complex on tumor cells, leads to IFN-γ secretion by T cells. Consequently, this cytokine acts in a paracrine manner on the tumor cells, activating the signal transducer and activator of transcription (STAT) signaling pathway that promotes PD-L1 expression on the surface of tumor cells [28]. This phenomenon is referred to as "adaptive immune resistance" (Figure III B).

Accordingly, PD-L1 overexpression has been found in a plethora of different cancers (e.g. melanoma, non-small cell lung carcinoma and breast cancer) correlating with poor clinical outcomes [47-50]. Thus, interfering with this immune-checkpoint molecule has gained in interest as a complementary strategy for cancer therapy as discussed in section 1.5.

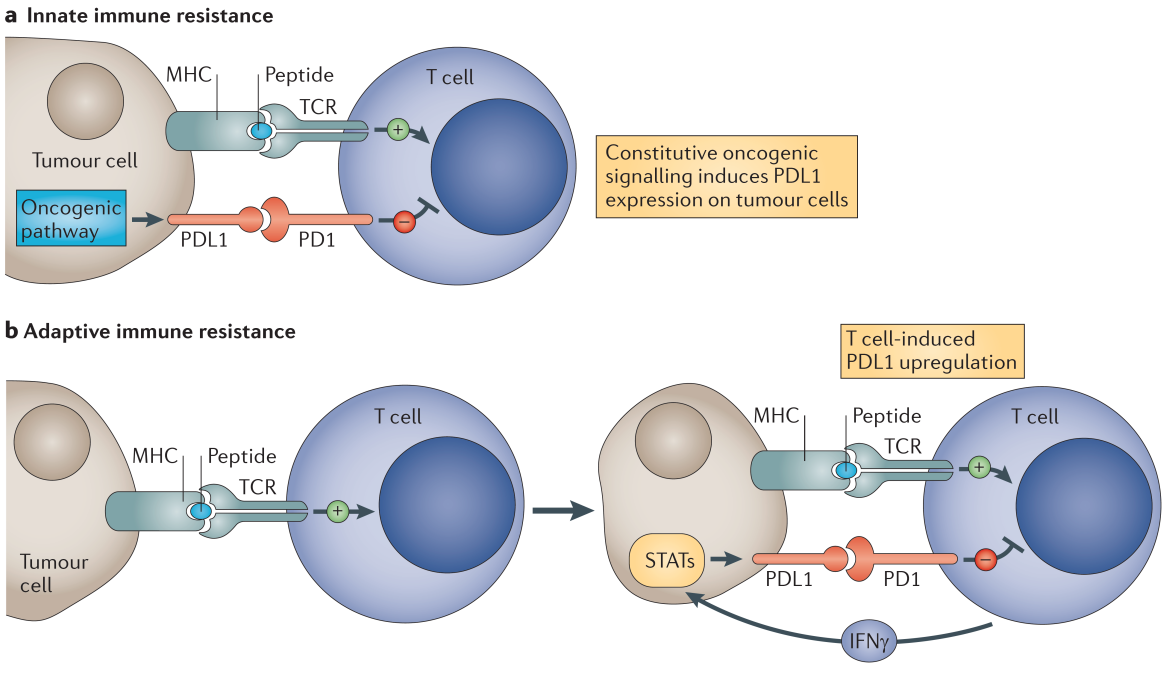

Figure III. Mechanisms of PD-1 expression on tumor cells. In the innate immune resistance mechanism, genomic instable cancer cells harbor altered molecular pathways and are able to induce the expression of inhibitory immune-checkpoints such as PD-L1 **(A)**. In the adaptive immune resistance mechanism the interaction between the MHC molecule and the TCR results in IFN-γ secretion by T cells. This cytokine in turn

acts on tumor cells activating the STAT signaling, responsible for PD-L1 expression on the surface of tumor cells. Adapted from Pardoll *et al*., Nat Rev Cancer, 2012 [28].

Besides hijacking inhibitory molecules to their advantage, tumor cells can also directly mediate the elimination of immune cells by using the Fas/FasL axis. Activated T cells express FasL, which interact with Fas expressed on the surface of tumor cells. This interaction induces the activation of the caspases-mediated apoptosis in the tumor cells [51]. Nevertheless, tumor cells can upregulate FasL as well, thus activating the apoptotic cascade in T cells which ultimately leads to effector T cell death [52-54]. Indeed, tumor cells induce pathways such as the activation-induced cell death of immune cells, which normally function to limit the immune response under physiological conditions, to dampen T cell responses. Thus, some tumor cells have developed different mechanisms to turn the immune system against itself.

1.4.2 Acquiring resistance to death effector mechanisms

As mentioned, the immunosurveillance theory postulates that the immune system is able to identify altered tumor cells and eliminate them. Thus, an effective way of escaping immune eradication is to prevent detection. Indeed, by reducing the expression or presentation of tumor-associated antigens, tumor cells can reduce their immunogenicity and remain invisible to the detection of the immune system. In this regard, tumor cells can escape their recognition by the immune system through two possible mechanisms:

1. *Loss of antigenicity*: Tumor cells induce cell intrinsic resistance mechanisms by expressing less antigens that can be seen as foreign by the immune system. This occurs by genetic deletion or frequent mutations thereby altering the immune-dominant epitopes on the antigen. For at least some of the mutated tumor antigens the available T cell repertoire is low, because these as “self” recognized antigens normally induce T cell tolerance [55]. Moreover, tumor cells can lose their antigens for instance by incorporating them via endocytosis or by releasing them from the tumor surface. Thus, loss of TAAs expression correlates with disease progression and less antigenic tumor cells become the

predominant cell population inside the tumor consequently being able to evade immune cell destruction.

2. *Impairment of the antigen-presentation machinery*: Besides the loss of antigenicity, tumor cells succeed to escape the immune system by interfering with the antigen-presenting machinery. Indeed, decreased or absent HLA class I expression is observed in many tumors [56, 57]. Alterations in the β-2 microglobulin (β2m) expression, a molecule responsible for the correct folding of the MHC-I complex, or defects in the intracellular antigen processing by alterations of the transporter associated with antigen processing (TAP) or proteasomal subunits (Figure 4.) [58], lead to loss of antigen presentation on the surface of tumor cells. Consequently, recognition by antigen-specific effector T cells does not take place, promoting tumor evasion.

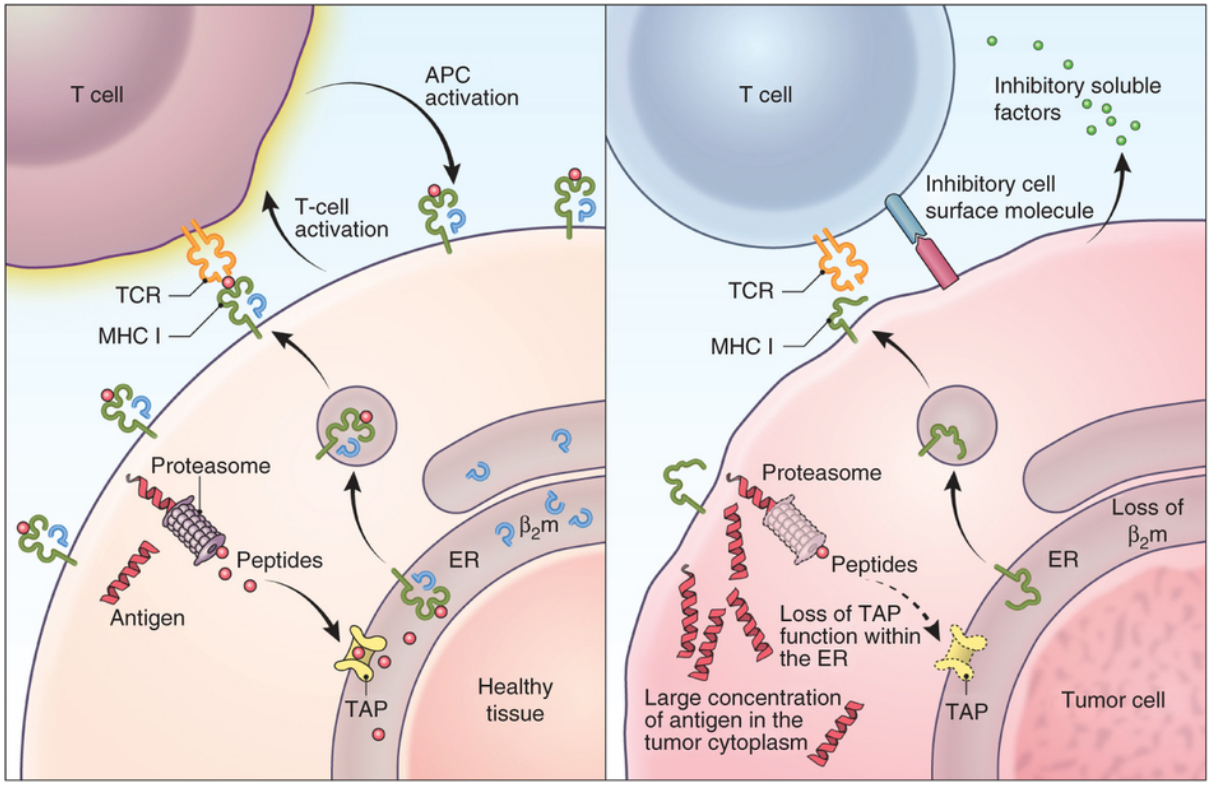

Figure IV. Impairment of the antigen-presenting machinery. Healthy tissues, possessing an intact antigen processing and presentation machinery, are susceptible to T cell-mediated killing **(left panel)**. Transformed cancer cells are prone to genomic instability and present defects in antigen processing such as dysfunction of TAP and proteasomal subunits or defects in antigen presentation, such as downregulation of MHC-I molecules or β2m **(right panel)**. Adapted from Hinrichs *et al.*, Nature Biotechnology, 2013 [58].

1.4.3 Resistance towards T cell induced apoptosis of tumor cells

The immune elimination of tumor cells is mediated by apoptosis that can be induced either by death receptor signaling (extrinsic pathway) or by the release of cytotoxic granules (intrinsic or mitochondrial pathway) [59]. Ligand-induced apoptosis (extrinsic apoptotic pathway), is mediated by death receptors, expressed on tumor cells such as Fas, DR3/DR4 and TNFR1, which belong to the tumor necrosis factor superfamily. The interaction with their respective ligands (FasL, TRAIL and TNF) induces apoptosis in the tumor cells via the death inducing signaling complex (DISC) [60, 61]. More specifically, the interaction between the receptors and the ligands induces oligomerization of the receptor [62, 63], which recruits and binds through its cytoplasmatic death domain (DD) the adaptor protein FADD (Fas associated death domain) in case of Fas and DR3/4 or TRADD (Tumor necrosis factor receptor type 1-associated death domain) in case of TNFR1. FADD carries a death effector domain (DED) and by homologous interaction it recruits the DED containing initiator pro-caspase-8 or pro-caspase-10 protein. This complex is referred to as DISC. After binding to DISC, pro-caspase-8 homodimers undergo a conformational change and autocatalytic processing, resulting in the generation of active caspase-8 and caspase-10. Subsequently, these initiator caspases can directly cleave and activate executioner caspases such as caspase-3, caspase-6 and caspase-7, which in turn cleave substrates within the cells, thus triggering the apoptotic signal [64]. In some cells, this pathway is sufficient to induce cell death. Nevertheless, in other cells, caspase-8 also triggers the cell-intrinsic (mitochondrial) pathway. This pathway involves the release of cytochrome-c from the mitochondria into the cytoplasm, upon cleavage of the pro-apoptotic molecule Bid (BH3 interacting-domain death agonist). Consequently, cytochrome-c interacts with the adaptor protein Apaf-1 (apoptotic protease activating factor-1) and forms the heptaric backbone of the apoptosome complex, which in turn recruits and activates caspase-9 through dimerization. Similar to active caspase-8, active caspase-9 cleaves and activates downstream effector caspases.

It is not surprising that tumors have evolved mechanisms through which they become resistant to death effector mechanisms, thereby becoming invulnerable to immune attack. Indeed, expression levels of both Fas and DR3/4 were found to be decreased in several tumors [65-68]. Moreover, decoy receptors, harboring a functional extracellular domain but lacking the intracellular DD have been found. Decoy receptor 3 (DcR3), is a soluble decoy receptor that is released by the tumor cells, it binds to FasL, thereby preventing apoptosis-

induced signaling in the tumor cells by Fas-FasL interaction [69]. Furthermore, tumor cells can interfere with the extrinsic apoptotic pathway by upregulating the endogenous inhibitor c-FLIP (FLICE (FADD like IL-1 beta-converting enzyme) inhibitory protein). c-FLIP possesses two DED and is thus capable of binding to the DISC, where it competitively inhibits the recruitment of caspase-8 thereby exerting an anti-apoptotic role [70]. The intrinsic apoptotic pathway can be inhibited by the production of anti-apoptotic molecules like BAX or BH3 proteins. In particular, Bcl-2 and Bcl-XL are commonly overexpressed in tumors, protecting cancer cells from apoptosis, by preventing cytochrome-c release [71]. Another important group of apoptosis-regulating proteins are so-called inhibitor of apoptosis proteins (IAPs). Through their baculovirus AIP repeat (BIR) domains, IAPs bind to and thereby inhibit caspases and through their ubiquitin-ligase RING zinc finger (RZF) activity they can block apoptosis by mediating proteosomal caspases degradation. Overexpression of several IAPs has been detected in several hematological malignancies including acute leukemias, myelodisplastic syndromes (MDS) and chronic myeloid leukemia (CML) as well as B-cell lymphoid malignancies correlating with poor prognosis [72-76].

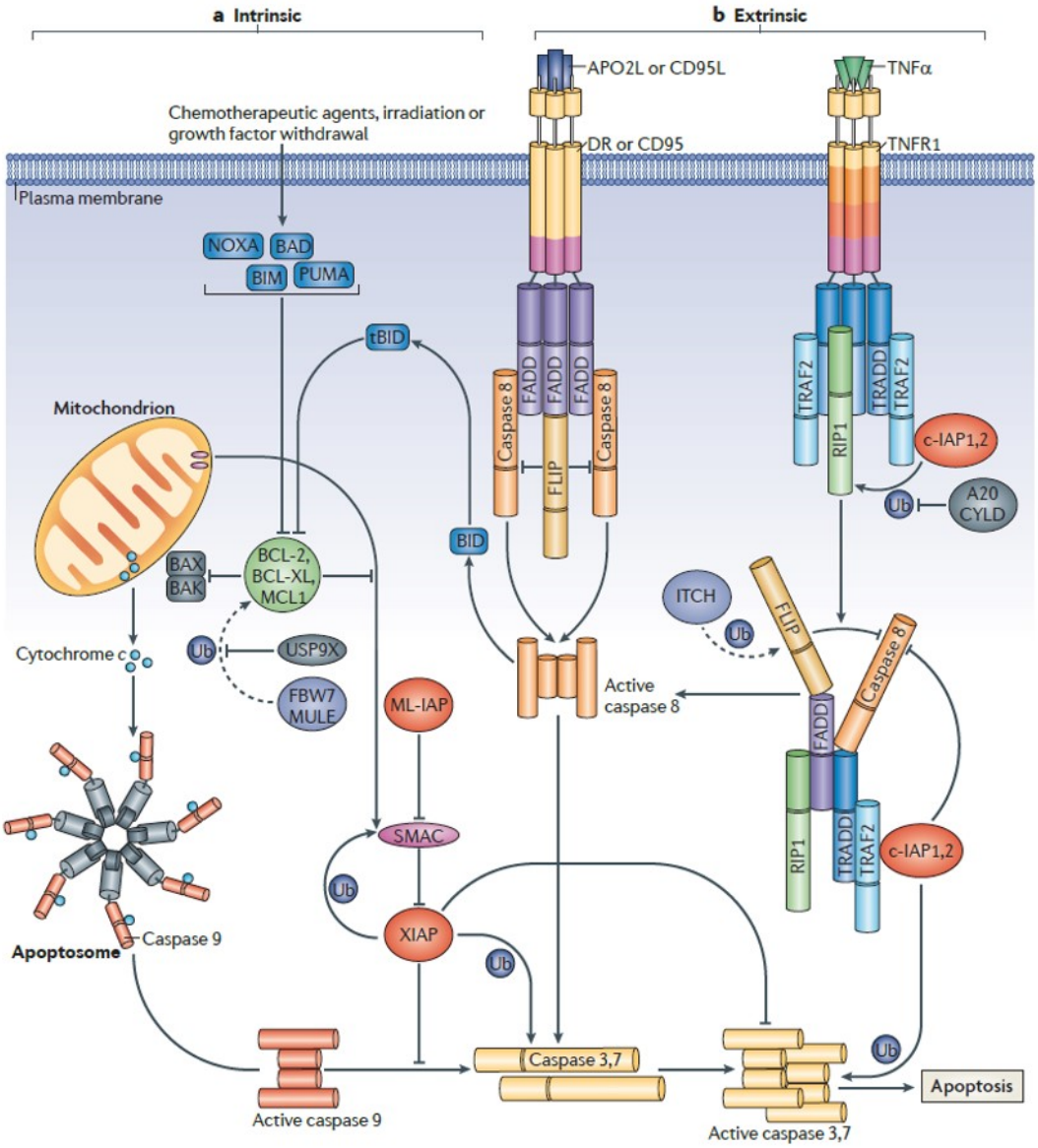

Figure V. The intrinsic and extrinsic apoptotic pathways. The intrinsic or mitochondrial apoptosis pathway is activated by chemotherapeutic agents, irradiation or growth factors' withdrawal. This leads to the activation of pro-apoptotic molecules such as BAD and BIM. Subsequently the disruption of the mitochondrial membrane results in cytochrome-c release that interacts with the adaptor protein Apaf-1 that in turn recruits and activates caspase-9 thus forming the apoptosome complex. This leads to the activation of caspase-3 and caspase-7, ultimately inducing apoptosis **(A)**. The extrinsic pathway is induced by death ligands such as FasL, TRAIL or TNF. Upon binding, the DISC complex is assembled which leads to the activation of caspase-8 and caspase-10 and the subsequent activation of effector caspases 3, 6 and 7. Several IAPs, which are upregulated in cancer cells, are involved in the inhibition of cell death **(B)**. Adapted from Vucic *et al.* Nat Rev Mol Cell Biol., 2011 [77].

To sustain tumor cell survival, cancer cells can upregulate pro-survival factors or counteract apoptosis by inducing molecular mechanisms responsible for cell cycle and tumor cell plasticity. In line, the transcription factor nuclear factor kappa B (NF-κB), important during inflammation and stress response, has been found to be elevated in Hodgkin lymphoma and T cell lymphoma. The activation of NF-κB results in the transcription of pro-tumorigenic genes such as cyclin D, which sustain cell proliferation, and anti-apoptotic genes, such as Bcl-2, Bcl-XL, x-linked inhibitor of apoptosis (XIAP) and c-IAP1/2. Notably, NF-κB activation prevents TNF-mediated apoptosis in tumor cells [78-80]. In physiologic conditions, by binding to its receptor, TNF triggers the apoptotic cascade. However, recent findings in our lab suggest that this pathway can be altered in tumor cells, supporting cell proliferation rather than tumor cell death (Sorrentino et. al., submitted).

1.4.4 The tumor microenvironment

Besides actively targeting immune cells or developing intrinsic mechanisms of immune-resistance, tumor cells can take advantage of the suppressive microenvironment. The tumor microenvironment includes a wide variety of malignant and non-malignant cells [81]. Although different immune effector cells are recruited to the tumor site, their anti-tumor functions are downregulated, mainly in response to immune-suppressive cytokines and growth factors released by cells encompassing the tumor microenvironment. Thus, tumor and stromal cells in the microenvironment prevent anti-tumor responses and support tumor growth by promoting tumor plasticity and resistance to cell death [82].

1.4.4.1 Immune-suppressive soluble factors

Tumor cells and the surrounding stroma cells in the microenvironment secrete a plethora of immune-suppressive factors such as growth factors and cytokines. Among them, transforming growth factor β (TGF-β), vascular endothelial growth factor (VEGF), interleukin 10 (IL-10), prostaglandin E2 (PGE2) and indoleamine 2,3-dioxygenase 1 (IDO) and arginase (Arg1) have been found to mediate a strong immunosuppressive response impairing a successful anti-tumor immunity. In particular, TGF-β is overexpressed in many tumors, where it inhibits T cell activation, proliferation and differentiation into mature effector cells [83]. Interestingly, upon induction of the transcription factor Foxp3, TGF-β

converts peripheral $CD4^+CD25^-$ naive T cells to $CD4^+CD25^+$ regulatory T cells, thus correlating with an aggressive tumor phenotype [84]. VEGF sustains angiogenesis and tumor proliferation [82]. IL-10 is mainly produced by M2 tumor associated macrophages (TAMs), which skew T helper cells to a Th2 polarization, thereby inducing immunosuppression [85]. Moreover, IL-10 contributes to immune escape mechanisms by downregulating TAP1 and TAP2 proteins responsible for a correct antigen presentation on the MHC complex. Furthermore, it has been shown that IL-10 sustains the Treg phenotype by inducing STAT3 signaling and activating the forkhead Box O1 (Foxo1) transcription factor [86]. In line, PGE2 induces the accumulation and function of Treg, impairs DCs ability to present antigen to T cells, thereby impairing CTL activation.

Metabolic changes in the TME can also lead to immune suppression. Indoleamine 2,3-dioxygenase (IDO) and arginase (Arg) are immunoregulatory enzymes that inhibit T cell proliferation by catabolizing the degradation of the amino acids tryptophan and L-arginine [87, 88] essential for immune cell survival. Furthermore, since tumor cells utilize glycolysis as main source of energy production, resulting in high production of lactic acid, the pH in the microenvironment decreases. It has been reported that a low pH impairs cytolytic activity and cytokine secretion in $CD8^+$ T cells [89].

1.4.4.2 Immune-suppressive cell populations

As previously mentioned, the developing tumor microenvironment comprises proliferating tumor cells, blood vessels, stroma and infiltrating immune cells. Via secretion of soluble factors, tumor cells recruit to the microenvironment a plethora of immune-suppressive cell populations in order to promote tumor progression and inhibit the anti-tumor immune response. These cell populations include regulatory T cells (Treg), myeloid-derived suppressor cells (MDSC), tumor-associated macrophages (TAM) and tolerogenic dendritic cells (tDC).

- *Regulatory T (Treg) cells*: are a subset of $CD4^+$, $CD25^+$ $Foxp3^+$ T lymphocytes. In physiologic conditions this cell population is responsible to induce peripheral tolerance to self-antigens and to prevent autoimmune diseases [90]. However, during tumor progression, Tregs are recruited to the tumor microenvironment to suppress effector T cells. Indeed, increased Tregs infiltration within the tumor

microenvironment has been correlated with poor patients' survival in different tumor entities [91-94]. The mechanism involved in suppressing the immune response comprises the modulation of APCs activity through the engagement of co-stimulatory immune-checkpoints. Indeed, CTLA-4 expressed on Tregs, having a higher affinity for CD80/86, outcompetes CD28 expressed on conventional T cells for CD80/86 ligation, thereby abrogating signals from DCs to T cells [95]. Moreover, Tregs secret cytokines such as TGF-β and IL-10, responsible for suppressing the activity of effector cells and APCs (see paragraph 1.4.4.1). Via secretion of cytotoxic granules as perforin and granzyme or through the engagement of death receptors, Tregs can directly exert a cytotoxic effect towards effector T cells [96, 97]. Tregs may also trigger metabolic disruption by stimulating DCs to generate enzymes that catabolize essential amino-acids (see paragraph 1.4.4.1). Finally, Tregs can also compete with effector cells for APC signals or cytokines, such as IL-2.

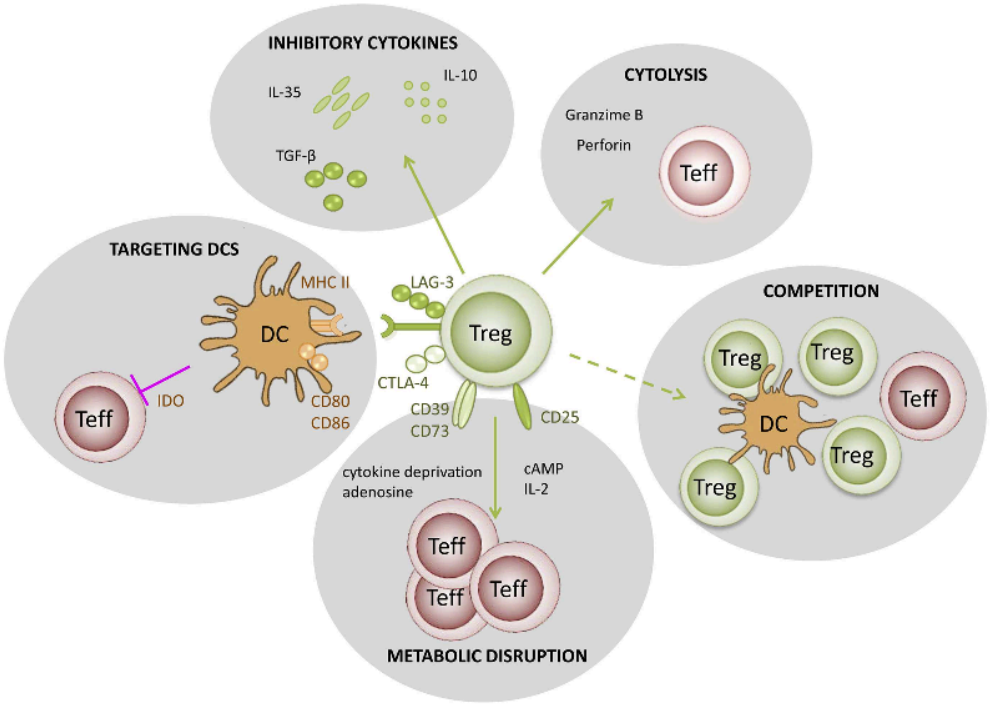

Figure VI. Putative mechanisms of immune-suppression used by Tregs. Immune-suppressive modes of Tregs include targeting of DCs via inhibitory receptors engagement, metabolic disruption that includes cytokine deprivation, cyclic AMP-mediated inhibition, and adenosine receptor (A2A)-mediated immunosuppression, competitive inhibition of effector T cells for the engagement with APCs, direct cytolysis of effector T cells through cytotoxic molecules and production of inhibitory cytokines like IL-10, IL-35, and TGF-β. Adapted from Caridade *et al*., Frontiers in immunology, 2013 [98].

- *Myeloid-derived suppressor cells (MDSCs)*: are a heterogeneous population of myeloid progenitor and immature mononuclear cells with a potent negative regulation of both the innate and adaptive immune responses. T cells are inhibited by MDSCs by depletion of arginine and cysteine, production of reactive oxygen species (ROS) and peroxynitrite and induction of Tregs. The innate immune system is suppressed by MDSCs that modulate the cytokine production of macrophages [99]. The recruitment of MDSCs in the TME is supported by growth factors and pro-inflammatory cytokines like GM-CSF, CCL2, CXCL12 and CXCL5 and has been shown to correlate with poor survival [100]. Indeed, besides their immunosuppressive function, MDSCs sustain tumor growth by remodeling the TME and triggering the epithelial-to-mesenchymal transition (EMT) [101].

- *Tumor-associated macrophages (TAM)*: are the most abundant leukocyte population of non-tumor cells inside the TME. TAMs are phagocytic cells that demonstrated a high degree of plasticity in response to the TME. Indeed, TAMs can undergo two differentiation states. INF-γ, LPS or TLR polarize macrophages into pro-inflammatory (M1) classically-activated macrophages, while exposure to Th2 and tumor-derived cytokines like IL-10, IL-4 or growth factors such as TGF-β propagates alternatively-activated anti-inflammatory (M2) macrophages. M2 macrophages suppress anti-tumor immunity and promote tumor development by eliminating M1 macrophages, promoting Tregs activity and impairing T cells activation. The latter can be achieved by TAMs downregulation of their MHC complex, thus losing their ability to present and activate antigen-specific T cells. TAMs can also directly induce T cell apoptosis through the expression of PD-L1 [102].

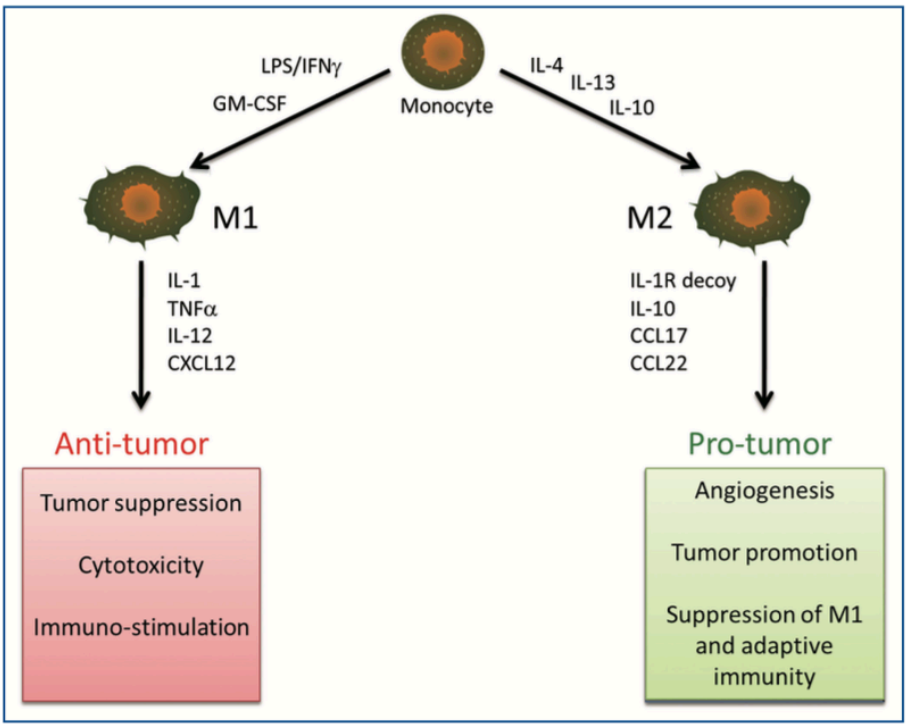

Figure VII. Differentiation state of macrophages. Depending on different stimuli, monocytes can polarize into M1 or M2 macrophages. INF-γ, LPS, TLR and GM-CSF induce pro-inflammatory and anti-tumorigenic (M1) classically-activated macrophages while IL4, IL-13 and IL-10 polarize macrophages to anti-inflammatory and pro-tumorigenic (M2) macrophages. Adapted from Leyva-Illades *et al.,* Transl Gastrointest Cancer, 2012 [103].

- *Tolerogenic dendritic cells (tDC)*: are a population of altered DCs in the TME. DCs are specialized antigen-presenting cells that maintain the balance between tolerance and immunity. However, in the TME, cancer cells and the associated stroma convert myeloid DCs into tumor-infiltrating tolerogenic DCs. These tolerogenic DCs can then be converted in Tregs and dampen the anti-tumor immunity [104, 105]. Moreover, tolerogenic DCs induce tolerance because they are poorly immunogenic, expressing only at low levels co-stimulatory molecules required for T cell activation. Furthermore, they have an impaired antigen-presenting machinery leading to T cell anergy.

1.5 Cancer immunotherapy

According to the immunosurveillance hypothesis, the immune system could suppress tumor growth. The confirmation of the validity of this hypothesis led to great enthusiasm for the development of immune-based anti-tumor therapies. Indeed, in the last years significant improvements in the field of immunotherapy have been accomplished and novel therapeutic strategies have been beneficial to numerous cancer patients, bringing immunotherapy to the forefront in cancer therapy.

Immunotherapy can be divided into active immunotherapy, which relies on cancer vaccines to stimulate the adaptive arm of the immune system directly *in vivo* and adoptive immunotherapy, which consists of the *ex vivo* isolation and expansion of TILs and their subsequent re-infusion into the patient.

1.5.1 Cancer vaccines

In the same way that vaccines work against diseases, cancer vaccines are made to induce immune cells recognizing TAAs on cancer cells. Cancer vaccination was the first method developed in cancer immunotherapy. Autologous tumor cell vaccination was introduced in the early 1970s pioneered by Hanna et al. when dissected hepatocellular carcinoma cells were irradiated and re-injected into a guinea pig model together with immune-stimulatory adjuvants. This method induced a protective immunity against subsequent challenge with syngeneic non-irradiated tumor cells [106]. Being able to overcome tumor-induced immune suppression and promoting the recruitment and maturation of specialized APCs, the granulocyte macrophage colony-stimulating factor (GM-CSF) is the most commonly used cytokine to boost anti-tumor immunity [107-109]. Based on these observations autologous melanoma tumor cells, transduced with GM-CSF (GVAX), were applied clinically. This vaccination approach induced the priming of $CD8^+$ T cells by DCs and showed a durable anti-tumor immune response in a variety of pre-clinical studies [110]. Nevertheless, advanced Phase III clinical studies failed to show efficacy of this vaccine. Allogeneic vaccines have significant advantages over autologous tumor vaccines in terms of availability for patients in all stages of the disease. Canvaxin, a polyvalent irradiated melanoma vaccine, is an example of allogeneic cancer vaccine that significantly improved overall survival in melanoma patients (Phase II trial) however failed to show a significant

effect in randomized Phase III trials [111]. The first FDA approved therapeutic cancer vaccine was the DC-based vaccine sipuleucel-T in 2010 for the treatment of prostate cancer [112]. Sipuleucel-T showed overall survival benefit to patients in three double-blind randomized phase III clinical trials. Moreover in 2014 a small phase I clinical trial demonstrated a synergistic effect of sipuleucel-T and ipilimumab, a monoclonal antibody targeting CTLA-4, that were administered as combination therapy to patients with advanced prostate cancer [113].

Similarly, several pre-clinical studies were conducted to establish cancer vaccines for hematological malignancies. Indeed, different phase I/II clinical trials confirmed that *ex vivo* generated monocyte-derived DCs stimulate T cell responses in multiple myeloma (MM) patients [114, 115]. Thus subcutaneous and intravenous administration of DC vaccination for refractory MM using patient-specific tumor idiotype proteins was shown to induce anti-MM T cell responses [116]. Despite recent advances in cancer vaccination, this method remains a challenging approach and further research needs to be conducted to discover novel TAA as well as vaccination approaches to improve this immunotherapeutic strategy.

1.5.2 Adoptive cell transfer (ACT)

Adoptive cell transfer (ACT) is an example of a specific adoptive immunotherapeutic approach that has proven to be one of the most powerful immunotherapies against metastatic melanoma to date. ACT was established by Rosenberg and consists in the isolation and *ex vivo* expansion of autologous tumor infiltrating lymphocytes (TILs) and the re-infusion into cancer patients. *In vitro* tests can identify the exact populations and effector functions required for cancer regression, which can then be selected for expansion. Subsequently, these cells can be activated and expanded in the laboratory free from endogenous inhibitory factors and can thus be induced to exhibit the required anti-tumor effector functions [117]. This approach showed an overall response rate of 34% in 86 patients treated with autologous TILs plus high-dose IL-2 [118]. Nevertheless, most of the responses were transient, and patients had limited persistence of the transferred cells. Further studies suggested that, prior host conditioning with lymphodepleting chemotherapy, improves TILs–mediated responses. This is due to higher TILs engraftment and elimination of immunosuppressive cells such as Tregs in the TME [112]. Unfortunately, TIL-based therapy is limited to resectable tumors such as melanoma, and in some patients, TILs are unable to expand *ex vivo* [119]. For this reason,

much effort has been put forward to generate genetically modified T cells to provide the desired antigen specificity and effector functions also in those tumor entities with reduced TILs applicability.

1.5.2.1 The potential of ACT with CAR-redirected T cells

T cell adoptive immunotherapy requires large cell numbers with high proliferative potential in order to be effective for cancer treatment. However, human tumor-specific T cells are relatively rare in cancer patients. To overcome this hindrance, T lymphocytes have been genetically engineered and redirected against tumors, through the genetic transfer of high avidity clonal T cell receptors (TCRs) or chimeric antigen receptors (CARs) specific for tumor-associated antigens (TAA). These strategies have solved the need of isolating rare antigen specific T cells from clinical specimens.

CARs are monomeric receptors constructed by fusing the single-chain variable fragment (scFv), derived from a tumor-specific monoclonal antibody, with the CD3ζ chain of the TCR complex. Thus, CARs are artificial fusion proteins and CAR T cells are prepared from autologous T cells that are genetically modified to express a specific CAR upon lentiviral or retroviral vector transduction. CARs harbor advantages over monoclonal antibodies and adoptively transferred tumor reactive T cells. Indeed, being expressed on T cells, CARs have a wider biodistribution, improved persistence, ability to infiltrate tissues, expand *in vivo* and migrate through chemokine gradients. Most importantly these receptors recognize tumor cells independently of the MHC complex. Recent clinical trials have underscored the potential of CAR-redirected T cells in patients with advanced, refractory chronic lymphocytic leukemia (CLL) after transfer of T cells redirected with an anti-CD19 CAR [120, 121]. The results of the first clinical trials demonstrated modest efficacy in cancer patients, and soon it became evident that CAR-mediated CD3ζ signaling alone termed “first generation CAR” (1G) was not sufficient to generate a durable T cell response. Thus, much work has been done in the optimization of the CAR design producing second (2G) and third (3G) generation CARs containing the endodomains of co-stimulatory receptors, such as CD28, 4-1BB or OX40 in addition to CD3ζ to sustain proliferation and cytokine production and to increase T cell survival and *in vivo* persistence. Following CAR constructs optimization, a number of clinical trials in phase I/II have obtained striking results, especially the ones using CD19-specific

CAR T cells containing a 4-1BB co-stimulatory domain for the treatment of CLL and acute lymphoid leukemia (ALL) [122, 123].

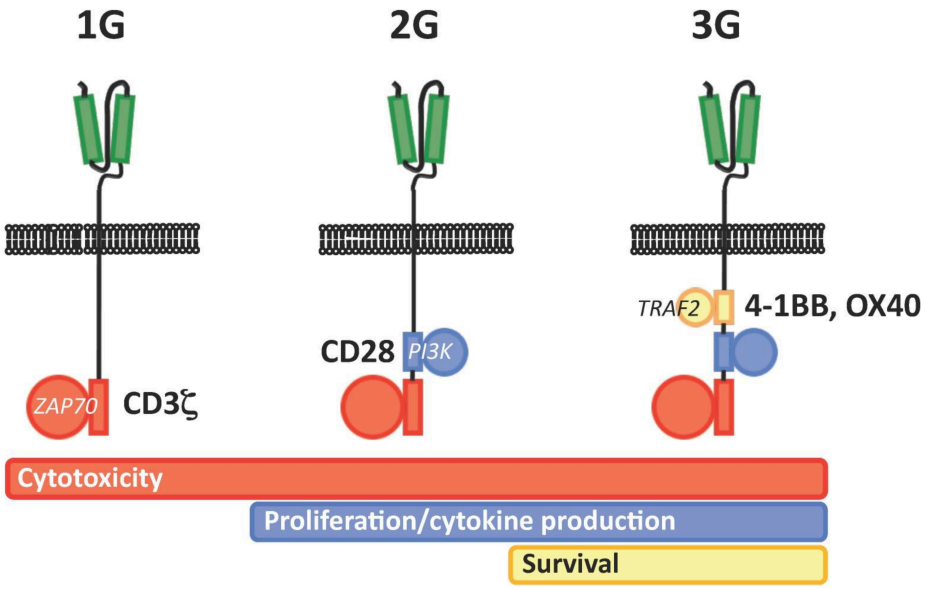

Figure VIII. Improving CAR design. First generation (1G) CARs contain only the CD3ζ to transmit activation signaling (left). Second generation (2G) CARs combine the CD3ζ to a single co-stimulatory molecule endodomain like CD28 that increases T cell proliferation and release of cytokines (middle). Third generation (3G) CARs incorporate two co-stimulatory molecule endodomains such as CD28 and 4-1BB or OX4O, which further improve T cell survival (right). Adapted from Casucci *et al.,* Journal of Cancer 2011 [124].

1.5.2.2 TCR gene transfer and TCR gene editing

An alternative approach to extend the use of adoptive T cell therapy, while overcoming immune tolerance to TAAs comes from the genetic engineering of T cells to express high-avidity tumor-reactive T cell receptors (TCR). Tumor-specific TCRs can be transferred into T cells thus redirecting the specificity of these immune cells towards cancer cells. In 2006 the first clinical trial using autologous-engineered T cells demonstrated the feasibility and safety of this therapeutic approach that induced clinical responses [125]. Phase I/II clinical trial showed clinical responses ranging from 19 to 50%, depending on clinical conditions, tumor type, target antigen, and TCR [126]. In order to avoid competition between the endogenous and the exogenously transferred TCR, zinc finger nucleases (ZFNs) were designed to permanently knockdown the endogenous TCR. In fact, ZFNs promote the disruption of endogenous TCR β- and α-chain genes and via lentiviral vectors transduction tumor specific TCR can be administered to T cells. This gene editing approach demonstrated

superior tumor antigen recognition compared to unedited cells, thus improving anti-tumor activity *in vivo* [127].

1.5.3 Immune-checkpoint blockade

As discussed in section 1.5.1, anticancer vaccines target TAAs thereby stimulating effector T cell responses. Although the approval of sipuleucel-T indicates effectiveness of cancer vaccines, the limited improved overall survival over placebo suggests that other factors may inhibit effector T cell responses. As described earlier, activated T cells can be suppressed by increased expression of CTLA-4 and PD-1 upon binding to their respective ligands on tumor cells or tumor associated cell populations. Therefore, other immunotherapy approaches such as immune-checkpoint blockade have been developed to target the regulatory mechanisms responsible for immune suppression [128]. During the last years remarkable clinical success was achieved by blocking inhibitory pathways induced in immune cells by cancer cells. In particular, CTLA-4 and PD-1 are two immune-checkpoint molecules that have been most actively studied in the context of clinical therapy [28]. In 2011, ipilimumab, a human monoclonal antibody (mAb) blocking CTLA-4, was the first-in-line treatment that achieved FDA approval for patients with metastatic melanoma [129-131]. In phase III trials ipilimumab treatment resulted in overall survival benefit, inducing durable disease control in patients who failed to respond to prior treatments [132].

The success of ipilimumab was followed by the generation of two PD-1 blocking antibodies, pembrolizumab and nivolumab, that were approved by the FDA in 2014 and 2015 respectively for the treatment of metastatic melanoma, non-small cell lung cancer (NSCLC) and renal carcinoma [133, 134]. The objective response rates (ORR) induced by nivolumab reached 30-40% in melanoma and 15% in progressive NSCLC [134-136]. In line, pembrolizumab showed equivalent results in melanoma, NSCLC and other solid tumors [137]. Remarkably, PD-L1 expression on tumor cells cannot be considered a useful biomarker for PD-1/PD-L1 blockade, since it has been shown that some patients not expressing this immune-checkpoint molecule can benefit from this therapy [138]. Indeed, in melanoma patients, 49% of PD-L1-positive and 26.2% of PD-L1-negative tumors react to anti-PD-1/PD-L1 therapy. In contrast, other tumor entities, like multiple myeloma do not respond to anti-PD-1/PD-L1 therapy despite the expression of these immune-checkpoints [139, 140]. Several others immune-checkpoint blockade therapies are being developed, that

could be used to treat patients that do not respond to anti-PD-1/PD-L1 therapy or to increase the effect achieved by anti-PD-1/PD-L1 therapy. Indeed, many immune inhibitory pathways do not overlap, suggesting that a combination of different immune-checkpoint blockade may potentiate the effect of a monotherapy [141]. Recent studies showed that the combination of nivolumab and ipilimumab significantly improved objective response in patients with metastatic melanoma with an ORR of 61% against 11% in patients treated with ipilimumab alone [142]. Although combination therapies may represent a more effective strategy to treat cancer, correlating with an increased T cell activation and efficacy, in some cases severe life-threatening side effects such as elevated circulating levels of several cytokines known as cytokine release syndrome (CRS) may occur, leading to abrogation of the treatment. Thus much effort is put in developing novel immune-checkpoint blocking antibodies that might help reducing systemic side effects and improve the treatment of patients that do not benefit from the existing mono- or combination therapy.

1.6 Immunopathogenesis and immunotherapy of multiple myeloma

Despite the advent of novel therapies leading to increased survival, multiple myeloma (MM) still remains an incurable disease. In order to improve patients' survival, elucidation on the mechanisms of anti-tumor immune dysfunction is critical.

1.6.1 Immune dysfunction in MM

Multiple myeloma is the second most common hematological malignancy worldwide due to the uncontrolled proliferation of malignant plasma cells in the bone marrow. It mainly affects elderly patients with a median age of 67. All MM patients have a pre-existing non-malignant phase defined as monoclonal gammopathy of undetermined significance (MGUS) [143]. The mechanism of progression from MGUS to MM is not limited to genetic mutations in the plasma cells since alterations in the microenvironment (the bone marrow) and loss of immunosurveillance play a significant role in tumor development. Genetic abnormalities such as translocations account for 40–50% of primary or initiating mutagenic events in myeloma and strongly influence disease phenotype [144]. In particular translocations involving the

immunoglobulin heavy chain (IgH) region on chromosome 14q32 are responsible for the pathogenesis of MM and the incidence of the translocation increases with the stage of the disease. For example, in the translocation t(8;14)(q24;q32), the IgH locus is juxtaposed to the proto-oncogene MYC. This translocation leads to increased transcription of MYC target genes, such as Cyclin A/D1/E, eIF-2α/-4E (eukaryotic initiation factor) and p53 increasing the capability of myeloma cells to drive cell proliferation.

Despite being a B cell lineage disorder, the T cell compartment is frequently affected showing a reduction in the CD4/CD8 ratio as well as the loss of NKT cells is a hallmark for progression from MGUS to MM [145]. Moreover, NK cells from MM patients upregulate PD-1 expression, allowing PD-L1 expressing MM cells to inhibit the cytotoxic function of NK cells [146]. Also, DCs are functionally impaired, demonstrating a reduction or loss of co-stimulatory expression, thus inhibiting antigen-specific T cell activation and proliferation. The inhibition of induction and maturation of DCs is likely related to exposure to myeloma-derived cytokines such as IL-6, IL-10 and TGF-β and growth factors like VEGF. Immunosuppressive cells like Tregs, TAMs and MDCS, harboring tumor promoting activities, also inhibit anti-tumor immunity and are therefore associated with disease progression in MM patients [147].

1.6.2 Immunotherapeutic treatments for MM patients

Standard treatments for MM patients include chemotherapy, proteasome inhibitors and immunomodulatory drugs (IMiDs). These treatment options have improved overall response rates. Nevertheless, MM remains an incurable disease, since the majority of patients experience relapse. Allogeneic stem cell transplantation (allo-SCT) has been associated as the only treatment being able to induce complete remission. Unfortunately the effect attributed to the graft versus myeloma is limited by the high treatment mortality due to graft versus host disease (GvHD) [148].

1.6.2.1 Immunomodulatory drugs (IMiDs)

With the introduction of immunomodulatory drugs (IMiDs) the survival rate of MM patients significantly increased. Thalidomide, a first generation IMiD, with anti-inflammatory and anti-angiogenic properties demonstrated a 32% overall response rate (ORR) in patients

with relapsed or refractory MM (RRMM) [149]. In particular, thalidomide stimulates T cell-mediated interactions between CD80 and the co-stimulatory molecule CD28 expressed on T cells thereby facilitating an antigen-specific effector response [150]. Second and third generation IMiDs, lenalidomide and pomalidomide also induce anti-tumor effects by decreasing the production of IL-6 and VEGF by the tumor cells and the surrounding stromal cells. Moreover they induce the activation of caspases leading to tumor cell death and induction of tumor suppression genes through cyclin-dependent kinase inhibitors [151].

1.6.2.2 Vaccination strategies

In the past decades, clinical trials using two different vaccination approaches were performed. One approach comprises DCs pulsed with TAAs. The first peptide-based vaccine used idiotype proteins (Id), however being poor immunogenic, this approach did not meet expectations, showing modest biologic responses. With the identification of TAAs such as MAGE, NY-ESO and WT-1, promising outcomes were achieved. Indeed, by using TAAs as targets, specific cytotoxic T cells were generated, eliciting increased immune responses [152]. Furthermore, the second vaccination approach involves the fusion of DCs with myeloma cells following autologous stem cell transplantation. This method showed efficient tumor-specific T cells proliferation as well as induction of tumor specific antibody responses thereby inducing complete response in 24% of treated MM patients [153, 154]. A clinical trial taking advantage of DC/myeloma vaccine in combination with PD-1 blockade following stem cell transplantation is ongoing (NCT01067287).

1.6.2.3 Antibody therapies

The lack of uniquely expressed target molecules on malignant plasma cells hampered the development of effective cytotoxic mAb therapies for the treatment of MM. The first approved monoclonal antibody for the treatment of MM was elotuzumab, a humanized IgG1 kappa immunostimulatory monoclonal antibody targeting the signaling lymphocytic activation molecule family 7 (SLAMF7) (also referred to as CS1). SLAMF7 is a glycoprotein expressed on both normal and malignant plasma cells as well as on NK cells. Elotuzumab showed remarkable *in vitro* activity, exerting anti-MM efficacy via NK-mediated antibody dependent cellular cytotoxicity (ADCC) and enhancing NK function. Nevertheless, in a phase

I trial, elotuzumab alone did not show any clinical effect. However, in a phase III trial the combination of elotuzumab with lenalidomide and dexamethasone elicited an impressive effect in relapsed/refractory MM patients with an 82% objective clinical response [155]. Daratumumab, another fully humanized IgG1 kappa monoclonal antibody, targeting CD38 showed tremendous effects in relapsed MM patients. CD38 is a type II transmembrane glycoprotein expressed on activated B and T lymphocytes, NK cells and DCs. Daratumumab as monotherapy, yielded remarkable responses inducing 36% overall response rate. In line, the efficacy of daratumumab combined with dexamethasone achieved 93% ORR including 43% complete responses. Daratumumab increases anti-myeloma T cell immunity via CD8 T cell expansion and inhibition of immunosuppressive cells such as Tregs and MDSCs. Moreover, daratumumab acts on myeloma cells inducing ADCC, complement-dependent cytotoxicity (CDC), antibody-dependent cellular phagocytosis (ADCP), and induction of apoptosis as well as loss of enzymatic activity. Several other novel antibodies are under development. Among them antibodies targeting the B cell maturation antigen (BCMA), which is crucial for long-term plasma cells survival and antibodies against CD138.

1.6.2.4 CAR T and TCR transgenic T cell therapies

CAR T cell therapy represents a major breakthrough in immunotherapy. So far, different CAR T cell therapy for MM patients have been reported. Interestingly, although primary myeloma cells express very low levels of CD19, CD19 targeted CAR T cells induced sustained remission in MM patients without cytokine release syndrome [156]. Recently, encouraging results were also reported from BCMA-CAR T cell therapy inducing a high ORR in refractory MM patients [157]. New CAR T cell therapies are being developed including more effective CAR constructs to prolong survival and increase T cell cytotoxicity. Furthermore, the infusion of autologous T cells engineered to express NY-ESO-1- or LAGE-1-specific TCRs showed increase overall survival of MM patients [158]. However, as TCR-edited T cells are HLA dependent, this approach has limited advantages compared to HLA-independent CAR T cell therapy.

1.6.2.5 Immune-checkpoint inhibitors treatment

The PD-1/PD-L1 pathway plays an important role in the pathophysiology of multiple myeloma. Indeed, PD-L1 expression has been detected to higher degrees in plasma cells from MM patients compared to MGUS patients and healthy donors. High expression of this immune-checkpoint is associated with disease progression and has been found upregulated at relapse or in the refractory stage. Also, PD-1 expression was found to be significantly higher in the myeloma microenvironment, in particular on CD8 and NK cells [159]. These results suggested that targeting the PD-1/PD-L1 pathway would have led to potential treatment with the anti-PD-1 antibody nivolumab. Surprisingly, preliminary results of a phase I trial were disappointing. Indeed no objective responses were reported among the 27 multiple myeloma patients enrolled in the clinical trial. Nevertheless, 67% of the patients remained in stable disease [139]. Furthermore, a phase II clinical trial with pembrolizumab combined with pomalidomide and dexamethasone reached an ORR of 60% indicating an excellent efficacy of this combination therapy [160].

1.6.3 Limitations

Despite the development of novel immunotherapeutic agents for the treatment of multiple myeloma, a large number of patients still exhibit lack of responses so far. As previously mentioned, several clinical trials using immune-checkpoint blockade failed to achieve objective responses. Thus, these unsatisfactory results emphasize the need to discover additional therapeutic targets that could induce clinical efficacy in a broad range of hematological malignancies. Indeed, since tumor cells are heterogeneous entities and employ diverse immunosuppressive mechanisms, there is a strong rationale to believe that other immune-checkpoint molecules, different than the ones that are currently being targeted in the clinics, may play a crucial role in tumor escape mechanisms. Thus, for successful immunotherapy, dissection of the whole “immune modulatome” is required.

1.7 High-throughput (HTP) RNAi-based screens to discover novel immune-checkpoint molecules

High-throughput screenings, based on the principle of RNA interference (RNAi), have arisen as powerful approaches to uncover gene functions and pathways in a high-throughput (HTP) fashion. In particular, HTP screenings take advantage of RNAi mechanisms to knockdown target genes. This gene silencing mechanism was discovered in 1998, when the introduction of double stranded RNA (dsRNA) into cells was shown to interfere by sequence homology with the messenger RNA (mRNA) of targeted genes thereby causing gene silencing [161]. This intracellular defense mechanism was adopted to perform HTP screenings in order to identify novel immune-checkpoints in different tumor models [162]. In 2014, Zhou et al., transduced mouse $CD8^+$ T cells with a pooled short hairpin RNA (shRNA) that were subsequently injected into tumor-bearing mice. Performing deep sequencing they observed that shRNAs that targeted negative regulators of T cells were highly enriched in murine tumors because of increased T cell activation and proliferation [163]. A novel approach that targets human tumor cells and measures T cell cytotoxicity instead of proliferation was recently developed in our group by Dr. Khandelwal [164]. In a proof-of concept study, an arrayed siRNA library of 500 genes was employed to knockdown target genes in human breast cancer cells (MCF7) subsequently challenged with CTLs. Consequently, T cell-mediated tumor killing was measured. The C-C chemokine receptor type 9 (CCR9) was identified as a novel immune-checkpoint molecule impairing T cell function both *in vitro* and *in vivo*. This study successfully identified novel immune-checkpoints paving the way to utilize this approach with a broader library and on different human tumors. Finally, Borrello et al. showed for the first time that marrow-infiltrating T lymphocytes (MILs) can be expanded and lead to clinical anti-tumor immunity [165, 166]. This subset of MILs could be utilized as a T cell population with enhanced tumor specificity in bone marrow (BM)-derived malignancies to perform HTP screenings in hematological malignancies, leading to the discovery of novel immune-checkpoints utilized to escape immunosurveillance.

2 Aim of the study

Multiple myeloma (MM) is a B-cell malignancy, characterized by accumulation of plasma cell clones in the bone marrow. While novel therapeutic agents like immunomodulatory drugs and proteasome inhibitors have improved overall survival of MM patients, the disease remains incurable in most patients. Several studies showed that immune-checkpoint molecules are expressed by myeloma cells and induce tumor-related immune suppression [146, 167, 168]. Despite the promising results achieved by blocking CTLA-4 and the PD-1/PD-L1 axis in the treatment of various solid tumors and Hodgkin's lymphoma, targeting these checkpoints did not induce objective responses in Phase I/II trials in MM patients [139]. Therefore, identification of novel immune-checkpoints and elucidation of the subsequent molecular mechanisms of immune inhibition are essential for further improvement.

By utilizing a proof-of-concept approach developed in our laboratory [164], we aimed at:

- Identifying novel MM-related immune-checkpoint molecules by taking advantage of a high-throughput (HTP) RNAi screen.
- Validating the role of candidate molecules, whose blockade could potentially induce anti-tumor immunity in MM patients.
- Unraveling the mode of action underlying the immune suppressive function of the selected hit.
- Provide the rationale for the applicability of the selected candidate gene as a potential target for multiple myeloma immunotherapy.

3 Materials

3.1 Laboratory equipment

Instrument	Company
Bolt® Mini Gel Tank	Life Technologies
Casy cell counter	Innovatis
FACS Canto II Flow cytometer	BD
FACSARIA II cell sorter	BD
FACS Lyrics	BD
Gamma Cell 1000	Best Theratonics
Gamma Counter (Cobra Packard)	PerkinElmer
GeneMate Electrophoresis Systems	Starlab
Incucyte ZOOM	Essen bioscience
Infinite M200 plate reader	Tecan
MAGPIX system	Merk Millipore
Mini Trans-Blot Cell	Bio-Rad
Mithras LB 940 microplate reader	Berthold
Molecular Imager (ChemiDoc XRS+)	Bio-Rad
MultiDrop Combi I	Thermo scientific
NanoDrop 2000c UV-Vis Spectrophotometer	Peqlab
Phero-stab 500 Electrophoresis power supply	Biotec-Fischer
PowerPac 3000 Power supply	Bio-Rad
QuantStudio 3 Real-Time PCR System	Thermo scientific
Spark microplate reader	TECAN
Thermal Cycler	Thermo scientific
Thermomixer comfort / compact	Eppendorf
MyECL Imager	Thermo scientific

3.2 Chemicals, reagents and consumables

Material	Company
1 kb DNA Ladder (GeneRuler)	Thermo Scientific
100 bp Ladder (GeneRuler)	Thermo Scientific
2x MyTaq HS Red Mix	Bioline
Agarose	Life Technologies
Amersham ECL Prime Western Blotting Detection Reagent	GE Healthcare
Ampicillin	Sigma-Aldrich
Aqua ad iniectabilia	B. Braun
Assay Diluent	BD
Benzonase	Merck
Beta-mercaptoethanol	Gibco
Biocoll separating solution	Millipore
Bovine serum albumin (BSA)	Sigma-Aldrich
Cell signaling lysis buffer	Millipore
Conical centrifuge tubes (15 and 50 mL)	TPP
Cryogenic vials (2 ml)	Corning
Dimethyl sulfoxide (DMSO)	Sigma-Aldrich
Disposable needles (0,4 x 20 mm)	Henke Sass Wolf
Disposable syringes (1 mL)	Henke Sass Wolf
Disposable syringes (50 mL)	BD
DharmaFECT1 and 2 Transfection Reagents	Dharmacon, GE healthcare
Disposable needles (0,4 x 20 mm)	Henke Sass Wolf
Disposable syringes (1 mL)	Henke Sass Wolf
Disposable syringes (50 mL)	BD
EDTA 1% (w/v) without $Mg2^{+}$	Biochrom
Ethanol absolute	Sigma-Aldrich
FACS tubes	Falcon
Flat bottom plates (6 and 96 wells)	TPP

Freezing container (Mr. Frosty)	Nalgene, Thermo Scientific
GelRed Nucleic Acid Gel Stain	Biotium
Geneticin sulfate (G418)	Gibco
G-Rex100 Gas permeable cell culture device	Wilson Wolf Manufacturing
IL-2 (human, recombinant)	Novartis
Ionomycin calcium salt	Sigma-Aldrich
Isopropanol	Fluka
Jet-PEI	Polyplus-transfection
Kiovig	Baxter
Lipofectamine LTX with Plus™ Reagent	Thermo Scientific
Lipofectamine RNAiMAX	Life Technologies
Loading dye solution (6x)	Fermentas
LumaPlates	Perkin Elmer
MES SDS running buffer (20x)	Life Technologies
Methanol	Sigma
Negative control siRNA 1 and 2	Ambion
Nuclease free water	Ambion
NuPAGE 4-12% Bis-Tris Gels	Thermo Scientific
NuPAGE LDS Sample Buffer	Thermo Scientific
OptiPlate-384 white opaque	Greiner
OptiPlate-96 white opaque	Perkin Elmer
Pacific orange dye	Thermo Scientific
PageRuler Prestained Protein Ladder	Thermo Scientific
pEGFP-Luc plasmid	Provided by Dr. Rudolf Haase. LMU Munich
Phorbol 12-myristate 13-acetate (PMA)	Sigma-Aldrich
Phosphatase inhibitor III	Sigma-Aldrich
Phytohaemagglutinin (PHA)	Sigma-Aldrich
Pipette filter tips (10 µl - 1000 µl)	Thermo Scientific
Polystyrene round bottom tubes with caps	Falcon

Ponceau S solution	Sigma-Aldrich
Protease Inhibitor Cocktail Set III, EDTA-Free	Calbiochem
Puromycin (10 mg/mL)	GIBCO
RNAiMAX	Thermo Scientific
Round-bottom plate (96 well)	TPP
Safe-lock tubes (0.5, 1.5, 2.0 mL)	Eppendorf
Syringe filter units (0.22 µm-pores)	Millipore
Tissue culture flask/filter cap (25, 75, 150 cm2)	TPP
Triton X-100	Fluka
Trypan blue solution (0.4 %)	Fluka
Trypsin-EDTA (1x)	Sigma-Aldrich
Tween 20	Sigma-Aldrich
Vakuumtitration 500 „rapid“-Filtermax	TPP
YOYO-1	Thermo Scientific
Whatman 3 mm gel blot paper	Sigma-Aldrich

3.3 Assay kits

Material	**Company**
Active Caspase-3 Magnetic Bead MAPmate	Merck Millipore
Cell-Titer-Glo Luminescent Cell Viability Assay kit	Promega
Human Granzyme B ELISA development kit	Mabtech
Human IFN-γ ELISA Set	BD OptEIA
Human IL-2 ELISA kit	BD OptEIA
Human TNF ELISA Set	BD OptEIA
MILLIPLEX MAP Early Phase Apoptosis 7-plex-kit - Cell Signaling Multiplex Assay	Merck Millipore
MILLIPLEX MAP Multi-Pathway Magnetic Bead 9-Plex - Cell Signaling Multiplex Assay	Merck Millipore
MyTaq HS Red Mix	Bioline
Pierce BCA Protein Assay Kit	Thermo Scientific

QuantiFast SYBR Green PCR Kit	Qiagen
QuantiTect Reverse Transcription Kit	Qiagen
RNeasy Mini Kit	Qiagen

3.4 Primers

Gene	**Primer sequence 5'-3'**
β-Actin (Sigma-Aldrich)	Forward: AGAAAATCTGGCACCACA Reverse: GGGGTGTTGAAGGTCTCAAA
CCR9 (Sigma-Aldrich)	Forward: CAGTGAACCCCTGGACAACT Reverse: TGCCACTCAACAGAACAAGC
CEACAM-6 (Sigma-Aldrich)	Forward: CAAAAGGAACGATGCAGGAT Reverse: TGGCAGGAGAGGTTCAGATT
HLA-A2 (Sigma-Aldrich)	Forward: TTGAGAGCCTACCTGGATGG Reverse: TGGTGGGTCATATGTGTCTTG
PD-L1 (Sigma-Aldrich)	Forward: GTACCTTGGCTTTGCCACAT Reverse: CCAACACCACAAGGAGGAGT
CAMK1A (Sigma-Aldrich)	Forward: TCCTGGCAGAAGATAAGAGGA Reverse: CAATGTTGGGGTGCTTGAT
CAMK1G (Sigma-Aldrich)	Forward: GATGGAACAGAATGGCATCA Reverse: CCTTGCTGTAGGGTTTCTGG
RT² qPCR Primer Assay for Human PNCK	Qiagen
RT² qPCR Primer Assay for Human CAMK1D	Qiagen
RT² qPCR Primer Assay for Human PTK2B	Qiagen
RT² qPCR Primer Assay for Human ITGB1	Qiagen
RT² qPCR Primer Assay for Human BEST1	Qiagen
RT² qPCR Primer Assay for Human RGS14	Qiagen

RT² qPCR Primer Assay for Human DGKQ	Qiagen
RT² qPCR Primer Assay for Human HLA-G	Qiagen
RT² qPCR Primer Assay for Human ADORA2B	Qiagen
RT² qPCR Primer Assay for Human Caspase-3	Qiagen
RT² qPCR Primer Assay for Human Caspase-6	Qiagen
RT² qPCR Primer Assay for Human Caspase-7	Qiagen

3.5 siRNAs and siRNA libraries

Material	Company
siGENOME set of four upgrade siRNAs against: CAMK1D, PTK2B, ITGB1, BEST1, RGS14, DGKQ, HLA-G, ADORA2B, CASPASE-6	Dharmacon, GE healthcare
siGENOME smart pools against: CCR9, PD-L1, FLuc, UBC, CHK1, COPB2, CASPASE-3, CASPASE-7	Dharmacon, GE healthcare
AllStars Hs Cell Death Control siRNA	Qiagen
Silencer Negative control 1 (scr1)	Thermo Scientific
Silencer Negative control 2 (scr2)	Thermo Scientific
Sub-library of the siGENOME library for the primary screen	Dharmacon, GE healthcare
Customized siRNA library for the secondary screen	Dharmacon, GE healthcare

3.6 Buffers

Buffer	Ingredients	Volume
Phosphate saline buffer (PBS)	PBS 10x (Sigma-Aldrich) ddH2O	100 mL 900 mL
Tris Buffer Saline (TBS)	TBS 10x (Sigma-Aldrich) ddH2O	100 mL 900 mL
Immunoblot washing solution (TBS-T)	TBS (10x) ddH2O Tween-20	100 mL 900 mL 0.5 mL
Immunoblot blocking solution for phosphorylated proteins	Immunoblot washing solution BSA	50 mL 5 g
Immunoblot transfer buffer (10x)	Tris base Glycine ddH2O	30.3 g 144 g 1 L
SDS-PAGE running buffer	MES SDS running buffer (20x) ddH2O	50 mL 950 mL

Tris-acetate-EDTA (TAE) buffer (50x)	Tris Glacial acetic acid 0.5 M EDTA ddH2O pH	242 g (2 M) 57.1 mL 100 mL 1 L 8.5
BL Buffer	ddH2O HEPES (50 mM) EDTA (0,5 mM) Phenylacetic acid (0,33 mM) Oxalic acid (0,07 mM) pH	84,8 mL 5 mL 0,1 mL 0,033 mL 0.07 mL 7,6
B2 Buffer	ddH2O DDT (415 mM) ATP (33 mM) AMP (0,996)	85 mL 6,4 g 1,82 g 0,035 g
Lysis buffer for the luciferase-based cytotoxicity assay	BL buffer 10% Triton-X-100	48,5 mL 1,5 mL
Luciferase assay buffer	BL buffer B2 buffer D-Luciferase (10mg/mL) 1M $MgSO_4$	44,35 mL 5 mL 0,65 mL 751 µL
FACS buffer	FCS PBS	2 % 500 mL

3.7 Cell media and supplements

Material	**Company**
Ab serum (heat-inactivated), human	Valley Biomedical
AIM-V with L-glutamine, streptomycin sulfate, gentamycin sulfate	Gibco
PROLEUKIN (rHuIL2)	Novartis Pharma
Beta-mercaptoethanol	Gibco
DMEM; high glucose (4.5 g/l), L-glutamine, sodium pyruvate, $NaHCO_3$	Sigma-Aldrich
Dulbecco-PBS without Ca^{2+}, $MgCl_2$ (1x)	Sigma-Aldrich
Fetal calf serum (FCS) (heat-inactivated)	Biochrom
Ham's F12 Nutrient Mixture	Gibco
HEPES buffer (1 M)	PAA
Human rIL-2	Novartis
Penicillin/Streptomycin (P/S; 100X)	PAA
RPMI 1640 with L-glutamine	Gibco

RPMI 1640 with L-glutamine and NaHCO3	Sigma-Aldrich
Opti-MEM	Thermo Scientific

Medium	**Component**	**Amount**
Freezing Medium for Tumor Cells	FCS	90 %
	DMSO	10 %
MIL freezing medium Solution A	FCS	60 %
	RPMI	40 %
MIL freezing medium Solution B	FCS	80 %
	DMSO	20 %
Complete Lymphocyte Medium (CLM)	RPMI	500 mL
	AB serum	50 mL
	P/S	5 mL
	HEPES	5 mL
	Beta-mercaptoethanol	50 µL
MIL expansion medium with feeder cells	CLM	50 %
	AIM-V	50 %
	Feeder cells	100x TILs
	OKT3	30 ng/mL
	rHuIL-2	3,000 U/mL
MIL expansion medium without feeder cells	CLM	50 %
	AIM-V	50 %
	rHuIL-2	3,000 U/mL
Complete RPMI	RPMI	500 mL
	FCS	50 mL
	P/S	5 mL
Complete RPMI with G418	RPMI	500 mL
	FCS	50 mL
	P/S	5 mL
	G418	1,5 mL
Complete Melanoma Medium (CMM)	DMEM	300 mL
	RPMI	100 mL
	Ham's F12 Nutrient Mixture	100 mL
	FCS	50 mL
	P/S	5 mL
	HEPES	5 mL
Complete DMEM	DMEM	500 mL
	FCS	50 mL
	P/S	5 mL

3.8 Cell lines

Cell Line	Origin	Culture Medium
KMM-1	Multiple myeloma	Complete RPMI
KMM-1-luc	Multiple myeloma	Complete RPMI with G418
U266	Multiple myeloma	Complete RPMI
RPMI8226	Multiple myeloma	Complete RPMI
HEK293T	Human embryonic kidney	Complete DMEM
M579	Melanoma patient-derived primary cell culture	Complete melanoma medium
MCF7	Breast adenocacinoma	Complete DMEM
PANC-1	Pancreatic ductal adenocarcinoma	Complete DMEM
SW480	Colorectal cancer	Complete DMEM
Mel27c	Uveal melanoma	Complete DMEM
Survivin antigen-specific T cells	Peripheral blood of breast cancer patient	RPMI, 10% Human AB serum, 1% P/S
MILs	Multiple myeloma patient-derived	Complete lymphocyte medium

3.9 Antibodies and recombinant proteins

3.9.1 Western blot

Specificity	Species	Isotype	Conjugate	Company	Application
Anti-CAMK1D	rabbit	IgG		Abcam	WB; 1:20000
Anti-PTK2B	rabbit	IgG		Abcam	WB; 1:20000
Anti-Caspase-3	rabbit	IgG		Abcam	WB; 1:750
Anti-Caspase-6	rabbit	IgG		Abcam	WB; 1:2000
Anti-Caspase-7	rabbit	IgG		Cell Signaling	WB; 1:1000
Anti-Caspase-7	mouse	IgG1		Thermo Scientific	WB; 1:1000
Anti-Caspase-3 (phospho S150)	rabbit	IgG		Abcam	WB; 1:850
Anti-Caspase-6 (phospho S257)	rabbit	IgG		Abcam	WB; 1:250
Anti-Sodium Potassium ATPase	rabbit	IgG		Abcam	WB; 1:20000

Anti-PD-L1	mouse	IgG1		R&D systems	WB; 1:500
Anti-β-actin	mouse	IgG1		Abcam	WB; 1:5000
Secondary anti-mouse	goat	IgG	HRP	Santa Cruz	WB; 1:4000
Secondary anti-rabbit	goat	IgG	HRP	Santa Cruz	WB; 1:4000
Anti-Caspase-3	rabbit	IgG		Cell Signaling	IP; 1:50
Anti-Caspase-6	rabbit	IgG		Abcam	IP; 1:50
Anti-Caspase-7	rabbit	IgG		Abcam	IP; 1:100

3.9.2 FACS antibodies

Specificity	**Species**	**Isotype**	**Conjugate**	**Company**	**Dilution**
Anti-HLA-A2	mouse	IgG2b	APC	BioLegend	1:20
Isotype	mouse	IgG2b	APC	BioLegend	1:20
Anti-CD3	mouse	IgG1	Pacific Blue	BD	1:50
Anti-CD4	mouse	IgG1	APC-Cy7	BD	1:50
Anti-CD8	mouse	IgG2a	PerCP-Cy5.5	BD	1:50
anti-PD1	mouse	IgG1	PE/Cy7	BioLegend	1:20
Isotype	mouse	IgG1	PE/Cy7	BioLegend	1:20
Anti-CCR9	mouse	IgG2a	Alexa Fluor 647	BD	1:20
Isotype	mouse	IgG2a	Alexa Fluor 647	BD	1:20
Anti-LAG3	Goat	IgG2	FITC	R&D system	1:20
Isotype	Goat	IgG2	FITC	R&D system	1:20
Anti-CTLA4	mouse	IgG1	APC	BioLegend	1:20
Isotype	mouse	IgG1	APC	BioLegend	1:20
Anti-CD95	mouse	IgG1	APC	BioLegend	1:20
Isotype	mouse	IgG1	APC	BioLegend	1:20
Anti-CD95	mouse	IgG1	PE	BD	1:20
Isotype	mouse	IgG1	PE	BD	1:20
Anti-CD45RA	mouse	IgG2b	FITC	BD	1:20

Anti-CD62L	mouse	IgG1	APC	BioLegend	1:20
Anti CD178	mouse	IgG1	APC	BD	1:20
Isotype	mouse	IgG1	APC	BD	1:20

3.9.3 Functional assays

Specificity	**Species**	**Isotype**	**Cat. N.**	**Company**	**Application**
Anti-MHC-I Cone W6/32	mouse	IgG2a	-	Prof. Moldenhauer (DKFZ – Heidelberg)	Functional test
Isotype	Mouse	IgG2a	-	Prof. Moldenhauer (DKFZ – Heidelberg)	Functional test
Anti-FasL	mouse	IgG1κ	306409	Biolegend	Functional test
Isotype	mouse	IgG1κ	400153	Biolegend	Functional test
rHuFasL	-	-	589404	Biolegend	Functional test
rHuTNFα	-	-	-	Prof. Männel (UKR - Regensburg)	Functional test
rHuTRAIL	-	-	PHC1634	Thermo Scientific	Functional test
W-7	-	-	0369	Tocris	Functional test
STO609	-	-	1551	Tocris	Functional test

3.10 Software

Software	**Developer**
Endnote (X7)	Adept Scienctific
Graph Pad Prism (6)	GraphPad Software
Microsoft Office 2013	Microsoft, USA
ImageJ	Wayane Rasband
Adobe Illustrator	Adobe system
FlowJo	Tree Star
cellHTS2	Boutros et al [169]

4 Methods

4.1 Cell culture methods

4.1.1 Tumor cell lines

KMM-1, U266 and RPMI8226 (multiple myeloma cell lines) are semi-adherent cell lines and were kindly provided by Prof. Witzens-Harig (University Hospital Heidelberg). PANC-1 (pancreatic ductal adenocarcinoma), MCF7 (breast carcinoma), SW480, (colorectal cancer) cell lines were acquired from the American Type Cell Culture (ATCC). The uveal melanoma cell line Mel27c was kindly provided by Prof. Berneburg (UKR, Regensburg). KMM-1-luc cells were generated after transfection with a plasmid encoding for the GFP-luciferase fusion protein (pEGFP-Luc plasmid) and for the G418-resistance gene. The plasmid was kindly provided by Dr. Haase (LMU Munich). Lipofectamine LTX was used as transfection reagent according to the manufacturer´s instructions (section 4.2.10). Transfected cells were selected for 14 days with G418-containing medium (0,6 mg/mL). The optimal concentration of G418 was established by titration of the toxic dosage of G418 in KMM-1 cells. The lowest concentration inducing completely tumor cell death was selected. Afterwards, KMM-1-luc cells were sorted twice for the expression of GFP by flow cytometry and cultured in the presence of 0,6 mg/mL G418. Cell sorting was conducted in collaboration with the DKFZ sorting core facility, using the FACSARIA II cell sorter (BD). M579 were kindly provided by Prof. Michal Lotem (Hadassah Hebrew University Medical Center, Israel). These cells carried the expression of the HLA-A2 and the luciferase gene. All cell lines were cultured with the described culture media and maintained at 37°C, 5% CO_2, except for M579 cells, which were maintained at 8% CO_2.

4.2 Molecular biology techniques

4.2.1 Reverse Transcription

Total RNA was isolated from the cell pellets using the RNeasy Mini kit (Qiagen) according to the manufacturer's guidelines. RNA quality and concentration was analyzed using the Scan Drop (AnalytikJena). 1 µg of RNA from each sample was reverse transcribed to complementary DNA (cDNA) using the QuantiTect reverse transcription kit (Qiagen) according to the manufacturer's protocol (including gDNA digestion). Briefly, 1 µg (= x µL) of RNA was incubated with 12-x µL H_2O and 2 µL gDNAse for 3 min. Subsequently, the master mix consisting of 4 µL buffer, 1 µL primer and 1 µL reverse transcriptase (RT) was added. To investigate genomic DNA contamination, water was added instead of reverse transcriptase (-RT controls). The mix was incubated for 20 min at 42°C and finally incubated for 3 min at 95°C for enzyme inactivation. cDNA was stored at -20°C.

4.2.2 End-point PCR

Gene expression was measured using end-point PCR. Synthesized cDNA was amplified using conventional PCR. PCR samples were set up in a 25 µL volume using 2x MyTaq HS Red Mix (Bioline), 500 nM of gene-specific primer mix (list of primers in section 3.4) and 100 ng of template cDNA. Water was added to the reaction mix instead of cDNA for contamination controls. The PCR program was set as the following: 95°C for 3 min, 35 cycles of 3 repetitive steps of denaturation (95°C for 30 s), annealing (60°C for 30 s) and extension (72°C for 30 s), and a final step at 72°C for 5 min. PCR products were run on a 2% agarose gel in TAE buffer using a gel electrophoresis system (Thermo Scientific) and DNA bands were visualized using UV light of myECL Imager (Thermo Scientific).

4.2.3 Quantitative PCR (qPCR)

Knockdown efficiency of siRNA sequences was measured by quantitative PCR. For qPCR, 10 ng of template cDNA, 2x QuantiFast SYBR Green PCR mix (Qiagen) and 300 nM of gene-specific primer mix was used per 20 µL reaction and each sample was prepared in

triplicates. Reactions were run using the QuantStudio 3 (Applied Biosystems). Expression of several genes was normalized to the expression of β-actin gene and the analysis was performed using comparative Ct method. For gene-specific primer list see section 3.4.

4.2.4 Reverse siRNA transfection

Gene knockdown in tumor cells was induced using reverse siRNA transfection. Several transfection reagents (RNAiMAX, Dharmafect 1 and Dharmafect 2) were tested for their transfection efficacy in KMM-1 cells. Lipofectamine RNAiMAX (Thermo Scientific) showed the best results and was used for all subsequent experiments. Briefly, 200 µL of 250 nM siRNA solution was added to each well of a 6-well plate. 4 µl of RNAiMAX transfection reagent was diluted in 196 µL of RPMI (Sigma-Aldrich) and incubated for 10 min at room temperature (RT). 400 µL of additional RPMI was added and 600 µL of RNAiMAX mix was given to the siRNA coated wells and incubated for 30 min at RT. 3,5 x 10^5 KMM-1 (WT or luc) 2 x 10^5 PANC-1 and 3,5 x 10^5 M579 cells were resuspended in 1,2 mL of antibiotic-free RPMI (for KMM-1) or DMEM (for PANC-1 and M579) culture medium supplemented with 10% FCS, seeded in the siRNA-RNAiMAX containing wells and incubated for 48 h at 37°C, 5% CO_2. For reverse transfection in a 96-well plate, 10 µL of siRNAs (250 nM) were mixed with 9,9 µL RPMI for 10 min. Subsequently, 20 µL of RPMI were added and the diluted transfection regent was given to each siRNA-containing well and incubated for 30 min. Afterwards, 1 x 10^4 KMM-1 (WT or luc) or M579, 2 x 10^3 PANC-1, MCF7 or SW480 and 8 x 10^3 Mel27c cells were resuspended in 30 µL of antibiotic-free RPMI or DMEM culture medium supplemented with 10% FCS and incubated for 48 h at 37°C, 5% CO_2.

For reverse transfection in 384-well plate, 5 µL of siRNAs (250 nM) were mixed with 4,95 µL of RPMI for 10 min. Afterwards 15 µL of RPMI were added and the diluted transfection regent was given to each siRNA-containing well and incubated for 30 min. Next, 5 x 10^3 KMM-1 (WT or luc) cells were resuspended in 30 µL of antibiotic-free RPMI culture medium supplemented with 10% FCS and incubated for 48 h at 37°C, 5% CO_2.

Final siRNA concentration was 25 nM in all cases. The utilized siRNA sequences are listed in section 3.5.

4.2.5 Phospho-Protein Isolation

To isolate phosphorylated proteins from cells, tumor cells were pelleted at 0,5 x g for 5 min and washed once with PBS at 4°C. The cell pellets were lysed with one pellet volume of Phosphoplex Lysis Buffer (Merck Millipore) containing protease inhibitor cocktail (Cabliochem, 1:100) and phosphatase inhibitor cocktail (Sigma-Aldrich, 1:100) at 4 °C for 15 min on a rotator. Samples were centrifuged at 17,000 g at 4 °C for 15 min. Supernatants containing the protein lysates were collected into fresh tubes and quantified using the BCA kit according to the manufacturer's protocol. Proteins were stored at -20 °C.

4.2.6 BCA Protein Assay

Proteins concentration was measured with the help of a standard curve. Samples were diluted 1:5 in water. The BCA working reagent (Solution A and Solution B, 50:1) (Thermo Scientific) was added to the samples and incubated at 37 °C for 30 min. The absorbance was measured with a TECAN-Reader at the wavelengths of 562 nm and 620 nm.

4.2.7 SDS-PAGE

30 µg of protein lysates were denaturated in 4x NuPAGE LDS Sample Buffer (Thermo Scientific) containing 10 % ß-mercaptoethanol (PAN) at 70 °C for 10 min. Samples were spun down and separated on the NuPAGE 4-12% Bis-Tris Gels (Thermo Scientific) along with PageRuler Prestained Protein Ladder (Thermo Scientific) and run at 115-150 V for 1 h 30 min.

4.2.8 Semi-Dry Western Blot

To transfer the proteins from the gel to a PVDF membrane (Millipore) a semi-dry western blot method was used. The gel and whatman papers were equilibrated in 1-Step Transfer Buffer (Thermo Science). The PVDF blotting membrane (Merck Millipore) was activated in 100 % methanol (Merck Millipore) for 1 min and afterwards placed in Transfer Buffer until use. Blots were assembled from anode to cathode as follows: 4 whatman papers –

membrane – gel – 4 whatman papers. Blots were run at 24 V for 10 min. To see if proteins were transferred from the gel to the membrane, gels were stained with Coomassie Brilliant Blue (Thermo Scientific) for 1 h and kept in Coomassie Destaining Solution overnight. Membranes were washed in 1x TBS and then placed in blocking solution (5 % BSA/0.05 % TBST) for 2 h to prevent unspecific binding of the antibody. Membranes were washed twice with TBST for 5 min. Primary antibodies (anti-CAMK1D (Abcam) 1:20000, anti-PTK2B (Abcam) 1:2000, Anti-Caspase-3 (Abcam) 1:750, Anti-Caspase-6 (Abcam) 1:2000, Anti-Caspase-7 (Thermo Scientific) 1:1000, Anti-Caspase-3 (phospho S150) (Abcam) 1:850, Anti-Caspase-6 (phospho S257) (Abcam) 1:250 and Sodium Potassium ATPase (Abcam) 1:20000) were diluted in 5 % BSA/0.05 % TBST and kept on the membrane overnight at 4°C on a rotator. Membranes were then washed three times for 10 min with 1 % BSA/0.05 % TBST. Afterwards, HRP- conjugated secondary antibodies (anti-rabbit 1:4000, Santa Cruz or anti-mouse 1:4000, Santa Cruz) were added to 1 % BSA/TBST and kept on the membrane at room temperature for 1h on a shaker. Thereafter, the membranes were washed for 10 min with 1 % BSA/TBST, then TBST and lastly with TBS. The blots were incubated with the ECL Detection Reagent (Reagent A and Reagent B, 1:1, GE Healthcare) for 4 min and the chemiluminescence was detected with myECL Imager (Thermo Scientific).

4.2.9 Co-immunoprecipitation assay

For detection of direct protein-protein interaction, co-immunoprecipitation was performed. Briefly, 10 M tumor cells were seeded in 10 cm^2 petri dishes. The next day, cells were stimulated for 4 h with 100 ng/ml rHuFasL. Unstimulated cells were used as negative control. Afterwards, tumor cells were detached, resuspended in ice cold TBS and centrifuged at 400 g for 6 min at 4°C. Supernatant was discarded, cell pellet was resuspended in 1,5 ml TBS and centrifuged at 500 g for 8 min at 4°C. Cell pellet was lysed with 1,5 ml lysis buffer (50 mM Tris-HCl, 150 mM NaCl, 0,5% NP40 or Triton-X) containing protease inhibitor (Roche complete 25x) and kept on a rotator for 1 h at 4°C. Afterwards, cells were centrifuged for 20 min at 20000 g at 4°C. Supernatant was collected and centrifuged for further 5 min at 20000 g at 4°C. Meanwhile, protein-G agarose was washed with 1 ml TBS and centrifuged for 1 min at 12000 g. 1ml of cell supernatant containing cytoplasmatic proteins was added to 60 µl protein-G agarose, incubated with anti-caspase-3 (1:50), anti-caspase-6 (1:50) or anti-caspase-7 (1:100) antibodies and incubated overnight on a rotator at 4°C. 90 µl of cell lysates

were frozen at -20°C. The next day, the immunoprecipitated samples were centrifuged at 12000 g at 4°C for 1 min. Supernatant was discarded and protein-G agarose was washed three times with lyses buffer and centrifuged at 12000 g at 4°C for 1 min. 2x LDS containing 10% β-mercaptoethanol was added to the immunoprecipitated samples, while 4x LDS containing 10% β-mercaptoethanol was added to the lysates. Samples were denaturated for 10 min at 95°C on a thermocycler. Samples were spun down and separated on NuPAGE 4-12% Bis-Tris Gels (Thermo Scientific) along with PageRuler Prestained Protein Ladder (Thermo Scientific) and run at 115-150 V for 1h30. After electrophoresis proteins were transferred on a PVDF membrane (Millipore) as explained in section 4.2.8. Anti-CAMK1D antibody (1:10000) was diluted in 5 % BSA/0.05 % TBST and kept on the membrane overnight at 4°C on a rotator. Membranes were then washed three times for 10 min with 1 % BSA/0.05 % TBST. Afterwards, HRP- conjugated secondary antibodies (anti-rabbit 1:3000) was added to 1 % BSA/TBST and kept on the membrane at room temperature for 1h on a shaker. The membrane was washed as explained in section 4.2.8. The blot was incubated with the ECL Detection Reagent (Reagent A and Reagent B, 1:1, GE Healthcare) for 4 min and the chemiluminescence was detected with myECL Imager (Thermo Scientific).

4.2.10 Plasmid transfection

For transient transfection of the pEGFP-Luc plasmid into KMM-1 and U266 multiple myeloma cell lines, different transfection reagents (Lipofectamine LTX with PLUS Reagent and JetPei) were tested for optimal plasmid expression. Lipofectamine LTX (Thermo Scientific) showed the best result and was used for subsequent experiments. Tumor cells (3,5 x 10^5 KMM-1 and U266 cells) were seeded in a 6 well plate and incubated at 37°C overnight. The following day 7,5 µL or 15 µL Lipofectamine LTX reagent were diluted in 150 µl Opti-MEM medium (Gibco). Simultaneously, 3.5 µg of DNA was diluted in 175 µL Opti-MEM medium and 3.5 µL of PLUS Reagent was added. 150 µl of diluted DNA was added to 150 µL diluted Lipofectamine LTX (Life Technologies) reagent and incubated for 5 min at RT. DNA-lipid complex was then added to the growth medium of the myeloma cells. Cells were incubated at 37°C for 48 hours before investigation of transfection efficacy by flow cytometry.

4.3 Immunological techniques

4.3.1 Isolation of PBMCs

PBMCs were isolated from buffy coats of healthy donors via density gradient centrifugation. Briefly, buffy coats were diluted 1:1 in PBS and added to 50 mL conical centrifuge tubes, containing 15 mL of Biocoll solution (Biochrom). Density gradient centrifugation was performed at 2000 rpm for 20 min at room temperature using low brake. Afterwards PBMCs were collected, washed three times and resuspended at the desired concentration.

4.3.2 Isolation of marrow infiltrating lymphocytes (MILs)

Marrow infiltrating lymphocytes (MILs) were isolated using untouched Human T cells Dynabeads (Thermo Fisher Scientific) according to the manufacturer's protocol. Briefly, an antibody mix towards non-T cells was added to the samples and allowed to bind to the cells. Dynabeads were added and allowed binding to the antibody-labeled cells during an incubation time of 20 min on ice. The bead-bound cells were separated on a magnet and discarded. The remaining negative isolated fraction represented untouched human T-cells that were used for further expansion using the rapid expansion protocol (REP).

4.3.3 Rapid expansion protocol (REP) for MILs

MILs were isolated from the bone marrow of patients with multiple myeloma. MILs cultures were *ex vivo* expanded using the Rapid Expansion Protocol (REP). $2x10^6$ of freshly isolated MILs were diluted to $6\ x10^5$ cell/mL in CLM supplemented with 3000 U/mL rHuIL-2 (Novartis). Cells were incubated in 25 cm^2 tissue culture flask for 48h at 37°C and 5% CO_2. PBMCs form three different buffy coats (at a ratio of 1:1:1) were irradiated with 60 Gy (Gammacell 1000) and used as feeder cells to support MILs expansion. $2x10^6$ MILs were co-incubated with $2x10^8$ feeder cells (in a ratio 1:100) in 400 mL of MIL expansion medium (CLM/AIM-V) with 30 ng/mL OKT3 antibody and 3000 IU/mL IL-2 for 5 days without moving in a G-Rex 100 cell culture flask. Afterwards, 250 mL of supernatant was changed

with 150 mL of fresh media and IL-2 was replenished to keep the concentration at 3000 U/mL. On day 7, MILs were divided into three G-Rex100 flasks in a final volume of 250 mL medium each and media was again replenished on day 11. On day 14 of the expansion, MILs were counted and frozen in aliquots of $40x10^6$ cells/mL in freezing media A and B (1:1). Solution A consists of 60% RPMI and 40% FCS and solution B consists of 80% RPMI supplemented with 20% DMSO. Frozen MILs were kept in the liquid nitrogen tank.

4.3.4 Generation of flu-antigen specific $CD8^+$ T cells (FluT cells)

For the generation of Flu-specific $CD8^+$ T cells (FluT cells), PBMCs from HLA-A2 healthy donors were isolated. Total $CD8^+$ T cells were sorted from PBMCs by magnetic separation (day 0), and expanded in the presence of A2-matched Flu peptide (GILGFVFTL) for 14 days. Irradiated autologous $CD8^-$ fraction was used as feeder cells during the first 7 days of expansion. Afterwards, irradiated T2 cells were used as fresh feeder cells. On day 1 and day 8, 100 U/mL IL2 and 5 ng/µL IL15 were added to the expansion. The percentage of Flu-antigen specific T cells was determined by pentamer staining on day 7 and 14 via flow cytometry analysis.

4.3.5 Generation of supernatants of activated MILs

For the generation of the supernatant of polyclonally activated MILs, 1 x 10^6 MILs were suspended in 1 mL of CLM collected in a 15 mL tube and stimulated with 25 µL of Dynabeads Human T-Activator CD3/CD28 (Thermo Scientific).
Afterwards, only the supernatant (100 uL/well) of activated T cells was added to knocked down tumor cells and incubated overnight at 37°C, 5% CO_2. Subsequently, luciferase-based cytotoxicity assay was performed.
Alternatively, MILs were stimulated with tumor cells at an E:T ratio of 10:1. After 20 h co-culture, plates were centrifuged at 450 x g for 5 minutes and 100 µL/well of the supernatant was collected for cytokines detection (ELISA).

4.3.6 Luciferase-based cytotoxicity assay

KMM-1-luc cells were reverse transfected with the desired siRNA sequences in white 96-well-plate (Perkin Elmer) and incubated for 48 h at 37°C, 5% CO_2. At the same day of transfection MILs were thawed and treated with benzonase (Merck; 100 U/mL) to prevent clumping. Cell density was adjusted to 0,6 x 10^6 cells/mL in CLM supplemented with 3000 U/mL rhuIL-2 (Novartis) for 48 h. IL-2 was depleted 24 h before the co-culture. FluT-cells were thawed on the same day of co-culture (6 h before co-culture). For the cytotoxicity setting, MILs, FluT cells, the supernatant of activated MILs or rHuFasL were added to transfected tumor cells at desired E:T ratio/concentration, and incubated for 20 h at 37°C, 5% CO_2. For the viability setting, only CLM was added to the tumor cells.
After co-culture, supernatant was removed, remaining tumor cells were lysed using 40 µL/well of cell lysis buffer for 10 min. After tumor cell lysis, 60 µL/well of luciferase assay buffer was added and luciferase intensity was measured by using the Infinite M200 plate reader (Tecan) with a counting time of 100 msec. Luciferase activities (relative luminescence units = RLUs) were either represented as raw luciferase values or as normalized data to scramble or unstimulated controls.

4.3.7 Real-time live-cell imaging assay

Target genes in KMM-1 or U266 tumor cells were knocked down with reverse siRNA transfection for 48 h as described in section 4.2.4. The reverse siRNA transfection was performed using transparent 96 well microplates (TPP). In parallel, MILs were thawed and prepared as described in section 4.3.3. After 48 h MILs (E:T 10:1) or rHuFasL (100 ng/mL) were added to the target cells in CLM with YOYO-1 (final concentration 1:5000) and co-cultured at 37 °C. For viability controls the according amount of CLM with YOYO-1 (final concentration 1:5000) was added. MILs or rHuFasL-mediated tumor lysis was imaged on the green channel using an IncuCyte ZOOM live cell imager (ESSEN BioScience) for the indicated time points at a 10x magnification. Data were analyzed with the Incucyte ZOOM 2016A software by creating a top-hat filter-based mask for the calculation of the area of YOYO-1 incorporating cells (indicating dead cells).

4.3.8 ELISA

Tumor cells were transfected with the indicated siRNAs in a 96-well plate. Afterwards, T cells were added at the indicated E:T ratio for 20 h and 100 µL of supernatants were harvested for the detection of IFN-γ (Human IFN-γ ELISA Set; BD OptEIA™), IL-2 (Human IL-2 ELISA Set; BD OptEIA™), Granzyme B (Human Granzyme B ELISA development kit; Mabtech) and TNF (Human TNF ELISA Set; BD OptEIA™). Experiments were performed according to the manufacturer´s instructions. Polyclonal anti-CD3/anti-CD28 magnetic beads stimulation was used as positive control. Absorbance was measured at λ = 450 nm, taking λ = 570 nm as reference wavelength using the Spark microplate reader (TECAN).

4.3.9 Flow cytometry (FACS)

Flow cytometry was used for the detection of proteins expressed on the plasma membrane of tumor and T cells. Intracellular staining was performed for the detection of caspase-3 according to manufacturer's instruction. Adherent and semiadherent cells were detached form plates using PBS-EDTA and centrifuged at 500 x g for 5 min. Cells were resuspended in FACS buffer and distributed in FACS tubes (5 x 10^5 cells/tube). To reduce unspecific antibody binding FC receptors were blocked with 166 µg Kiovig (Baxter) in 100 µL FACS buffer for 20 min on ice combined with Live/Dead fixable dead cell staining kit (Thermo Scientific) (1:1000 in 100 µL FACS buffer) for 15 min in the dark on ice. Next, samples were washed two times in FACS buffer and incubated with either fluorophore-conjugated primary antibodies or isotype control at the concentrations indicated in section 3.9.2 for 20 min on ice in the dark. Afterwards, cells were washed twice and acquired with the FACS Canto II cell analyzer machine (BD Bioscience) or FACSLyrics Flow cytometer and data was analyzed using FlowJo (Tree Star).

4.3.10 Functional neutralization

For the functional blockade of MHC-I molecules, KMM-1-luc cells seeded in 96-well plates at a density of 1 x 10^4 cells/well. 50 µL of the MHC-I antibody (at a concentration of

60, 20 and 6,67 µg/mL) or isotype control (both generated by Prof. Gerd Moldenhauer – DKFZ – Heidelberg), were added to the tumor-containing wells for 30 min at 37°C, 5% CO_2. Afterwards, 50 µL of MILs (E:T = 10:1) were added and incubated for 20 h at 37°C, 5% CO_2. T cell-mediated cytotoxicity was measured via luciferase-based cytotoxicity assay as explained in section 4.3.6.

For the functional neutralization experiment in section 5.4.5, anti-FasL or isotype control (section 3.9.3) were pre-incubated with MILs for 1h at 37°C, 5% CO_2. As negative control, antibodies were cultivated in the absence of T cells. Afterwards, antibody-containing supernatants were used to stimulate KMM-1-luc cells, which were reverse transfected with the indicated siRNAs. The final concentration of the neutralizing antibodies was 100 ng/mL for anti-FasL and isotype control. As positive control recombinant FasL protein (100 ng/ml, BioLegend) was added to the tumor cells instead of T cells. 20 h after co-culture luciferase intensity was measured.

4.3.11 Blocking assays

For the experiments using the anti-Calmodulin (W7) (Tocris) and CAMKK (STO609) (Tocris) inhibitors, 1 x 10^4 KMM-1-luc (scr or CAMK1D-transfected) cells were seeded in white 96-well plates (Perkin Elmer) in 100 µL of RPMI 10 % FCS. Small molecule inhibitors were added at the indicated concentrations for 1 h at 37 °C, before 100 ng/ml rHuFasL or medium control was added. DMSO treatment served as negative control. After 20 h stimulation, luciferase-based cytotoxicity assay was performed.

4.3.12 Luminex assays

KMM-1 cells were reverse transfected with scr and siCAMK1D siRNA sequences in 6-well plates as described in section 4.2.4. Tumor cells were stimulated with rHuFasL (100 ng/mL) for 15min, 30min, 1h, 2h, 4h and 8h. Unstimulated cells served as control. For the detection of intracellular phosphorylated analytes a general pathway (MILLIPLEX MAP Multi-Pathway Magnetic Bead 9-Plex kit, Millipore) was used. While, for the detection of proteins involved in the activation of apoptosis the MILLIPLEX MAP Early Phase Apoptosis 7-plex-kit (Millipore) together with Active Caspase-3 Magnetic Bead MAPmate (Millipore)

was used. Beads specific for GAPDH served as normalization control. Briefly, tumor cells were lysed using the lysis buffer provided in the kit and protein concentration was quantified using the BCA Protein Assay Kit (Thermo Scientific) according to manufacturer's instructions (section 4.2.6). Afterwards 20 µg of protein lysates were diluted in 25 µL assay diluent (provided in the kit) and incubated with 25 µL of beads detecting different analytes present in the MILLIPLEX MAP Multi-Pathway Magnetic Bead 9-Plex kit (ERK/MAP kinase 1/2 (Thr185/Tyr187), Akt (Ser473), STAT3 (Ser727), JNK (Thr183/Tyr185), p70 S6 kinase (Thr412), NF-kB (Ser536), STAT5A/B (Tyr694/699), CREB (Ser133), and p38 (Thr180/Tyr182)) and in the MILLIPLEX MAP Early Phase Apoptosis 7-plex-kit (phosphorylated Akt (Ser473), JNK (Thr183/Tyr185), Bad (Ser112), Bcl-2 (Ser70), p53 (Ser46), cleaved Caspase-8 (Asp384), cleaved Caspase-9 (Asp315) and active Caspase-3 (Asp175)). The assay was performed according to the manufacturer´s instructions and samples were measured using the MAGPIX Luminex instrument (Merck Millipore).

4.4 High-throughput RNAi screening

4.4.1 Primary RNAi screening

The primary RNAi screening was conducted using a sub-library of the genome-wide siRNA library siGENOME (Dhamacon, GE healthcare), which comprised 2887 genes (1288 genes for GPCR/kinase and 1599 genes for custom library). The library was prepared in Prof. Boutros´s group (DKFZ, Heidelberg) as described in [170]. The following 384-well plates of the genome-wide library were included: 1, 2, 3, 13, 14, 15, 17, 65, 67, 68. Each well contained a pool of four non-overlapping siRNAs (SMARTpool) targeting the same gene. This arrayed screening approach was performed in duplicates and was adopted from Khandelwal et al [164]. Samples siRNA sequences were distributed in the 384-well plates and positive and negative siRNA controls were added in empty wells. Final concentration of all siRNA sequences was 25 nM. Reverse transfection was performed as explained in section 4.2.4. The read-out was performed using Mithras LB 940 microplate Reader with a counting time of 100 msec. The screening procedure was run in parallel with a CellTiter-Glo luminescent cell viability (CTG) assay on luciferase-negative KMM-1 cells without the

addition of MILs in order to exclude genes affecting cell viability in general. Briefly, for the read-out, supernatant was removed in each well containing siRNA-transfected tumor cells and 20 µL of the CTG reagent (pre-diluted 1:4 in RPMI) were added. After 15 min incubation in the dark, plates were measured using the Mithras reader as described above.
For the screening analysis the raw RLUs from the primary screening, were processed using the cellHTS2 package in R/Bioconductor [169]. Values from both conditions were quantile normalized against each other using the aroma.ligh package in R. Differential scores (cytotoxicity vs. viability) were calculated using the LOESS local regression method. To identify candidate hits, the following thresholds were applied on the z-scores of the samples: for the viability setting, genes showing a $z > 2,0$ or $z < 2,0$ were excluded. For the cytotoxicity setting, CCR9 was used as threshold score. Additionally genes having a z-score $> 0,5$ or $< 0,5$ in the CTG-based viability screening were filtered out from the candidate list. Data analysis was performed by Dr. Tillmann Michels (DKFZ, Heidelberg; RCI, Regensburg).

4.4.2 Secondary screening

For the secondary screening, a customized library containing the 128 genes from the primary screening was distributed in several 96-well plates along with positive and negative siRNA controls. Reverse transfection was performed as described in section 4.2.4. For the cytotoxicity setting MILs (10:1 ratio) were added to knocked down tumor cells (1×10^4 cells/well). Instead, CLM medium was added to the viability plates. After 20h, luciferase based read-out was performed as described in section 4.3.6. Cytotoxicity/viability ratios were calculated according to the formula

C*ytotoxicity/viability ratio* = (*Norm. RLU cytotoxicity setting / Norm. RLU viability setting).*

by using scr2 as negative control. The hit-list was generated by including only hits with improved T cell mediated cytotoxicity over scr2 transfection, (Cytotoxicity/viability ratio < 1). Pearson´s correlation was calculated with Microsoft Excel.

4.5 Statistical evaluation

For statistical analysis, GraphPad Prism 6 software was used. If not differently stated, statistical differences between the control and the test groups were determined by using two-tailed unpaired Student's t-test. In all statistical tests, a p-value ≤ 0.05 was considered significant with * = $p \leq 0.05$, ** = $p \leq 0.01$, *** = $p \leq 0.001$ and **** = $p \leq 0.0001$.

5 Results

5.1 Set-up of a HTP RNAi screening for the identification of novel immune-checkpoint molecules in multiple myeloma

In order to identify novel genes involved in escape mechanisms of cancer immunosurveillance, the human multiple myeloma cell line (KMM-1) was used as tumor model in this work. To discover potential immune-checkpoint molecules in MM, a high-throughput (HTP) screening approach was developed. This method was previously established in this laboratory by Dr. Khandelwal et al. [164], and subsequently adapted and improved in this work. Briefly, MM-tumor cells were stably transfected with firefly luciferase and reverse transfected for 48h with a siRNA library targeting 2887 genes encoding for protein kinases, G-protein coupled receptors and surface proteins. The workflow of the screening approach comprises a cytotoxicity setup and a viability control setup. In the cytotoxicity setting, T cells were added to the co-culture after the knockdown occurred in the tumor cells. After 20h, the supernatant containing T cells and dead tumor cells was removed, remaining tumor cells were lysed and luciferase activity was measured. Luciferase activity is proportional to the amount of living cells. The cytotoxicity setting allows identifying those genes whose knockdown increases the susceptibility towards T cell-mediated killing of tumor cells resulting in decreased luciferase activity. In order to exclude genes whose knockdown has an impact on cell viability *per se*, tumor cells were transfected with the siRNA library and subsequently cultivated in the absence of T cells (viability setup).

The ideal read-out would be represented by a loss of luciferase activity, when a potential immune-checkpoint molecule is knocked down compared to the negative control in the presence of T cells (cytotoxicity setup), while no difference in luciferase intensity in the viability setup is detected (Figure 1).

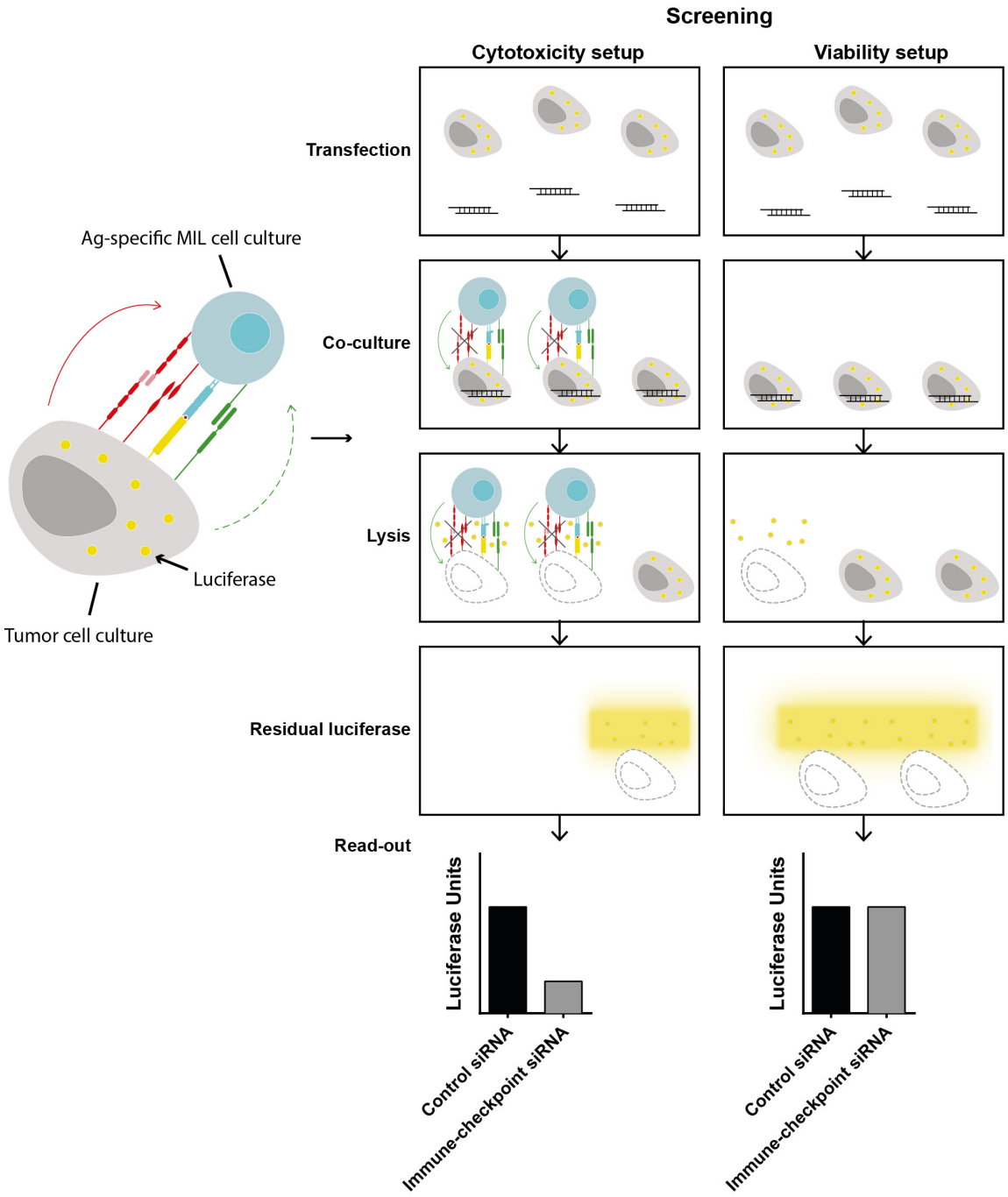

Figure 1. HTP-screening scheme for novel immune-checkpoints in MM. A siRNA library of 2887 genes is arrayed in a 384-well format. Each well contains a pool of four non-overlapping siRNA sequences targeting the same gene. Luciferase-expressing KMM-1 (KMM-1-luc) tumor cells are seeded in each well (reverse transfection). In the cytotoxicity setup, 48h after transfection, patient-derived HLA-matched MILs (marrow infiltrating lymphocytes) are added and co-cultured with transfected tumor cells for 20h. Supernatant is removed and luciferase activity of remaining tumor cells is measured after tumor cell lysis. To identify candidate immune-checkpoint molecules, cytotoxicity (tumor cell death) should increase (lowering luciferase activity) upon gene silencing (grey bar) compared to control siRNA (black bar). The HTP-assay also includes viability controls per gene knockdown to which no MILs are added to exclude genes with intrinsic impact on cell survival.

Before performing the HTP-screening, a series of adaptation and optimization procedures were essential, in order to ensure reliability and robustness of the methods. These procedures are described in further details in the next paragraphs.

5.1.1 Selection of HLA-A2$^+$ multiple myeloma cells for pEGFP-Luc transfection

As the HTP-screen is based on the co-culture of tumor cells and marrow infiltrating lymphocytes (MILs), HLA-A2$^+$ MM cell lines had to be identified to match with HLA-A2$^+$ MILs. To this end, two different multiple myeloma cell lines (KMM-1 and U266) were tested to be used in the luciferase-based screening. Flow cytometry (FACS) and end-point polymerase chain reaction (PCR) -analysis were performed to assess HLA-A2 expression. Both, U266 and KMM-1 cells resulted to be HLA-A2 positive as shown by FACS (Figure 2A) and by conventional PCR (Figure 2B). As the readout of the screening is based on luciferase activity, tumor cells need to express the luciferase reporter gene. Therefore, KMM-1 and U266 cell lines were transiently transfected with a pEGFP-Luc vector, encoding a fusion of enhanced green fluorescent protein (EGFP) and luciferase (Luc) from the firefly *Photinus Pyralis* transcribed from the same cytomegalovirus (CMV) promoter. This construct, allows transfected cells to be FACS-sorted by the GFP protein expression, thereby assuring luciferase expression of the sorted cells. Moreover, the vector backbone contains the neomycin-resistance gene that allows stably transfected cells to be selected using the selection antibiotic geneticin (G418). Even if the transfection efficacy was low (3,84%), as assessed by FACS analysis of GFP positive cells (Figure 2C), we generated stable clones by selecting KMM-1 and U266 cells with 0,6 mg/ml G418 antibiotic, previously titrated on both myeloma cell lines (Figure 2D). Upon 52 days of selection, GFP$^+$ cells were enriched to an appropriate number to perform FACS-sorting. After two rounds of cell-sorting, 90% of KMM-1 cells were GFP$^+$ and expressed considerable amount of the firefly-luciferase gene (Figure 2C). Differently, U266 GFP$^+$ cells did not further expand after sorting and consequently only KMM-1 cells were selected for subsequent optimization experiments.

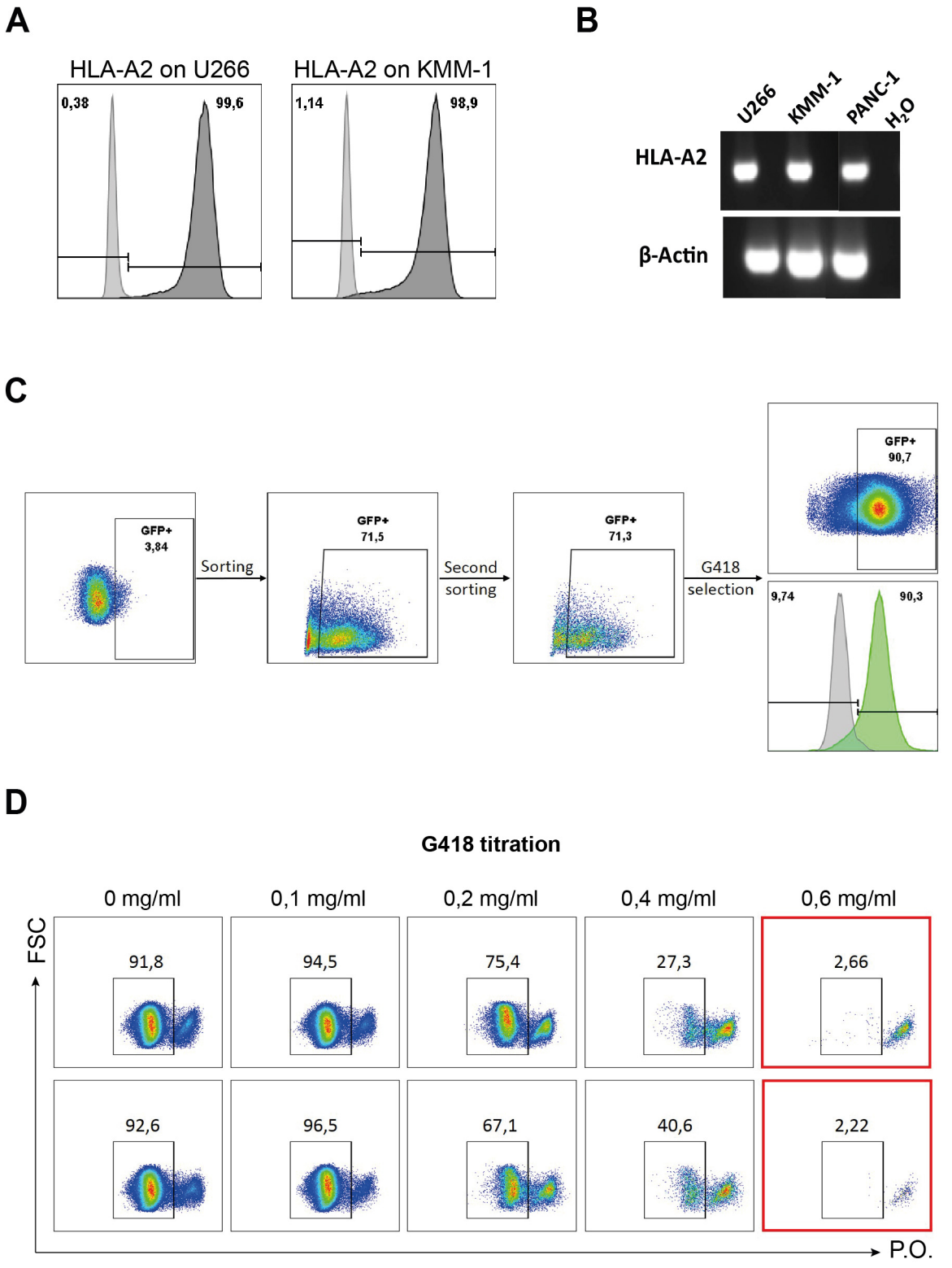

Figure 2. Selection of HLA-A2 luciferase positive multiple myeloma cell lines. (A) FACS-analysis of HLA-A2 on U266 and KMM-1 cells. Both myeloma cell lines were stained with an anti-HLA-A2 antibody and subsequently analyzed by FACS. Dark grey histogram: anti-HLA-A2 staining; Isotype control is shown as light grey histogram. **(B)** End-point polymerase chain reaction (PCR) assay for detection of HLA-A2 mRNA abundance in U266 and KMM-1 cells. PANC-1 tumor cells were used as positive control. Water served as no template control. **(C)** FACS analysis of GFP expression in KMM-1 tumor cells. Left panel: GFP expression after 14 days of tumor cells' selection with G418. Right

panel: GFP expression after two rounds of FACS-sorting. Histogram showing 90% of FACS-sorted cells carrying the pEGFP-Luc plasmid. Grey histogram: KMM-1 wild type (WT) cells; Green histogram: KMM-1-luc cells. **(D)** Titration of G418 on KMM-1 (upper panels) and U266 (lower panels) cell lines assessed by FACS. A live/dead stain kit was used to determine the viability of multiple myeloma cells. Cells were measured by flow-cytometry and gated on living cells. Pacific Orange (P.O.) was used to discriminate between live and dead cells. Gate defines living cells upon G418 titration. Red box defines the concentration of 0,6 mg/ml of G418 as the lowest concentration at which all non-transfected cells died.

5.1.2 Transfection optimization and setup of viability controls for the screening

KMM-1 cells were tested for their usability in the luciferase-based screening. Myeloma cells were seeded in different cell numbers (5000, 2500, 1250, 625) in 384-well plates and the luciferase activity was measured after cell lysis (Figure 3A). A linear relationship was observed between the seeded KMM-1-luc cell number and the luciferase activity (r^2 = 0,9927) (Figure 3B). Even 625 seeded KMM-1-luc cells could be distinguished from the background. The correlation between cell number and luciferase activity was used to determine the appropriate cell number to avoid overcrowded tumor cell density that could lead to saturation of the luciferase signal. Expecting that the knockdown of a potential immune-checkpoint in the tumor cells co-cultured with T cells drastically decreases the luciferase activity, an optimal luciferase intensity level was achieved with 5000 KMM-1-luc cells per well. Furthermore, as each cell line varies with regard to its sensitivity to a given transfection reagent, different transfection reagents (Dharmafect 1, Dharmafect 2 and RNAiMAX) were tested. We measured the transfection efficacy by transfecting KMM-1-luc cells with 25nM of different lethal siRNAs targeting genes essential for cell survival like ubiquitin C (UBC) [171], checkpoint kinase 1 (CHK1) [172], coatomer protein complex subunit beta 2 (COPB2) [173, 174], and “cell death” (CD) that comprises a mixture of several siRNAs targeting ubiquitously expressed human genes (Table 1). Loss of viability would lead to a decrease in luciferase intensity indicating high transfection efficacy. As the selected clones exhibited high luciferase activity, we silenced the signal using a firefly luciferase (FLuc)-targeting siRNA. RNAiMAX elicited the highest transfection efficacy with 5000 cells per well for all siRNA sequences (Figure 3C). Transfection with UBC, cell death, CHK1 and COPB2 markedly decreased cell viability as well as targeting the luciferase gene induced a reduction of the luciferase signal after 48h in comparison to the negative controls determined by two scrambled siRNA sequences (scr1; scr2) and a mock-control. Thus, siFLuc as well as

the lethal siRNA sequences were ideal choices for transfection and viability controls for the RNAi screen, respectively. Moreover, we tested whether increasing the concentration of the siRNA sequences to 50nM (transfecting 5000 KMM-1) or decreasing the cell number per well to 2500 (while maintaining 25nM as siRNA concentration) would increase the transfection efficiency. In both settings we did not observe an increase in transfection efficiency compared to transfecting 5000 KMM-1 with 25nM siRNA (Figure 3D). Therefore, all subsequent experiments were performed with 25nM siRNA concentration.

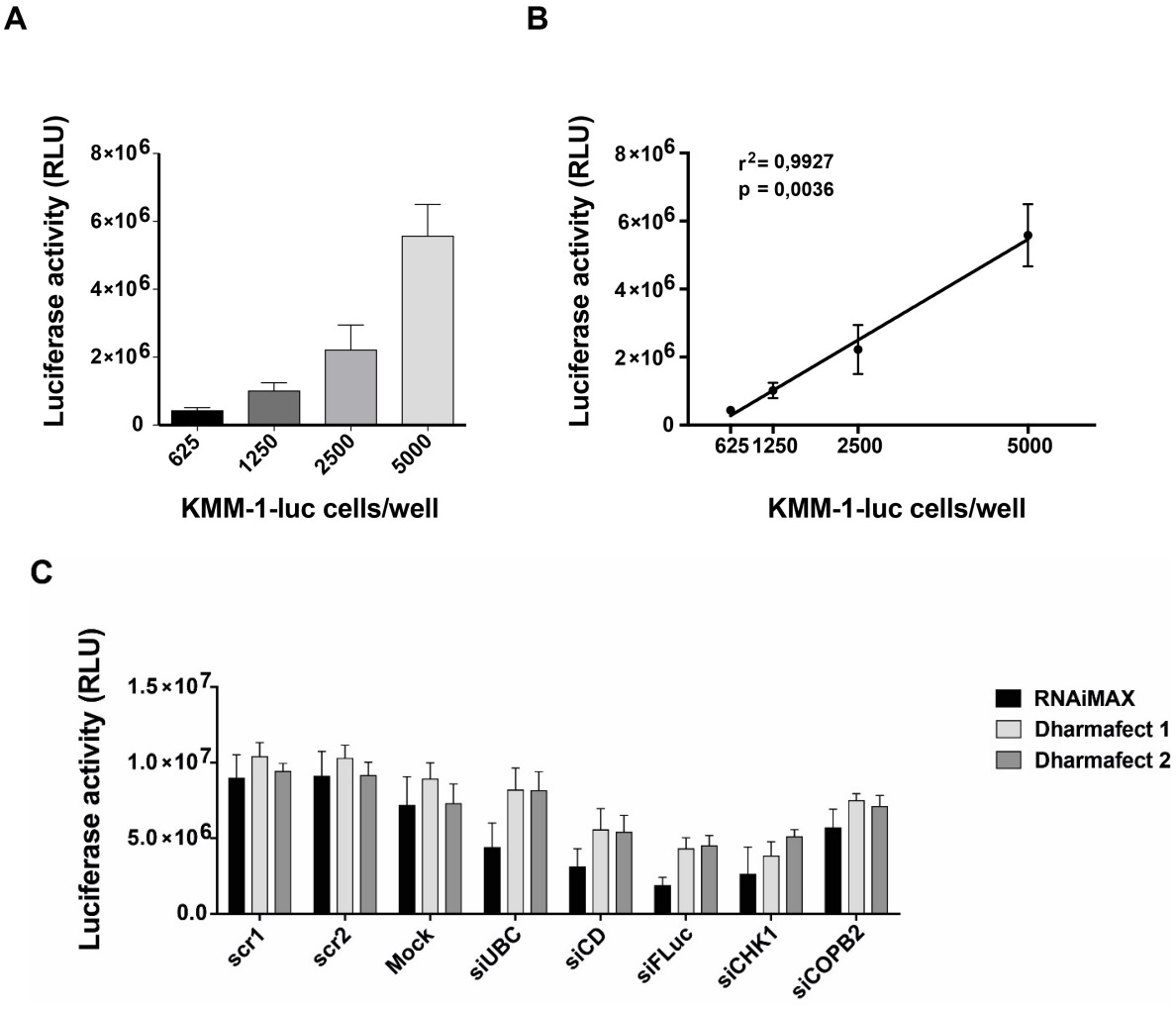

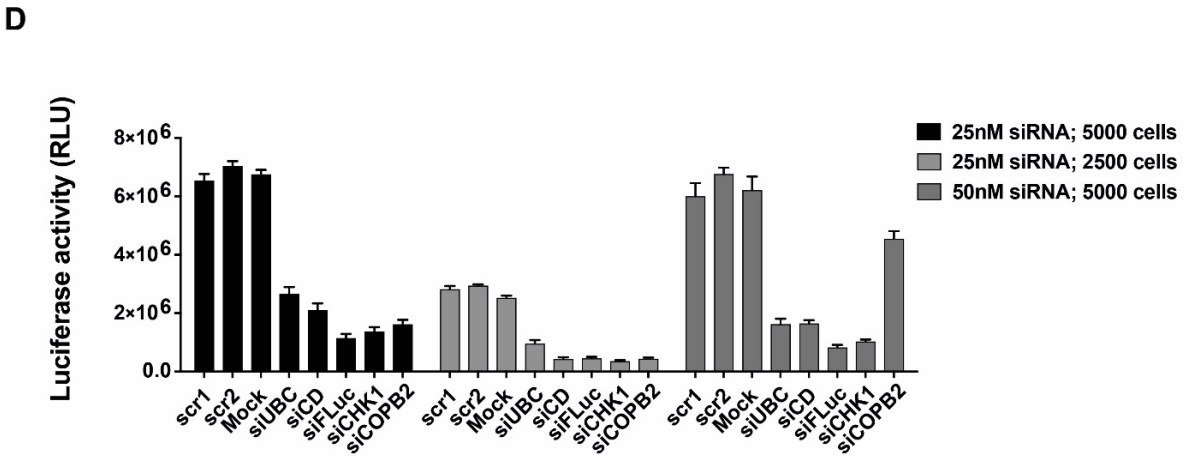

Figure 3. Determination of KMM-1-luc cell number, transfection reagents and viability controls. **(A)** KMM-1-luc were seeded in different cell numbers (5000, 2500, 1250, 625) in 384-well plates to assess the optimal cell number for the screening. Luciferase activity was measured after lysis. **(B)** Linear relationship between seeded KMM-1-luc cell number and the luciferase activity. **(C)** Dharmafect 1, Dharmafect 2 and RNAiMAX transfection reagents were used to transfect cells with different lethal siRNAs and siFLuc to determine the best transfection reagent. **(D)** 2500 and 5000 KMM-1-luc cells were seeded in 384-well plates and transfected with 25nM and 50nM siRNA concentration respectively. Loss of luciferase activity was compared to transfection of 5000 KMM-1-luc cells with 25nM siRNA concentration. Graphs show cumulative data of at least two independent experiments. Columns show mean +/- standard deviation (SD).

Table 1. Description of the candidate genes used as proper viability controls.

siRNA	Function
UBC	Ubiquitin C. Polyubiquitin precursor, involved in DNA repair, cell-cycle regulation, protein degradation.
Cell Death	A commercially available cocktail of several siRNAs targeting 5 essential genes for cell survival.
FLuc	A siRNA targeting the firefly luciferase encoded gene.
CHK1	Checkpoint kinase 1 is required for checkpoint mediated cell cycle arrest in response to DNA damage.
COPB2	Coatomer subunit beta 2 is essential for Golgi budding and vesicular trafficking.

5.1.3 MILs isolation, expansion and functional characterization

To be effective in the treatment of cancer, T cell adoptive immunotherapy requires large cell numbers with high proliferative potential and intact effector functions. As KMM-1 cells are immortalized tumor cells, the necessary target cell number for the screening was easily achievable. On the contrary, MILs are primary cells with limited proliferative potential. In order to reach the required number of T cells, the rapid expansion protocol (REP) established by Rosenberg et al., [175] and adapted in our laboratory was used. To this end, T lymphocytes were isolated from bone marrow cells from multiple myeloma patients depleted of $CD138^+$ cells using untouched Human T cells Dynabeads and subsequently expanded using the rapid expansion protocol. Before T cell purification, the cells were stained for CD3, CD4 and CD8 and tested for HLA-A2 positivity (Figure 4A). T cell growth was regularly monitored for a period of 15 days. On average, MIL numbers increased around 1000-fold after rapid expansion at day 15 of REP. Next, the killing ability of expanded MILs towards KMM-1-luc target cells was assessed. Different effector to target (E:T) ratios (20:1, 10:1 and 5:1) were tested. KMM-1 were seeded in different cell numbers and co-cultured with MILs (Figure 4B) or with Survivin specific T cell clones (Figure 4C). 20h after T cells co-culture, culture medium was removed and the remaining luciferase activity was measured. Co-culture of MILs or Survivin T cells with tumor cells elicited specific lysis of KMM-1-luc cells. Hence MILs, being patient-derived T cells and mimicking a physiological system, were selected for further experiments.

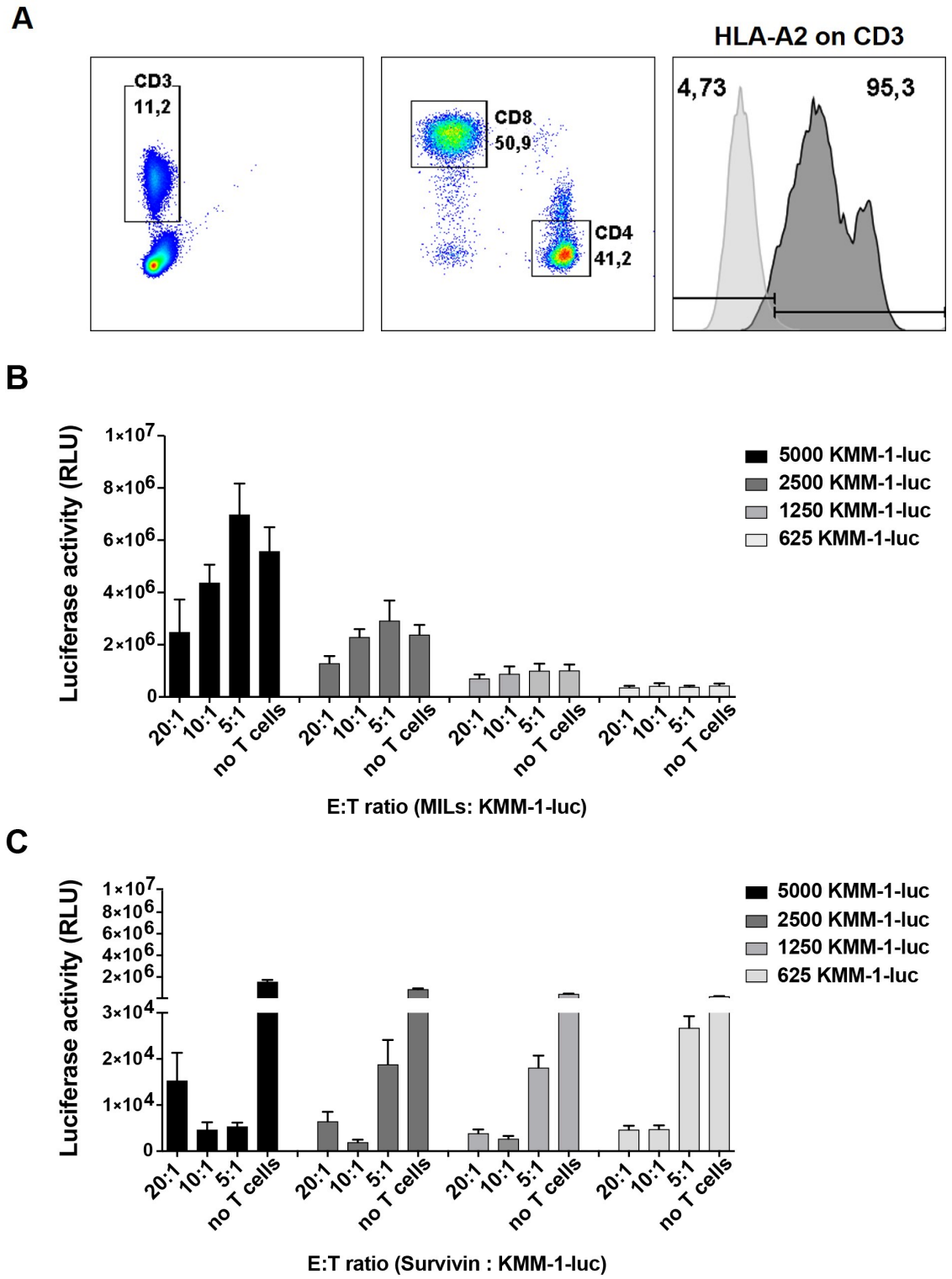

Figure 4. Assessment of E:T ratios of HLA-A2$^+$ MILs and Survivin T cells. (A) FACS-staining of the negative fraction of CD138-sorted bone marrow cells from a multiple myeloma patient, before T cell isolation. Cells were stained for anti-CD3, anti-CD4 and anti-CD8 and tested for HLA-A2 positivity (dark grey histogram). Light grey histogram: isotype control. **(B and C)** KMM-1-luc cells were co-cultured with either **(B)** MILs or **(C)** Survivin T cells in different E:T ratios (20:1, 10:1 and 5:1) and luciferase activity of lysed tumor cells was measured. Columns show mean +/- standard deviation (SD) of two independent experiments.

5.1.4 MHC-I restricted T cell mediated killing of multiple myeloma tumor cells

Furthermore, the modality by which MILs were killing KMM-1 cells was addressed. Both, the tumor cells and the T cells expressed the HLA-A2 haplotype (as described in section 5.1.1 and 5.1.3), however the cultures were derived from two different patients. Consequently, T cells could induce tumor cell death via TCR-MHC-I recognition or by TCR-independent mechanisms (e.g. unspecific cytokine secretion) or even by induction of apoptosis upon binding to members of the TNF-superfamily like FasL, TRAIL or TNF. To assess the TCR engagement, MILs were co-cultured with KMM-1 cells in the presence of a MHC-I blocking antibody. A reduced T cell mediated killing of the tumor cells was observed in a dose-dependent manner using the anti-MHC-I antibody (Figure 5A). Furthermore, INF-γ secretion can be used as an indicator of TCR activation. Thus, KMM-1 cells were co-cultured with MILs and INF-γ secretion by the T cells was measured and compared to unstimulated T cells (T cells that were not co-cultured with the tumor cells). A significant increase of INF-γ was measured upon MILs activation by tumor cells compared to unstimulated MILs. As expected, anti-CD3/anti-CD28 magnetic beads induced a strong secretion of IFN-γ by activated T cells (Figure 5B). Altogether, these data indicate that MIL-derived T cells remain functional after the expansion and could exhibit their functionality towards KMM-1 cells in a TCR dependent manner.

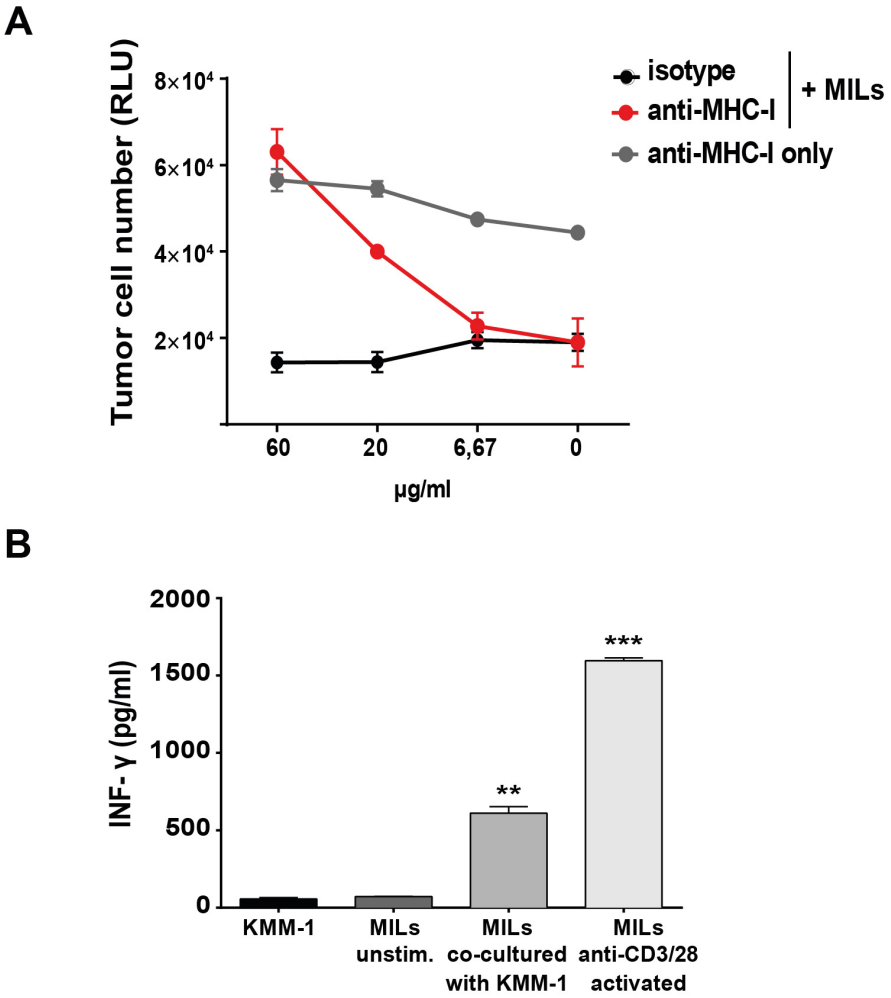

Figure 5. Functional characterization of MILs. (A) Luciferase-based killing assay for detection of T cell-mediated cytotoxicity in the presence of the indicated concentrations of anti-MHC-I antibody (red line) and IgG2a isotype as positive control (grey line). Anti-MHC-I antibody was added to KMM-1 cells in the absence of T cells as negative control (black line). **(B)** MILs and KMM-1 cells were co-cultured for 20h. IFN-γ secretion was measured by ELISA. As negative control, T cells were cultured in the absence of tumor cells (MILs unstim.). Background INF-γ was measured in KMM-1 cells alone. Anti-CD3/anti-CD28 magnetic beads stimulated MILs were used as positive control. **(A, B)** Graphs show mean +/- SD. **(B)** P-values were calculated using two-tailed student´s t-test. * $p \leq 0.05$; ** $p \leq 0.01$; *** $p \leq 0.001$. Representative data of at least 2 independent experiments.

5.1.5 Phenotypic characterization of marrow infiltrating lymphocytes

Marrow-infiltrating lymphocytes comprise a mixture of cytotoxic (CD8) and helper (CD4) T cells. Cytotoxic T cells are supposed to be the main effector T cell subpopulation mediating an anti-tumor immune response. For this reason, the memory and effector phenotypes of the T cell subsets were examined by expression of the surface markers CD45RA and CD62L. As expected, T cell populations show a strong memory phenotype, marked by CD95 expression. Both, CD4 and CD8 T cells revealed a central memory ($CD45RA^-$ $CD62L^+$) and an abundant effector memory ($CD45RA^-$ $CD62L^-$) phenotype, whereas no naïve ($CD45RA^+$ $CD62L^+$ $CD95^-$) or terminal effector memory ($CD45RA^+$ $CD62L^-$) T cells were present (Figure 6A). Based on the evidence that MILs showed a modest cytotoxic activity towards KMM-1 cells even at high E:T ratios, we hypothesized that this outcome was ascribed to T cell exhaustion [176]. Several studies demonstrate that tumor infiltrating lymphocytes from different tumor entities have impaired T cell effector activity and upregulate different receptors leading to dysfunctional T cells [177-180]. In concordance with their memory phenotype, MILs express high levels of exhaustion markers such as CTLA-4, LAG-3 and PD-1, suggesting a state of strong exhaustion. In particular CTLA-4 was detected in 77,2% and 83,5% of CD4 and CD8 T cells respectively. Moreover, 53,8% and 47,9% of CD4 and CD8 T cells expressed LAG-3 and PD-1 expression was detected in 49,4% and 44,8% of CD4 and CD8 T cells respectively (Figure 6B). Exhausted MILs have a higher probability to express receptor/ligands for potential immune-checkpoints, that might be identified by the RNAi screening.

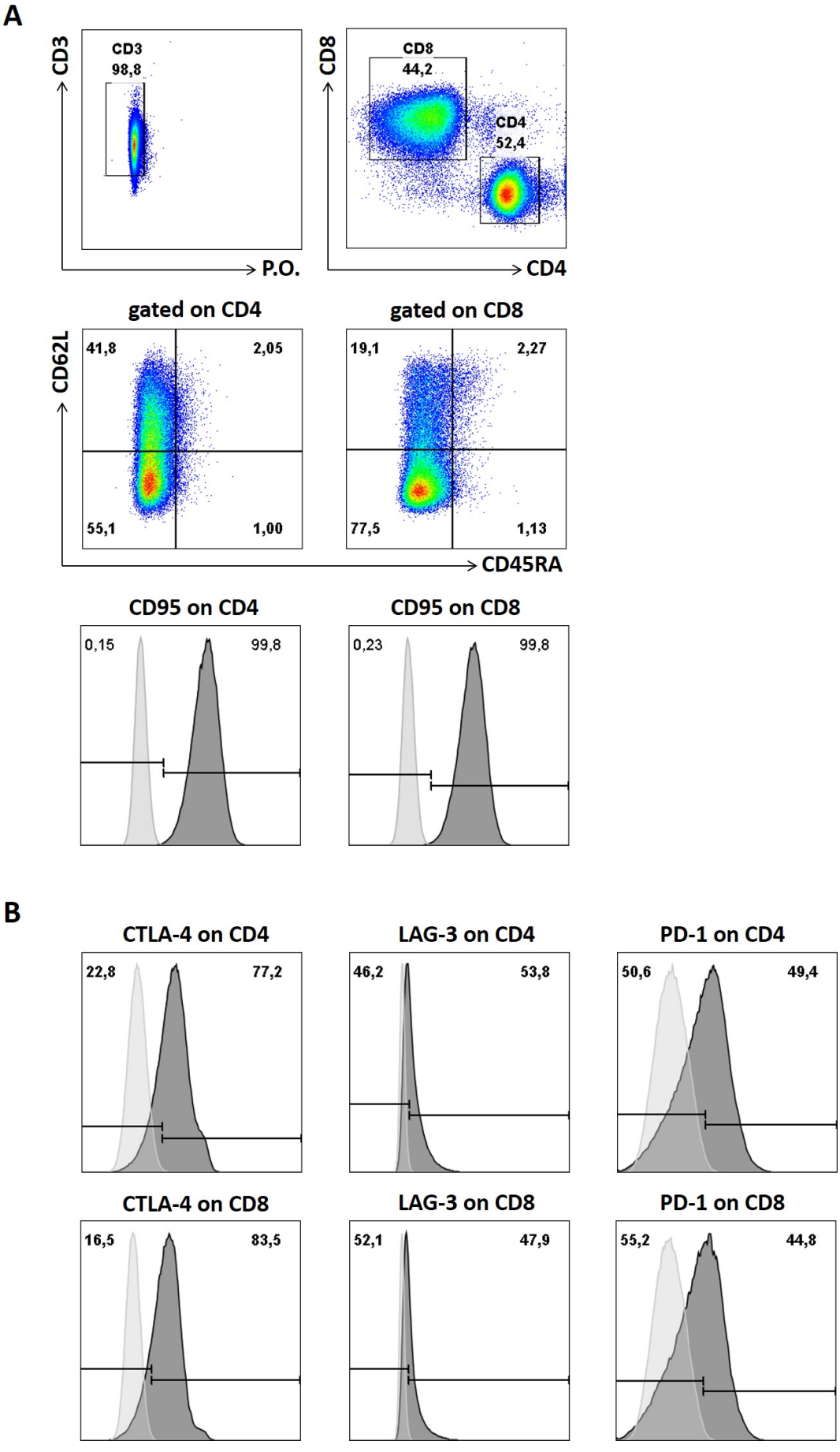
A
CD3
CD3
98,8
P.O.
CD8
CD8
44,2
CD4
52,4
CD4
gated on CD4
gated on CD8
CD62L
41,8
2,05
55,1
1,00
19,1
2,27
77,5
1,13
CD45RA
CD95 on CD4
CD95 on CD8
0,15
99,8
0,23
99,8
B
CTLA-4 on CD4
LAG-3 on CD4
PD-1 on CD4
22,8
77,2
46,2
53,8
50,6
49,4
CTLA-4 on CD8
LAG-3 on CD8
PD-1 on CD8
16,5
83,5
52,1
47,9
55,2
44,8

Figure 6. Phenotypical characterization of MILs. (A) FACS-analysis of CD4 and CD8 populations in $CD3^+$ MILs upon REP. Representative surface staining for CD45RA and CD62L to identify T cell subpopulations. Central memory (Tcm) cells are represented by $CD45RA^-$ $CD62L^+$ expression, whereas effector memory (Tem) are defined by $CD45RA^-$ $CD62L^-$. CD95 expression of CD4 and CD8 T cells marks the memory phenotype. **(B)** Flow cytometry analysis for the exhaustion markers CTLA-4, LAG-3 and PD-1 in CD4 and CD8 population of MILs. Light grey histogram: isotype control, dark grey histogram: anti-CTLA-4, anti-LAG-3 and anti-PD-1 staining.

5.1.6 Selection of immune-checkpoint controls

The selection of positive and negative immune-checkpoint controls is of high importance for the reproducibility and robustness of the HTP-screening [162]. Indeed, without appropriate controls it is not possible to evaluate the impact of a potential immune-checkpoint molecule on T cell mediated killing. Thus, positive immune-checkpoint controls are needed to i) set a threshold to identify effective hits and ii) to confirm the robustness of the HTP screening. Negative controls (e.g. scramble siRNA sequences) are included as a reference to calculate the effect of gene knockdown and to exclude those genes that have a viability impact. Only genes having a higher effect on T cell-mediated tumor lysis compared to the selected immune-checkpoint control, while having a minor impact on general cell viability, were considered as novel immune-checkpoint candidates.

In order to determine appropriate negative controls for the assay, the impact of two different scrambled siRNA sequences (scr1 and scr2) on KMM-1-luc cells was tested using the luciferase-based assay. Both scr1 and scr2 siRNA transfection did not alter cell viability compared to mock-control (tumor cells treated with transfection reagent in the absence of siRNAs) (Figure 7A). Therefore, both siRNA sequences were included in the HTP-screening. Furthermore, suitable positive controls for both viability and cytotoxicity needed to be established. Thus, to identify immune-checkpoints that alter cell viability, we knocked down genes essential for cell survival (as explained in section 5.1.2). Among them we targeted UBC and used a mixture of siRNAs (siCD) inducing cell death. Moreover, we targeted firefly-luciferase (FLuc) as an additional positive control for transfection efficacy. Using the luciferase-based readout system, we found that siUBC, siCD and siFLuc induced efficient tumor cell death and loss of luciferase expression with and without the addition of T cells, indicating effective transfection efficiency (Figure 7A). For the cytotoxicity setting, we tested T cell-mediated cytotoxicity after knockdown of several known immune-checkpoint molecules such as programmed death ligand 1 (PD-L1) [181] and C-C Motif Chemokine

Receptor 9 (CCR9) [164]. To this end, we validated their expression in the selected tumor cell line and assessed also the knockdown efficiency of the respective siRNA sequences. Both immune-checkpoint molecules were expressed by KMM-1 cells as revealed by flow-cytometry analysis (Figure 7B) and end-point PCR (Figure 7C) and both siRNA sequences reduced respectively PD-L1 and CCR9 transcription by 50% as observed by end point PCR (Figure 7C) and quantitative PCR (qPCR) (Figure 7D). Thus, we tested the impact of PD-L1 and CCR9 knockdown on T cell mediated killing of tumor cells. Tumor cells, in which these genes were knocked down, were co-cultured with T cells at different E:T ratios (5:1 and 10:1). A "no T cells-condition" was included to identify whether the knockdown caused a viability impact *per se*. Using the luciferase-based killing assay, we observed that PD-L1, although expressed by the tumor cells and efficiently knocked down upon siRNA transfection, did not improve the T cell-mediated cytotoxicity. Only by knocking down CCR9 an increased T cell-mediated killing of tumor cells was detected, without any impact on cell viability (in the viability setting). Thus, CCR9 was used as positive immune-checkpoint control in the HTP-screening.

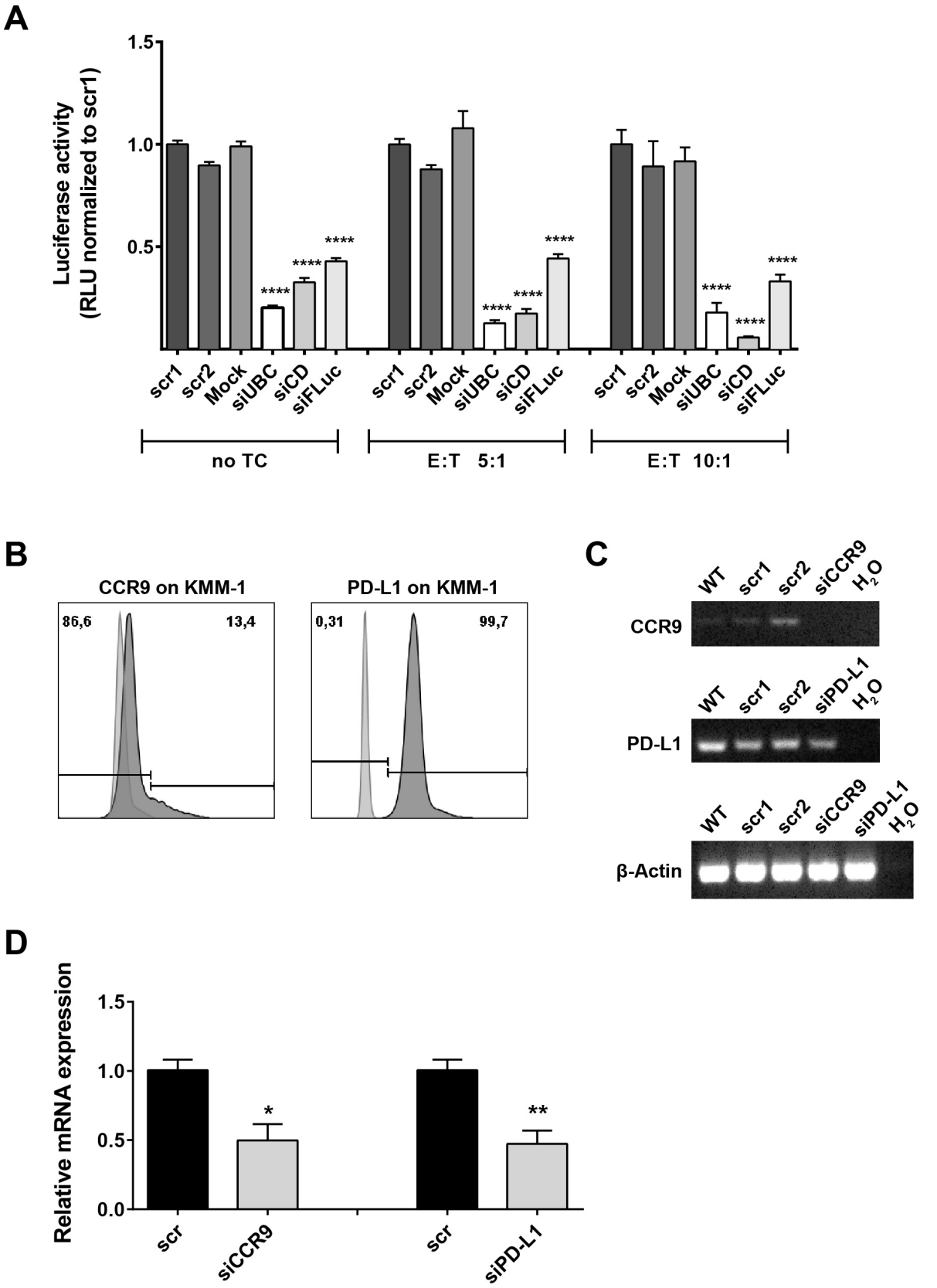
A
Luciferase activity (RLU normalized to scr1)
1.5
1.0
0.5
****
scr1
scr2
Mock
siUBC
siCD
siFLuc
no TC
E:T 5:1
E:T 10:1
B
CCR9 on KMM-1
PD-L1 on KMM-1
86,6
13,4
0,31
99,7
C
WT
scr1
scr2
siCCR9
siPD-L1
H2O
CCR9
PD-L1
β-Actin
D
Relative mRNA expression
1.5
1.0
0.5
0.0
*
**
scr
siCCR9
siPD-L1

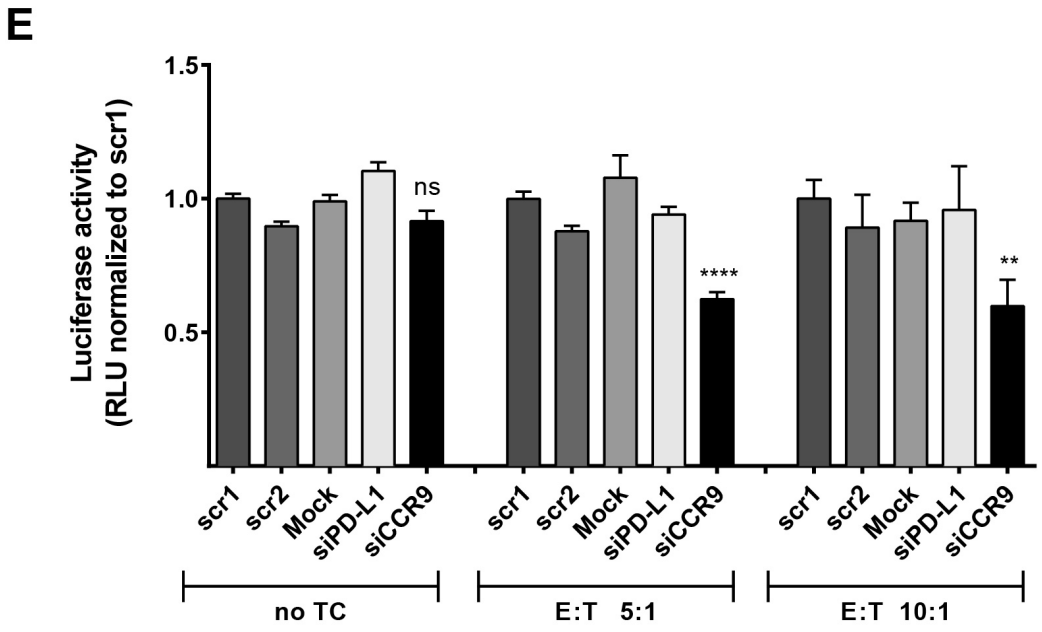

Figure 7. Assessment of positive and negative immune-checkpoint controls for the HTP-screen. **(A)** KMM-1-luc cells were transfected with the specified siRNA sequences. Loss of luciferase activity was compared to negative siRNA sequences. Statistical significance was calculated compared to scr1 siRNA sequence. Knocked down tumor cells were co-cultured with MILs in different E:T ratios. **(B)** FACS-analysis for CCR9 and PD-L1 expression on KMM-1 cells (dark grey histogram); Light grey histogram: isotype control. **(C)** End-point polymerase chain reaction (PCR) assay for the detection of CCR9 and PD-L1 mRNA abundance in WT or siRNA treated KMM-1 cells. **(D)** Quantitative PCR (qPCR) analysis of CCR9 and PD-L1 mRNA expression in KMM-1 cells after 48h siRNA transfection. Results are presented in terms of fold change after β-actin mRNA normalization. **(E)** KMM-1-luc cells were transfected with the indicated siRNA sequences for 48h. Luciferase-based viability assay was conducted (no TC control) and co-culture with MILs at indicated E:T ratios was performed for cytotoxicity assay. Cell survival was determined by measuring the remaining luciferase activity of tumor cells after 20h co-culture with MILs or culture medium (no TC). **(A, D, E)** Graphs show mean +/- SEM of three independent experiments. P-values were calculated using two-tailed student´s t-test. * $p < 0.05$, ** $p < 0.01$, *** $p < 0.001$, **** $p < 0.0001$

5.2 High-throughput RNAi screen performance

Once the optimization process was completed, the arrayed RNAi screen was performed in a 384-well format using MILs as T cell source and KMM-1-luc as target cells at an E:T ratio of 10:1. As explained in section 5.1, tumor cells were transfected with a siRNA library of 2887 genes comprising kinases, surface proteins and GPCRs. RNAiMAX was used as transfection reagent and T cells were added after 48h siRNA transfection when the knockdown was achieved (cytotoxicity setting). As a viability control, transfected tumor cells were cultured in the absence of MILs (viability setting). After 20h co-culture, the supernatant containing T cells and dead tumor cells was removed, remaining tumor cells were lysed and the residual luciferase activity (RLU: relative luminescence units) was measured (Schematic representation in Figure 1). An additional luciferase-independent CellTiter-Glo (CTG) screening, in which cell viability was determined by measuring intracellular ATP levels, was performed with wild-type KMM-1 cells in order to filter out genes, whose knockdown impacted cell viability. All sets (cytotoxicity, viability, CTG) were conducted in technical duplicates.

5.2.1 Performance of controls

To compare the RLU values from the transfected tumor cells within the library, plate normalization was performed. This step was required since the relatively short half-life of the luciferase could generate inter-plate variability. Overall, the residual luciferase intensities in the screening were normally distributed around the mean of the respective plate in all setups but showed a high variance and some row effects. Therefore, B score normalization was used for normalizing the data (Figure 8A). Next, the cytotoxicity and viability impact of each gene and control was summarized as a z-score (the number of standard deviations from the mean). To validate the overall screening performance, the performance of control genes, which were loaded in each plate of the library, was calculated. Negative control scr1 and scr2 siRNAs transfection as well as mock-control did neither affect tumor cell viability nor immune susceptibility of tumor cells as observed by no change in luciferase activity (compared to the respective plate mean) in both settings (Figure 8B and C). In contrast, transfection with UBC and CD siRNAs resulted in a clear loss of cell viability as observed by the abrogation of the luciferase signal independent of the addition of MILs and was even stronger when T cells

were added to the co-culture. Therefore, UBC and CD served as positive viability controls. In line with this, targeting the firefly luciferase with siFLuc abolished the luciferase signal under both conditions and served as an internal control for transfection efficacy. Depletion of CCR9 resulted in enhanced MIL-mediated tumor cell killing in the cytotoxicity setting, while a negligible effect in the viability setting was observed (Figure 8B and C). As expected, PD-L1 did not show any effect on T cell mediated cytotoxicity. To evaluate the technical quality and reproducibility of the assay, the Pearson correlation coefficient (r^2) was calculated for the three settings. We observed r^2 = 0,701 in the cytotoxicity setting and r^2 = 0,872 in the viability setting, confirming the technical robustness of the assay (Figure 8B). Independent assessment of all genes for their impact on cell viability was achieved using the CTG assay that showed r^2 = 0,810 (Figure 8C).

A

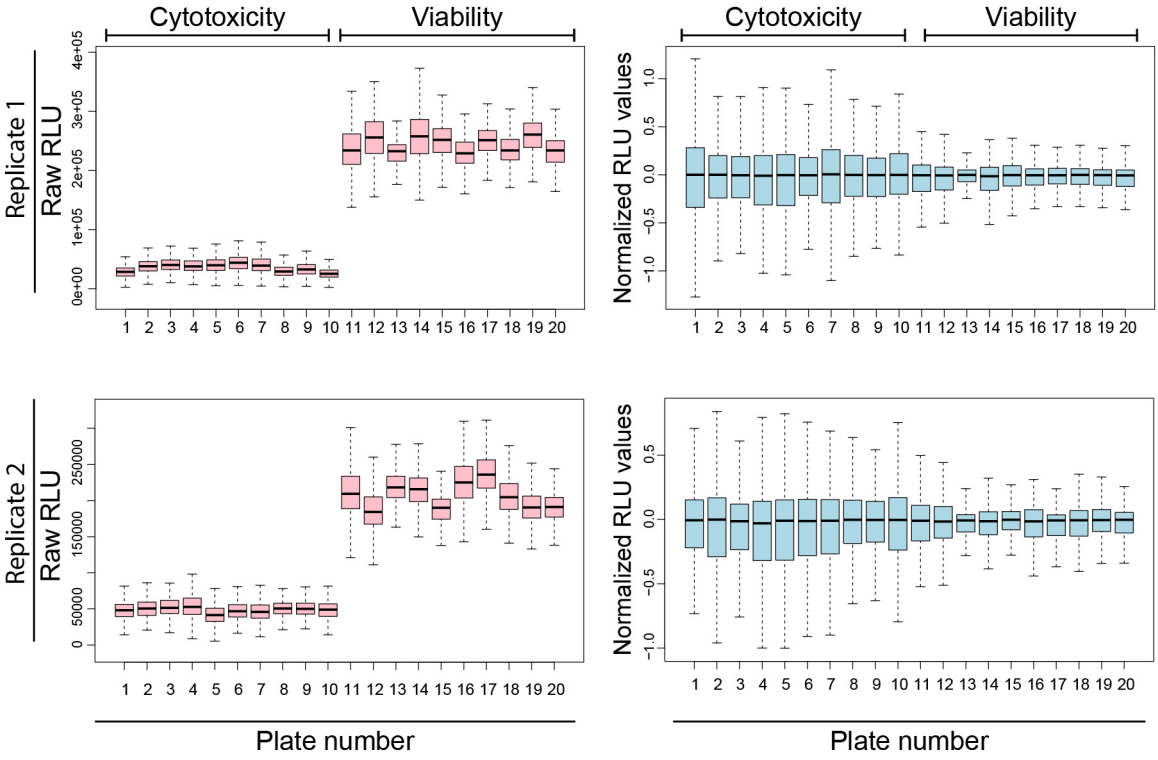

B

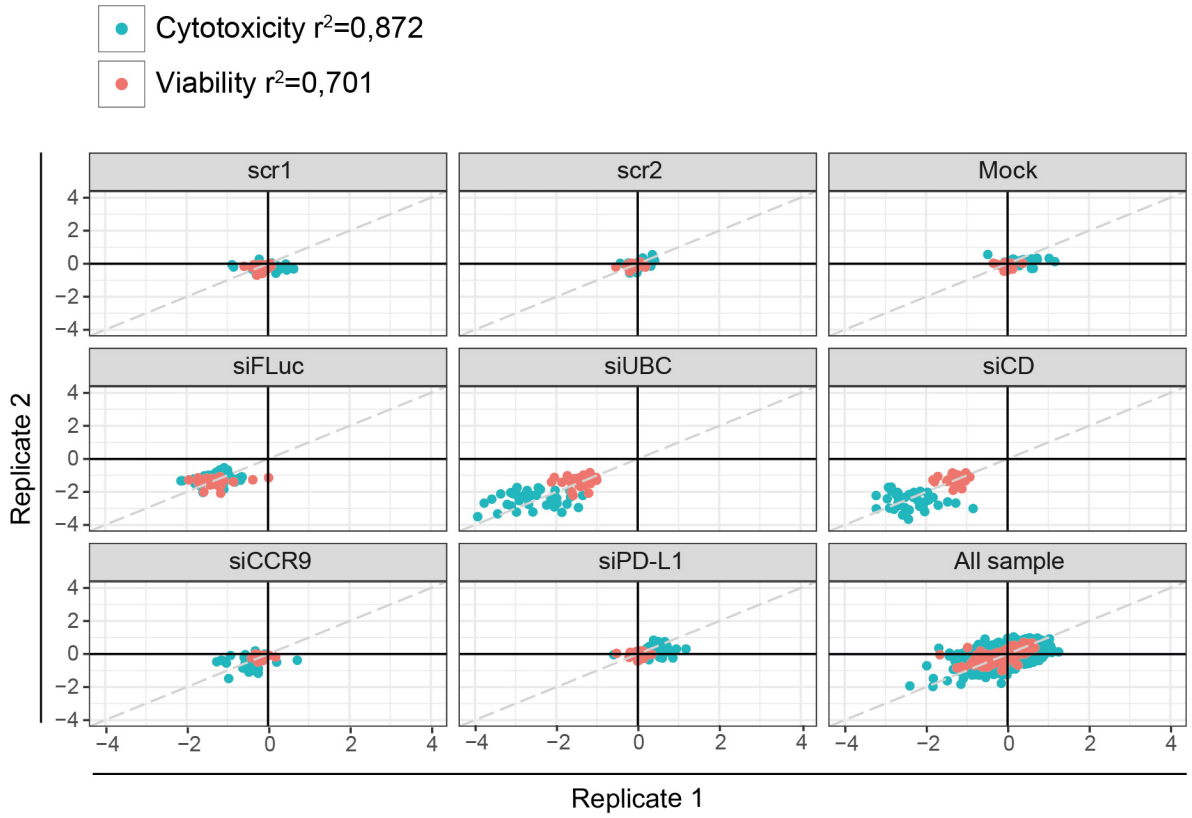
Cytotoxicity r²=0,872
Viability r²=0,701
scr1
scr2
Mock
siFLuc
siUBC
siCD
siCCR9
siPD-L1
All sample
Replicate 2
Replicate 1

C

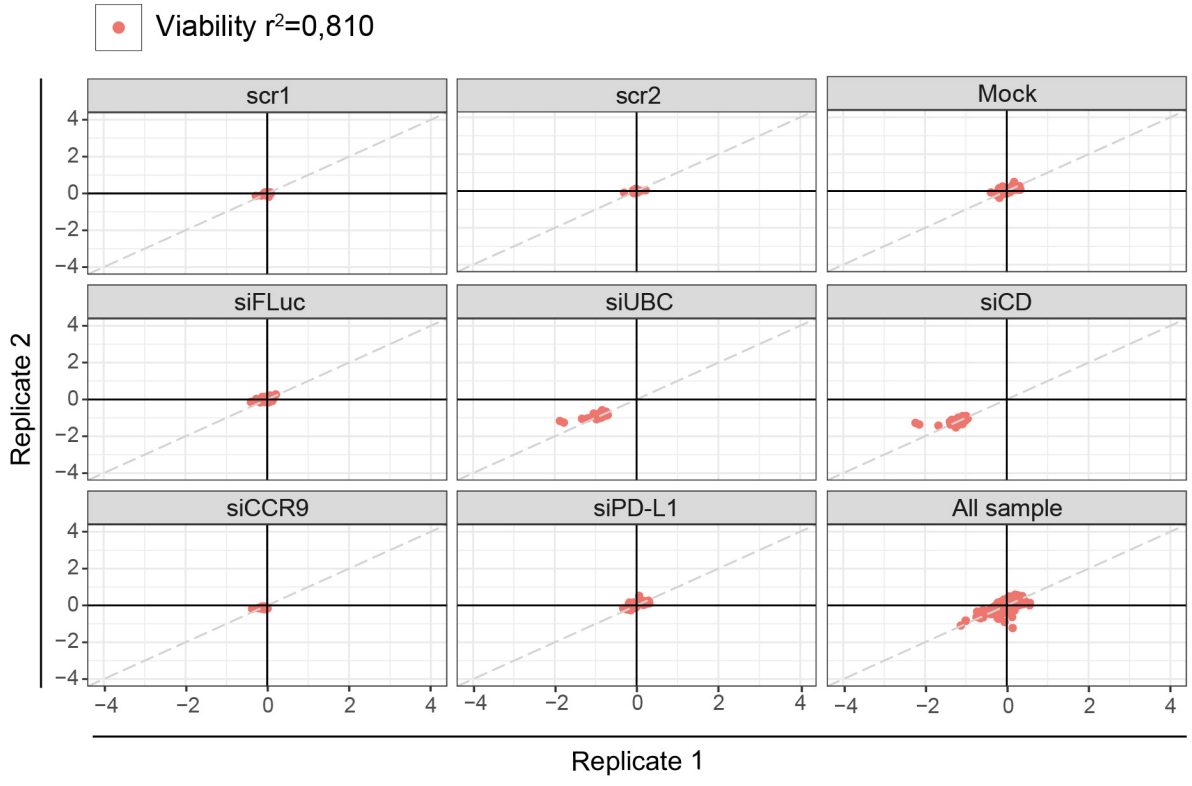
Viability r²=0,810
scr1
scr2
Mock
siFLuc
siUBC
siCD
siCCR9
siPD-L1
All sample
Replicate 2
Replicate 1

Figure 8. Performance of controls. (A) Raw luciferase activity (RLU) was measured for each well of 40 x 384-well plates (upper and lower left panels). To exclude intra- and inter-plate variability, RLU values were normalized using the B score method (upper and lower right panels). For each replicate set, plates from 1 to 10 were co-cultured with MILs at E:T 10:1 (cytotoxicity), while plates from 11 to 20 were cultured with medium control (viability). **(B)** Performance of controls in the HTP-screening. Dot plot shows normalized and scored RLUs after transfection of KMM-1-luc cells with several control siRNAs. Technical replicates were plotted against each other. Blue dots: cytotoxicity setting (with MILs). Red dots: viability setting (without MILs). Pearson correlation (r^2) between the 2 replicate values was calculated for each setting (cytotoxicity setting: $r^2 = 0{,}701$; viability setting: $r^2 = 0{,}872$). **(C)** Additional 20 x 384-well plates were subjected to the luciferase-independent CellTiter-Glo (CTG) screening performed on WT KMM-1 cells in which cell viability was determined by measuring intracellular ATP levels (viability setting: $r^2 = 0{,}810$).

5.2.2 Gating strategy for the identification of novel immune-checkpoint molecules

To identify potential immune-checkpoints, the RLU of each gene knockdown were transformed into z-scores, defined by the number of standard deviations between the single data point and the mean of the plate. To simplify subsequent analysis, each z-score was inverted by multiplication with -1. Next, we compared the impact of each gene knockdown in regulating T cell mediated killing and in modulating tumor viability (cytotoxicity versus viability). For the viability setting, we excluded genes showing a $z > 2{,}0$ or $z < -2$. Knockdown of genes which had a z-score higher than ubiquitin C in the CTG screen were excluded ($z > 0{,}5$). Also, knockdowns which were beneficial for tumor cell growth ($z < -0{,}5$ in CTG) were excluded from hit calling. For the cytotoxicity setting, we considered as potential immune-checkpoints only genes whose cytotoxicity score was higher than the knockdown of the control immune-checkpoint CCR9. The results of the high-throughput RNAi screen are depicted in Figure 9A. Finally, local regression (LOESS) was used to rank the hits. LOESS-derived scores incorporate the difference between the cytotoxicity and the viability (*z*) scores and therefore allow to identify candidates whose knockdown show the strongest immune-related phenotype (Figure 9B). The screen unraveled both inhibitory and stimulatory immune modulators of T cell-mediated killing. Nevertheless, our analysis was concentrated on the discovery of novel inhibitory immune-checkpoints, as the blockade of this class of proteins has shown improved clinical benefits in several tumor entities [182-186].

Our analysis revealed 128 potential negative regulators of T cell cytotoxicity stronger than CCR9, among them several confirmed immune-checkpoints (e.g. CD5, FES and PAK3), supporting the reliability of our screening approach. CD5, functions as a receptor for IL-6,

which in turn activates the transcription factor STAT3 via the JAK-STAT signaling thereby promoting cancer progression [187]. The serine/threonine protein kinase PAK3 acts as a signal transducer in several cancer signaling pathways, such as the canonical MAP kinase cascade of Ras/Raf/MeK/ERK [188], being important for cytoskeletal dynamics, cell survival and proliferation [189, 190]. FES, a cytoplasmic protein-tyrosine kinase already identified in a kinome-wide siRNA screen, contributes in cellular signaling cascades fostering cellular differentiation and inflammation as well as multiple myeloma cell growth and survival [191]. Moreover, in line with literature and with the previous setup of positive controls, PD-L1 did not show any effect on T cell mediated killing of multiple myeloma cells. The identification of these validated immune-checkpoints in combination with good immune-checkpoint control performance supported the robustness and sensitivity of our screening approach.

A

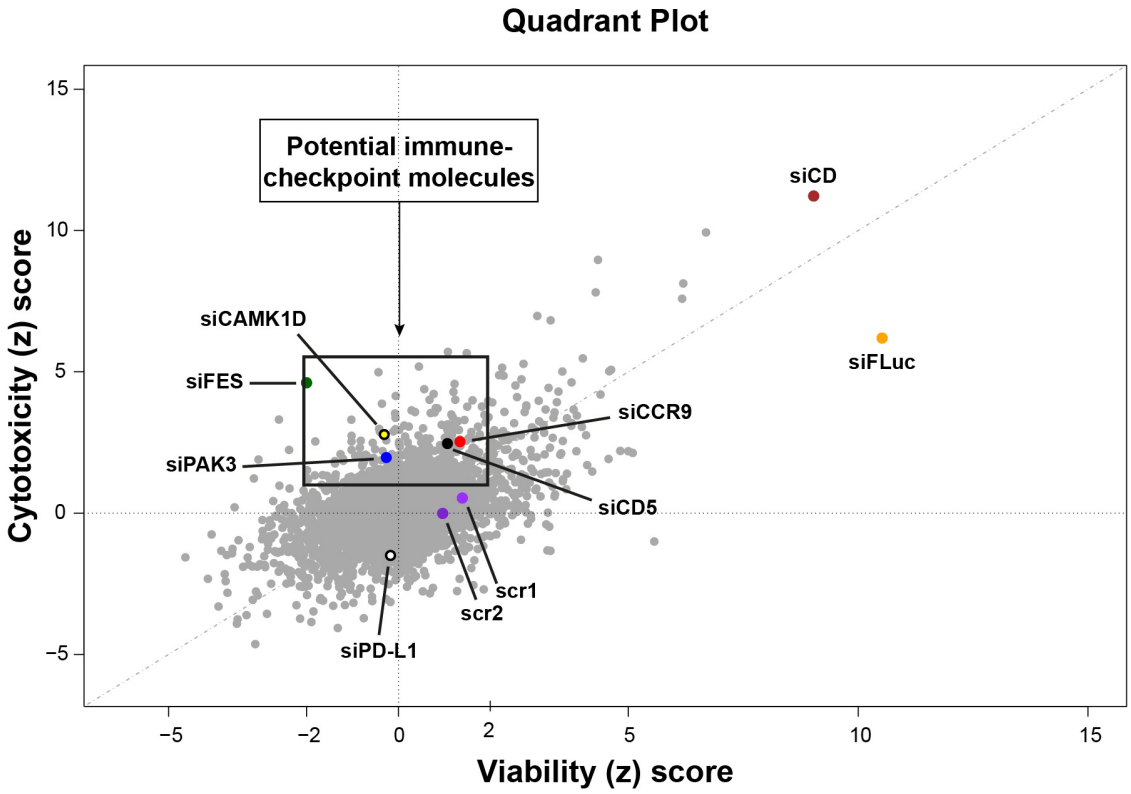
Quadrant Plot
Potential immune-checkpoint molecules
siCD
siFLuc
siCAMK1D
siFES
siCCR9
siPAK3
siCD5
scr1
scr2
siPD-L1
Cytotoxicity (z) score
Viability (z) score
15
10
5
0
−5
−5
−2
0
2
5
10
15

B

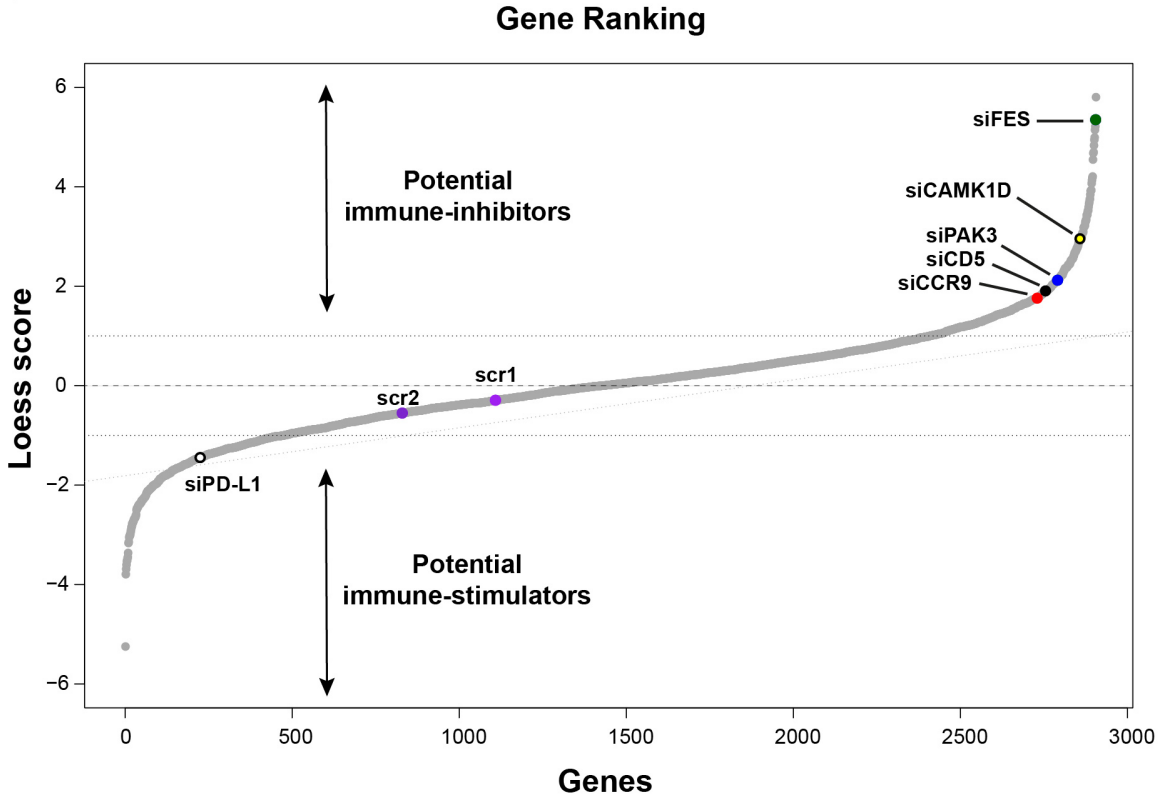
Gene Ranking
Potential immune-inhibitors
Potential immune-stimulators
siFES
siCAMK1D
siPAK3
siCD5
siCCR9
scr1
scr2
siPD-L1
Loess score
Genes
6
4
2
0
−2
−4
−6
0
500
1000
1500
2000
2500
3000

Figure 9. High-throughput screening results. (A) Quadrant plot showing z-scores of gene knockdown in transfected KMM-1-luc cells after co-culture with MILs (cytotoxicity z-score) or with culture medium (viability z-score), using a siRNA library of 2887 genes. The black box indicates genes, which were considered as potential negative immune modulators of T cell-mediated killing. **(B)** Gene ranking diagram showing differential score between cytotoxicity and viability z-scores using local regression (LOESS) rank. The upper panel classifies the potential immune-inhibitors with a high loess score, while the lower panel displays the potential immune-stimulators in multiple myeloma cells. Genes with differential score higher than CCR9 knockdown were selected as potential negative immune-modulators.

5.2.3 Secondary screening

To further validate the hits and the robustness of the screening, we re-tested the identified candidates in a secondary screening (Figure 10). As for the primary HTP-screening cytotoxicity and viability impact of each gene knockdown was calculated compared to the negative control (Figure 10A). Most of the hits identified in the HTP-screening induced a moderate loss of luciferase intensity indicating an increased T cell mediated killing of tumor cells. The strongest phenotypic effect (high cytotoxicity and no viability impact) was elicited by a serine/threonine protein kinase (CAMK1D) (Table 2). In order to determine if the tumor cell killing was mediated by cytokines or soluble proteins released by the T cells, an additional setting was included in the secondary screening. Hence, MILs were pre-activated with anti-CD3/anti-CD28 magnetic beads (polyclonal stimulation) for 20h and only the supernatant of the pre-activated T cells was added to the knocked down tumor cells. The knockdown of only few genes induced tumor cell susceptibility upon exposure to the T cells supernatant indicating a role in resistance to cytokine- or soluble protein-induced apoptosis. (Figure 10B). Noteworthy, this effect was reproducible when MILs were activated by siRNA-transfected tumor cells (Figure 10A). Nevertheless, most of the identified hits induced tumor cell killing only in the presence of T cells. These results provided a first indication that multiple myeloma cells express immune-checkpoint molecules that confer resistance to T cell interaction rather than molecules released upon T cell activation.

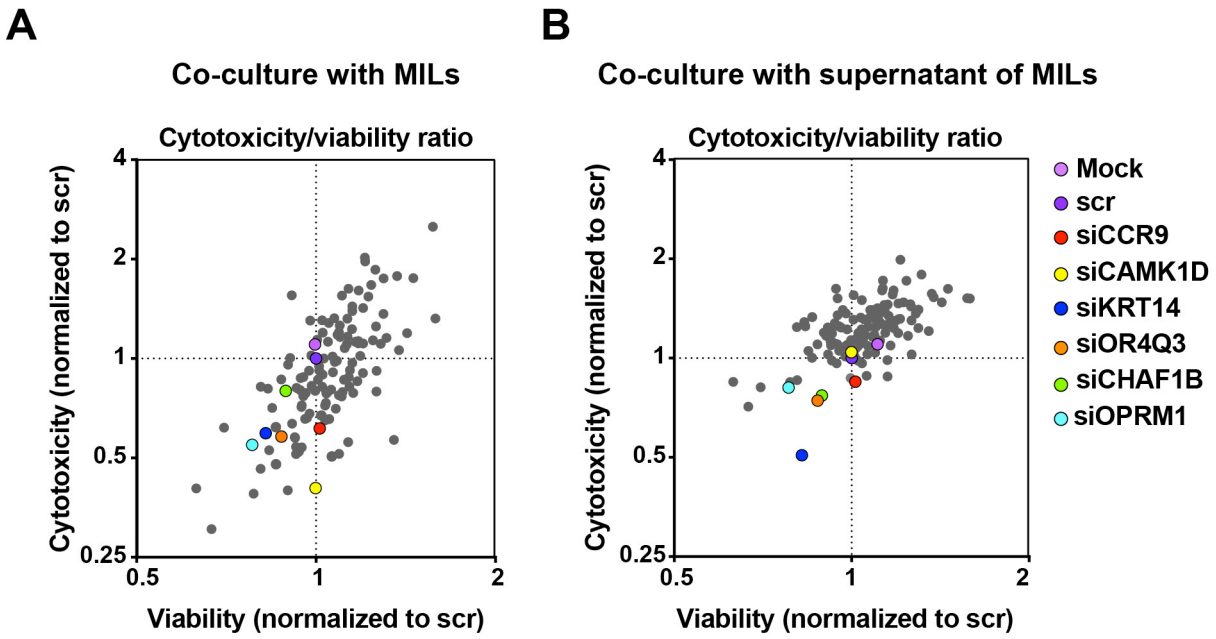

Figure 10. Secondary screening results. Luciferase-based secondary screening was performed using the hits obtained from the primary screening. Knocked down tumor cells were co-cultured with **(A)** MILs or **(B)** supernatant of anti-CD3/anti-CD28 magnetic beads activated MILs. RLUs were normalized to scr2 siRNA control. Log2 scale of cytotoxicity/viability ratio is depicted. Experiments were performed in duplicates. Mean is shown.

Table 2. Hit-list from the secondary screen. Hits are ranked according to their cytotoxicity/viability score in the MILs-based screening.

Rank	Hit	Score	Rank	Hit	Score	Rank	Hit	Score
1	CAMK1D	0,406	**25**	SLC12A2	0,657	**49**	PDK4	0,762
2	EED	0,419	**26**	NPR1	0,66	**50**	BMPR2	0,762
3	CD5	0,444	**27**	OR4Q3	0,663	**51**	DOK4	0,769
4	IL17A	0,455	**28**	ADGRG6	0,681	**52**	FES	0,773
5	SNU13	0,468	**29**	ALK	0,684	**53**	PLIN3	0,774
6	COPB2	0,47	**30**	AK2	0,684	**54**	MLKL	0,8
7	PTK2B	0,475	**31**	CD3D	0,695	**55**	LAT	0,801
8	OR5B2	0,493	**32**	DUSP5	0,695	**56**	IFNA6	0,807
9	PAK3	0,496	**33**	P2RY2	0,696	**57**	OR5M8	0,808
10	IGF2	0,554	**34**	APOM	0,698	**58**	PTPRU	0,817
11	AIP	0,558	**35**	OPRM1	0,701	**59**	SEPT7	0,833
12	PFKFB4	0,558	**36**	KIF1B	0,705	**60**	NMUR2	0,839
13	ADORA2B	0,558	**37**	TESK1	0,708	**61**	KRT76	0,839
14	APOC4	0,568	**38**	ETFB	0,714	**62**	KCNV2	0,84
15	ANGPT2	0,574	**39**	KRT14	0,721	**63**	PRKCG	0,843
16	BEST1	0,583	**40**	GK2	0,722	**64**	FLVCR1	0,851
17	DGKQ	0,623	**41**	RGS14	0,723	**65**	ADRBK2	0,852
18	FGF4	0,623	**42**	PKM	0,725	**66**	CLCA2	0,857
19	TPM2	0,627	**43**	BMX	0,727	**67**	IQCH	0,862
20	DUSP4	0,627	**44**	IRAK3	0,752	**68**	NR0B2	0,87
21	ITK	0,628	**45**	KRT15	0,753	**69**	TNFSF15	0,878
22	AK7	0,632	**46**	GPR31	0,754	**70**	DDI1	0,879
23	HLA-G	0,642	**47**	IL1RL2	0,756	**71**	ITGB1	0,881
24	RGS17	0,652	**48**	RPS6KA6	0,759	**72**	CHAF1B	0,896

5.3 Selection of potential immune-checkpoint molecules

As the hit-list contained a large number of potential immune-checkpoints, two main selection criteria for subsequent validation were considered. First, being interested in the identification of novel immune checkpoint molecules, only hits with an undetermined role in tumor escape mechanisms were considered. Second, surface or intracellular proteins, as kinases, were prioritized being feasible targets of blocking antibodies or small inhibitory molecules, respectively.
After an extensive literature research, we selected 8 potential immune-checkpoint molecules (Table 3) that were subjected to advanced validation.

Table 3. List of selected hits for further validation and their cellular location.

Hit	Extended Name	Cellular Location
PTK2B	Protein Tyrosine Kinase 2 Beta	Cytosol
CAMK1D	Calcium/Calmodulin Dependent Protein Kinase ID	Cytosol
ITGB1	Integrin Subunit Beta 1	Plasma membrane and extracellular
BEST1	Bestrophin 1	Plasma membrane
RGS14	Regulator Of G Protein Signaling 14	Plasma membrane
DGKQ	Diacylglycerol Kinase Theta	Cytosol and nucleus
HLA-G	Major Histocompatibility Complex, Class I, G	Plasma membrane
ADORA2B	Adenosine A2b Receptor	Plasma membrane

5.3.1 Expression of potential immune-checkpoints in different tumor entities

As a first validation step, the expression of candidate hits was investigated in the multiple myeloma cell line KMM-1 and different solid tumor cell lines namely M579 (melanoma), PANC-1 (pancreatic adenocarcinoma), SW480 (colon cancer) and MCF7 (breast cancer). Hits expression was measured at mRNA level using end-point (Figure 11) or quantitative PCR (data not shown). Those genes whose expression was absent in the multiple myeloma cell line (HLA-G and ADORA2B, an adenosine receptor member of the G protein-coupled receptor superfamily) were not considered for further validation, as off-target of the

siRNA might have been responsible for the phenotypic effect observed in the screenings. On the contrary, abundant gene expression was observed for PTK2B, CAMK1D, ITGB1, BEST1, RGS14 and DGKQ in the multiple myeloma cell line. The melanoma cell line M579 did not express CAMK1D while all the other tumor cell lines investigated showed a copious expression of the gene. MCF7 cells did not express PTK2B and DGKQ while very low expression of BEST1 and RGS14 was observed.

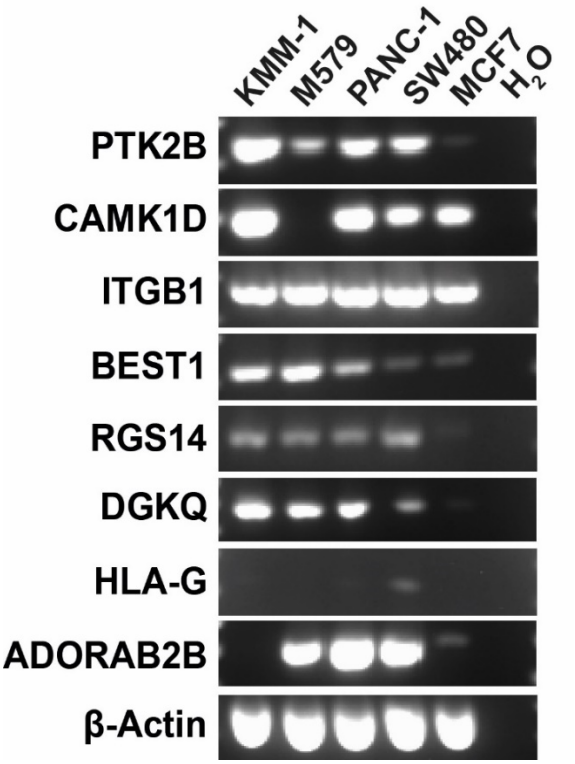

Figure 11. Expression of hits in various tumor cell lines. End-point PCR was performed in KMM-1, M579, PANC-1, SW480 and MCF7 for detection of PTK2B, CAMK1D, ITGB1, BEST1, RGS14, DGKQ, HLA-G and ADORA2B transcripts. β-actin was used as housekeeping gene. H_2O served as no template control.

5.3.2 Deconvolution assay to assess on-target of the siRNA sequences

In the HTP-screen a pool of four siRNAs was employed to target the same gene. Since single siRNA sequences out of the siRNA pools could bind in an unspecific manner to other unrelated mRNAs in the cytosol, thereby generating a false-positive result (off-target effect), the pooled siRNA sequences were "deconvoluted". To this end, KMM-1-luc cells were transfected with the pooled siRNA used in the screening or with the four single non-overlapping siRNAs out of the pool and either co-cultured with MILs or with medium control. Luciferase-based read-out was assessed and compared to CCR9 knockdown. The assay was performed for the 6 selected hits. On-target effect was only attributed to genes whose knockdown led to increase T cell-mediated killing with at least two single siRNA sequences. We further excluded siRNA sequences showing more than 30% viability effect in the absence of T cells.

We observed that the transfection of three out of four PTK2B siRNAs (s1, s2 and s3) and the pool siRNA, increased T cell mediated cytotoxicity while no viability impact of the siRNAs *per se* was detected (Figure 12A). Likewise, three siRNA sequences targeting CAMK1D improved T cell mediated tumor cell killing and no tumor cell death was observed in the viability setting (Figure 12B). RGS14 and BEST1 knockdown showed a phenotypic effect with two siRNA sequences (s2 and s3), nevertheless in both cases one siRNA sequence triggered a viability impact of about 30%, that was also visible in the pool knockdown (Figure 12C and 12D). DGKQ and in particular ITBG1 elicited a strong phenotypic effect but a drastic viability impact was observed with at least two siRNA sequences targeting DGKQ or even all four siRNA sequences targeting ITGB1 (Figure 12E and 12F). Thus, RGS14, BEST1 and DGKQ together with ITBG1 were excluded from further analysis.

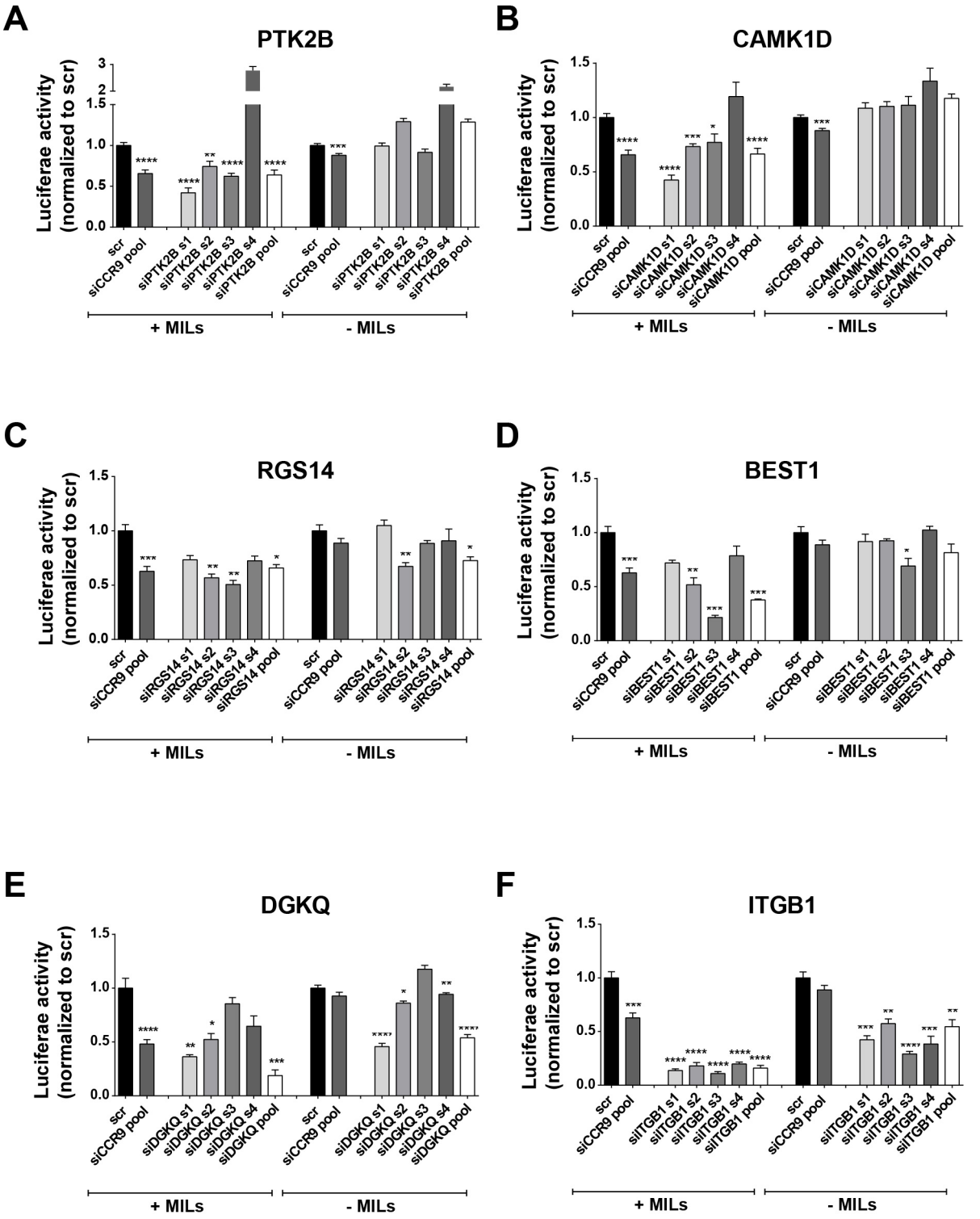

Figure 12. Validation of siRNA on-target effect. KMM-1-luc cells were transfected using single (s1, s2, s3, s4) or pooled non-overlapping siRNAs targeting **(A)** PTK2B, **(B)** CAMK1D, **(C)** RGS14, **(D)** BEST1, **(E)** DGKQ and **(F)** ITGB1. Control siRNA (scr) was used as a negative control whereas pooled siCCR9 served as positive control. Transfected cells were co-cultured with MILs at 10:1 E:T ratio for the cytotoxicity setting. For the viability setting, only culture medium was added instead of T cells. T cell-mediated cytotoxicity was measured using the luciferase-based cytotoxicity assay. Values were normalized to scr control in each setting. Graphs show median +/- SEM. Cumulative data of at least three independent experiments. P-values were calculated using two-tailed student´s t-test. * $p < 0.05$, ** $p < 0.01$, *** $p < 0.001$, **** $p < 0.0001$

Based on these data CAMK1D and PTK2B were selected for additional validation. The knockdown efficiency of deconvoluted and pooled siRNA sequences was assessed both at mRNA and protein level. For both hits all four siRNA sequences as well as the pool induced a strong reduction of gene expression (Figure 13A and B). CAMK1D knockdown also resulted in significant protein reduction with each tested siRNA sequences (Figure 13C). In line, PTK2B protein level was reduced after transfection ranging from 80% to 90%, depending on the used siRNA sequence (Figure 13D).

In summary, we successfully validated CAMK1D and PTK2B as novel regulators of T cell-mediated cytotoxicity. For each target, three non-overlapping siRNAs showed efficient gene silencing, which resulted in increased T cell mediated killing in luciferase-based assays.

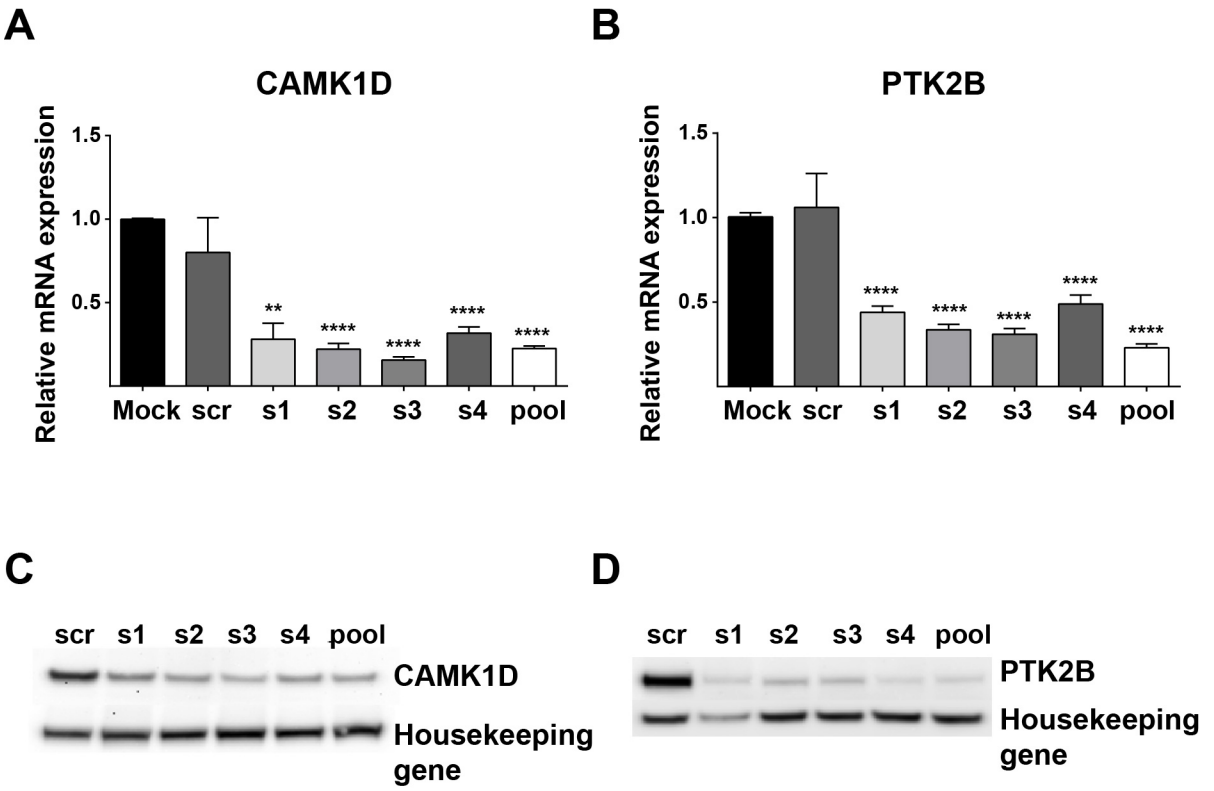

Figure 13. Evaluation of knockdown efficiency. Analysis of knockdown efficiency of siRNAs targeting **(A, C)** CAMK1D and **(B, D)** PTK2B. **(A and B)** KMM-1 cells were transfected with single (s1, s2, s3, s4) or pooled siRNAs and 48h later mRNA expression levels were determined by qPCR. Results are presented in terms of fold change after normalizing to β-actin mRNA. **(C and D)** Western blot analysis for detection of CAMK1D and PTK2B protein levels after 48h transfection of KMM-1 cells with single (s1, s2, s3, s4) or pooled siRNAs. Scramble siRNA sequence was used as negative control. The Sodium Potassium ATPase was used as housekeeping gene. **(C, D)** Representative data of at least two independent experiments. **(A, B)** Cumulative data of three independent experiments. Columns show mean +/- SEM. P-values were calculated using two-tailed student´s t-test. * $p < 0.05$, ** $p < 0.01$, *** $p < 0.001$, **** $p < 0.0001$

5.4 CAMK1D as a novel immune-checkpoint molecule in multiple myeloma

Based on the strength of the phenotype observed in the screens, as well as in the validation assays (section 5.3.2), CAMK1D was selected for detailed analysis of its function as a novel immunosuppressive protein with translational relevance. CAMK1D was the 35th strongest hit in the primary HTP-screen, whereas it was the first candidate in the secondary screen. CAMK1D is a serine/threonine protein kinase involved in the phosphorylation of different transcription factors such as CREB [192]. Analysis of patient´s tumor microarray data from the Oncomine^{TM} database, revealed CAMK1D being overexpressed not only in several multiple myeloma patients but also in B-Cell Childhood Acute Lymphoblastic Leukemia compared to healthy donors (Appendix Figure XI). Interestingly, its immune-related function in cancer evasion remained elusive for far.

5.4.1 Corroboration of CAMK1D on-target effect

As shown in the previous paragraph, CAMK1D knockdown efficiency was significantly achieved with all four siRNA sequences both at mRNA and protein level (Figure 13A and 13C) as well as three out of four siRNA sequences increased T cell mediated killing (Figure 12B). Surprisingly, although a significant knockdown was obtained with the siRNA sequence s4, no enhanced tumor cell death was observed upon co-culture with T cells. To further confirm that the outcome of CAMK1D was not the result of an off-target effect by targeting an alternative isoform of the CAMK1 family we i) investigated the expression of different CAMK1 isoforms in KMM-1 cells and ii) took advantage of small molecules targeting upstream activators of CAMK1D. The latter application will be addressed in section 5.4.7.

CAMK1D belongs to the Calcium/Calmodulin protein I family that contains four different isoforms namely CAMK1-alpha, CAMK1-beta, CAMK1-gamma and CAMK1-delta. Gene expression analysis revealed that the delta isoform is predominantly expressed by KMM-1 cells (Figure 14). On the other hand, CAMK1A isoform was expressed at very low levels while CAMK1B and CAMK1G were absent in KMM-1 cells (Figure 14). These results, together with the previous deconvolution experiments, suggest an on-target effect of the siRNA sequences to the delta isoform of the gene.

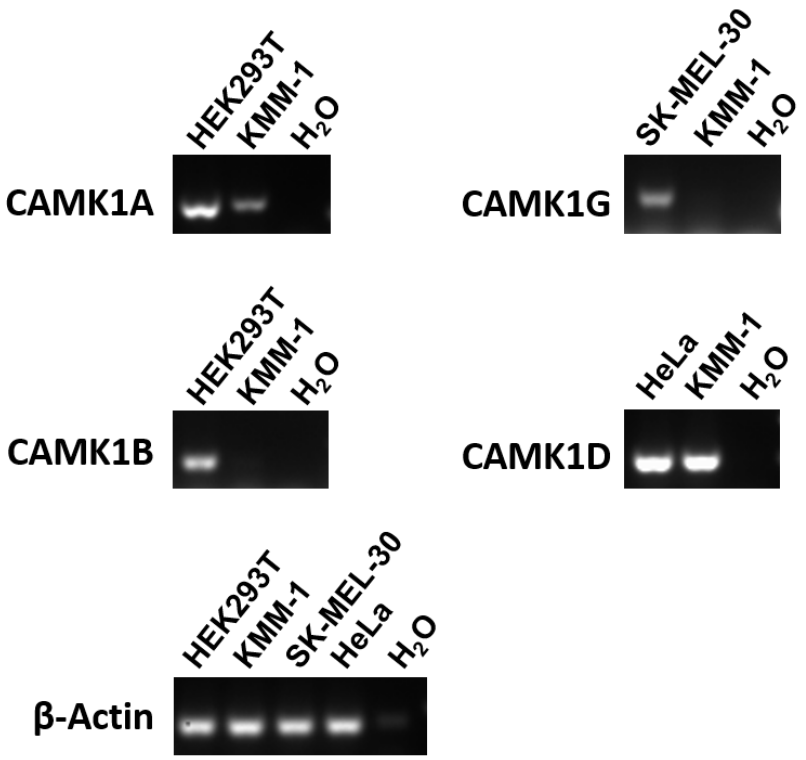

Figure 14. Gene expression of CAMK1 isoforms. End-point PCR analysis of CAMK1-alpha (CAMK1A), CAMK1-beta (CAMK1B), CAMK1-gamma (CAMK1G) and CAMK1-delta (CAMK1D) isoforms measuring mRNA abundance. HEK293T cells were used as positive cell line expressing CAMK1A and CAMK1B. The melanoma cell line SK-mel-30 was used as positive control for CAMK1G and HeLa cells were used as positive cell line expressing CAMK1D. β-actin was used as housekeeping gene. H_2O served as no template control.

5.4.2 CAMK1D knockdown increases MIL-mediated tumor lysis

To increase the confidence in CAMK1D as a reliable selected candidate gene, we took advantage of a live cell-imaging microscope to measure MIL-mediated apoptosis induction in tumor cells. By applying this method we can track tumor - T cell interactions in real-time. For this assay KMM-1 cells were either transfected with CAMK1D or scr siRNA sequences and co-cultured with MILs. A fluorescent dye (YOYO-1) was added as an indicator of apoptosis. We observed that after 16h of co-culture CAMK1D knocked down KMM-1 cells were susceptible to MIL-mediated tumor lysis reaching the highest levels after 24h of co-culture (Figure 15A and B). On the other hand, scr-transfected KMM-1 cells showed only modest tumor cell death upon co-culture with MILs. Thus, these results indicated CAMK1D to mediate resistance towards T cell attack.

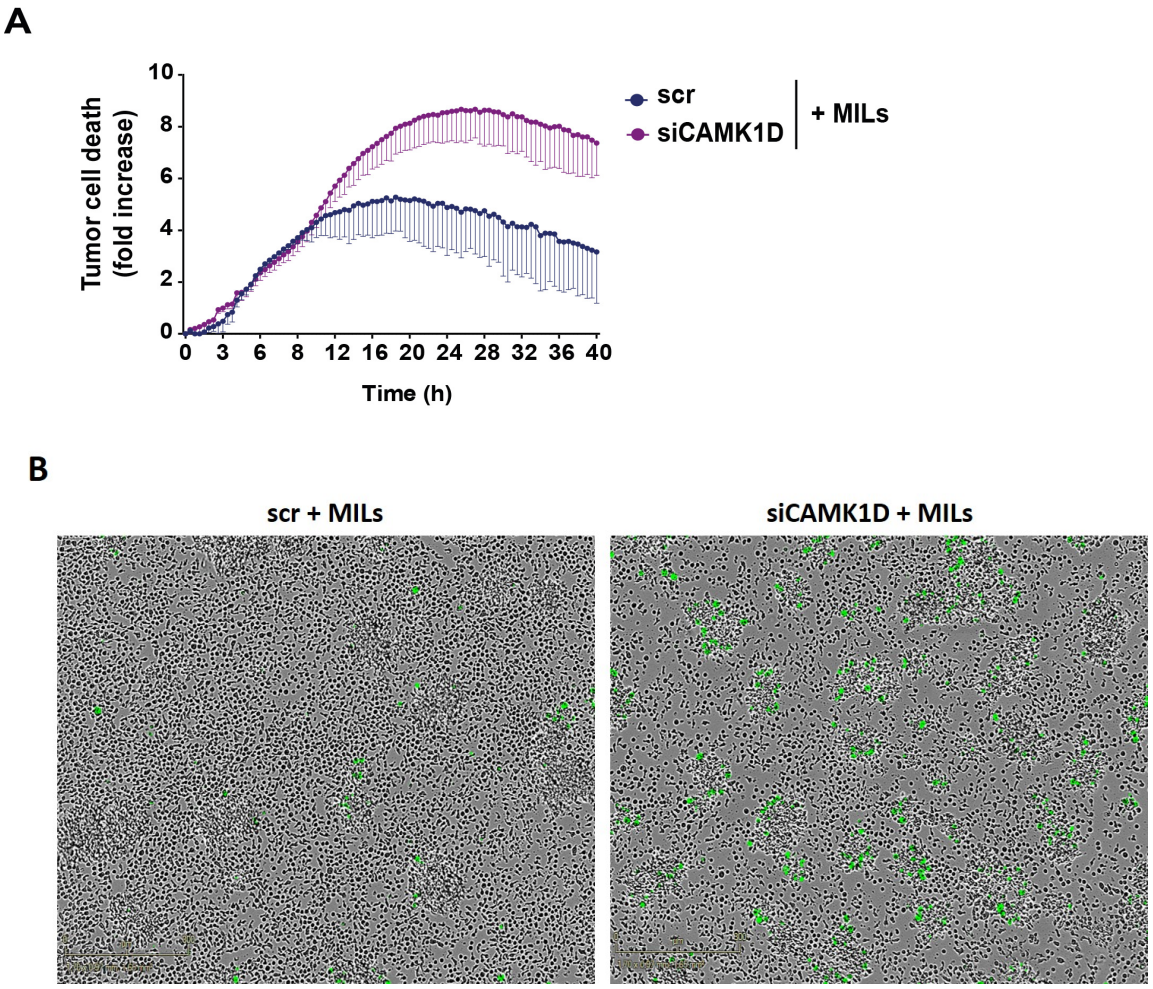

Figure 15. Assessment of T cell mediated tumor cell killing. (A) Live cell-imaging analysis. Tumor cells were transfected with CAMK1D or scr siRNA sequences. When co-cultured with MILs, a fluorescent dye (YOYO-1) was added as an indicator of apoptosis. The experiment is representative of three independent experiments. **(B)** Representative pictures from the live-cell microscopy. Left: scr-

transfected KMM-1 cells with the addition of MILs. Right: siCAMK1D transfected KMM-1 cells with the addition of MILs. YOYO-1 was added in the co-culture to detect apoptotic cells. A filtered-based mask was applied to apoptotic cells (indicated by the green color). **(A)** Values denote mean ± SEM.

5.4.3 The knockdown of CAMK1D does not increase T cell function

Next, we wanted to investigate the mode of action of CAMK1D-mediated resistance to T cell attack. Tumor cells can evade the immune system by taking advantage of different mechanisms [193, 194]. Thus, we assessed whether CAMK1D modulated T cell activity or interfered with tumor susceptibility towards T cell attack. To determine whether the knockdown of CAMK1D in tumor cells increased T cell activity and cytotoxic potential, different cytokines were measured and compared to scr transfected KMM-1 cells co-cultured with T cells. Interestingly, the knockdown of CAMK1D did not increase INF-γ, Granzyme B, IL-2 or TNF-α secretion (Figure 16A-D), suggesting that CAMK1D does not interfere with T cell activation or cytotoxicity.

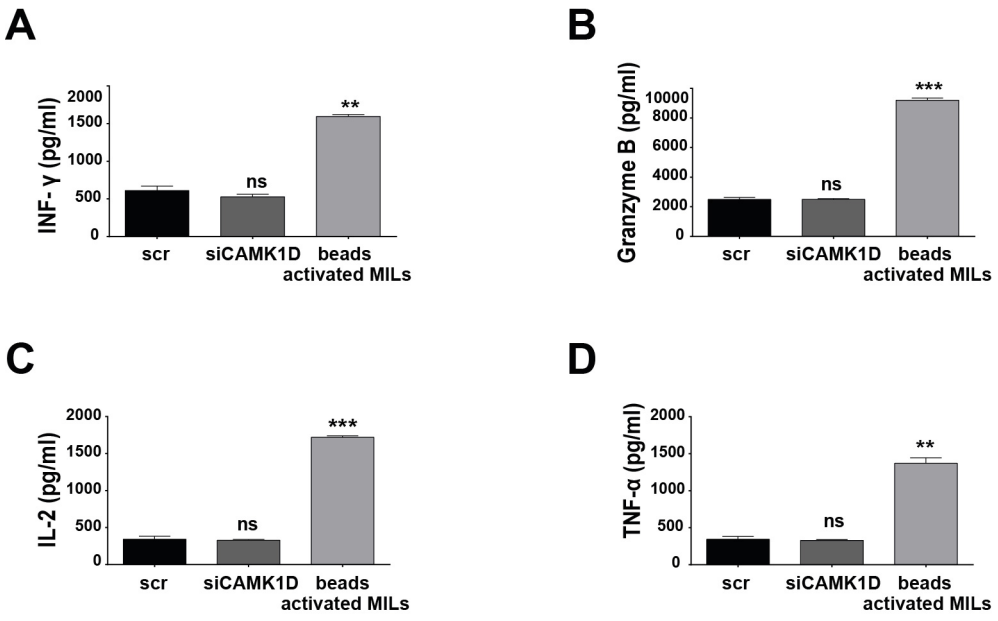

Figure 16. Silencing CAMK1D in the tumor cells does not increase T cell function. KMM-1 cells were transfected with scr or CAMK1D siRNA for 48h. Afterwards MILs were added at an E:T ratio of 10:1 and **(A)** INF-γ, **(B)** Granzyme B, **(C)** IL-2 and **(D)** TNF-α secretion was measured 20h after co-culture. Anti-CD3/anti-CD28 magnetic beads stimulation served as a positive control. Representative data of two independent experiments. Columns show mean +/- SD. P-values were calculated using two-tailed student´s t-test. * $p \leq 0.05$; ** $p \leq 0.01$; *** $p \leq 0.001$.

5.4.4 The knockdown of CAMK1D sensitizes tumor cells towards ligands expressed on T cells

Although we consistently detected increased T cell mediated tumor cell killing after CAMK1D knockdown in KMM-1 cells, functional analysis of T cells did not reveal any increased T cell function after interaction with CAMK1D-deficient tumor cells. We therefore hypothesized that CAMK1D might desensitize myeloma cells against T cell-derived effector molecules and therefore we exposed KMM-1 cells to recombinant FasL (rHuFasL), TRAIL (rHuTRAIL) or TNF (rHuTNF). These antibodies/proteins mimic ligands expressed on- or factors released by- T cells. Recombinant FasL and, to a much lesser degree recombinant TRAIL, induced a dramatic reduction of luciferase activity in CAMK1D knocked down MM cells but not in CAMK1D-proficient cells (Figure 17). In line with the secondary screening, where only the supernatant of activated T cells was added to the knocked down tumor cells, silencing of CAMK1D and exposure to recombinant TNF, an effector molecule secreted by T cells, did not show an effect on tumor cell death. Thus, these results suggest that CAMK1D mediates intrinsic tumor resistance to Fas-signaling induced by activated T cells.

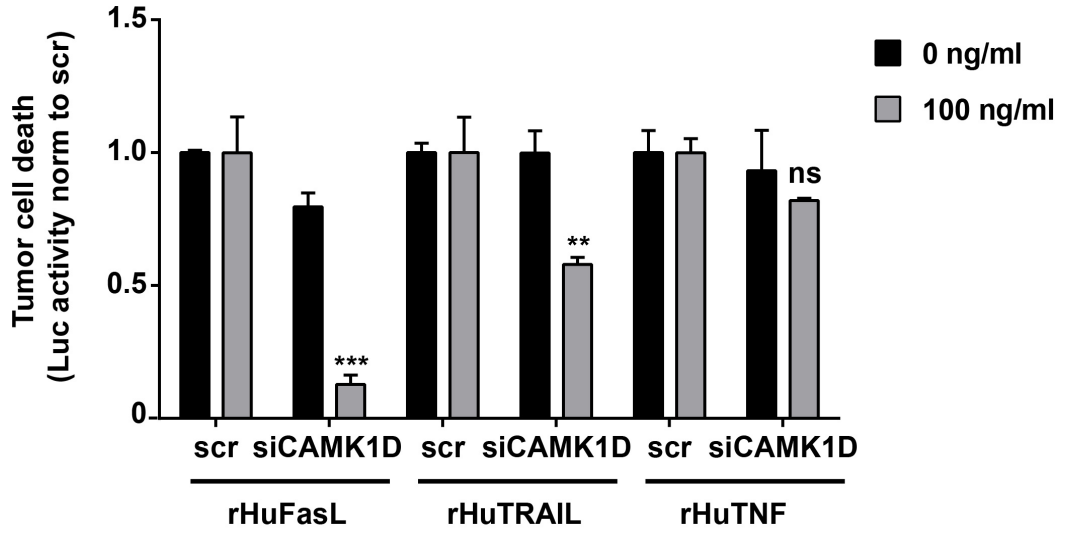

Figure 17. Assessment of susceptibility to ligands expressed on/or cytokines released by T cells. KMM-1-luc cells were transfected with scr or CAMK1D siRNAs and treated with recombinant FasL, TRAIL or TNF. Luciferase activity was measured after 20h of treatment. Experiments were performed in triplicates and representative results of three independent experiments are shown. Values denote mean ± SEM, and statistical significance was calculated using unpaired, two-tailed Student's t-test with * $p \leq 0.05$; ** $p \leq 0.01$; *** $p \leq 0.001$.

5.4.5 Recombinant FasL mimics T cell mediated killing of multiple myeloma cells

In order to confirm Fas ligand (FasL) as the main effector molecule in KMM-1 – T cell interactions we investigated the expression of Fas receptor (Fas) and FasL on tumor cells and T cells, respectively. We observed that 100% of the tumor cells expressed Fas and 28,2% and 16,1% of CD4 and CD8 T cells in the MIL preparations expressed the corresponding ligand, respectively (Figure 18A). To further confirm the relevance of the Fas pathway, we took advantage of a live cell-imaging microscope to measure Fas-mediated apoptosis induction in tumor cells. We observed that after 15h of rHuFasL exposure CAMK1D knocked down KMM-1 cells were susceptible to tumor cell death at a higher degree compared to scr and siCCR9-transfected tumor cells (Figure 18B). Real-time live-cell microscope was used to determine the kinetic of rHuFasL-mediated cytotoxicity and to compare cell death to untreated tumor cells (Figure 18C). In line with this, we found that U266 myeloma cells expressed CAMK1D (Figure 18D) and similar to KMM-1 cells the knockdown was successfully achieved (Figure 18E). Moreover, the addition of rHuFasL showed a strong impact on tumor cell death upon CAMK1D knockdown compared to scr-transfected cells (Figure 18F).

Finally, to corroborate FasL as the effector molecule inducing tumor cell death, we blocked FasL expressed on the T cells *via* a FasL neutralizing antibody. Knocked down tumor cells were co-culture with MILs together with an isotype control, whereby the expected increased tumor cell killing was observed in CAMK1D knocked down tumor cells compared to scr control. Remarkably, when tumor cells were co-cultured with MILs together with a FasL neutralizing antibody a complete rescue of tumor cell death was observed regardless CAMK1D knockdown (Figure 18G). Altogether these results corroborate FasL as the main effector molecule through which the T cells kill the tumor cells.

A

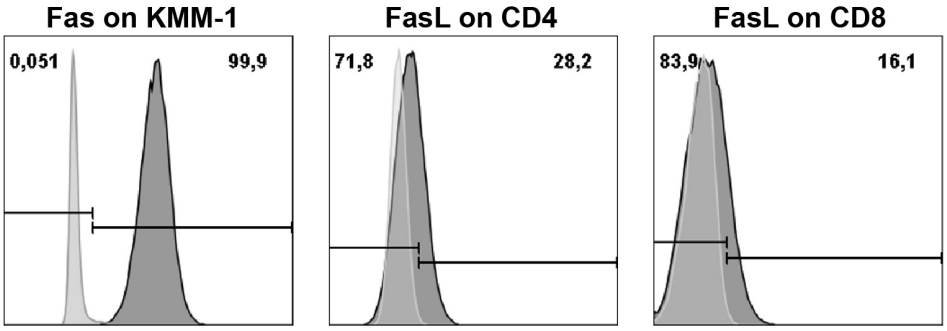
Fas on KMM-1
0,051
99,9
FasL on CD4
71,8
28,2
FasL on CD8
83,9
16,1

B

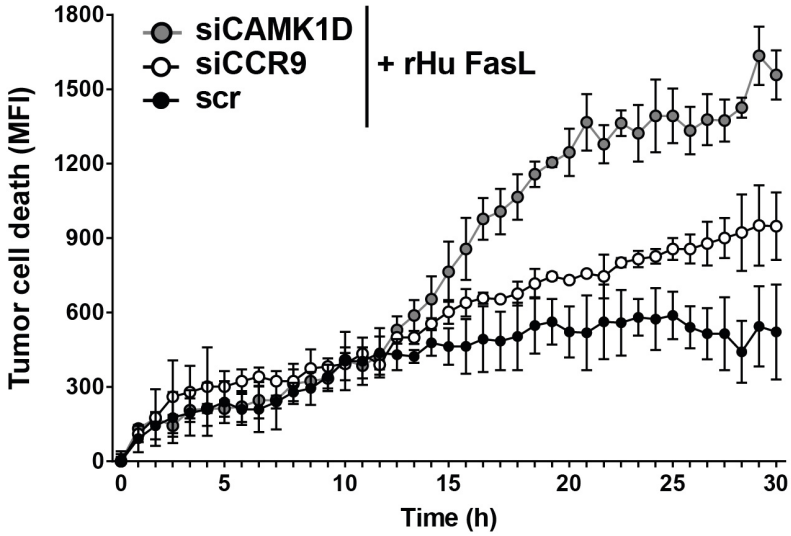
siCAMK1D
siCCR9
scr
+ rHu FasL
Tumor cell death (MFI)
1800
1500
1200
900
600
300
0
0
5
10
15
20
25
30
Time (h)

C

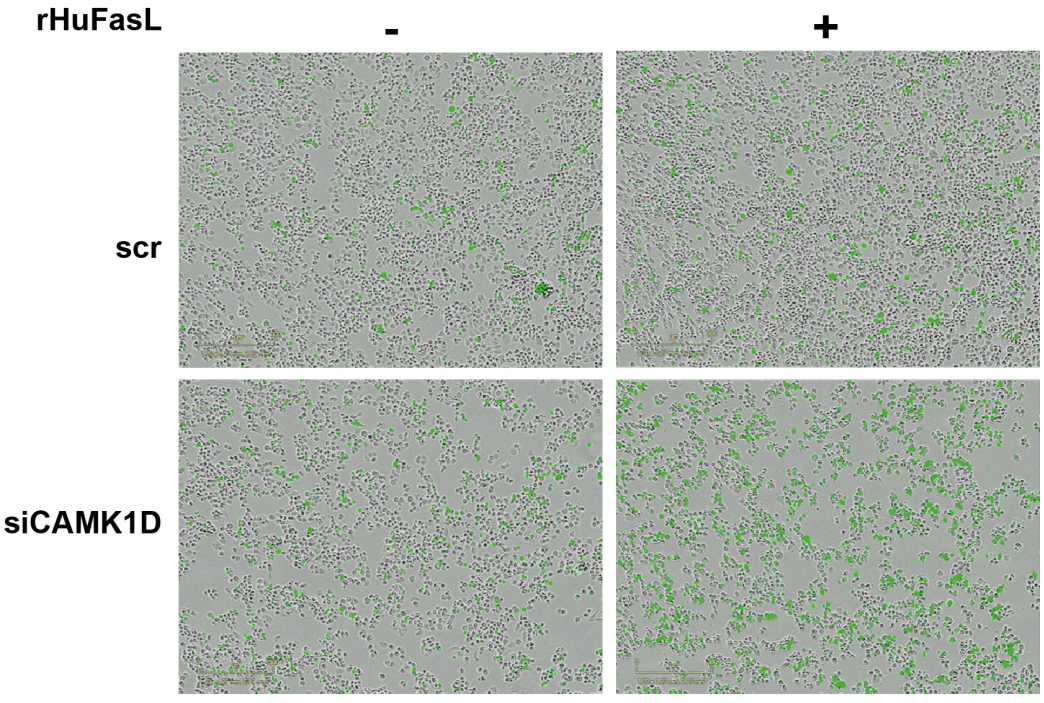
rHuFasL
-
+
scr
siCAMK1D

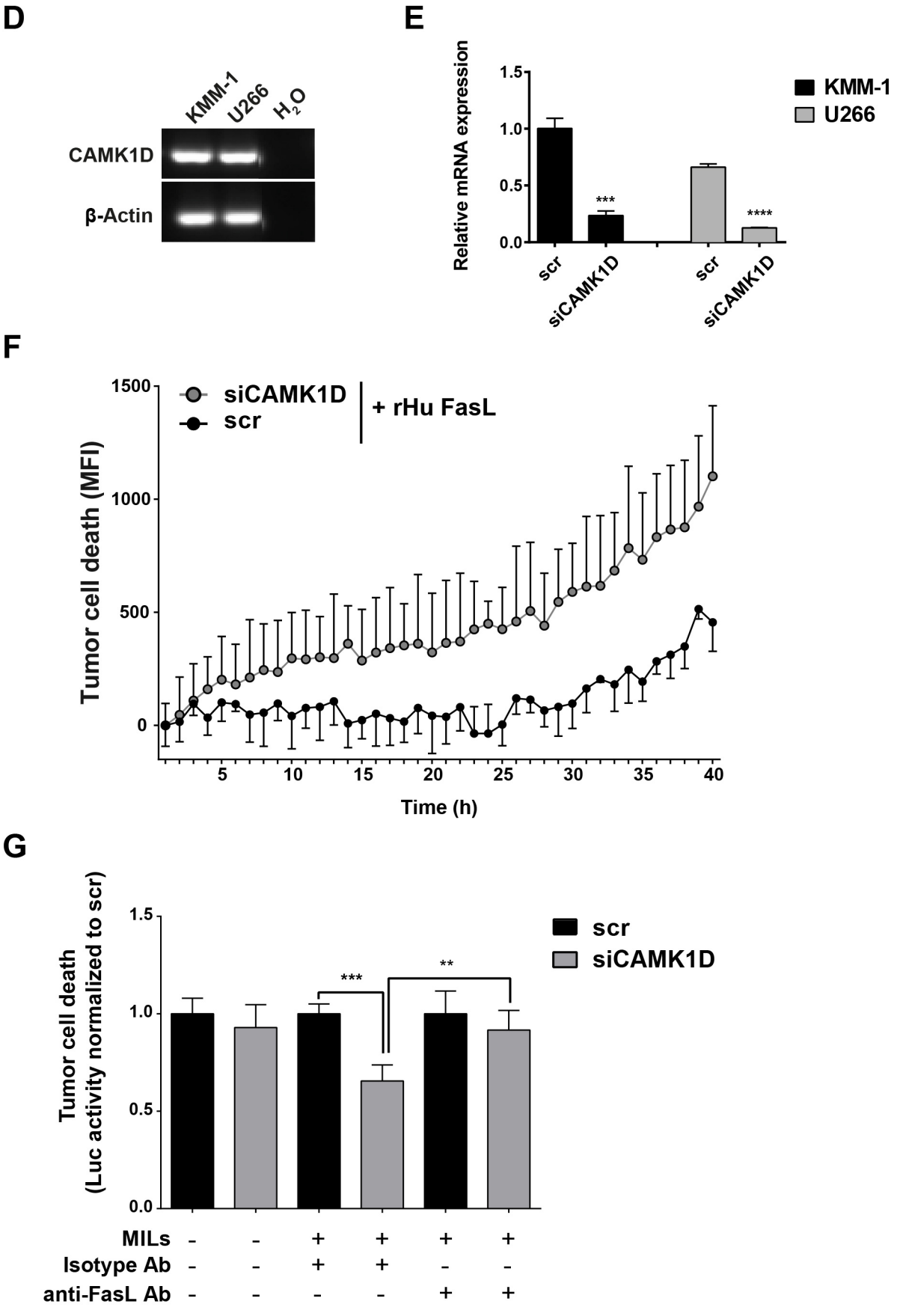
D
KMM-1
U266
H2O
CAMK1D
β-Actin
E
Relative mRNA expression
1.5
1.0
0.5
0.0
***
****
scr
siCAMK1D
scr
siCAMK1D
KMM-1
U266
F
siCAMK1D
scr
+ rHu FasL
Tumor cell death (MFI)
1500
1000
500
0
5
10
15
20
25
30
35
40
Time (h)
G
Tumor cell death
(Luc activity normalized to scr)
1.5
1.0
0.5
0.0
***
**
scr
siCAMK1D
MILs - - + + + +
Isotype Ab - - + + - -
anti-FasL Ab - - - - + +

Figure 18. FasL is the main effector molecule inducing tumor cell death in MM cells. (A) Representative FACS analysis of Fas and FasL expression. Tumor cells and T cells were stained with conjugated antibodies against Fas and FasL. Cell surface expression was measured by flow cytometry. Histograms show the percentage of Fas positive KMM-1 cells as well as CD4 and CD8 positive FasL cells (dark grey histograms). Isotype controls are shown in light grey. **(B)** Live cell-imaging analysis showing KMM-1 tumor cells transfected with siCAMK1D, siCCR9 or scr siRNA sequences upon exposure to rHuFasL. A fluorescent dye (YOYO-1) was added as an indicator of apoptosis. A filtered-based mask was applied to apoptotic cells (indicated by the green color). **(C)** Real-time live-cell imaging showing scr and siCAMK1D transfected KMM-1 cells 30h upon 100 ng/ml rHuFasL or medium control. YOYO-1 depicts apoptotic cells (shown in green). A filtered-based mask was applied to apoptotic cells (indicated by the green color). **(D)** End-point PCR analysis of CAMK1D expression in U266 cells. KMM-1 cells were used as positive control. β-actin was used as housekeeping gene. H_2O served as no template control. **(E)** Quantitative PCR (qPCR) showing CAMK1D knockdown efficiency in KMM-1 and U266 cell lines. Results are presented in terms of fold change after normalization to β-actin mRNA. **(F)** Live-cell imaging analysis showing scr and siCAMK1D transfected U266 cells upon 100 ng/ml rHuFasL. A fluorescent dye (YOYO-1) was added as an indicator of apoptosis. **(G)** Luciferase-based assay: scr or siCAMK1D transfected MILs were co-cultured with a FasL neutralizing (anti-FasL) antibody or with an isotype control. Loss of luciferase activity is measured. **(B, F, G)** Representative experiment of three independent experiments. Values denote mean ± SEM and statistical significance was calculated using unpaired, two-tailed Student's t-test with * $p \leq 0.05$; ** $p \leq 0.01$; *** $p \leq 0.001$.

5.4.6 CAMK1D knockdown induces tumor cell death in different tumor entities and with different T cell sources

As shown in section 5.3.1, CAMK1D expression was detected in different solid tumors (PANC-1 and MCF-7) (Figure 11) and in the multiple myeloma cell lines KMM-1 and U266 (Figure 18D). Although expressed in different tumor entities, the knockdown of CAMK1D in the solid tumor cell lines PANC-1 and MCF-7 did not show any effect on T cell-mediated tumor cell death (data not shown). Interestingly, here we observed that Fas expression was very low compared to myeloma cells (Figure 19A). These results suggest that Fas expression is indispensable for MILs-mediated killing of CAMK1D deficient tumor cells. Although CAMK1D was not expressed in the melanoma cell line M579 (Figure 11) we found CAMK1D expression in uveal melanoma cells. Thus, we tested CAMK1D and Fas expression in the uveal melanoma cell line Mel27c. Both, CAMK1D (Figure 19B) and Fas (Figure 19C) were found to be expressed in Mel27c cells. Moreover, by taking advantage of the live-cell imaging microscope, we observed that the addition of rHuFasL to CAMK1D knocked down tumor cells triggered increased apoptosis compared to scr-transfected Mel27c cells (Figure 19D and E). A negligible viability impact was detected by the siRNA *per se* in this cell line as well (Figure 19D and E).

To corroborate these findings, we analyzed RNA-Seq data from the TCGA database. Interestingly, we found that high levels of CAMK1D expression in uveal melanoma patients correlated with poor prognosis, while patients with low levels of CAMK1D showed increased survival (Figure 19F).

Furthermore, to confirm that CAMK1D knockdown sensitizes tumor cells to FasL, an additional T cell source was utilized. To this end, influenza-specific T cells (FluT cells) that recognize flu-specific peptide presented by HLA-A2 were co-cultured with KMM-1 cells. Before the co-culture, knocked down tumor cells were pulsed with different flu-peptide concentrations. In this setup, the presence or absence of the peptide ensures the interaction of the TCR with the HLA-A2 molecule. FluT cells were co-cultured for 20h with scr or CAMK1D knocked down tumor cells at an E:T ratio of 10:1. Similar to KMM-1 cells co-cultured with patient derived MILs, or U266 cells exposed to rHuFasL, the knockdown of CAMK1D induced an increased tumor cell death compared to CAMK1D-proficient cells upon co-culture with FluT cells (Figure 19G). Flow cytometry-analysis revealed that like MILs, FluT cells express 12,7% of FasL on the surface (Figure 19H), consequently being able to induce the Fas-signaling pathway in the Fas expressing tumor cell line KMM-1.

In summary, we identified CAMK1D as potential immune-checkpoint molecule in two different multiple myeloma cell lines as well as in the uveal melanoma cell line Mel27c, whose knockdown increases susceptibility towards different T cell sources namely MILs and FluT cells, both inducing Fas-mediated apoptosis of the tumor cells.

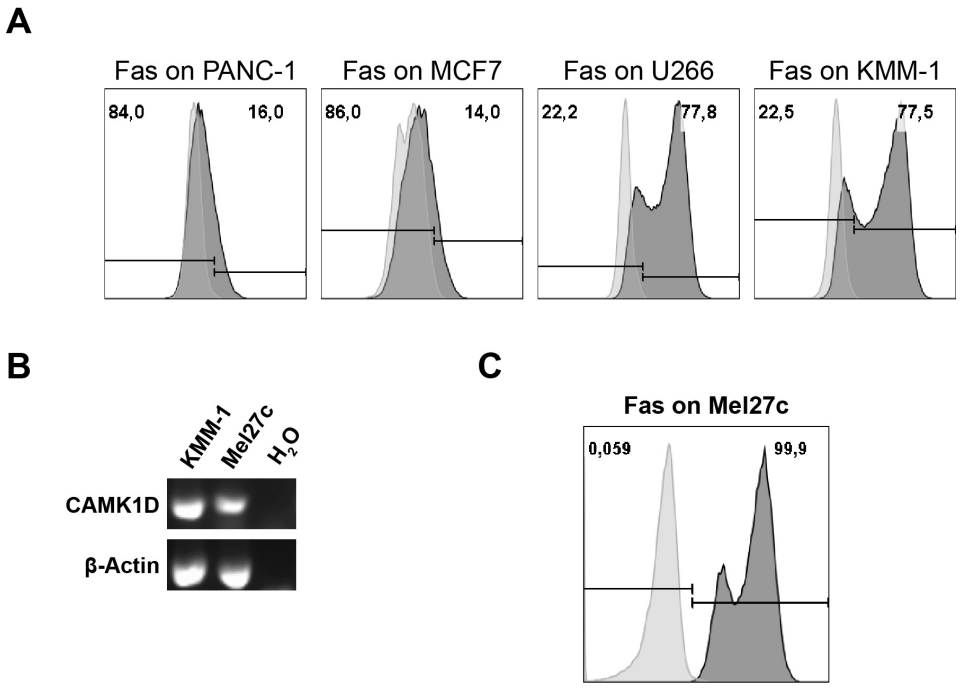
A
Fas on PANC-1
84,0
16,0
Fas on MCF7
86,0
14,0
Fas on U266
22,2
77,8
Fas on KMM-1
22,5
77,5
B
KMM-1
Mel27c
H2O
CAMK1D
β-Actin
C
Fas on Mel27c
0,059
99,9
D
Tumor cell death (MFI)
3×10^7
2×10^7
1×10^7
0
0 2 4 6 8 10 12 14 16 18 20 22 24 26 28 30
Time (h)
scr
siCAMK1D
+ rHuFasL
scr
siCAMK1D
E
rHuFasL
-
+
scr
siCAMK1D

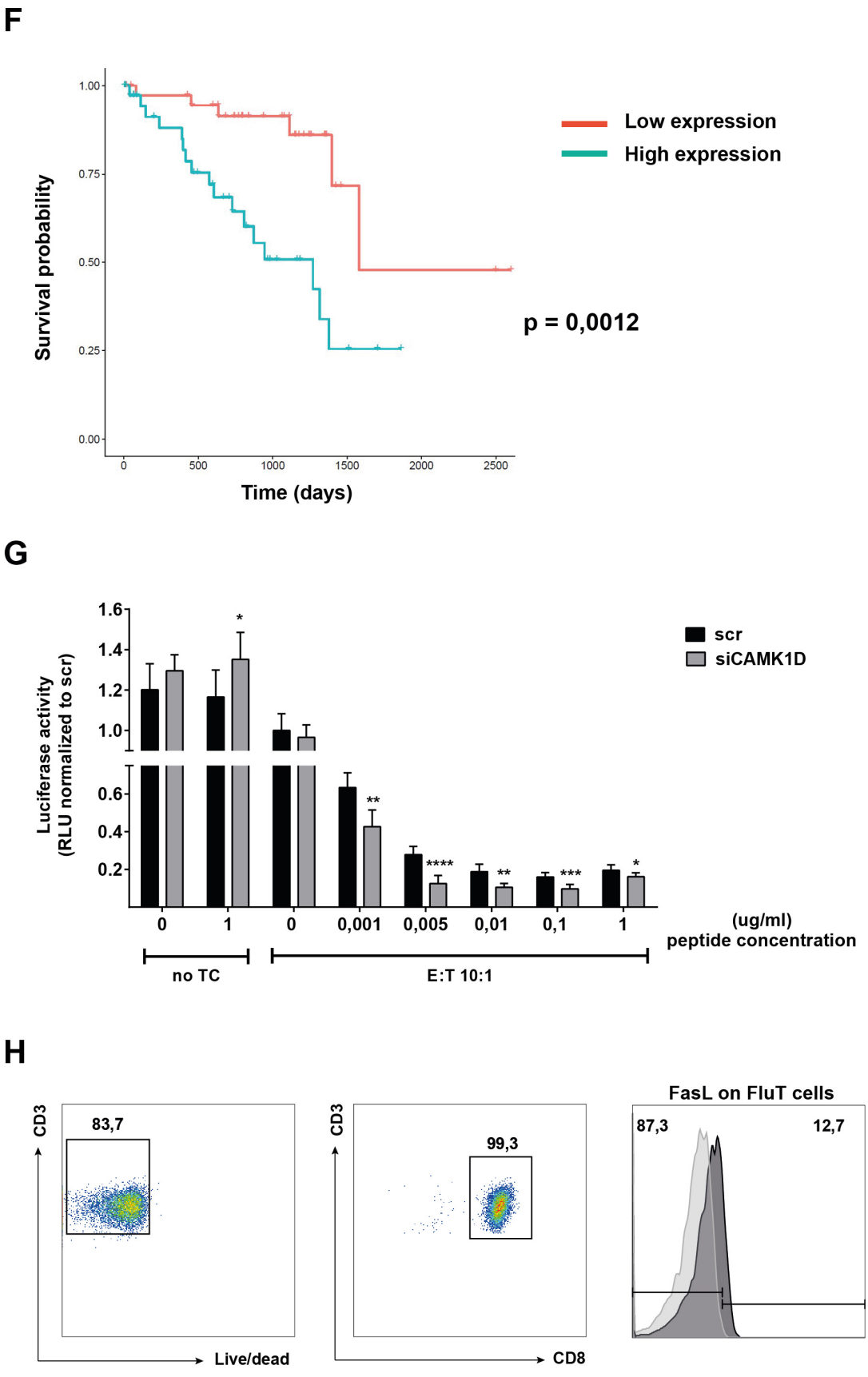

Figure 19. Effect of CAMK1D knockdown in different tumor entities and upon distinct T cell sources. (A) Representative FACS analysis of Fas expression in PANC-1, MCF7, U266 and KMM-1

cells. Tumor cells were stained with conjugated antibodies against Fas. Cell surface expression was measured by flow cytometry. Histograms show the percentage of Fas positive tumor cells (dark grey histograms). Isotype controls are shown in light grey. **(B)** End-point PCR showing CAMK1D expression in the uveal melanoma cell line Mel27c. KMM-1 multiple myeloma cells were used as positive control. β-actin was used as housekeeping gene. Water served as no template control **(C)** Representative FACS analysis of Fas expression on Mel27c cells. Tumor cells were stained with conjugated antibodies against Fas. Cell surface expression was measured by flow cytometry. Histograms show the percentage of Fas positive Mel27c cells (dark grey histograms). Isotype control is shown in light grey. **(D)** Live cell-imaging analysis showing uveal melanoma cells transfected with siCAMK1D or scr siRNA sequence upon exposure to rHuFasL. A fluorescent dye (YOYO-1) was added as an indicator of apoptosis. Knockdown of CAMK1D increased Mel27c cell lysis compared to scr control. The experiment is representative of two independent experiments. Values denote mean ± SEM. **(E)** Representative pictures from the live-cell microscopy. Upper panels: scr-transfected Mel27c cells with or without the addition of rHuFasL. Bottom panels: siCAMK1D transfected Mel27c cells with or without the addition of rHuFasL. YOYO-1 was added in the co-culture to detect apoptotic cells. A filtered-based mask was applied to apoptotic cells (indicated by the green color). **(F)** Correlation of CAMK1D expression and patient survival in UVM. Uveal melanoma patients were divided in CAMK1D high and low expression according to the median of CAMK1D expression. Kaplan-Meier curves showing the correlation between CAMK1D expression and patients' survival probability were generated using TCGA clinical data. Significance was calculated using the log-rank test. The analysis was performed by Dr. Tillmann Michels (AG Beckhove, RCI Regensburg). **(G)** KMM-1-luc were pulsed with different concentrations (0,001; 0,005; 0,01; 0,1 and 1 µg/ml) of flu-derived peptide for 1 hour before co-culture with flu-specific T cells or medium control (viability setting) for 20 h. T cell-mediated lysis or viability impact of target knockdown was measured by luciferase assay. Flu-specific T cells and peptides were generated by Ayse Nur Menevse (RCI, Regensburg). **(H)** Representative FACS analysis of FasL expression on FluT cells. T cells were stained with conjugated antibodies against CD3, CD8 and FasL. Dead cells were excluded by using Live/dead Zombie dye. Cell surface expression was measured by flow cytometry. Histograms show the percentage of FasL positive CD8 FluT cells (dark grey histograms). Isotype control is shown in light grey. Experiment was performed in collaboration with Dr. Slava Stamova (AG Beckhove, RCI, Regensburg)**. (G)** Experiment was performed in triplicate. Representative result of at least two independent experiments. Error bars denote ± SD, and statistical significance was calculated using unpaired, two-tailed Student's t-test with * $p \leq 0.05$; ** $p \leq 0.01$; *** $p \leq 0.001$; **** $p \leq 0.0001$. Experiment was performed in collaboration with Ayse Nur Menevse (AG Beckhove, RCI Regensburg).

5.4.7 Inhibition via small molecules recapitulates CAMK1D tumor cell killing upon siRNA gene silencing

As mentioned in section 5.4.1, the confirmation of an on-target effect of the siRNA sequences is pivotal for the validation of a potential immune-checkpoint. Accordingly, targeting the selected candidate at protein level would prove CAMK1D as potential therapeutic target in multiple myeloma patients.

Due to the lack of CAMK1D specific small molecules, we decided to target upstream activators of CAMK1D. CAMK1D is a protein kinase dependent on calmodulin (CaM) binding thereby inducing a conformational change allowing the CAMK-kinase (CAMKK) to phosphorylate and fully activate CAMK1D. Thus, we took advantage of the cell permeable calmodulin antagonist W7 that blocks calmodulin interactions with target proteins by binding to calcium-binding domains in each calmodulin molecule [195], to investigate whether we were able to recapitulate the effect observed in CAMK1D-deficient cells. To this end, CAMK1D-proficient cells were treated with increasing concentrations of anti-calmodulin small molecule compound and either exposed to rHuFasL or to medium control. Only CAMK1D-proficient cells treated with rHuFasL and the small molecule exhibited the same tumor cell susceptibility towards rHuFasL as CAMK1D knocked down tumor cells *via* siRNA. Interestingly, the additional knockdown of CAMK1D in tumor cells co-cultured with anti-calmodulin and exposed to rHuFasL did not display a significant additive effect, suggesting CAMK1D to be the decisive target of calmodulin (Figure 20A).

Driven by these results we decided to target CAMKK to investigate whether the inhibition of the kinase responsible for CAMK1D complete activation increases tumor susceptibility towards rHuFasL stimulation as well. To this end, we exploited the use of the small molecule compound STO609, a selective, cell-permeable inhibitor of Ca^{2+}-calmodulin-dependent protein kinase kinase that competes for the ATP-binding site. The effects observed were weaker compared to W7 small molecule. Indeed, in CAMK1D proficient cells only a concentration of 2 μM of STO609 induced an increased tumor cell death when rHuFasL was added to the co-culture. Interestingly, this concentration caused the same tumor cell susceptibility towards rHuFasL as the knockdown of CAMK1D induced by siRNA and rHuFasL stimulation (Figure 20B). Altogether these results support CAMK1D to play a specific role in tumor escape mechanisms.

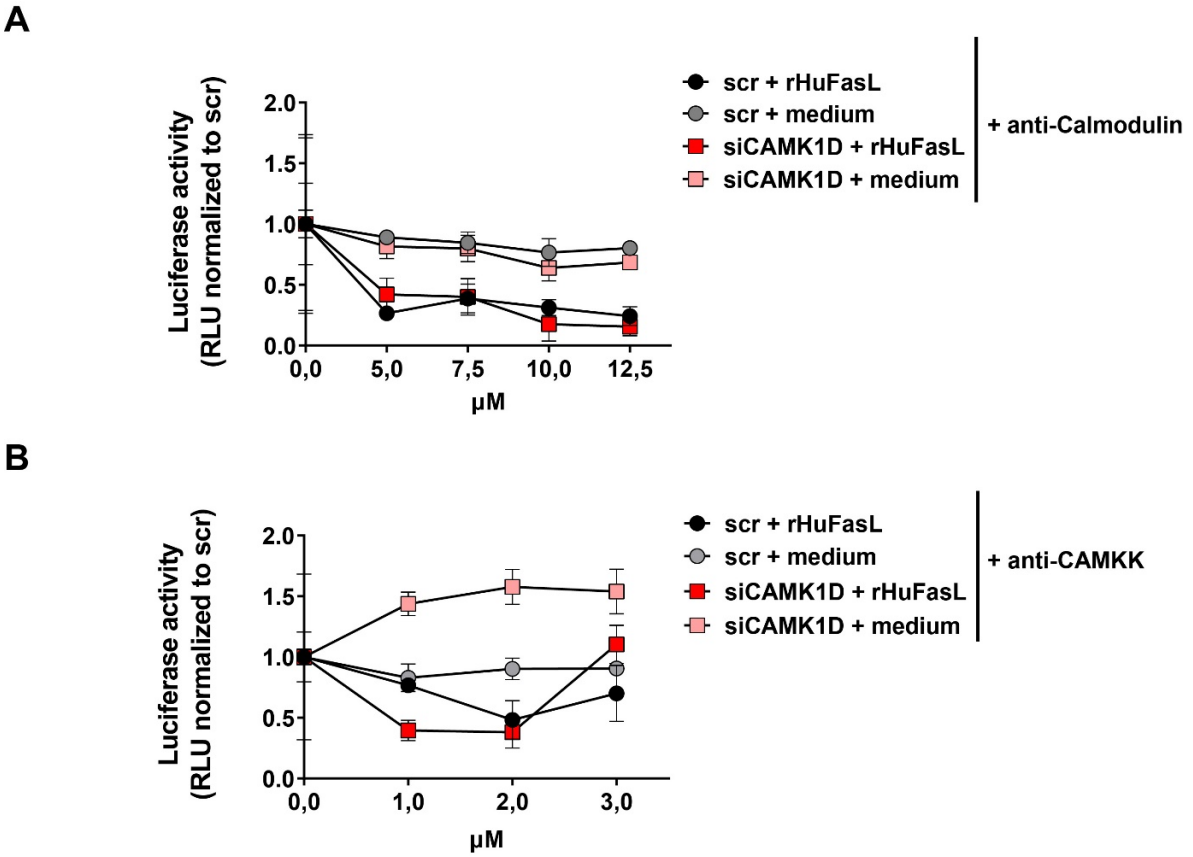

Figure 20. CAMK1D inhibition via small molecules. CAMK1D proficient and deficient KMM-1-luc cells were treated with the indicated concentrations of **(A)** Calmodulin inhibitor (W7 compound) or **(B)** CAMKK inhibitor (STO609) for 20h. Either rHuFasL or medium control was added to the culture upon 30min pre-incubation of the inhibitors with the tumor cells. Cytotoxicity was measured by luciferase-based killing assay and data were normalized using the cytotoxicity/viability ratio. Representative results of at least three independent experiments. Graphs show mean +/- SD.

5.4.8 CAMK1D hampers FasL induced apoptosis

FasL binding to Fas receptor results in complex signaling events leading on the one hand to caspases activation that mediates cell apoptosis and on the other hand to Ca^{2+} influx in the cytoplasm, which has been shown among others to activate CAMK1D [196, 197]. To investigate the mode of action of CAMK1D in the Fas-signaling cascade, Luminex assays were performed, where different apoptosis or phosphorylated proteins were simultaneously measured. To this end, CAMK1D-proficient and -deficient cells were stimulated with rHuFasL for different time frames. We observed a strong increase in caspase-3 activation starting 1h upon rHuFasL stimulation, which showed a peak upon 2h in CAMK1D knockdown KMM-1 cells compared to CAMK1D proficient cells. Caspase-3 activation gradually decreased after 4h and 8h rHuFasL stimulation (Figure 21A). In line, we observed that the levels of phosphorylated thus, activated Bcl-2, an anti-apoptotic protein, were maintained in CAMK1D proficient cells regardless of rHuFasL stimulation. On the contrary, upon CAMK1D knockdown, the levels of Bcl-2 significantly dropped for all measured time-points (Figure 21B). Moreover, we also observed that the phosphorylation, and therefore activation of the transcription factor cAMP response element-binding protein (CREB), was increased in CAMK1D-proficient cells (Figure 21C). This is in line with the higher/maintained expression of Bcl-2 in CAMK1D proficient cells since CREB is responsible for the transcription of the anti-apoptotic molecule [198]. The Extracellular Signal-regulated Kinases, ERK1/2, have a known role in cellular proliferation, differentiation, and survival, and their inappropriate activation is a common occurrence in human cancers [199]. We observed that at early time-points (15min, 30min and 1h) of rHuFasL stimulation the phosphorylation and thus activation levels of these kinases were enhanced in wild-type cells, while the knockdown of CAMK1D re-established basal levels (Figure 21D). The altered activation of the presented proteins implies that CAMK1D plays a role in interfering with the apoptotic machinery of KMM-1 cells leading to tumor cell resistance towards FasL stimulation.

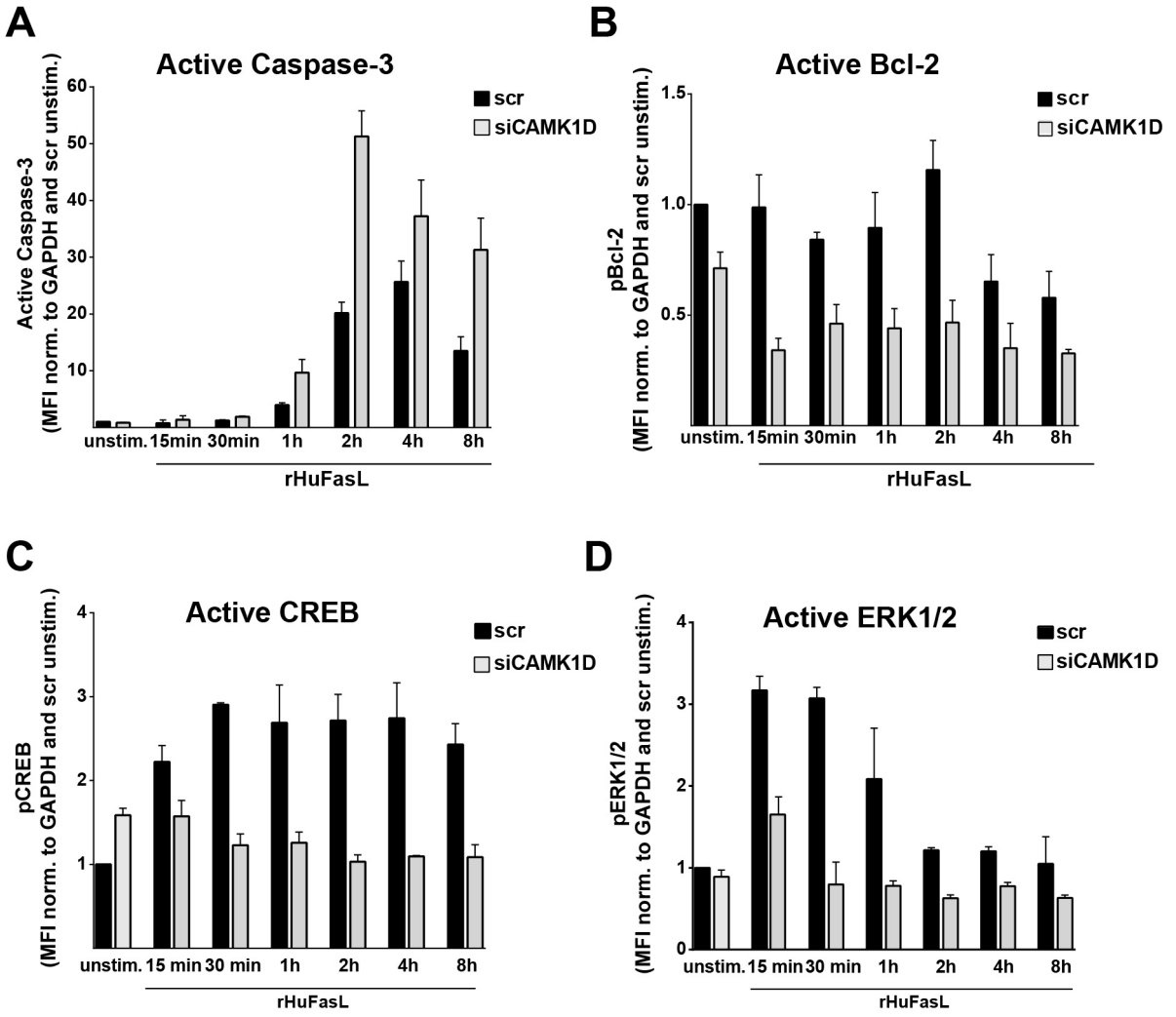

Figure 21. Luminex assay measuring apoptosis and phosphorylated proteins. CAMK1D-proficient and -deficient cells were stimulated with rHuFasL for different time frames (15min, 30min, 1h, 2h, 4h and 8h). Protein levels were normalized to GAPDH and compared to scr-unstimulated cells. The amount of **(A)** activated caspase-3 **(B)** pBcl-2, **(C)** pCREB and **(D)** pERK1/2 was measured. The experiment is representative of three independent experiments. Values denote mean ± SD.

5.4.9 CAMK1D interferes with effector caspases

As mentioned in the previous paragraph, FasL stimulation can trigger caspases activation leading to programmed cell death. In the Luminex analyses we did not observe a difference in the activation of the initiator caspases, caspase-8 and caspase-9 (data not shown) in CAMK1D-proficient vs. -deficient cells. Thus, we hypothesized that CAMK1D may interfere with downstream effector caspases as first observed in the Luminex analyses for caspase-3 activation. Caspases are synthesized within the cell as inactive zymogens lacking protease activity. In particular the effector caspases, caspase-3, caspase-6 and caspase-7 are produced as inactive pro-caspase homodimers that need to be cleaved from initiator caspases between the large and the small subunit to allow the formation of a functional mature protease [200]. To further validate the results observed in the Luminex analyses we performed a flow cytometry analysis measuring the levels of active caspase-3. For this purpose, CAMK1D-proficient and -deficient KMM-1 cells were stimulated with rHuFasL and the percentage of active caspase-3 was measured. In line with the Luminex analyses, upon 2h a two-fold increase of active caspase-3 was measured and showed a peak at 4h rHuFasL stimulation in CAMK1D-deficient cells. Increased levels of active caspase-3 were maintained for all subsequent measured time-points in CAMK1D knocked down tumor cells compared to proficient cells (Figure 22A). Likewise, via western blot analysis we were able to detect an increased protein level of caspase-3 cleavage at 2h and 4h rHuFasL stimulation (Figure 22B). Furthermore, not only an increased cleavage thus activation of caspase-3 was observed in CAMK1D-deficient cells compared to CAMK1D proficient cells upon rHuFasL stimulation, but also enhanced cleavage levels of caspase-6 and caspases-7 were present after 2h and 4h (Figure 22C and 22D). These results suggest that CAMK1D regulates these effector caspases.

A

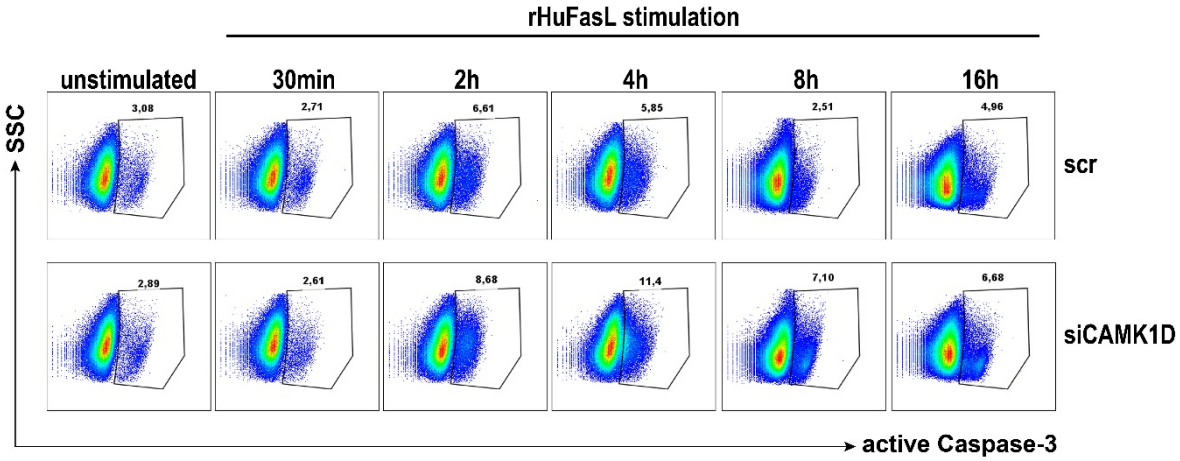
rHuFasL stimulation
unstimulated
30min
2h
4h
8h
16h
SSC
3,08
2,71
6,61
5,85
2,51
4,96
scr
2,89
2,61
8,68
11,4
7,10
6,68
siCAMK1D
active Caspase-3

B

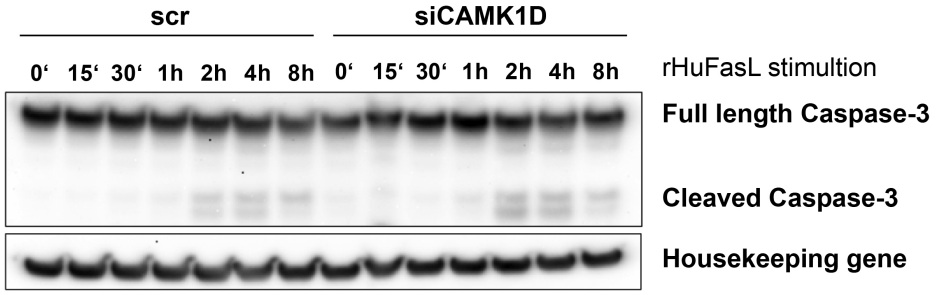
scr
siCAMK1D
0‘ 15‘ 30‘ 1h 2h 4h 8h 0‘ 15‘ 30‘ 1h 2h 4h 8h
rHuFasL stimultion
Full length Caspase-3
Cleaved Caspase-3
Housekeeping gene

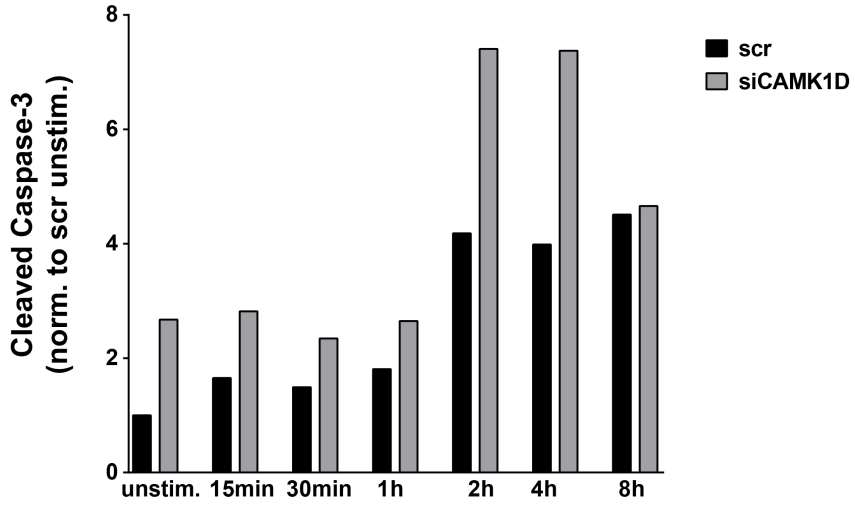
Cleaved Caspase-3
(norm. to scr unstim.)
0
2
4
6
8
unstim.
15min
30min
1h
2h
4h
8h
scr
siCAMK1D

C

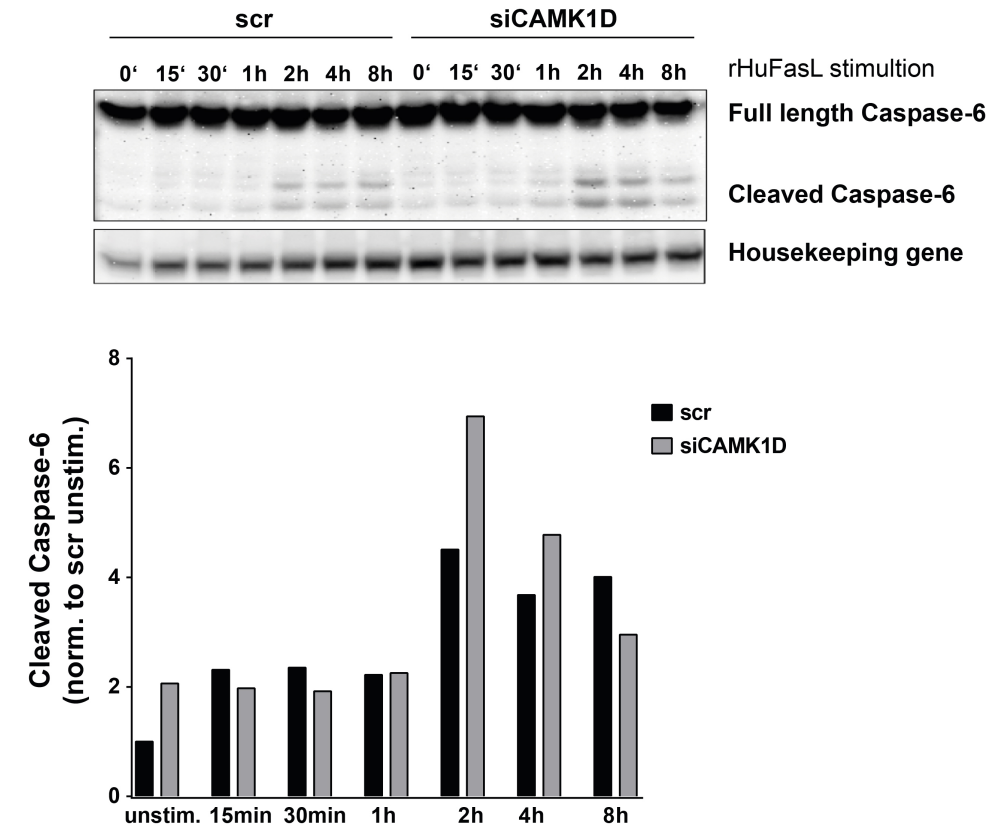
scr
siCAMK1D
0‘ 15‘ 30‘ 1h 2h 4h 8h 0‘ 15‘ 30‘ 1h 2h 4h 8h
rHuFasL stimultion
Full length Caspase-6
Cleaved Caspase-6
Housekeeping gene
Cleaved Caspase-6 (norm. to scr unstim.)
0
2
4
6
8
unstim. 15min 30min 1h 2h 4h 8h
scr
siCAMK1D

D

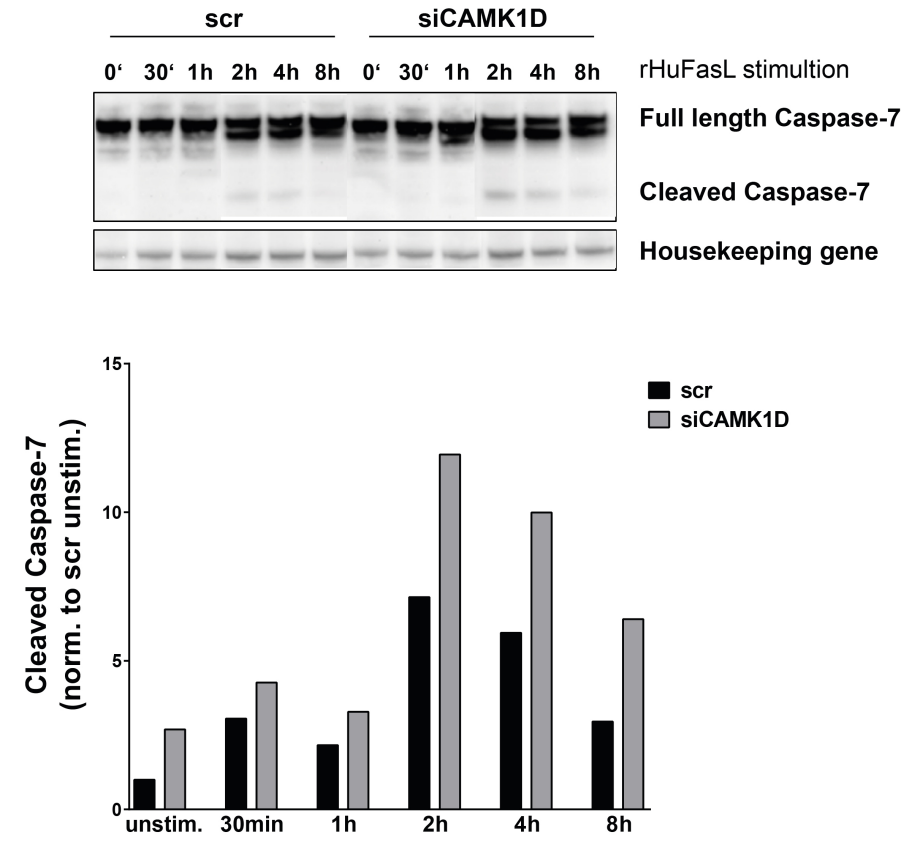
scr
siCAMK1D
0‘ 30‘ 1h 2h 4h 8h 0‘ 30‘ 1h 2h 4h 8h
rHuFasL stimultion
Full length Caspase-7
Cleaved Caspase-7
Housekeeping gene
Cleaved Caspase-7 (norm. to scr unstim.)
0
5
10
15
unstim. 30min 1h 2h 4h 8h
scr
siCAMK1D

Figure 22. CAMK1D interference with effector caspases. (A) FACS analysis of scr and CAMK1D transfected KMM-1 cells treated for the given time frames with rHuFasL. Gate marks active caspase-3 labeled cells. **(B)** Top: Western blot measuring full length and cleaved caspase-3 upon rHuFasL stimulation. Bottom: quantification of cleaved caspase-3. **(C)** Top: Western blot measuring full length and cleaved caspase-6 upon rHuFasL stimulation. Bottom: Quantification of cleaved caspase-6. **(D)** Top: Western blot measuring full length and cleaved caspase-7 upon rHuFasL stimulation. Bottom: quantification of cleaved caspase-7. **(B, C, D)** The Sodium Potassium ATPase was used as housekeeping gene. Representative results of at least two independent experiments.

5.4.10 The susceptibility of CAMK1D deficient cells towards FasL is rescued by effector caspases knockdown

Effector caspases seem to be a fundamental downstream target of CAMK1D, thereby increasing tumor cell resistance to T cell attack. We thus hypothesized that by silencing the effector caspases in CAMK1D deficient cells, we would observe a rescue of tumor cell death upon rHuFasL stimulation. To validate this hypothesis, we knocked down caspase-3, caspase-6 and caspase-7 alone or in a combined manner with siCAMK1D and performed a luciferase-based read-out. The knockdown efficiency of the caspases genes was assessed via end-point (Figure 23A) or quantitative (Figure 23B) PCR. Specificity of the caspases siRNA sequences was observed, since only the targeted caspase showed a reduced gene expression not interfering with the other effector caspases (Figure 23B). As expected, when we silenced the effector caspases alone and stimulated the knocked down tumor cells with rHuFasL, an increased luciferase activity was detected, displaying a reduced tumor cell death compared to the loss of luciferase activity in CAMK1D knocked down cells (Figure 23C). Interestingly the co-knockdown of each single caspase (siCasp-3, siCasp-6 and siCasp-7) together with siCAMK1D completely abolished tumor cell death upon rHuFasL (Figure 23C). No viability impact of the siRNA sequences *per se* was observed in the viability setting (Figure 23D). In conclusion, we confirmed our hypothesis that CAMK1D interacts with the effector caspases, leading to an increased resistance to tumor cell death.

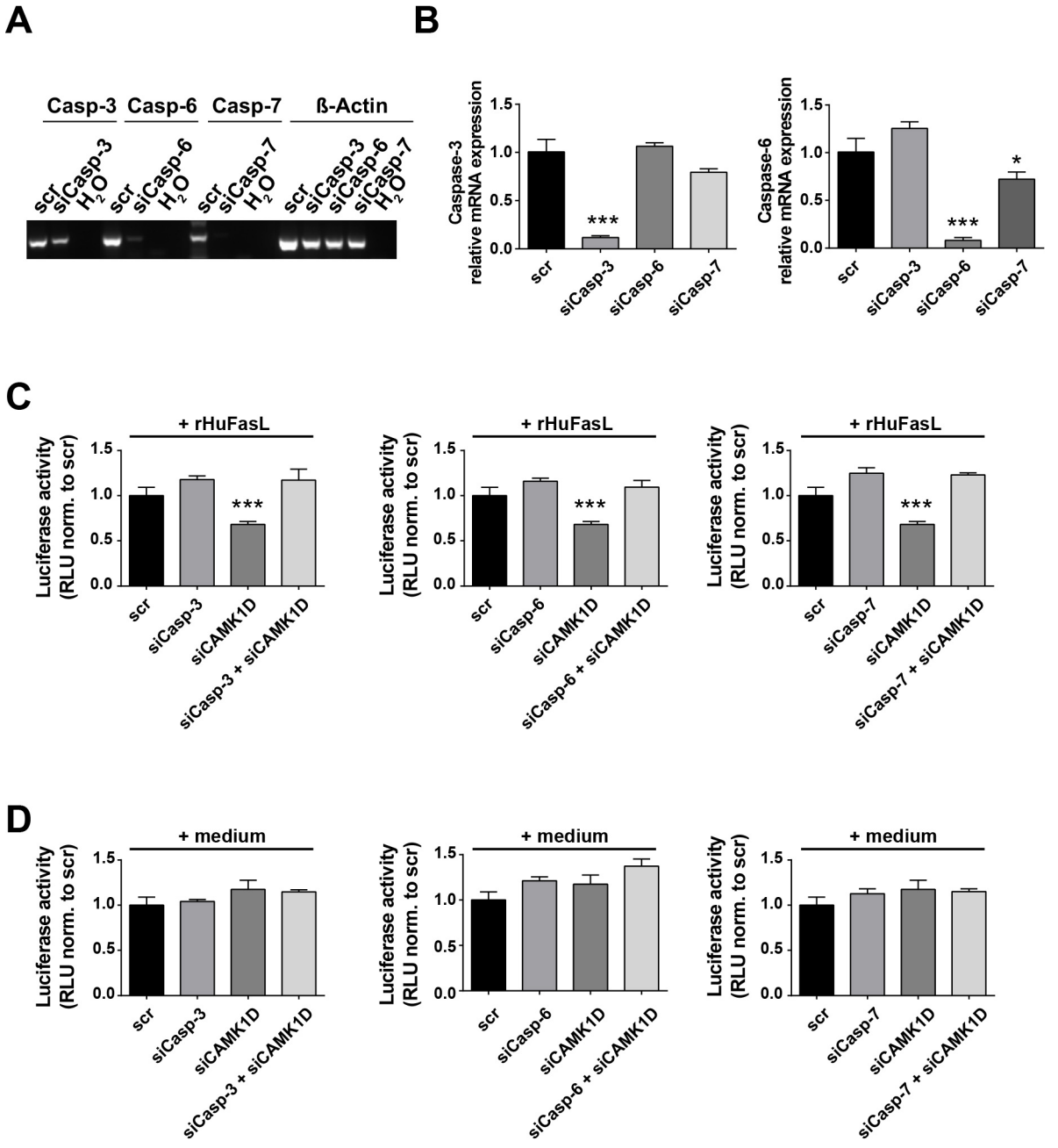

Figure 23. CAMK1D interferes with effector caspases. KMM-1 cells were transfected with siCasp-3, siCasp-6 or siCasp-7. Effector caspases expression and knockdown were measured via **(A)** end-point or **(B)** qPCR. β-actin was used as housekeeping gene. **(C, D)** Effector caspases were knocked down alone or in combination with CAMK1D and **(C)** stimulated with rHuFasL or **(D)** with medium control. Graphs show representative data of at least two independent experiments. Experiments were performed in quadruplicates and show mean ± SD. Statistical significance was calculated using unpaired, two-tailed Student's t-test with * $p \leq 0.05$; ** $p \leq 0.01$; *** $p \leq 0.001$; **** $p \leq 0.0001$.

5.4.11 CAMK1D immunoprecipitates with effector caspases

Next, we wanted to investigate whether CAMK1D directly interacts with the effector caspases or elicits its effect on caspases indirectly through accessory proteins. For this purpose, we decided to perform a co-immunoprecipitation (co-IP) assay with the effector caspases (caspase-3, caspase-6 or caspase-7) and CAMK1D. Thus, we stimulated CAMK1D-proficient cells with rHuFasL for 4h to induce the signaling cascade leading to CAMK1D activation. Unstimulated cells were used as negative control. As expected, CAMK1D was found in the lysates of unstimulated and stimulated cells (Figure 24A-C). Interestingly, we observed that CAMK1D immunoprecipitated with all three effector caspases. Remarkably, upon rHuFasL stimulation the levels of CAMK1D interaction with the effector caspases were found to be slightly increased compared to the unstimulated samples (Figure 24A-C), suggesting that CAMK1D activation increases the interaction with the effector caspases. However, although CAMK1D directly interacted with the effector caspases, we still detected caspase-3 cleavage upon rHuFasL stimulation. Basal activation levels of caspase-6 and caspase-7 were also measured regardless of rHuFasL stimulation (Figure 24A-C). These results confirmed a direct interaction between CAMK1D and the effector caspases and suggested that CAMK1D inhibits the activity of the effector caspases through posttranslational modifications or by inhibiting their binding to downstream targets.

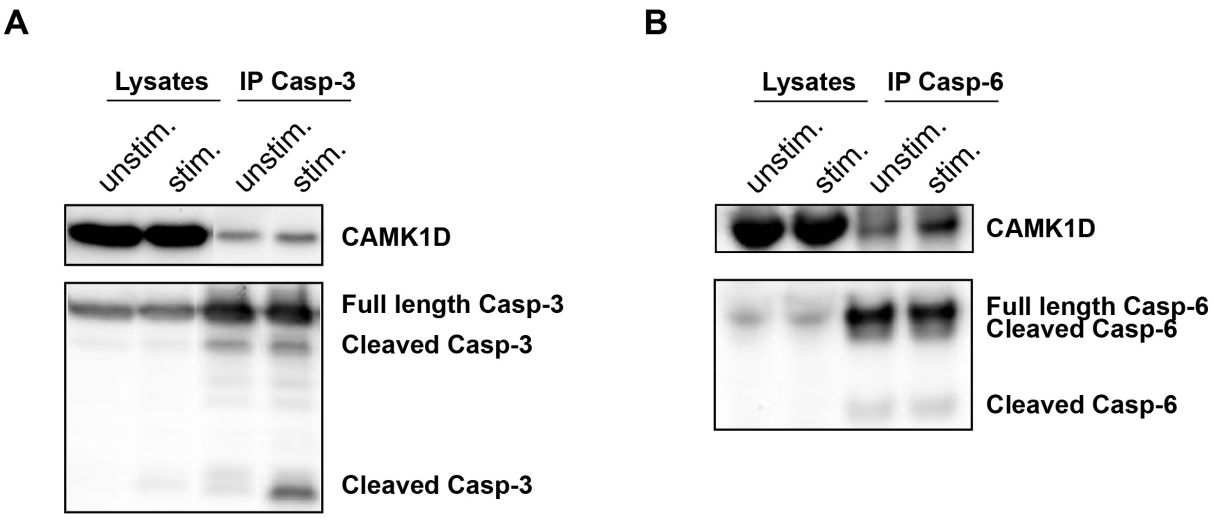

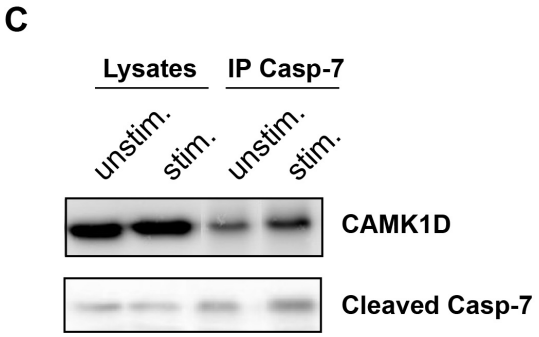

Figure 24. CAMK1D directly interacts with effector caspases. Representative blots showing co-immunoprecipitation of **(A)** caspase-3 and CAMK1D, **(B)** caspase-6 and CAMK1D and **(C)** caspase-7 and CAMK1D. KMM-1 cells were stimulated with rHuFasL for 4h. Unstimulated cells were used as negative control. Cells were lysed and **(A)** anti-caspase-3, **(B)** anti-caspase-6 or **(C)** anti-caspase-7 antibodies were incubated overnight with protein-G beads that have specific binding sites for IgGs. Proteins in the cell lysates and immunoprecipitated (IP) samples were separated by electrophoresis; Proteins were transferred on a membrane and incubated overnight with anti-CAMK1D antibody. Unstimulated and stimulated cell lysates were used as positive control for CAMK1D detection. Subsequently, the blots were incubated overnight to detect the presence of activated effector caspases in the samples.

5.4.12 CAMK1D inhibits the effector caspases via phosphorylation

Caspases are regulated by a variety of cellular factors. In particular, posttranslational modifications like phosphorylation or ubiquitylation can inhibit their enzymatic activity [201]. Having established a direct interaction between the effector caspases (caspase-3, caspase-6 or caspase-7) and CAMK1D, we hypothesized that CAMK1D may be responsible for effector caspases inactivation by phosphorylation, thereby inhibiting caspases cleavage and/or activity. We confirmed this theory by validating that upon rHuFasL stimulation the protein levels of phosphorylated caspase-3 increased in scr transfected KMM-1 cells and were higher compared to CAMK1D knocked down tumor cells (Figure 24A and B). Similarly, the levels of phosphorylated caspase-6 were higher in CAMK1D-proficient cells (Figure 24A and C). Altogether these data suggest that CAMK1D modulates resistance to apoptosis by inhibiting the activation and activity of the effector caspases after FasL stimulation in KMM-1 cells.

Taken together, these results describe CAMK1D as a novel potential immunotherapeutic target, whose blockade sensitizes tumor cells towards immune cell attack.

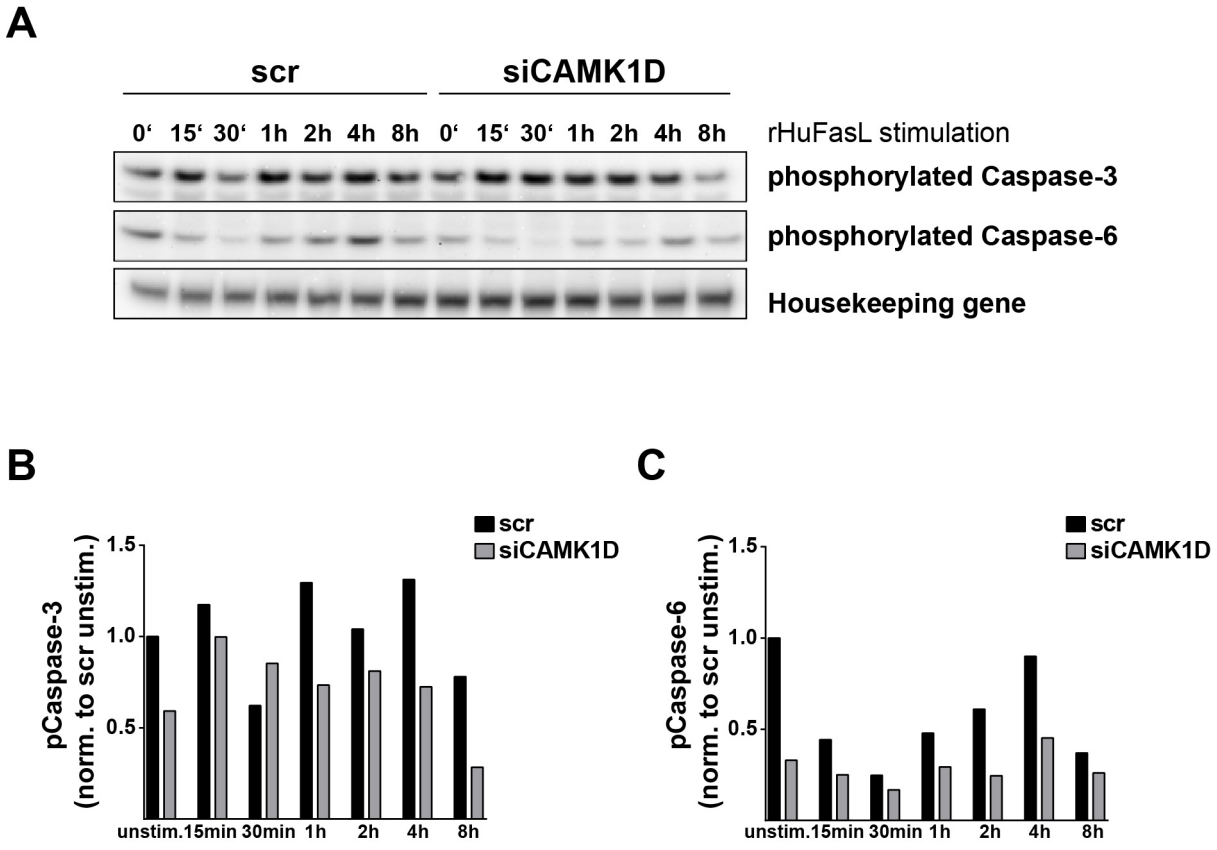

Fig 24. Caspases inactivation via phosphorylation. (A) Western blot measuring phosphorylated caspase-3 and caspase-6 upon rHuFasL stimulation. The Sodium Potassium ATPase was used as housekeeping gene. **(B, C)** Quantification of **(B)** phosphorylated caspase-3 and **(C)** phosphorylated caspase-6 upon rHuFasL stimulation. Representative results of at least two independent experiments.

6 Discussion

Despite noteworthy improvements in the field of immunotherapy, where immune-checkpoint blockade provided clinical success in different cancer entities [131, 182, 184-186, 202] a significant proportion of cancer patients lack response to anti-CTLA-4 or anti-PD-1/PD-L1 antibody therapies [138, 203-205]. This implies that up to now undiscovered immune-checkpoint molecules might be employed by tumor cells to escape the anti-tumor immune response. Therefore, a systemic identification and targeting of additional immune-checkpoint molecules would thoroughly improve immunotherapy.

In the current study, we developed a patient-derived MM-MIL model to screen in a high-throughput manner for novel immune-checkpoints. The primary HTP-screen revealed 128 candidate genes whose knockdown increased anti-tumor response. Among them, CAMK1D was chosen for further validation and mode of action analysis. The role of CAMK1D in immune escape mechanisms has not been described so far. In particular, we found that CAMK1D increases the resistance of tumor cells towards T cell-mediated killing by modulating the activation and activity of effector caspases. Thus, rather than inhibiting T cells, CAMK1D alters the susceptibility of tumor cells towards the cytotoxic potential of T cells mediated by FasL. Interestingly, the underlying pathway exerted by CAMK1D is independent from PD-L1-mediated inhibition, suggesting that this immune-checkpoint molecule could be targeted in both mono- and combination therapy to synergistically improve the survival of cancer patients. In line with this, we addressed the translational impact of CAMK1D by indirectly inhibiting this immune-checkpoint via small molecules.

6.1 High-throughput RNAi screen for tumor-associated immune-checkpoints

During the last years, several HTP-screening platforms have been established to expand the discovery of potential immune-checkpoints. In 2012, Bellucci and colleagues took advantage of a lentiviral shRNA library targeting more than 1000 human genes (kinases and phosphatases) to transduce multiple myeloma cells that were subsequently co-cultured with

NK cells. As read-out system they measured IFN-γ secretion as a marker of natural killer cell activity and identified 83 genes that, when silenced in the tumor cells, increased IFN-γ secretion. Among the identified hits they found that JAK1/2 knockdown improved IFN-γ secretion by NK cells [206]. Two years later, the group of Wucherpfennig performed an *in vivo* shRNA screening by transducing OT-1 T cells. They demonstrated that shRNAs knocking down negative regulators of T cells, thereby restoring CD8 T cell function and proliferation, were enriched within the tumor. In particular, by deep-sequencing of the shRNA cassette, they found that genes involved in T cell resistance to the tumor microenvironment were over-represented [163]. Recently, Restifo and colleagues performed a CRISPR-Cas9 screening by taking advantage of a lentiviral-based library of 123,000 sgRNAs. They transduced human melanoma cells, thereby mimicking loss-of-function mutations and co-cultured the transduced tumor cells with human T cells. In this work different genes whose loss in the tumor cells reduced T cells effector function were identified. Among them, genes essential for antigen presentation and genes playing a role in IFN-γ signaling [207].

These screening strategies have relied on the release of IFN-γ as an indicator of anti-tumor immune cell reactivity or have focused on T cell proliferation as a readout system. However, the release of IFN-γ by immune cells does not always correlate with cellular cytotoxicity [208, 209]. Thus, the detection of a direct tumor cell lysis by T cells might improve immunotherapeutic strategies. In line, the group of Haining developed a CRISPR/Cas9 *in vivo* screening to identify genes that synergize with or trigger resistance to anti-PD-1 therapy in mice. Melanoma cells were transduced with sgRNAs against 2,368 genes and transplanted into immune-competent or -deficient mice in combination with PD-1 therapy. Genes involved in the NF-κB signaling, antigen presentation and the unfolded protein response were identified as being responsible for immunotherapy unresponsiveness [210].

6.1.1 HTP-screen design and rationale

In the current study, we adopted the high-throughput RNAi screening approach developed in our laboratory by Dr. Khandelwal [164] to identify immune-checkpoints that inhibit T cell-mediated tumor lysis. The following adaptations were applied in order to improve the qualitative and quantitative aspects of the screen:

- Multiple myeloma cells were used instead of breast cancer cells. Considering cancer as a highly heterogenic disease, it is clear that different tumor entities might take advantage of distinctive immune-checkpoints to evade the immune system. In fact, anti-PD-L1 and anti-CTLA-4 therapies have been shown to improve the survival of melanoma patients. On the other hand, although PD-L1 is highly expressed on malignant plasma cells and PD-1 expression is found on CD8 T cells and NK cells of multiple myeloma patients, these patients failed to respond to anti-PD-1 therapy in a phase I clinical trial [139]. Thus, performing a RNAi screen in MM cells could expand the repertoire of immune-checkpoints discovered so far, increasing the chances to an immunotherapeutic response.

- Marrow-infiltrating lymphocytes were chosen instead of polyclonally activated PBMCs or antigen-specific lymphocytes, as T cell source. MILs co-cultured with patient-derived multiple myeloma cells better resemble the "physiological" situation found in cancer patients. Importantly, MILs have been shown to be an effective T cell source for adoptive T cell therapy. Noonan and colleagues performed a phase I study to assess the safety and efficacy of this approach. Here, MILs from 25 multiple myeloma patients were harvested, expanded, activated *ex vivo* and re-infused into the patients. The treatment efficacy was shown by a reduction of 90% in tumor burden, whereby 6 patients experienced complete remission [166]. Immune response was attributes to MILs i) possessing endogenous tumor specificity, ii) being able to efficiently traffic to the bone marrow upon infusion by highly expressing the chemokine receptor CXCR4 and iii) being enriched in Tcm cells, thereby persisting over time and maximizing the overall efficacy of adoptive T-cell therapy. Thus, these unique features not found in the PBL counterparts, make MILs an ideal source of T cells for adoptive T cell therapies. Nevertheless, in line with published data, we observed that MILs isolated from MM patients exhibit an exhausted phenotype [211]. Exhaustion markers can in turn function as receptors for inhibitory ligands expressed on tumor cells [212]. Thus, the hampered reactivity against tumor cells represent an ideal feature for the RNAi screen, since we aimed at identifying genes whose knockdown increased T cell mediated killing of tumor cells.

- A siRNA library targeting 2887 genes enriched for kinases, GPCRs and other surface molecules was used instead of the siRNA library comprising only 500 GPCRs utilized in the breast cancer screening. GPCRs represent interesting targets for cancer immunotherapy since they are expressed on the plasma membrane thus being accessible targets for an antibody-therapy. Moreover, many are orphan receptors whose role in immune inhibition remains still unaddressed. Nevertheless, GPCRs constitute only a small fraction of all surface molecules (surfaceome). Since in this work we aimed at increasing the coverage of surface proteins for their potential role as immune checkpoints, we took advantage of a siRNA library enriched in surface molecules (representing around 50% of the surfaceome) comprising also cytoplasmatic and surface-bound protein kinases. The latter can be targeted via small molecule inhibitors. Indeed it has been shown that tumor cells treated with tyrosine-kinase inhibitors improved cancer immunotherapy treatments [213].

6.1.2 Performance and data interpretation of the HTP-screen

RNAi-screens, unraveling novel immune-checkpoints, can be technically challenging, emphasizing the need for extensive set-ups to ensure robustness and reproducibility of the methodology. In particular, the luciferase-based read-out system is designed for adherent cells, as the luciferase activity is measured in the leftover live tumor cells upon removal of dead cells and T cells by aspiration of the cell culture supernatant. KMM-1 cells are semi-adherent multiple myeloma cells, thus they required a deeper assessment in order to optimize the conditions to be used in HTP-screenings. We first optimized the siRNA transfection protocol and found that RNAiMAX induced the best transfection efficacy as observed by a significant reduction of the luciferase activity upon siFLuc transfection. In line, the transfection of siUBC targeting ubiquitin C as well as transfection with the commercially available siRNA pool “cell death”, were ideal choices to identify and exclude genes whose knockdown affected cell viability *per se*, as these siRNAs abrogate cell viability in the absence of T cells. To exclude any effect of siRNA transfection *per se*, the “select negative control no. 2”, a siRNA with no significant sequence similarity to mouse, rat, or human mRNA sequences, was used. To verify the robustness of the assay, the correlation among the

technical duplicates of each setting in the screening was calculated. The correlation was relatively high (r^2=0,701 in the cytotoxicity setting and r^2=0,872 in the viability setting) indicating a robust quality of the approach. An additional viability assay (CellTiter-Glo) was included to exclude genes affecting cell viability (r^2=0,810). In this luciferase-independent assay, the viability impact of siRNA sequences *per se* is measured by the ATP concentration in the tumor cells [214]. Next, after normalization of the plates, the cytotoxicity scores were fitted to the viability scores using local regression (LOESS), allowing to rank the hits according to their phenotypic effect. Additionally, genes having a high score in the CTG screen, were excluded. Importantly, the read-out of the RNAi-screen is only meaningful if proper controls have been set-up. Indeed, the performance of assay controls is of high importance for the RNAi-screen analysis and data interpretation. As discussed in the introduction, multiple myeloma cells express the immune-checkpoint molecule PD-L1. Nevertheless, in line with literature, PD-L1 cannot be considered a reliable positive control for HTP-screenings in multiple myeloma cells, since the blockade of this immune-checkpoint does not positively impact on tumor cell death [139]. On the other hand, the C-C motif chemokine receptor 9 (CCR9), which was previously identified as an immune checkpoint in breast cancer and melanoma [164], was successfully identified as a negative immune modulator in multiple myeloma cells. Of note, positive assay controls are of fundamental importance to define an appropriate cut-off parameter for the identification of potential hits. Thus, in this work, CCR9 was used as a reference gene to identify novel immune-checkpoints exhibiting a stronger phenotypic effect. 128 potential immune-checkpoint molecules were identified in the HTP-screening, eliciting a stronger T cell-mediated cytotoxicity than the positive control CCR9. Confirming the robustness of our screening-approach, the HTP-screen revealed several genes with known cancer immune regulatory functions such as CD5, FES and PAK3. CD5, also known as Leu-1 in humans, is a type I transmembrane glycoprotein belonging to the scavenger receptor cysteine-rich (SRCR) superfamily and is expressed on the surface of T cells and a subset of mature B cells (B1a cells) [187]. Recently, Zhang and colleagues discovered CD5 as a novel receptor for IL-6, which in turn activates STAT3 through the JAK-STAT signaling pathway, thereby promoting tumor growth and progression [187]. Fittingly, constitutive STAT3 activation has been demonstrated in a variety of human tumors such as lung [215], brain [216, 217], pancreatic [218], melanoma [219], multiple myeloma [220, 221] and leukemia [222]. In line with these findings, the abrogation of CD5 in multiple myeloma, being a malignant B-cell neoplasm characterized by mutated plasma cells

within the bone marrow, enhanced T cell-mediated killing in our HTP-screening. Moreover, IL-6 plays an essential role in the pathogenesis of multiple myeloma. This pleiotropic, pro-inflammatory cytokine has been shown to be a key player in tumor growth, proliferation and survival of myeloma cells as well as exerting a stimulatory effect on osteoclasts, leading to bone disruption. PAK3 (p21 (RAC1) Activated Kinase 3) is a serine/threonine protein kinase with important roles in cytoskeletal dynamics, cell survival and proliferation [189, 190]. It acts as a signal transducer in several cancer signaling pathways, including the canonical MAP kinase cascade of Ras/Raf/MeK/ERK [188]. FES is a cytoplasmic protein-tyrosine kinase that participates in cellular signaling cascades responsible for cellular differentiation, survival and inflammation. Moreover in 2010, a kinome-wide siRNA screen identified FES as an essential kinase for multiple myeloma cell growth and survival [191].
Besides immune-inhibitors, the established HTP-screen also revealed potential activators of the immune system. However, lacking appropriate positive co-stimulatory controls, we could not delineate a proper threshold for the identification of novel immune-stimulatory molecules of T cells. Currently, in our laboratory Ayse Nur Menevse is adopting the high-throughput screening approach to autoimmune disease models such as multiple sclerosis (MS). MS is a severe autoimmune disease characterized by the infiltration of auto-reactive CD8 T cells into the brain [223, 224]. Thus, with this screening the blockade of co-stimulatory molecules resulting in decreased T cell activation would unravel fundamental activatory molecules that will be further validated as potential candidates to fight MS.

Despite the robustness of the primary HTP-screen, RNAi screens can generate false-positive hits due to off-target effects. Therefore, we performed a secondary screen with an enriched library comprising the 128 hits derived from the primary screening. To have a first hint on the mechanism of action of the selected hits, besides the tumor - T cell co-culture setting, we included a setting where the knockdown tumor cells were co-cultured only with the supernatant of pre-activated T cells. This approach would reveal if soluble molecules such as cytokines released by T cells would have an impact on tumor cell death and whether target genes mediate resistance to these molecules. Indeed, in a HTP-screen performed by Dr. Sorrentino in our laboratory, the knockdown of the salt-inducible kinase 3 (SIK3) in pancreatic ductal adenocarcinoma cells (PDAC) induced tumor cells to be susceptible towards TIL-secreted TNF thereby inducing apoptosis of the cancer cells (Sorrentino *et al*, submitted).

Interestingly, most of the examined hits induced myeloma cell death only in the presence of MILs. These results further suggested that different tumor entities take advantage of diverse escape mechanisms.
Various hits showed a different performance in the primary and secondary screens, ranking higher or lower in the two screenings. Therefore an extensive validation of selected hits was necessary to identify authentic immune-checkpoints.

6.1.3 Comparative analysis of high-throughput RNAi screens

Over the last years, a series of HTP-screens were performed in our laboratory on different tumor entities. After the pilot breast cancer screen performed by Dr. Khandelwal using a GPCR siRNA library combined with PBMC or antigen-specific T cells [164], Dr. Michels performed a HTP-screen with a surfaceome-enriched library on patient-derived melanoma cells using HLA-A2-matched TILs. Likewise, Dr. Sorrentino performed a similar screening on PDAC with patient-derived TILs. In the presented work, we show the applicability of this approach also for hematological malignancies as multiple myeloma. As mentioned in the previous paragraph, since tumors are heterogenic malignancies, thus taking advantage of distinctive escape mechanisms/pathways such as the expression of unique immune-checkpoints, performing HTP-screenings on different cancer entities would increase the repertoire of potential immune-checkpoint molecules. Indeed, by comparing the three screens performed with the same library (Figure IX A), the analysis revealed only a very small overlap between the melanoma, PDAC and multiple myeloma hit-list (Figure IX B). The two solid tumors shared 12 immune-checkpoints, while MM shared only 4 and 7 hits with melanoma and PDAC, respectively. Only one candidate overlapped in all three screenings, namely the regulator of G protein signaling 14 (RGS14). Interestingly, we observed that different members of the same gene family were found as targets in different tumor entities. The calcium/calmodulin-dependent protein kinase 1 family was found to play a role in melanoma and multiple myeloma. Expression analysis revealed that the delta and alpha isoforms of the CAMK1-family were either expressed in one or the other tumor entity. CAMK1-delta was found to be expressed in MM cells but not in melanoma cells while CAMK1-alpha was expressed in melanoma but not MM cells. Thus, the unique expression of proteins belonging to the same family generates the hypothesis that family members can exert similar functions in different tumors.

These results further confirmed the unique landscape of immune modulators used by different tumors and therefore screening different tumor entities would be beneficial for the development of more efficient immunotherapy.

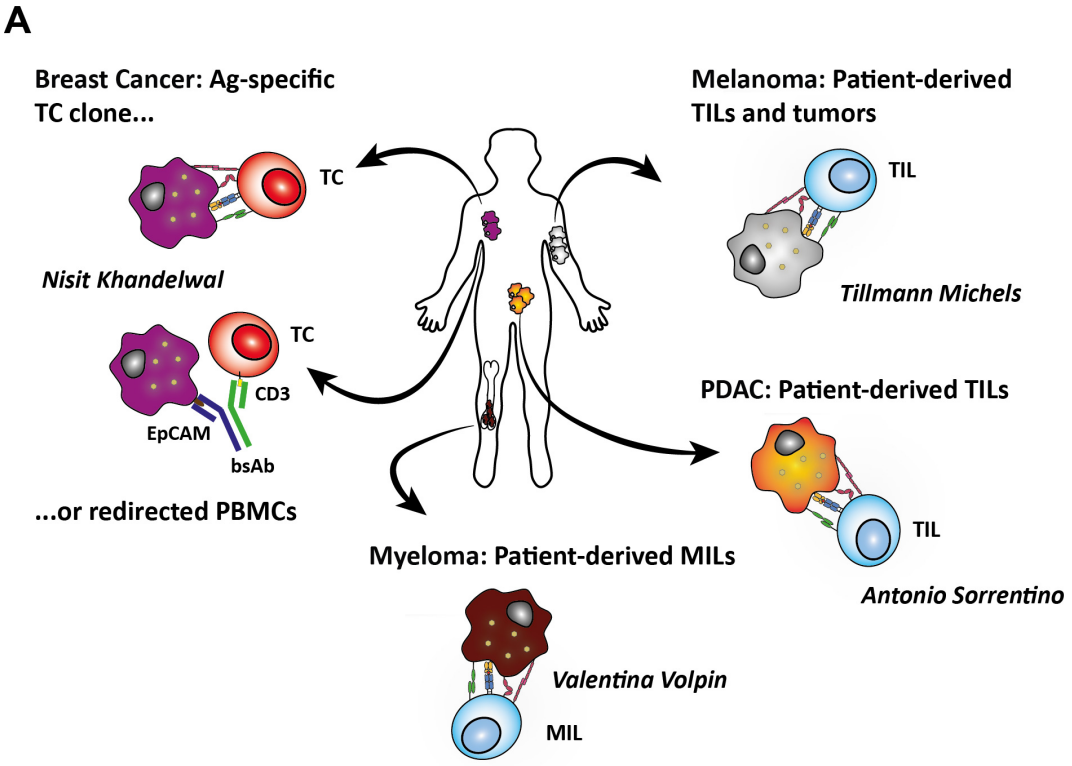

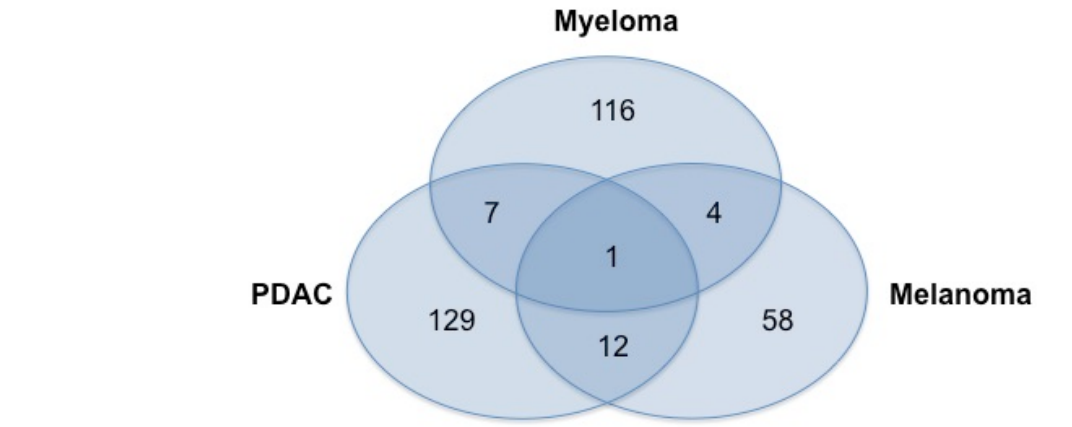

Figure IX. Comparative analysis of RNAi screens. (A) Schematic representation of the HTP-screens performed in breast cancer, melanoma, PDAC and multiple myeloma, including the sources of T cells. **(B)** Venn diagram representation of the overlapping candidate genes after the primary HTP-screens in melanoma, PDAC and multiple myeloma. Breast cancer was omitted due to a distinct library. The analysis was performed by Dr. Tillmann Michels (AG Beckhove, RCI Regensburg).

6.1.4 Rationale for hits selection

After the primary and secondary screening, several potential immune-checkpoints emerged as appealing targets to follow-up. Importantly, as we aimed at discovering novel targets for clinical applications, the candidate genes that we selected for further validation needed to fulfill different criteria. First of all, their role as immune-regulators should not be described. Moreover, proteins with a great potential to become "druggable" targets were favored. To this, protein kinases and surface molecules, due to their cellular localization were prioritized representing reasonable molecules to target via small molecules or blocking antibodies, respectively. Indeed, although progresses have been made, some classes of proteins like transcription factors and phosphatases, are difficult to target and remain undruggable so far [225]. Furthermore, differential expression between healthy tissue and cancer cells would be a major advantage for a targeted therapy. Indeed, if the potential immune-checkpoint is ubiquitously expressed, the risk of developing severe side effects upon targeting the molecule of interest increases. To this end we took advantage of databases for gene expression (e.g. TCGA) to investigate the differential expression between tumor and healthy tissue.

As already mentioned, off-target effects are a major concern of HTP-RNAi-screens leading to an incorrect identification of candidate genes [226]. Consequently, a fundamental validation step is to rule out potential off-target effects of the distinct siRNA sequences used in the RNAi screening. Different issues are responsible for causing an off-target effect [227] namely i) the generation of siRNAs with nearly identical sequence similarity to an unrelated mRNA sequence, ii) sequence similarities in the 5' region of the siRNA from the 2^{nd} to $7^{th}/8^{th}$ nucleotide (referred to as the "seed sequence") could lead to binding at the 3' UTR of unrelated mRNAs and inducing their degradation and iii) the delivery of double stranded siRNA sequences can lead to the binding of the complementary strand rather than the guide strand to the transcription machinery.
To decrease off-target effects, in the current HTP-screen different strategies were adopted. First of all, the siRNA library was designed by the manufacturer in order to increase the stability and potency of the siRNA sequences, such as low G/C content and absence of inverted nucleotide repeats. Moreover, we used four non-overlapping siRNA sequences targeting the same mRNA ("pooled approach"), instead of single siRNAs, to diminish off-

target effects. Indeed, the incidence of off-target effects is concentration dependent therefore, by reducing the concentration of single siRNA sequences, the pooled approach decreases the probability of off-targets [228]. Nevertheless, off-target effects cannot be completely excluded, therefore, the selected candidates needed to undergo further validation. To this, siRNA sequences from the pool needed to be "deconvoluted". Thus, the luciferase-based killing assay was repeated by using the individual siRNAs present in the pool. Likewise, the knockdown efficiency of each single siRNA sequence was validated. Candidate hits that showed an on-target effect of at least two siRNA sequences in the luciferase-based assay were considered for further mode of action investigation.
Among the validated hits, CAMK1D was selected as potential immune-checkpoint due to the strength of the phenotype and biological relevance.

6.2 CAMK1D as a novel immune-checkpoint molecule in cancer

6.2.1 Structure, distribution and function of Ca^{2+}/Calmodulin protein kinases

Members of the calcium/calmodulin (Ca^{2+}/CaM) protein kinase family are classified as serine/threonine kinases as their substrate target site of phosphorylation contains either a serine or a threonine. The family of Ca^{2+}/CaM-kinases is divided in two main categories, namely the multifunctional CaM-kinases comprising CAMKI, CAMKII, CAMKIV and CAMKK (CAMK-kinase) and the substrate-specific CaM-kinases, CAMKIII and MLCK (myosin light chain kinase). The multifunctional CaM-kinases have multiple downstream targets, while the substrate-specific CaM-kinases have only one known target as their name implies. The activation of Ca^{2+}/CaM-kinases is dependent on the initial binding of calcium and calmodulin. The general structure of Ca^{2+}/CaM-kinases comprises a bi-lobed catalytic domain followed by a regulatory domain (the catalytic domain) that harbors an autoinhibitory domain and a CaM-binding domain. The autoinhibitory domain overlaps with the CaM-binding domain at basal Ca^{2+} levels, retaining Ca^{2+}/CaM-kinases in an inactivated state. Only upon binding of the Ca^{2+}/CaM-complex the autoinhibitory domain is removed from the catalytic site, allowing the binding of substrates.

Although the multifunctional CaM-kinases CAMKI, CAMKII and CAMKIV can phosphorylate the cAMP response element binding protein (CREB) thereby activating CREB-dependent gene transcription, CAMKI and CAMKIV differ from CAMKII in their activation mechanisms. Indeed, CAMKI and CAMKIV are fully activated upon phosphorylation by the CAMK-kinase CAMKK, thereby inducing the CREB-dependent transcription. On the other hand, CAMKII is regulated by autophosphorylation and through an additional phosphorylation on Ser142 inhibits CREB-dependent transcription [229, 230].

CAMKI was originally purified from bovine brain on the basis of its ability to phosphorylate synapsin I, a protein associated to synaptic vesicles [231]. In particular, CAMKI family members, CAMK1-alpha, CAMK1-beta, CAMK1-gamma and CAMK1-delta differ in their cellular and subcellular localization. CAMK1-alpha exhibits predominantly a cytosolic localization, while CAMK1-beta is localized both in the cytoplasm and in the nucleus [232]. CAMK1-gamma was found to localize to the Golgi and the intracellular part of the plasma membrane [232]. Interestingly, CAMK1-delta (CAMK1D) exhibits a cytosolic localization but translocates to the nucleus in response to stimuli triggered by intracellular calcium influx [196].

CAMK1D is a monomeric protein kinase of 42kDa abundantly expressed in the primary hippocampal neurons. Sakagami and colleagues demonstrated that one minute after neurons' stimulation with KCl, that induces cell depolarization, the percentage of CAMK1D within the nucleus is increased by two-fold and returns at basal levels within 30 minutes. Moreover, activation of CAMK1D is indispensable for nuclear translocation. Indeed, point mutations into the ATP-binding site (the catalytic domain) or the threonine residue that is necessary for fully activation by CAMKK, hamper CAMK1D nuclear translocation. Once in the nucleus, CAMK1D is able to phosphorylate CREB [196]. Likewise, in the hippocampal pyramidal neurons CAMKIV, having a constitutive nuclear localization, is responsible for the early phase of CREB phosphorylation. Thus, the function of different CAMKs could converge playing a role in distinct spatial and temporal kinetics. Indeed, CAMK1D is shown to be inactivated more slowly than CAMKIV, although remaining Ca^{2+}/Calmodulin-dependent, further sustaining CREB phosphorylation.

In order to acquire more information on CAMK1D expression, we took advantage of the GTEx database [233]. This analysis proposed a ubiquitous expression of CAMK1D mRNA in several human tissues with the highest expression in the brain (Appendix Figure XII). Nevertheless, these results need to be further confirmed by deeper experimental procedures.

6.2.2 The role of Ca^{2+}/CaM kinases in cancer

To date, several reports described an emerging role of CAMKII in cancer. Indeed, Liang and colleagues demonstrated that the suppression of CAMKII in normal and neoplastic B-lymphoid cells prevents B-cell malignancies via the excessive B-cell activating factor (BAFF) [234]. Further studies showed that inhibition of CAMKII-gamma suppresses the proliferation of myeloid leukemia cells [235]. B cell-proliferation was ascribed to CAMKII activation of the NF-kB pathway as well as multiple oncogenic signaling pathways in non-small cell lung cancer (NSCLC) [236, 237]. Despite strong evidences demonstrating CAMKII as a key protein in modulating cell proliferation and invasion, little is known about the role of CAMK1D in cancer. In 2008, Bergamaschi and colleagues demonstrated that the levels of CAMK1D expression were elevated in invasive carcinomas compared to carcinoma in situ [238]. Moreover, by engineering CAMK1D in non-tumorigenic breast epithelial cells they observed an increased proliferation and phenotypic switch involving loss of cell-cell adhesion molecules and increased cell migration and invasion, hallmarks implying an epithelial-to-mesenchimal transition (EMT). Hence, they correlate CAMK1D as a novel oncogene linked to EMT in breast cancer. As CAMK1-alpha has been shown to activate cyclin D1/cdk4 complexes in fibroblasts [239], CAMK1D might promote proliferation of cancer cells through similar mechanisms. Undoubtedly, additional studies are needed to determine the role of CAMK1D in cancer progression.

In this regard, we took advantage of the Oncomine™ database to compare the expression of CAMK1D in healthy tissue versus cancer biopsies [240]. CAMK1D mRNA was found to be significantly overexpressed in B-cell childhood acute lymphoblastic leukemia (Appendix Figure XI A). Moreover, CAMK1D is overexpressed in several multiple myeloma patients, while the levels are similar to healthy donors in patients with MGUS (a stage prior to multiple myeloma) as well as in patients experiencing plasma cell leukemia (Appendix Figure XI B).

Finally, the expression of CAMK1D together with the functional data highlighted the relevance of CAMK1D as a promising candidate for further validation analysis.

6.2.3 CAMK1D induces intrinsic tumor resistance towards T cell attack

CAMK1D was the 35th hit in the primary and the 1st candidate in the secondary multiple myeloma screening. Validation assays showed significant increases in T cell-mediated tumor lysis upon CAMK1D knockdown with three non-overlapping siRNA sequences. Tumor cell killing in CAMK1D-deficient cells was independent of the T cell source, as both MILs and PBMC-derived flu-specific CD8^{+} T cells were able to reproduce the same effect. Remarkably, tumor cell viability was not affected without the addition of T cells. As explained in the introduction, tumor cells can evade the immune system in several ways (section 1.4). Particularly, they can either hamper immune cell activation or intrinsically increase tumor cell resistance towards the immune system. Our data demonstrated that CAMK1D-deficient tumor cells did not enhance T cell function, while they caused tumor cells to be more susceptible towards T cell attack. Furthermore, we observed that the mechanisms through which T cells mediate tumor cell killing is via ligands expressed on their surface, as the merely addition of the supernatant of pre-activated T cells, containing soluble cytotoxic molecules such as INF-γ, TNF and Granzyme B, did not show any impact on tumor cell death. These data suggest that CAMK1D acts as central mediator of intrinsic tumor resistance towards T cells.

6.2.4 CAMK1D impairs FasL-mediated apoptotic signaling in tumor cells

In the current study, FasL was identified as the key effector molecule inducing tumor cell death in CAMK1D-deficient cells. FasL is a homotrimeric type-II transmembrane protein that belongs to the tumor necrosis factor (TNF) family and is expressed on activated T cells. The binding of FasL to its receptor (CD95) induces caspases-mediated apoptosis in the tumor cells [51]. Besides mediating tumor cell death, Fas signaling is involved in peripheral deletion of autoimmune cells and activation induced T cell death. Indeed, mutations in the Fas gene trigger the autoimmune lymphoproliferative syndrome (ALPS), caused by an abnormal accumulation of white blood cells [241].

It is not surprising that tumor cells have evolved mechanisms to evade this immune regulation. Indeed, to counteract the immune system, tumor cells can upregulate FasL on their surface and induce apoptosis in T cells [52, 53]. On the other hand, tumor cells can downregulate Fas expression as it has been shown for a variety of malignancies including

melanoma, pulmonary adenocarcinomas and esophageal cancer [242-245]. Consequently these tumors develop resistance to FasL and acquire the advantage to spread within the body.
In this work, both MILs and flu-specific T cells were found to express FasL (CD178) on their surface. In line, the expression of Fas-receptor was shown to be an indispensible requirement to induce tumor cell death. Indeed, although CAMK1D was expressed in several solid tumors such as PDAC (PANC-1 cells) and in the breast cancer cell line MCF7, the knockdown of CAMK1D in these cell lines did not show any impact upon T cell-mediated killing. To this, FACS-analysis revealed that the percentage of Fas-expressing tumor cells was very low compared to the multiple myeloma cell lines. These results suggest that different tumor entities express a diverse panel of molecules responsible for their regulation.
Moreover, the blockade of FasL on activated MILs abrogated the cytotoxic effect exerted by the T cells in CAMK1D-deficient cells. Accordingly, these results further corroborate FasL to be the key effector molecule inducing tumor cell death and CAMK1D being responsible to interfere with the Fas/FasL induced signaling pathway.
Although CAMK1D was not expressed in skin melanoma cells, we observed CAMK1D expression in uveal melanoma cells. Being the most common intraocular malignancy, with an aggressive metastatic progression, made this tumor entity an interesting model for further examination of our findings. We observed a high expression of both CAMK1D and Fas-receptor and remarkably the treatment with recombinant human FasL increased tumor cell death in CAMK1D-deficient cells.
Furthermore, we investigated CAMK1D expression in RNA-Seq data from around 11,500 tumor samples from 36 tumor entities (TCGA; doi:10.7908/C11G0KM9) using TCGA2STAT for R and correlated the results with survival. Interestingly, patients experiencing uveal melanoma, correlated with better survival if CAMK1D expression was absent or low. On the other hand, patients with high expression of CAMK1D had a worse survival probability (significant; $p = 0{,}0012$). These expression patterns made CAMK1D an interesting target for further validation.

6.2.5 Molecular aspects of CAMK1D inhibition of the Fas/FasL pathway

To obtain a better insight into the mode of action of CAMK1D, we performed a Luminex assay. This assay enabled us to identify several molecules differing in their activation/inhibition status in CAMK1D-proficient and -deficient cells upon rHuFasL stimulation. Interestingly, the extracellular signal-regulated kinase (ERK) was one of the identified proteins belonging to the mitogen-activated protein kinases (MAPK). Upon extracellular stimuli, ERK is phosphorylated and activated subsequently regulating cell proliferation, differentiation and survival [246]. Our results indicated an increased phosphorylation of ERK (pERK) in CAMK1D-proficient cells, indicating a hyperactivation of the mitogenic pathway. In line, in a recent study Fan and colleagues identified that multiple myeloma patients exhibit high levels of pERK which was associated with a poor prognosis [247]. Respectively, our data demonstrate an increased tumor cell killing in CAMK1D-deficient cells, thus CAMK1D could mediate resistance towards T cell-mediated apoptosis by interacting with the ERK pathway. Moreover, Vanhoutte and colleagues detected CAMK-kinase to be involved in the activation of the ERK pathway in neurons, which in turn activates CREB [248]. Nevertheless, further investigations are required to identify a direct interaction between CAMK1D and ERK.

Furthermore, the levels of activated Bcl-2, an anti-apoptotic molecule, were found to be higher in CAMK1D-proficient cells. These results are in line with the findings of Puthier and colleagues who demonstrated higher expression of Bcl-2 in malignant plasma cells from both the bone marrow and peripheral blood [249]. Accordingly, Wilson and colleagues verified the upregulation of Bcl-2 expression upon antigen ligation in B cells. They demonstrated that the *Bcl-2* gene is under the control of the transcription factor CREB [198]. Fitting with these results, we observed an increase phosphorylation of CREB upon stimulation with FasL in KMM-1 cells. It is now well established that CAMK-family members are responsible for the phosphorylation, hence activation of CREB inducing downstream gene transcription. In breast cells, activated CREB levels were associated with CAMK1D overexpression [238]. The fact that CREB mediates transcription of several genes promoting proliferation and differentiation (e.g. cyclin D1) and anti-apoptotic genes such as *Bcl-2* through the regulation via CAMK1D, makes CAMK1D an appealing target for molecular-targeted therapy.

Along with the enhanced expression of Bcl-2, the increased phosphorylation of CREB and the sustained activation of the ERK-pathway, we observed higher levels of activated caspase-

3 in CAMK1D-deficient cells upon FasL stimulation. Caspases are endoproteases responsible for the regulation of programmed cell death. Upon activation these cysteine-dependent aspartate-driven proteases subsequently cleave key intracellular substrates to promote cell death [250, 251]. Indeed, B cells lacking caspase-3 exhibit an increased proliferation *in vivo* and hyperproliferation after mitogenic stimulation *in vitro* [252]. Hence, the increased levels of caspase-3 activation prompted us to investigate whether other caspases were implicated in this pathway as well. Interestingly, the initiator caspases (caspase-8 and caspase-9) did not seem to be affected by CAMK1D (data not shown). On the other hand, effector caspases (caspase-3, caspase-6 and caspase-7) showed an impaired activation in the presence of CAMK1D. Caspases can be regulated by post translational modifications such as phosphorylation and ubiquitylation that can block caspases activation and activity [201]. Phosphorylation on different sites can generate opposite effects. Indeed, although the phosphorylation site has not been identified yet, the phosphorylation of caspase-3 by PKC-delta appears to enhance caspase-3 activity, while the phosphorylation of caspase-3 by p38 at Ser150, directly inhibits caspase-3, hindering Fas-induced apoptosis in neutrophils [253]. Likewise, Suzuki and colleagues demonstrated that in the colon cancer cell line SW480, caspase-6 is inhibited by the phosphorylation of the kinase ARK5, leading to the evasion of Fas-induced apoptosis [254]. Also caspase-7 can be inhibited posttranslationally by PAK2-medited phosphorylation at Ser30, Thr173 and Ser239, which negatively regulates caspase-7 activity [255]. Besides being regulated at a posttranslational level by modifications that alter caspases activation or activity, the endoproteases can be controlled at the level of protein stability through ubiquitylation by inhibitor of apoptosis proteins (IAPs), leading to proteasome-dependent degradation and increased resistance to apoptosis [201, 256]. Indeed, several IAPs, such as the X-linked inhibitor of apoptosis protein (XIAP) contain a carboxyl-terminal RING domain that is critical for the protein's ubiquitin ligase activity [257]. Additionally, IAPs can also act as direct stoichiometric inhibitors of caspases by binding to the active site and in the case of caspase-9 preventing the dimerization necessary for its activation and subsequently precluding downstream activation of the effector caspases [258-260].

In line with increased caspases activation in CAMK1D-deficient cells, we also detected a reduced inhibitory phosphorylation of caspase-3 and caspase-6. These results, together with the observation that CAMK1D co-immunoprecipitates with the effector caspases, suggest that CAMK1D can directly bind and inhibit caspases activation by acting as a stoichiometric

inhibitor as well as hindering caspases binding to downstream target substrates. Moreover, by phosphorylating activated caspases, CAMK1D can inhibit their activity thus reducing the overall apoptosis of cancer cells. Unfortunately, antibodies detecting the phosphorylation of caspase-7 are not commercially available, but due to sequence similarity between caspase-3 and caspase-7, as well as an increased activation of caspase-7 in CAMK1D deficient cells, we suppose that caspase-7 is subjected to CAMK1D-mediated phosphorylation similar to the other effector caspases.

The caspases-dependent apoptotic pathway is triggered by signaling through the TNF-family. On the other hand, Fas/FasL interaction also increases calcium levels in the cytoplasm released from the endoplasmatic reticulum (ER). In particular, Fas-mediated apoptosis requires a biphasic release of calcium from the ER in a mechanism dependent on phospholipase C (PLC) activation. A quick kinetic of calcium release is caused by the binding of inositol 1,4,5-triphosphate (IP_3) to its receptors (IP_3R) on the ER. IP_3 is generated upon PLC-dependent hydrolysis of phosphatidyl 4,5-bisphosphate (PIP_2). IP_3 binding to IP_3R on the ER causes a quick release of calcium in the cytoplasm. Accordingly, cytochrome-c binding to the IP_3R is responsible for a delayed and sustained calcium release [197].

We propose a model where FasL stimulation increases calcium release from the ER, thereby binding to calmodulin, the upstream activator of CAMK1D. The activation and consequently binding of calmodulin to CAMK1D releases the autoinhibitory domain of CAMK1D allowing CAMK-kinase to phosphorylate and fully activate CAMK1D. As a consequence, CAMK1D inhibits effector caspases activation via binding and therefore acting as a direct stoichiometric inhibitor as well as reduces effector caspases activity through subsequent phosphorylation. Moreover, activated CAMK1D translocates into the nucleus where it phosphorylates and activates CREB, leading to the transcription of the anti-apoptotic molecule Bcl-2 (Figure X). This mechanism proposes CAMK1D as a novel immune-checkpoint molecule interfering with tumor cell death, sustaining anti-apoptotic pathways.

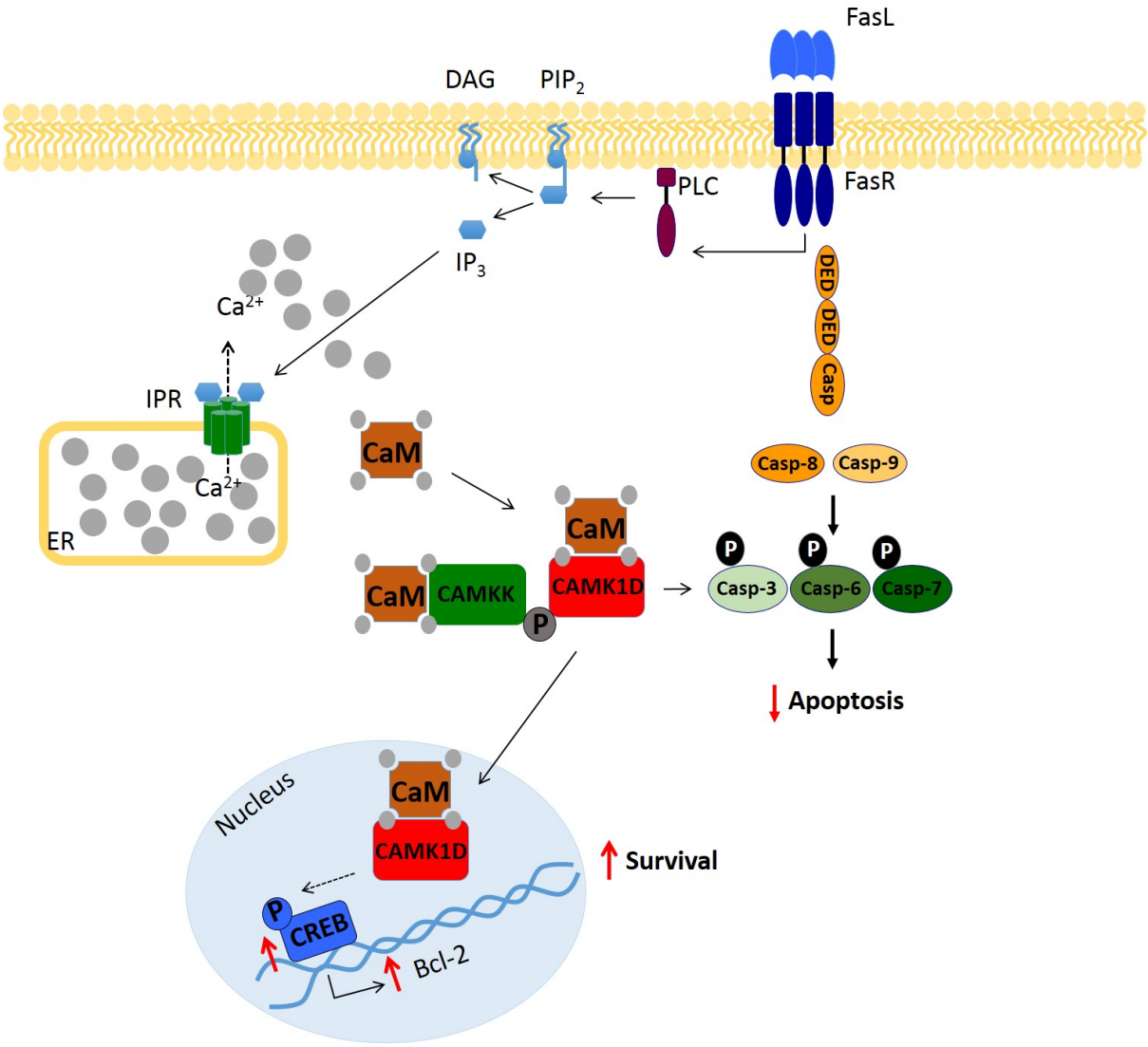

Figure X. Proposed mode of action of CAMK1D-mediated resistance to FasL. Upon FasL binding to Fas the phospholipase C (PLC) catalyzes phosphatidyl 4,5-bisphosphate (PIP_2) in diacylglycerol (DAG) and inositol 1,4,5-triphosphate (IP_3). IP_3 binding to the IP_3 receptors (IP_3R) on the endoplasmatic reticulum (ER) leads to calcium (Ca^{2+}) influx into the cytoplasm. Four calcium ions bind to calmodulin (CaM), which in turn can bind and activate CAMK1D. CaM binds also to CAMK-kinase (CAMKK), which is subsequently activated and phosphorylates CAMK1D thereby leading to full activation of the kinase. In parallel, Fas/FasL pathway triggers the apoptotic signaling cascade by activation of caspase-8 and caspase-9, which in turn cleave and activate the effector caspases caspase-3, caspase-6 and caspase-7. Activated CAMK1D directly binds to the effector caspases thereby reducing caspases activation and hindering caspases binding to downstream targets. Moreover, via phosphorylation CAMK1D inhibits effector caspases activity subsequently reducing the overall apoptosis of cancer cells. Upon activation, CAMK1D also translocates into the nucleus where it phosphorylates the transcription factor cAMP response element-binding protein (CREB). Increased pCREB leads to the transcription of anti-apoptotic genes such as Bcl-2 leading to enhance survival of the tumor cells.

6.2.6 Translational aspects of CAMK1D as a target for cancer immunotherapy

The principal goal of this project was to identify novel immune-checkpoint molecules to use as potential targets for the development of cancer immunotherapy. By taking advantage of a HTP-screening platform, we identified CAMK1D as a potential target for immunotherapeutic approaches in multiple myeloma and uveal melanoma. Several aspects suggesting a translational relevance of CAMK1D inhibition in cancer therapy have already been discussed (section 6.2.2, 6.2.3 and 6.2.4).

To support the clinical applicability of CAMK1D blockade, we took advantage of small molecule compounds. Due to the lack of CAMK1D-specific inhibitors, direct activators of CAMK1D, namely calmodulin and CAMKK, were targeted with protein-specific small molecules. Both small molecules block the respective hydrophobic pockets thereby inhibiting the anchoring ability to the target protein CAMK1D. Inhibition of either calmodulin or CAMKK resulted in a dose-dependent increase of tumor cell death upon FasL stimulation.

One concern about CAMK1D target therapy is its ubiquitous expression particularly in T cells and neurons. Thus, inhibition of this protein kinase could on the one hand increase tumor susceptibility towards T cell attack, but on the other hand impair T cell activity. In line, Bellucci and colleagues demonstrated that the blockade of the tyrosine kinase, JAK2, sensitized multiple myeloma tumor cells towards the attack of NK cells [206]. Nevertheless, recent clinical studies showed that JAK1/2 inhibitors impair the functionality of NK cells and T cells in myeloproliferative neoplasms [261-263]. Consequently, supplementary studies must be conducted to clarify the exact role of CAMK1D inhibition in T cells and which consequences a targeted therapy would have on neurons.

Nonetheless, CAMK1D remains an interesting target for cancer immunotherapy, in particular for those patients who experience relapse or demonstrate unresponsiveness to conventional therapies. Indeed, despite advances in treatments such as novel immunomodulatory drugs (IMiDs), proteasome inhibitors and adoptive T cell therapy (section 1.6), MM remains largely incurable. It is now widely accepted that successful treatments are more likely to be achieved with combination therapies. Thus the combination of CAMK1D blockade with for example the third generation IMiDs, lenalidomide and pomalidomide that hamper tumor cell production of IL-6 and VEGF, could potentially increase the overall response rate of MM patients by increasing the susceptibility towards immune cell attack. As it has been shown in a phase III trial for the combination of elotuzumab, a monoclonal antibody targeting

SLAMF7, with lenalidomide and dexamethasone, which elicited a prominent effect in multiple myeloma patients, targeting CAMK1D in combination with FDA-approved monoclonal antibodies may result in enhanced anti-tumor activity, thereby improving the efficacy of combination therapies.

7 Conclusion

With the advent of immune-checkpoint modulation, cancer immunotherapy has enhanced anti-tumor immune responses. However, MM remains an incurable disease and most patients succumb to relapse. In this regard, several immune-inhibitory mechanisms are exploited by tumor cells and the microenvironment, leading to treatment failure. To this end, we aimed to generate a high-throughput discovery platform to unravel novel immune-checkpoint molecules as targets for immune-checkpoint blockade in multiple myeloma. The narrow overlap of immune-checkpoints discovered by HTP-screenings in other tumor entities revealed the substantial heterogeneity of escape mechanisms used by tumor cells. Consequently, the cancer-specific arsenal of immune-checkpoints justifies the partial response of cancer patients to current therapies.

Among the genes identified as potential immune-checkpoints we identified the serine/threonine protein kinase CAMK1D as a key modulator of tumor intrinsic resistance towards immune cell attack.

The discovery of new potential immune-checkpoints is encouraging for the future of MM treatment and offers the chance to improve patients' survival through the implementation of rationally designed combination therapies.

8 References

1. Stewart, B.W., et al., *World cancer report 2014*. 2014, Lyon, France
Geneva, Switzerland: International Agency for Research on Cancer
WHO Press. xiv, 630 pages.
2. Hanahan, D. and R.A. Weinberg, *The hallmarks of cancer.* Cell, 2000. **100**(1): p. 57-70.
3. Lemmon, M.A. and J. Schlessinger, *Cell signaling by receptor tyrosine kinases.* Cell, 2010. **141**(7): p. 1117-34.
4. Witsch, E., M. Sela, and Y. Yarden, *Roles for growth factors in cancer progression.* Physiology (Bethesda), 2010. **25**(2): p. 85-101.
5. Bieging, K.T., S.S. Mello, and L.D. Attardi, *Unravelling mechanisms of p53-mediated tumour suppression.* Nat Rev Cancer, 2014. **14**(5): p. 359-70.
6. Burkhart, D.L. and J. Sage, *Cellular mechanisms of tumour suppression by the retinoblastoma gene.* Nat Rev Cancer, 2008. **8**(9): p. 671-82.
7. Curto, M., et al., *Contact-dependent inhibition of EGFR signaling by Nf2/Merlin.* J Cell Biol, 2007. **177**(5): p. 893-903.
8. Adams, J.M. and S. Cory, *The Bcl-2 apoptotic switch in cancer development and therapy.* Oncogene, 2007. **26**(9): p. 1324-37.
9. Hanahan, D. and J. Folkman, *Patterns and emerging mechanisms of the angiogenic switch during tumorigenesis.* Cell, 1996. **86**(3): p. 353-64.
10. Blackburn, E.H., *Telomerase and Cancer: Kirk A. Landon--AACR prize for basic cancer research lecture.* Mol Cancer Res, 2005. **3**(9): p. 477-82.
11. Berx, G. and F. van Roy, *Involvement of members of the cadherin superfamily in cancer.* Cold Spring Harb Perspect Biol, 2009. **1**(6): p. a003129.
12. Chen, F., et al., *New horizons in tumor microenvironment biology: challenges and opportunities.* BMC Med, 2015. **13**: p. 45.
13. Hanahan, D. and R.A. Weinberg, *Hallmarks of cancer: the next generation.* Cell, 2011. **144**(5): p. 646-74.
14. Semenza, G.L., *HIF-1: upstream and downstream of cancer metabolism.* Curr Opin Genet Dev, 2010. **20**(1): p. 51-6.
15. Burnet, F.M., *The concept of immunological surveillance.* Prog Exp Tumor Res, 1970. **13**: p. 1-27.
16. Chen, D.S. and I. Mellman, *Oncology meets immunology: the cancer-immunity cycle.* Immunity, 2013. **39**(1): p. 1-10.
17. Ferguson, T.A., J. Choi, and D.R. Green, *Armed response: how dying cells influence T-cell functions.* Immunol Rev, 2011. **241**(1): p. 77-88.
18. Franciszkiewicz, K., et al., *Role of chemokines and chemokine receptors in shaping the effector phase of the antitumor immune response.* Cancer Res, 2012. **72**(24): p. 6325-32.
19. Vesely, M.D., et al., *Natural innate and adaptive immunity to cancer.* Annu Rev Immunol, 2011. **29**: p. 235-71.
20. MacEwan, D.J., *TNF ligands and receptors--a matter of life and death.* Br J Pharmacol, 2002. **135**(4): p. 855-75.

21. Warren, H.S. and M.J. Smyth, *NK cells and apoptosis.* Immunol Cell Biol, 1999. **77**(1): p. 64-75.
22. Dunn, G.P., et al., *Cancer immunoediting: from immunosurveillance to tumor escape.* Nat Immunol, 2002. **3**(11): p. 991-8.
23. Aguirre-Ghiso, J.A., *Models, mechanisms and clinical evidence for cancer dormancy.* Nat Rev Cancer, 2007. **7**(11): p. 834-46.
24. Bhatia, A. and Y. Kumar, *Cancer-immune equilibrium: questions unanswered.* Cancer Microenviron, 2011. **4**(2): p. 209-17.
25. Dunn, G.P., L.J. Old, and R.D. Schreiber, *The three Es of cancer immunoediting.* Annu Rev Immunol, 2004. **22**: p. 329-60.
26. Mittal, D., et al., *New insights into cancer immunoediting and its three component phases--elimination, equilibrium and escape.* Curr Opin Immunol, 2014. **27**: p. 16-25.
27. Dong, Y., Q. Sun, and X. Zhang, *PD-1 and its ligands are important immune checkpoints in cancer.* Oncotarget, 2017. **8**(2): p. 2171-2186.
28. Pardoll, D.M., *The blockade of immune checkpoints in cancer immunotherapy.* Nat Rev Cancer, 2012. **12**(4): p. 252-64.
29. Chen, L. and D.B. Flies, *Molecular mechanisms of T cell co-stimulation and co-inhibition.* Nat Rev Immunol, 2013. **13**(4): p. 227-42.
30. Krummel, M.F. and J.P. Allison, *CD28 and CTLA-4 have opposing effects on the response of T cells to stimulation.* J Exp Med, 1995. **182**(2): p. 459-65.
31. Walunas, T.L., et al., *CTLA-4 can function as a negative regulator of T cell activation.* Immunity, 1994. **1**(5): p. 405-13.
32. Stojanovic, A., et al., *CTLA-4 is expressed by activated mouse NK cells and inhibits NK Cell IFN-gamma production in response to mature dendritic cells.* J Immunol, 2014. **192**(9): p. 4184-91.
33. Azuma, M., et al., *B70 antigen is a second ligand for CTLA-4 and CD28.* Nature, 1993. **366**(6450): p. 76-9.
34. Waterhouse, P., et al., *Lymphoproliferative disorders with early lethality in mice deficient in Ctla-4.* Science, 1995. **270**(5238): p. 985-8.
35. Chambers, C.A., T.J. Sullivan, and J.P. Allison, *Lymphoproliferation in CTLA-4-deficient mice is mediated by costimulation-dependent activation of CD4+ T cells.* Immunity, 1997. **7**(6): p. 885-95.
36. Marengere, L.E., et al., *Regulation of T cell receptor signaling by tyrosine phosphatase SYP association with CTLA-4.* Science, 1996. **272**(5265): p. 1170-3.
37. Chuang, E., et al., *The CD28 and CTLA-4 receptors associate with the serine/threonine phosphatase PP2A.* Immunity, 2000. **13**(3): p. 313-22.
38. Tai, X., et al., *Basis of CTLA-4 function in regulatory and conventional CD4(+) T cells.* Blood, 2012. **119**(22): p. 5155-63.
39. Krummey, S.M. and M.L. Ford, *Braking bad: novel mechanisms of CTLA-4 inhibition of T cell responses.* Am J Transplant, 2014. **14**(12): p. 2685-90.
40. Kwiecien, I., et al., *Elevated regulatory T cells, surface and intracellular CTLA-4 expression and interleukin-17 in the lung cancer microenvironment in humans.* Cancer Immunol Immunother, 2017. **66**(2): p. 161-170.
41. Walker, L.S. and D.M. Sansom, *Confusing signals: recent progress in CTLA-4 biology.* Trends Immunol, 2015. **36**(2): p. 63-70.
42. Agata, Y., et al., *Expression of the PD-1 antigen on the surface of stimulated mouse T and B lymphocytes.* Int Immunol, 1996. **8**(5): p. 765-72.

43. Zinselmeyer, B.H., et al., *PD-1 promotes immune exhaustion by inducing antiviral T cell motility paralysis.* J Exp Med, 2013. **210**(4): p. 757-74.
44. Chemnitz, J.M., et al., *SHP-1 and SHP-2 associate with immunoreceptor tyrosine-based switch motif of programmed death 1 upon primary human T cell stimulation, but only receptor ligation prevents T cell activation.* J Immunol, 2004. **173**(2): p. 945-54.
45. Sheppard, K.A., et al., *PD-1 inhibits T-cell receptor induced phosphorylation of the ZAP70/CD3zeta signalosome and downstream signaling to PKCtheta.* FEBS Lett, 2004. **574**(1-3): p. 37-41.
46. Yokosuka, T., et al., *Programmed cell death 1 forms negative costimulatory microclusters that directly inhibit T cell receptor signaling by recruiting phosphatase SHP2.* J Exp Med, 2012. **209**(6): p. 1201-17.
47. Ghebeh, H., et al., *The B7-H1 (PD-L1) T lymphocyte-inhibitory molecule is expressed in breast cancer patients with infiltrating ductal carcinoma: correlation with important high-risk prognostic factors.* Neoplasia, 2006. **8**(3): p. 190-8.
48. Hino, R., et al., *Tumor cell expression of programmed cell death-1 ligand 1 is a prognostic factor for malignant melanoma.* Cancer, 2010. **116**(7): p. 1757-66.
49. Liu, J., et al., *Plasma cells from multiple myeloma patients express B7-H1 (PD-L1) and increase expression after stimulation with IFN-{gamma} and TLR ligands via a MyD88-, TRAF6-, and MEK-dependent pathway.* Blood, 2007. **110**(1): p. 296-304.
50. Sznol, M. and L. Chen, *Antagonist antibodies to PD-1 and B7-H1 (PD-L1) in the treatment of advanced human cancer.* Clin Cancer Res, 2013. **19**(5): p. 1021-34.
51. Green, D.R. and T.A. Ferguson, *The role of Fas ligand in immune privilege.* Nat Rev Mol Cell Biol, 2001. **2**(12): p. 917-24.
52. Igney, F.H. and P.H. Krammer, *Tumor counterattack: fact or fiction?* Cancer Immunol Immunother, 2005. **54**(11): p. 1127-36.
53. O'Connell, J., et al., *The Fas counterattack: Fas-mediated T cell killing by colon cancer cells expressing Fas ligand.* J Exp Med, 1996. **184**(3): p. 1075-82.
54. Zeytun, A., et al., *Fas-Fas ligand-based interactions between tumor cells and tumor-specific cytotoxic T lymphocytes: a lethal two-way street.* Blood, 1997. **90**(5): p. 1952-9.
55. Kvistborg, P., M.M. van Buuren, and T.N. Schumacher, *Human cancer regression antigens.* Curr Opin Immunol, 2013. **25**(2): p. 284-90.
56. Ferrone, S. and F.M. Marincola, *Loss of HLA class I antigens by melanoma cells: molecular mechanisms, functional significance and clinical relevance.* Immunol Today, 1995. **16**(10): p. 487-94.
57. Garrido, F., et al., *Natural history of HLA expression during tumour development.* Immunol Today, 1993. **14**(10): p. 491-9.
58. Hinrichs, C.S. and N.P. Restifo, *Reassessing target antigens for adoptive T-cell therapy.* Nat Biotechnol, 2013. **31**(11): p. 999-1008.
59. Mellier, G., et al., *TRAILing death in cancer.* Mol Aspects Med, 2010. **31**(1): p. 93-112.
60. Ashkenazi, A., *Targeting the extrinsic apoptosis pathway in cancer.* Cytokine Growth Factor Rev, 2008. **19**(3-4): p. 325-31.
61. Kischkel, F.C., et al., *Cytotoxicity-dependent APO-1 (Fas/CD95)-associated proteins form a death-inducing signaling complex (DISC) with the receptor.* EMBO J, 1995. **14**(22): p. 5579-88.

62. Danial, N.N. and S.J. Korsmeyer, *Cell death: critical control points.* Cell, 2004. **116**(2): p. 205-19.
63. Trauth, B.C., et al., *Monoclonal antibody-mediated tumor regression by induction of apoptosis.* Science, 1989. **245**(4915): p. 301-5.
64. Lavrik, I., et al., *The active caspase-8 heterotetramer is formed at the CD95 DISC.* Cell Death Differ, 2003. **10**(1): p. 144-5.
65. Dechant, M.J., et al., *Mutation analysis of the apoptotic "death-receptors" and the adaptors TRADD and FADD/MORT-1 in osteosarcoma tumor samples and osteosarcoma cell lines.* Int J Cancer, 2004. **109**(5): p. 661-7.
66. Maeda, T., et al., *Fas gene mutation in the progression of adult T cell leukemia.* J Exp Med, 1999. **189**(7): p. 1063-71.
67. Petak, I., et al., *Hypermethylation of the gene promoter and enhancer region can regulate Fas expression and sensitivity in colon carcinoma.* Cell Death Differ, 2003. **10**(2): p. 211-7.
68. Volkmann, M., et al., *Loss of CD95 expression is linked to most but not all p53 mutants in European hepatocellular carcinoma.* J Mol Med (Berl), 2001. **79**(10): p. 594-600.
69. Pitti, R.M., et al., *Genomic amplification of a decoy receptor for Fas ligand in lung and colon cancer.* Nature, 1998. **396**(6712): p. 699-703.
70. Kober, A.M., et al., *Caspase-8 activity has an essential role in CD95/Fas-mediated MAPK activation.* Cell Death Dis, 2011. **2**: p. e212.
71. Yi, X., X.M. Yin, and Z. Dong, *Inhibition of Bid-induced apoptosis by Bcl-2. tBid insertion, Bax translocation, and Bax/Bak oligomerization suppressed.* J Biol Chem, 2003. **278**(19): p. 16992-9.
72. Akyurek, N., et al., *Expression of inhibitor of apoptosis proteins in B-cell non-Hodgkin and Hodgkin lymphomas.* Cancer, 2006. **107**(8): p. 1844-51.
73. de Graaf, A.O., et al., *Expression of C-IAP1, C-IAP2 and SURVIVIN discriminates different types of lymphoid malignancies.* Br J Haematol, 2005. **130**(6): p. 852-9.
74. Granziero, L., et al., *Survivin is expressed on CD40 stimulation and interfaces proliferation and apoptosis in B-cell chronic lymphocytic leukemia.* Blood, 2001. **97**(9): p. 2777-83.
75. Nakagawa, Y., et al., *Differential expression of survivin in bone marrow cells from patients with acute lymphocytic leukemia and chronic lymphocytic leukemia.* Leuk Res, 2004. **28**(5): p. 487-94.
76. Vaux, D.L. and J. Silke, *Mammalian mitochondrial IAP binding proteins.* Biochem Biophys Res Commun, 2003. **304**(3): p. 499-504.
77. Vucic, D., V.M. Dixit, and E.G. Wertz, *Ubiquitylation in apoptosis: a post-translational modification at the edge of life and death.* Nat Rev Mol Cell Biol, 2011. **12**(7): p. 439-52.
78. Beg, A.A. and D. Baltimore, *An essential role for NF-kappaB in preventing TNF-alpha-induced cell death.* Science, 1996. **274**(5288): p. 782-4.
79. Karin, M. and A. Lin, *NF-kappaB at the crossroads of life and death.* Nat Immunol, 2002. **3**(3): p. 221-7.
80. Liu, J. and A. Lin, *Role of JNK activation in apoptosis: a double-edged sword.* Cell Res, 2005. **15**(1): p. 36-42.
81. Siveen, K.S. and G. Kuttan, *Role of macrophages in tumour progression.* Immunol Lett, 2009. **123**(2): p. 97-102.

82. Bhatia, A. and Y. Kumar, *Cellular and molecular mechanisms in cancer immune escape: a comprehensive review.* Expert Rev Clin Immunol, 2014. **10**(1): p. 41-62.
83. Ludviksson, B.R. and B. Gunnlaugsdottir, *Transforming growth factor-beta as a regulator of site-specific T-cell inflammatory response.* Scand J Immunol, 2003. **58**(2): p. 129-38.
84. Chen, W., et al., *Conversion of peripheral CD4+CD25- naive T cells to CD4+CD25+ regulatory T cells by TGF-beta induction of transcription factor Foxp3.* J Exp Med, 2003. **198**(12): p. 1875-86.
85. Gabrilovich, D.I., S. Ostrand-Rosenberg, and V. Bronte, *Coordinated regulation of myeloid cells by tumours.* Nat Rev Immunol, 2012. **12**(4): p. 253-68.
86. Hsu, P., et al., *IL-10 Potentiates Differentiation of Human Induced Regulatory T Cells via STAT3 and Foxo1.* J Immunol, 2015. **195**(8): p. 3665-74.
87. Munder, M., *Arginase: an emerging key player in the mammalian immune system.* Br J Pharmacol, 2009. **158**(3): p. 638-51.
88. Uyttenhove, C., et al., *Evidence for a tumoral immune resistance mechanism based on tryptophan degradation by indoleamine 2,3-dioxygenase.* Nat Med, 2003. **9**(10): p. 1269-74.
89. Calcinotto, A., et al., *Modulation of microenvironment acidity reverses anergy in human and murine tumor-infiltrating T lymphocytes.* Cancer Res, 2012. **72**(11): p. 2746-56.
90. Sakaguchi, S., et al., *Regulatory T cells and immune tolerance.* Cell, 2008. **133**(5): p. 775-87.
91. Curiel, T.J., et al., *Specific recruitment of regulatory T cells in ovarian carcinoma fosters immune privilege and predicts reduced survival.* Nat Med, 2004. **10**(9): p. 942-9.
92. Kono, K., et al., *CD4(+)CD25high regulatory T cells increase with tumor stage in patients with gastric and esophageal cancers.* Cancer Immunol Immunother, 2006. **55**(9): p. 1064-71.
93. Liu, F., et al., *CD8(+) cytotoxic T cell and FOXP3(+) regulatory T cell infiltration in relation to breast cancer survival and molecular subtypes.* Breast Cancer Res Treat, 2011. **130**(2): p. 645-55.
94. Schmidt, H.H., et al., *HLA Class II tetramers reveal tissue-specific regulatory T cells that suppress T-cell responses in breast carcinoma patients.* Oncoimmunology, 2013. **2**(6): p. e24962.
95. Qureshi, O.S., et al., *Trans-endocytosis of CD80 and CD86: a molecular basis for the cell-extrinsic function of CTLA-4.* Science, 2011. **332**(6029): p. 600-3.
96. Gondek, D.C., et al., *Cutting edge: contact-mediated suppression by CD4+CD25+ regulatory cells involves a granzyme B-dependent, perforin-independent mechanism.* J Immunol, 2005. **174**(4): p. 1783-6.
97. Ren, X., et al., *Involvement of cellular death in TRAIL/DR5-dependent suppression induced by CD4(+)CD25(+) regulatory T cells.* Cell Death Differ, 2007. **14**(12): p. 2076-84.
98. Caridade, M., L. Graca, and R.M. Ribeiro, *Mechanisms Underlying CD4+ Treg Immune Regulation in the Adult: From Experiments to Models.* Front Immunol, 2013. **4**: p. 378.

99. Sinha, P., et al., *Cross-talk between myeloid-derived suppressor cells and macrophages subverts tumor immunity toward a type 2 response.* J Immunol, 2007. **179**(2): p. 977-83.
100. Gabitass, R.F., et al., *Elevated myeloid-derived suppressor cells in pancreatic, esophageal and gastric cancer are an independent prognostic factor and are associated with significant elevation of the Th2 cytokine interleukin-13.* Cancer Immunol Immunother, 2011. **60**(10): p. 1419-30.
101. Marvel, D. and D.I. Gabrilovich, *Myeloid-derived suppressor cells in the tumor microenvironment: expect the unexpected.* J Clin Invest, 2015. **125**(9): p. 3356-64.
102. Kuang, D.M., et al., *Activated monocytes in peritumoral stroma of hepatocellular carcinoma foster immune privilege and disease progression through PD-L1.* J Exp Med, 2009. **206**(6): p. 1327-37.
103. Leyva-Illades, D., et al., *Cholangiocarcinoma pathogenesis: Role of the tumor microenvironment.* Transl Gastrointest Cancer, 2012. **1**(1): p. 71-80.
104. Gabrilovich, D., *Mechanisms and functional significance of tumour-induced dendritic-cell defects.* Nat Rev Immunol, 2004. **4**(12): p. 941-52.
105. Ghiringhelli, F., et al., *Tumor cells convert immature myeloid dendritic cells into TGF-beta-secreting cells inducing CD4+CD25+ regulatory T cell proliferation.* J Exp Med, 2005. **202**(7): p. 919-29.
106. Hanna, M.G., Jr. and L.C. Peters, *Immunotherapy of established micrometastases with Bacillus Calmette-Guerin tumor cell vaccine.* Cancer Res, 1978. **38**(1): p. 204-9.
107. Disis, M.L., et al., *Granulocyte-macrophage colony-stimulating factor: an effective adjuvant for protein and peptide-based vaccines.* Blood, 1996. **88**(1): p. 202-10.
108. Dranoff, G., *GM-CSF-based cancer vaccines.* Immunol Rev, 2002. **188**: p. 147-54.
109. Jager, E., et al., *Granulocyte-macrophage-colony-stimulating factor enhances immune responses to melanoma-associated peptides in vivo.* Int J Cancer, 1996. **67**(1): p. 54-62.
110. Copier, J. and A. Dalgleish, *Whole-cell vaccines: A failure or a success waiting to happen?* Curr Opin Mol Ther, 2010. **12**(1): p. 14-20.
111. Sondak, V.K., M.S. Sabel, and J.J. Mule, *Allogeneic and autologous melanoma vaccines: where have we been and where are we going?* Clin Cancer Res, 2006. **12**(7 Pt 2): p. 2337s-2341s.
112. Longo, D.L., *New therapies for castration-resistant prostate cancer.* N Engl J Med, 2010. **363**(5): p. 479-81.
113. Scholz, M., et al., *Phase I clinical trial of sipuleucel-T combined with escalating doses of ipilimumab in progressive metastatic castrate-resistant prostate cancer.* Immunotargets Ther, 2017. **6**: p. 11-16.
114. Brown, R.D., et al., *Dendritic cells from patients with myeloma are numerically normal but functionally defective as they fail to up-regulate CD80 (B7-1) expression after huCD40LT stimulation because of inhibition by transforming growth factor-beta1 and interleukin-10.* Blood, 2001. **98**(10): p. 2992-8.
115. Ratta, M., et al., *Dendritic cells are functionally defective in multiple myeloma: the role of interleukin-6.* Blood, 2002. **100**(1): p. 230-7.
116. Curti, A., et al., *Phase I/II clinical trial of sequential subcutaneous and intravenous delivery of dendritic cell vaccination for refractory multiple myeloma using patient-specific tumour idiotype protein or idiotype (VDJ)-derived class I-restricted peptides.* Br J Haematol, 2007. **139**(3): p. 415-24.

117. Rosenberg, S.A., et al., *Adoptive cell transfer: a clinical path to effective cancer immunotherapy.* Nat Rev Cancer, 2008. **8**(4): p. 299-308.
118. Rosenberg, S.A., et al., *Use of tumor-infiltrating lymphocytes and interleukin-2 in the immunotherapy of patients with metastatic melanoma. A preliminary report.* N Engl J Med, 1988. **319**(25): p. 1676-80.
119. Phan, G.Q. and S.A. Rosenberg, *Adoptive cell transfer for patients with metastatic melanoma: the potential and promise of cancer immunotherapy.* Cancer Control, 2013. **20**(4): p. 289-97.
120. Boesteanu, A.C. and P.D. Katsikis, *Memory T cells need CD28 costimulation to remember.* Semin Immunol, 2009. **21**(2): p. 69-77.
121. Porter, D.L., et al., *Chimeric antigen receptor-modified T cells in chronic lymphoid leukemia.* N Engl J Med, 2011. **365**(8): p. 725-33.
122. Grupp, S.A., et al., *Chimeric antigen receptor-modified T cells for acute lymphoid leukemia.* N Engl J Med, 2013. **368**(16): p. 1509-1518.
123. Kalos, M., et al., *T cells with chimeric antigen receptors have potent antitumor effects and can establish memory in patients with advanced leukemia.* Sci Transl Med, 2011. **3**(95): p. 95ra73.
124. Casucci, M. and A. Bondanza, *Suicide gene therapy to increase the safety of chimeric antigen receptor-redirected T lymphocytes.* J Cancer, 2011. **2**: p. 378-82.
125. Morgan, R.A., et al., *Cancer regression in patients after transfer of genetically engineered lymphocytes.* Science, 2006. **314**(5796): p. 126-9.
126. Cieri, N., et al., *Adoptive immunotherapy with genetically modified lymphocytes in allogeneic stem cell transplantation.* Immunol Rev, 2014. **257**(1): p. 165-80.
127. Provasi, E., et al., *Editing T cell specificity towards leukemia by zinc finger nucleases and lentiviral gene transfer.* Nat Med, 2012. **18**(5): p. 807-815.
128. Mittendorf, E.A. and P. Sharma, *Mechanisms of T-cell inhibition: implications for cancer immunotherapy.* Expert Rev Vaccines, 2010. **9**(1): p. 89-105.
129. Farkona, S., E.P. Diamandis, and I.M. Blasutig, *Cancer immunotherapy: the beginning of the end of cancer?* BMC Med, 2016. **14**: p. 73.
130. Grosso, J.F. and M.N. Jure-Kunkel, *CTLA-4 blockade in tumor models: an overview of preclinical and translational research.* Cancer Immun, 2013. **13**: p. 5.
131. Hodi, F.S., et al., *Improved survival with ipilimumab in patients with metastatic melanoma.* N Engl J Med, 2010. **363**(8): p. 711-23.
132. Ascierto, P.A., et al., *Clinical experience with ipilimumab 3 mg/kg: real-world efficacy and safety data from an expanded access programme cohort.* J Transl Med, 2014. **12**: p. 116.
133. Sharma, P. and J.P. Allison, *Immune checkpoint targeting in cancer therapy: toward combination strategies with curative potential.* Cell, 2015. **161**(2): p. 205-14.
134. Topalian, S.L., et al., *Survival, durable tumor remission, and long-term safety in patients with advanced melanoma receiving nivolumab.* J Clin Oncol, 2014. **32**(10): p. 1020-30.
135. Rizvi, N.A., et al., *Activity and safety of nivolumab, an anti-PD-1 immune checkpoint inhibitor, for patients with advanced, refractory squamous non-small-cell lung cancer (CheckMate 063): a phase 2, single-arm trial.* Lancet Oncol, 2015. **16**(3): p. 257-65.
136. Robert, C., et al., *Nivolumab in previously untreated melanoma without BRAF mutation.* N Engl J Med, 2015. **372**(4): p. 320-30.

137. Benosman, S., et al., *Interleukin-1 receptor-associated kinase-2 (IRAK2) is a critical mediator of endoplasmic reticulum (ER) stress signaling.* PLoS One, 2013. **8**(5): p. e64256.
138. Carbognin, L., et al., *Differential Activity of Nivolumab, Pembrolizumab and MPDL3280A according to the Tumor Expression of Programmed Death-Ligand-1 (PD-L1): Sensitivity Analysis of Trials in Melanoma, Lung and Genitourinary Cancers.* PLoS One, 2015. **10**(6): p. e0130142.
139. Lesokhin, A.M., et al., *Nivolumab in Patients With Relapsed or Refractory Hematologic Malignancy: Preliminary Results of a Phase Ib Study.* J Clin Oncol, 2016. **34**(23): p. 2698-704.
140. Yousef, S., et al., *Immunomodulatory molecule PD-L1 is expressed on malignant plasma cells and myeloma-propagating pre-plasma cells in the bone marrow of multiple myeloma patients.* Blood Cancer J, 2015. **5**: p. e285.
141. Swart, M., I. Verbrugge, and J.B. Beltman, *Combination Approaches with Immune-Checkpoint Blockade in Cancer Therapy.* Front Oncol, 2016. **6**: p. 233.
142. Postow, M.A., et al., *Nivolumab and ipilimumab versus ipilimumab in untreated melanoma.* N Engl J Med, 2015. **372**(21): p. 2006-17.
143. Korde, N., S.Y. Kristinsson, and O. Landgren, *Monoclonal gammopathy of undetermined significance (MGUS) and smoldering multiple myeloma (SMM): novel biological insights and development of early treatment strategies.* Blood, 2011. **117**(21): p. 5573-81.
144. Kuehl, W.M. and P.L. Bergsagel, *Early genetic events provide the basis for a clinical classification of multiple myeloma.* Hematology Am Soc Hematol Educ Program, 2005: p. 346-52.
145. Dhodapkar, M.V., et al., *A reversible defect in natural killer T cell function characterizes the progression of premalignant to malignant multiple myeloma.* J Exp Med, 2003. **197**(12): p. 1667-76.
146. Benson, D.M., Jr., et al., *The PD-1/PD-L1 axis modulates the natural killer cell versus multiple myeloma effect: a therapeutic target for CT-011, a novel monoclonal anti-PD-1 antibody.* Blood, 2010. **116**(13): p. 2286-94.
147. Tamura, H., *Immunopathogenesis and immunotherapy of multiple myeloma.* Int J Hematol, 2018. **107**(3): p. 278-285.
148. Kocoglu, M. and A. Badros, *The Role of Immunotherapy in Multiple Myeloma.* Pharmaceuticals (Basel), 2016. **9**(1).
149. Singhal, S., et al., *Antitumor activity of thalidomide in refractory multiple myeloma.* N Engl J Med, 1999. **341**(21): p. 1565-71.
150. Haslett, P.A., et al., *Thalidomide costimulates primary human T lymphocytes, preferentially inducing proliferation, cytokine production, and cytotoxic responses in the CD8+ subset.* J Exp Med, 1998. **187**(11): p. 1885-92.
151. Quach, H., et al., *Mechanism of action of immunomodulatory drugs (IMiDS) in multiple myeloma.* Leukemia, 2010. **24**(1): p. 22-32.
152. Bae, J., et al., *Myeloma-specific multiple peptides able to generate cytotoxic T lymphocytes: a potential therapeutic application in multiple myeloma and other plasma cell disorders.* Clin Cancer Res, 2012. **18**(17): p. 4850-60.
153. Rosenblatt, J., et al., *Vaccination with dendritic cell/tumor fusions following autologous stem cell transplant induces immunologic and clinical responses in multiple myeloma patients.* Clin Cancer Res, 2013. **19**(13): p. 3640-8.

154. Rosenblatt, J., et al., *Vaccination with dendritic cell/tumor fusion cells results in cellular and humoral antitumor immune responses in patients with multiple myeloma.* Blood, 2011. **117**(2): p. 393-402.
155. Lonial, S., et al., *Elotuzumab in combination with lenalidomide and low-dose dexamethasone in relapsed or refractory multiple myeloma.* J Clin Oncol, 2012. **30**(16): p. 1953-9.
156. Garfall, A.L., et al., *Chimeric Antigen Receptor T Cells against CD19 for Multiple Myeloma.* N Engl J Med, 2015. **373**(11): p. 1040-7.
157. Ali, S.A., et al., *T cells expressing an anti-B-cell maturation antigen chimeric antigen receptor cause remissions of multiple myeloma.* Blood, 2016. **128**(13): p. 1688-700.
158. Rapoport, A.P., et al., *NY-ESO-1-specific TCR-engineered T cells mediate sustained antigen-specific antitumor effects in myeloma.* Nat Med, 2015. **21**(8): p. 914-921.
159. Gorgun, G., et al., *Lenalidomide Enhances Immune Checkpoint Blockade-Induced Immune Response in Multiple Myeloma.* Clin Cancer Res, 2015. **21**(20): p. 4607-18.
160. Badros, A., et al., *Pembrolizumab, pomalidomide, and low-dose dexamethasone for relapsed/refractory multiple myeloma.* Blood, 2017. **130**(10): p. 1189-1197.
161. Fire, A., et al., *Potent and specific genetic interference by double-stranded RNA in Caenorhabditis elegans.* Nature, 1998. **391**(6669): p. 806-11.
162. Boutros, M. and J. Ahringer, *The art and design of genetic screens: RNA interference.* Nat Rev Genet, 2008. **9**(7): p. 554-66.
163. Zhou, P., et al., *In vivo discovery of immunotherapy targets in the tumour microenvironment.* Nature, 2014. **506**(7486): p. 52-7.
164. Khandelwal, N., et al., *A high-throughput RNAi screen for detection of immune-checkpoint molecules that mediate tumor resistance to cytotoxic T lymphocytes.* EMBO Mol Med, 2015. **7**(4): p. 450-63.
165. Borrello, I. and K.A. Noonan, *Marrow-Infiltrating Lymphocytes - Role in Biology and Cancer Therapy.* Front Immunol, 2016. **7**: p. 112.
166. Noonan, K.A., et al., *Adoptive transfer of activated marrow-infiltrating lymphocytes induces measurable antitumor immunity in the bone marrow in multiple myeloma.* Sci Transl Med, 2015. **7**(288): p. 288ra78.
167. Jing, W., et al., *Combined immune checkpoint protein blockade and low dose whole body irradiation as immunotherapy for myeloma.* J Immunother Cancer, 2015. **3**(1): p. 2.
168. Hallett, W.H., et al., *Immunosuppressive effects of multiple myeloma are overcome by PD-L1 blockade.* Biol Blood Marrow Transplant, 2011. **17**(8): p. 1133-45.
169. Boutros, M., L.P. Bras, and W. Huber, *Analysis of cell-based RNAi screens.* Genome Biol, 2006. **7**(7): p. R66.
170. Gilbert, D.F., et al., *A novel multiplex cell viability assay for high-throughput RNAi screening.* PLoS One, 2011. **6**(12): p. e28338.
171. Ryu, K.Y., et al., *The mouse polyubiquitin gene UbC is essential for fetal liver development, cell-cycle progression and stress tolerance.* EMBO J, 2007. **26**(11): p. 2693-706.
172. Liu, Q., et al., *Chk1 is an essential kinase that is regulated by Atr and required for the G(2)/M DNA damage checkpoint.* Genes Dev, 2000. **14**(12): p. 1448-59.
173. Coutinho, P., et al., *Differential requirements for COPI transport during vertebrate early development.* Dev Cell, 2004. **7**(4): p. 547-58.

174. Gilsdorf, M., et al., *GenomeRNAi: a database for cell-based RNAi phenotypes. 2009 update.* Nucleic Acids Res, 2010. **38**(Database issue): p. D448-52.
175. Dudley, M.E., et al., *Generation of tumor-infiltrating lymphocyte cultures for use in adoptive transfer therapy for melanoma patients.* J Immunother, 2003. **26**(4): p. 332-42.
176. Wherry, E.J., *T cell exhaustion.* Nat Immunol, 2011. **12**(6): p. 492-9.
177. Crespo, J., et al., *T cell anergy, exhaustion, senescence, and stemness in the tumor microenvironment.* Curr Opin Immunol, 2013. **25**(2): p. 214-21.
178. Fourcade, J., et al., *Upregulation of Tim-3 and PD-1 expression is associated with tumor antigen-specific CD8+ T cell dysfunction in melanoma patients.* J Exp Med, 2010. **207**(10): p. 2175-86.
179. Jiang, Y., Y. Li, and B. Zhu, *T-cell exhaustion in the tumor microenvironment.* Cell Death Dis, 2015. **6**: p. e1792.
180. Woo, S.R., et al., *Immune inhibitory molecules LAG-3 and PD-1 synergistically regulate T-cell function to promote tumoral immune escape.* Cancer Res, 2012. **72**(4): p. 917-27.
181. Zou, W., J.D. Wolchok, and L. Chen, *PD-L1 (B7-H1) and PD-1 pathway blockade for cancer therapy: Mechanisms, response biomarkers, and combinations.* Sci Transl Med, 2016. **8**(328): p. 328rv4.
182. Brahmer, J.R., et al., *Safety and activity of anti-PD-L1 antibody in patients with advanced cancer.* N Engl J Med, 2012. **366**(26): p. 2455-65.
183. Mellman, I., G. Coukos, and G. Dranoff, *Cancer immunotherapy comes of age.* Nature, 2011. **480**(7378): p. 480-9.
184. Slovin, S.F., et al., *Ipilimumab alone or in combination with radiotherapy in metastatic castration-resistant prostate cancer: results from an open-label, multicenter phase I/II study.* Ann Oncol, 2013. **24**(7): p. 1813-21.
185. Topalian, S.L., et al., *Safety, activity, and immune correlates of anti-PD-1 antibody in cancer.* N Engl J Med, 2012. **366**(26): p. 2443-54.
186. Yang, J.C., et al., *Ipilimumab (anti-CTLA4 antibody) causes regression of metastatic renal cell cancer associated with enteritis and hypophysitis.* J Immunother, 2007. **30**(8): p. 825-30.
187. Zhang, C., et al., *CD5 Binds to Interleukin-6 and Induces a Feed-Forward Loop with the Transcription Factor STAT3 in B Cells to Promote Cancer.* Immunity, 2016. **44**(4): p. 913-923.
188. King, A.J., et al., *The protein kinase Pak3 positively regulates Raf-1 activity through phosphorylation of serine 338.* Nature, 1998. **396**(6707): p. 180-3.
189. Jaffer, Z.M. and J. Chernoff, *p21-activated kinases: three more join the Pak.* Int J Biochem Cell Biol, 2002. **34**(7): p. 713-7.
190. Ye, D.Z. and J. Field, *PAK signaling in cancer.* Cell Logist, 2012. **2**(2): p. 105-116.
191. Tiedemann, R.E., et al., *Kinome-wide RNAi studies in human multiple myeloma identify vulnerable kinase targets, including a lymphoid-restricted kinase, GRK6.* Blood, 2010. **115**(8): p. 1594-604.
192. Senga, Y., et al., *The Phosphatase-Resistant Isoform of CaMKI, Ca(2)(+)/Calmodulin-Dependent Protein Kinase Idelta (CaMKIdelta), Remains in Its "Primed" Form without Ca(2)(+) Stimulation.* Biochemistry, 2015. **54**(23): p. 3617-30.
193. Topfer, K., et al., *Tumor evasion from T cell surveillance.* J Biomed Biotechnol, 2011. **2011**: p. 918471.

194. Vinay, D.S., et al., *Immune evasion in cancer: Mechanistic basis and therapeutic strategies.* Semin Cancer Biol, 2015. **35 Suppl**: p. S185-S198.
195. Osawa, M., et al., *Solution structure of calmodulin-W-7 complex: the basis of diversity in molecular recognition.* J Mol Biol, 1998. **276**(1): p. 165-76.
196. Sakagami, H., et al., *Prominent expression and activity-dependent nuclear translocation of Ca2+/calmodulin-dependent protein kinase Idelta in hippocampal neurons.* Eur J Neurosci, 2005. **22**(11): p. 2697-707.
197. Wozniak, A.L., et al., *Requirement of biphasic calcium release from the endoplasmic reticulum for Fas-mediated apoptosis.* J Cell Biol, 2006. **175**(5): p. 709-14.
198. Wilson, B.E., E. Mochon, and L.M. Boxer, *Induction of bcl-2 expression by phosphorylated CREB proteins during B-cell activation and rescue from apoptosis.* Mol Cell Biol, 1996. **16**(10): p. 5546-56.
199. Roberts, P.J. and C.J. Der, *Targeting the Raf-MEK-ERK mitogen-activated protein kinase cascade for the treatment of cancer.* Oncogene, 2007. **26**(22): p. 3291-310.
200. McIlwain, D.R., T. Berger, and T.W. Mak, *Caspase functions in cell death and disease.* Cold Spring Harb Perspect Biol, 2013. **5**(4): p. a008656.
201. Parrish, A.B., C.D. Freel, and S. Kornbluth, *Cellular mechanisms controlling caspase activation and function.* Cold Spring Harb Perspect Biol, 2013. **5**(6).
202. Page, D.B., et al., *Immune modulation in cancer with antibodies.* Annu Rev Med, 2014. **65**: p. 185-202.
203. Bu, X., K.M. Mahoney, and G.J. Freeman, *Learning from PD-1 Resistance: New Combination Strategies.* Trends Mol Med, 2016. **22**(6): p. 448-451.
204. Hugo, W., et al., *Genomic and Transcriptomic Features of Response to Anti-PD-1 Therapy in Metastatic Melanoma.* Cell, 2016. **165**(1): p. 35-44.
205. Royal, R.E., et al., *Phase 2 trial of single agent Ipilimumab (anti-CTLA-4) for locally advanced or metastatic pancreatic adenocarcinoma.* J Immunother, 2010. **33**(8): p. 828-33.
206. Bellucci, R., et al., *Tyrosine kinase pathways modulate tumor susceptibility to natural killer cells.* J Clin Invest, 2012. **122**(7): p. 2369-83.
207. Patel, S.J., et al., *Identification of essential genes for cancer immunotherapy.* Nature, 2017. **548**(7669): p. 537-542.
208. Bachmann, M.F., et al., *Distinct kinetics of cytokine production and cytolysis in effector and memory T cells after viral infection.* Eur J Immunol, 1999. **29**(1): p. 291-9.
209. Slifka, M.K., F. Rodriguez, and J.L. Whitton, *Rapid on/off cycling of cytokine production by virus-specific CD8+ T cells.* Nature, 1999. **401**(6748): p. 76-9.
210. Manguso, R.T., et al., *In vivo CRISPR screening identifies Ptpn2 as a cancer immunotherapy target.* Nature, 2017. **547**(7664): p. 413-418.
211. Chung, D.J., et al., *T-cell Exhaustion in Multiple Myeloma Relapse after Autotransplant: Optimal Timing of Immunotherapy.* Cancer Immunol Res, 2016. **4**(1): p. 61-71.
212. Pauken, K.E. and E.J. Wherry, *Overcoming T cell exhaustion in infection and cancer.* Trends Immunol, 2015. **36**(4): p. 265-76.
213. Diehl, P., D. Tedesco, and A. Chenchik, *Use of RNAi screens to uncover resistance mechanisms in cancer cells and identify synthetic lethal interactions.* Drug Discov Today Technol, 2014. **11**: p. 11-8.

214. Crouch, S.P., et al., *The use of ATP bioluminescence as a measure of cell proliferation and cytotoxicity.* J Immunol Methods, 1993. **160**(1): p. 81-8.
215. Harada, D., N. Takigawa, and K. Kiura, *The Role of STAT3 in Non-Small Cell Lung Cancer.* Cancers (Basel), 2014. **6**(2): p. 708-22.
216. Garg, N., et al., *CD133(+) brain tumor-initiating cells are dependent on STAT3 signaling to drive medulloblastoma recurrence.* Oncogene, 2017. **36**(5): p. 606-617.
217. Haftchenary, S., et al., *Potent Targeting of the STAT3 Protein in Brain Cancer Stem Cells: A Promising Route for Treating Glioblastoma.* ACS Med Chem Lett, 2013. **4**(11): p. 1102-7.
218. Corcoran, R.B., et al., *STAT3 plays a critical role in KRAS-induced pancreatic tumorigenesis.* Cancer Res, 2011. **71**(14): p. 5020-9.
219. Kortylewski, M., R. Jove, and H. Yu, *Targeting STAT3 affects melanoma on multiple fronts.* Cancer Metastasis Rev, 2005. **24**(2): p. 315-27.
220. Bharti, A.C., et al., *Nuclear factor-kappaB and STAT3 are constitutively active in CD138+ cells derived from multiple myeloma patients, and suppression of these transcription factors leads to apoptosis.* Blood, 2004. **103**(8): p. 3175-84.
221. Catlett-Falcone, R., et al., *Constitutive activation of Stat3 signaling confers resistance to apoptosis in human U266 myeloma cells.* Immunity, 1999. **10**(1): p. 105-15.
222. Redell, M.S., et al., *Stat3 signaling in acute myeloid leukemia: ligand-dependent and -independent activation and induction of apoptosis by a novel small-molecule Stat3 inhibitor.* Blood, 2011. **117**(21): p. 5701-9.
223. Friese, M.A. and L. Fugger, *Autoreactive CD8+ T cells in multiple sclerosis: a new target for therapy?* Brain, 2005. **128**(Pt 8): p. 1747-63.
224. Gobel, K., et al., *Collateral neuronal apoptosis in CNS gray matter during an oligodendrocyte-directed CD8(+) T cell attack.* Glia, 2010. **58**(4): p. 469-80.
225. Lazo, J.S. and E.R. Sharlow, *Drugging Undruggable Molecular Cancer Targets.* Annu Rev Pharmacol Toxicol, 2016. **56**: p. 23-40.
226. Echeverri, C.J., et al., *Minimizing the risk of reporting false positives in large-scale RNAi screens.* Nat Methods, 2006. **3**(10): p. 777-9.
227. Sharma, S. and A. Rao, *RNAi screening: tips and techniques.* Nat Immunol, 2009. **10**(8): p. 799-804.
228. Jackson, A.L. and P.S. Linsley, *Recognizing and avoiding siRNA off-target effects for target identification and therapeutic application.* Nat Rev Drug Discov, 2010. **9**(1): p. 57-67.
229. Sun, P., et al., *Differential activation of CREB by Ca2+/calmodulin-dependent protein kinases type II and type IV involves phosphorylation of a site that negatively regulates activity.* Genes Dev, 1994. **8**(21): p. 2527-39.
230. Sun, P., L. Lou, and R.A. Maurer, *Regulation of activating transcription factor-1 and the cAMP response element-binding protein by Ca2+/calmodulin-dependent protein kinases type I, II, and IV.* J Biol Chem, 1996. **271**(6): p. 3066-73.
231. Nairn, A.C. and P. Greengard, *Purification and characterization of Ca2+/calmodulin-dependent protein kinase I from bovine brain.* J Biol Chem, 1987. **262**(15): p. 7273-81.
232. Swulius, M.T. and M.N. Waxham, *Ca(2+)/calmodulin-dependent protein kinases.* Cell Mol Life Sci, 2008. **65**(17): p. 2637-57.
233. Consortium, G.T., *The Genotype-Tissue Expression (GTEx) project.* Nat Genet, 2013. **45**(6): p. 580-5.

234. Liang, D., et al., *BAFF activates Erk1/2 promoting cell proliferation and survival by Ca2+-CaMKII-dependent inhibition of PP2A in normal and neoplastic B-lymphoid cells.* Biochem Pharmacol, 2014. **87**(2): p. 332-43.
235. Si, J. and S.J. Collins, *Activated Ca2+/calmodulin-dependent protein kinase IIgamma is a critical regulator of myeloid leukemia cell proliferation.* Cancer Res, 2008. **68**(10): p. 3733-42.
236. Chai, S., et al., *Ca2+/calmodulin-dependent protein kinase IIgamma enhances stem-like traits and tumorigenicity of lung cancer cells.* Oncotarget, 2015. **6**(18): p. 16069-83.
237. Ishiguro, K., et al., *Ca2+/calmodulin-dependent protein kinase II is a modulator of CARMA1-mediated NF-kappaB activation.* Mol Cell Biol, 2006. **26**(14): p. 5497-508.
238. Bergamaschi, A., et al., *CAMK1D amplification implicated in epithelial-mesenchymal transition in basal-like breast cancer.* Mol Oncol, 2008. **2**(4): p. 327-39.
239. Kahl, C.R. and A.R. Means, *Regulation of cyclin D1/Cdk4 complexes by calcium/calmodulin-dependent protein kinase I.* J Biol Chem, 2004. **279**(15): p. 15411-9.
240. Rhodes, D.R., et al., *Oncomine 3.0: genes, pathways, and networks in a collection of 18,000 cancer gene expression profiles.* Neoplasia, 2007. **9**(2): p. 166-80.
241. Magerus-Chatinet, A., et al., *Autoimmune lymphoproliferative syndrome caused by a homozygous null FAS ligand (FASLG) mutation.* J Allergy Clin Immunol, 2013. **131**(2): p. 486-90.
242. Hahne, M., et al., *Melanoma cell expression of Fas(Apo-1/CD95) ligand: implications for tumor immune escape.* Science, 1996. **274**(5291): p. 1363-6.
243. Leithauser, F., et al., *Constitutive and induced expression of APO-1, a new member of the nerve growth factor/tumor necrosis factor receptor superfamily, in normal and neoplastic cells.* Lab Invest, 1993. **69**(4): p. 415-29.
244. Shin, M.S., et al., *Alterations of Fas (Apo-1/CD95) gene in cutaneous malignant melanoma.* Am J Pathol, 1999. **154**(6): p. 1785-91.
245. Sprecher, E., et al., *Apoptosis, Fas and Fas-ligand expression in melanocytic tumors.* J Cutan Pathol, 1999. **26**(2): p. 72-7.
246. Mebratu, Y. and Y. Tesfaigzi, *How ERK1/2 activation controls cell proliferation and cell death: Is subcellular localization the answer?* Cell Cycle, 2009. **8**(8): p. 1168-75.
247. Fan, L., et al., *High Expression of Phosphorylated Extracellular Signal-Regulated Kinase (ERK1/2) is Associated with Poor Prognosis in Newly Diagnosed Patients with Multiple Myeloma.* Med Sci Monit, 2017. **23**: p. 2636-2643.
248. Vanhoutte, P., et al., *Glutamate induces phosphorylation of Elk-1 and CREB, along with c-fos activation, via an extracellular signal-regulated kinase-dependent pathway in brain slices.* Mol Cell Biol, 1999. **19**(1): p. 136-46.
249. Puthier, D., et al., *Differential expression of Bcl-2 in human plasma cell disorders according to proliferation status and malignancy.* Leukemia, 1999. **13**(2): p. 289-94.
250. Cerretti, D.P., et al., *Molecular cloning of the interleukin-1 beta converting enzyme.* Science, 1992. **256**(5053): p. 97-100.
251. Nicholson, D.W., et al., *Identification and inhibition of the ICE/CED-3 protease necessary for mammalian apoptosis.* Nature, 1995. **376**(6535): p. 37-43.
252. Woo, M., et al., *Caspase-3 regulates cell cycle in B cells: a consequence of substrate specificity.* Nat Immunol, 2003. **4**(10): p. 1016-22.

253. Alvarado-Kristensson, M., et al., *p38-MAPK signals survival by phosphorylation of caspase-8 and caspase-3 in human neutrophils.* J Exp Med, 2004. **199**(4): p. 449-58.
254. Suzuki, A., et al., *Regulation of caspase-6 and FLIP by the AMPK family member ARK5.* Oncogene, 2004. **23**(42): p. 7067-75.
255. Li, X., et al., *Phosphorylation of caspase-7 by p21-activated protein kinase (PAK) 2 inhibits chemotherapeutic drug-induced apoptosis of breast cancer cell lines.* J Biol Chem, 2011. **286**(25): p. 22291-9.
256. Choi, W.Y., et al., *Sanguinarine sensitizes human gastric adenocarcinoma AGS cells to TRAIL-mediated apoptosis via down-regulation of AKT and activation of caspase-3.* Anticancer Res, 2009. **29**(11): p. 4457-65.
257. Joazeiro, C.A. and A.M. Weissman, *RING finger proteins: mediators of ubiquitin ligase activity.* Cell, 2000. **102**(5): p. 549-52.
258. Deveraux, Q.L., et al., *X-linked IAP is a direct inhibitor of cell-death proteases.* Nature, 1997. **388**(6639): p. 300-4.
259. Riedl, S.J., et al., *Structural basis for the inhibition of caspase-3 by XIAP.* Cell, 2001. **104**(5): p. 791-800.
260. Shiozaki, E.N., et al., *Mechanism of XIAP-mediated inhibition of caspase-9.* Mol Cell, 2003. **11**(2): p. 519-27.
261. Dunn, G.P., et al., *IFN unresponsiveness in LNCaP cells due to the lack of JAK1 gene expression.* Cancer Res, 2005. **65**(8): p. 3447-53.
262. Parampalli Yajnanarayana, S., et al., *JAK1/2 inhibition impairs T cell function in vitro and in patients with myeloproliferative neoplasms.* Br J Haematol, 2015. **169**(6): p. 824-33.
263. Schonberg, K., et al., *JAK Inhibition Impairs NK Cell Function in Myeloproliferative Neoplasms.* Cancer Res, 2015. **75**(11): p. 2187-99.

9 Appendix

A

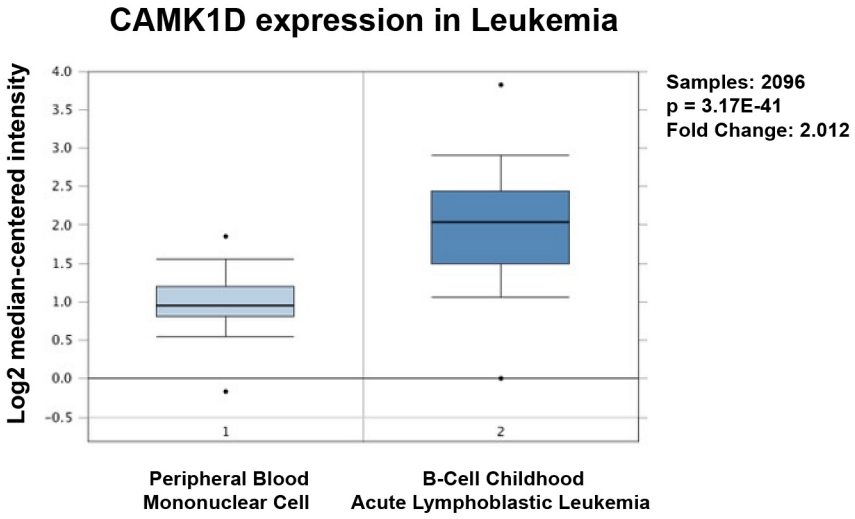

B

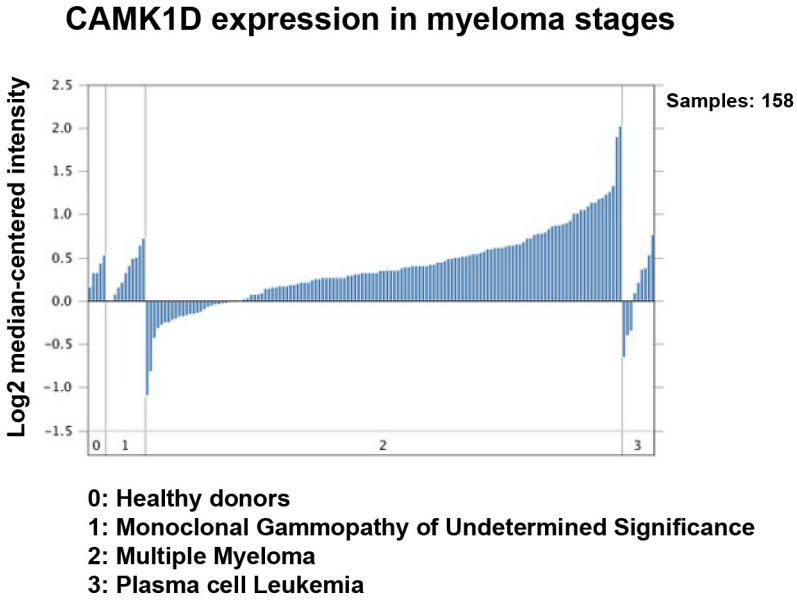

Figure XI. Comparison of CAMK1D mRNA expression. (A) Assessment of CAMK1D expression in PBMCs of healthy donors compared to B-cell Childhood Acute Lymphoblastic Leukemia. **(B)** CAMK1D expression in healthy donors compared to the three stages of myeloma (MGUS, MM and plasma cell leukemia). Data were obtained using the Oncomine™ cancer microarray database. P= p-value.

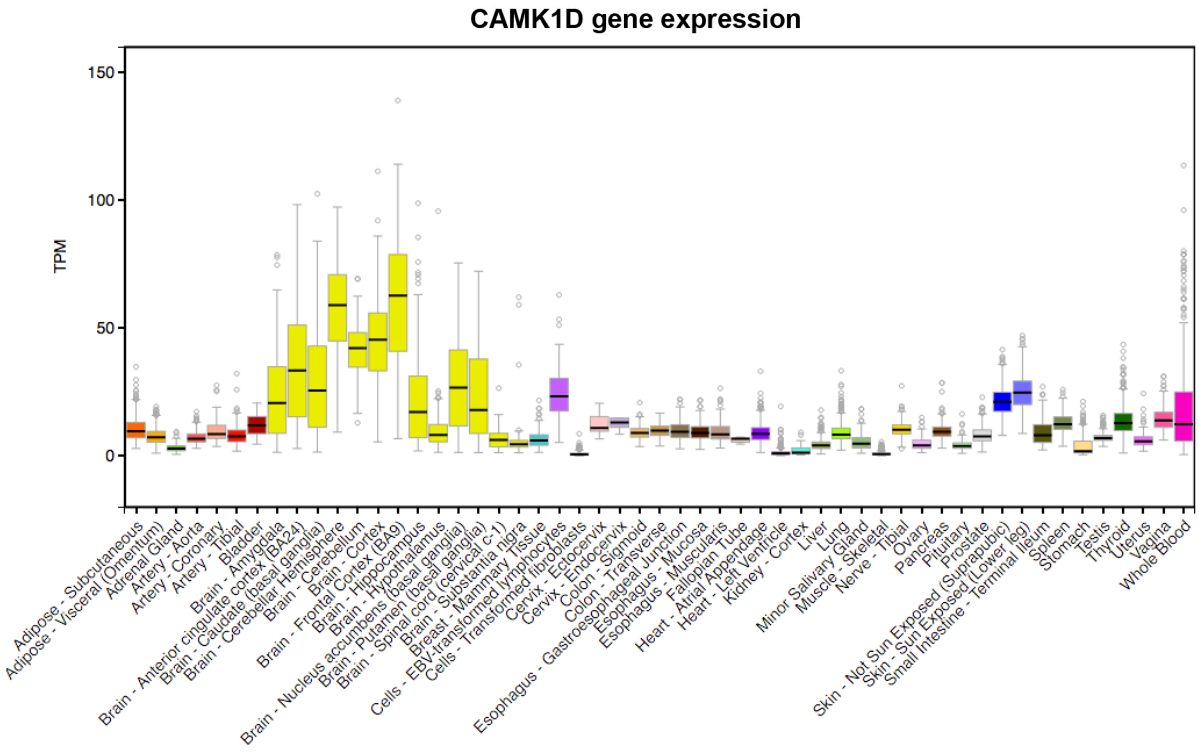

Figure XII. Gene expression for CAMK1D. CAMK1D gene expression levels throughout 53 human tissues. Data analysis from the Portal for the Genotype-Tissue Expression (GTEx) project.

10 Abbreviations and Definitions

A

AB	Human serum type AB
ACT	Adoptive cell transfer
APC	Antigen presenting cell
ATCC	American type culture collection
ATP	Adenosine triphosphate

B

BCL-2	B-cell lymphoma-2
BCL-xL	B-cell lymphoma-extra large
BCR	B cell receptor
BD	Becton Dickinson
bp	Base pair
BSA	Bovine serum albumin

C

Ca^{2+}	Calcium
CAMK1D	Calcium/calmodulin-dependent protein kinase type 1 delta
CAR	Chimeric antigen receptors
Casp	Caspase
CCL3	C-C chemokine ligand 3
CCR2	C-C chemokine receptor type 2
CCR9	C-C chemokine receptor type 9
CD	Cluster of differentiation
cDNA	complementary DNA
CEACAM6	Carcinoembryonic antigen related cell adhesion molecule 6
c-FLIP	Caspase-like apoptosis regulatory protein
CHK1	checkpoint kinase 1
CLM	Complete lymphocyte medium
CMM	Complete melanoma medium
CO_2	Carbon dioxide
COPB2	coatomer protein complex subunit beta 2
CREB	cAMP response element-binding protein
CTG	CellTiter-Glo
CTL	Cytotoxic T lymphocyte
CTLA-4	Cytotoxic T lymphocyte antigen 4
CXCL9	C-X-C chemokine ligand 9

D

DAG	diacylgycerol
DC	Dendritic cell
DcR3	Decoy receptor 3
DISC	Death inducing signaling complex
DKFZ	German Cancer Research Center - Heidelberg
DMEM	Dulbecco´s modified Eagle´s medium
DNA	Deoxyribonucleic acid

E

ECL	Enhanced Chemiluminescent
e.g.	Latin "exempli gratia" - "for example"
E:T	Effector to target ratio
EDTA	Ethylenediaminetetraacetic acid
ELISA	Enzyme-linked Immunosorbent Assay
EMT	Epithelial-mesenchymal transition
ERK1/2	extracellular signal-regulated kinases 1 and 2
et al.	Latin "et ali" - "and others"

F

FACS	Fluorescence-activated cell sorting
Fas	Fas cell surface death receptor/TNFRSF6
FasL	Fas ligand
FCS	Fetal calf serum
FDA	US Food and Drug Administration

FITC	Fluoerescein
Fluc	Firefly luciferase
FluT	Flu-antigen specific CD8+ T cells

G

g	gram
G418	Geneticin sulfate
gDNA	genomic DNA
GENT	Gene expression database of normal and tumor tissues
GFP	Green fluorescent protein
GM-CSF	Granulocyte macrophage colony-stimulating factor
GPCR	G-protein coupled receptor
GTEx	the portal for the genotype-tissue expression
GVAX	GM-CSF-transduced autologous tumor cell vaccine

H

h	Hours
HEPES	4-(2-hydroxyethyl)-1-piperazineethanesulfonic acid
HLA	Human leukocyte antigen
HRP	Horseradish peroxidase
HTTP	High-throughput

I

e.g.	Latin "id est"- "that is to say"
ICAM-1	Intracellular Adhesion Molecule 1
IDO	Indoleamine 2,3-dioxygenase
INFγ	Interferon-gamma
IgG	Immunoglobulin G
IgSF	Immunoglobulin super family
IHC	Immunohistochemistry
IL	Interleukin
IP_3	inositol 1,4,5-trisphosphate
IP_3R	inositol 1,4,5-trisphosphate receptor
ITIM	Tyrosine-based inhibitory motif

J

JAK	Janus kinase
JNK	C-Jun N-terminal protein kinase

K

kb	Kilobase
KD	Knockdown
kDA	Kilodalton
KMM-1	multiple myeloma cell line

L

L	Liter
LAG-3	Lymphocyte activation gene 3
LKB-1	Liver kinase B1
LOESS	LOcal regrESSion
LPS	Lipopolysaccharide
luc	luciferase

M

M	molar
mA	Milliampere
mAb	Monoclonal antibody
MAPK	Mitogen-activated protein kinase
MDSC	Myeloid-derived suppressor cell
MFI	mean fluorescence intensity
mg	Milligram
MGUS	monoclonal gammopathy of undetermined significance
MHC-I	Class I major histocompatibility molecules
MHC-II	Class II major histocompatibility molecules
MIL	Marrow infiltrating lymphocyte
min	minutes
miRNA	micro RNA
mL	milliliter
MM	Multiple Myeloma
mM	millimolar
mRNA	Messenger RNA
MS	Multiple sclerosis

N

NF-κB	Nuclear factor-kappa B
NK	Natural killer

ns	Not significant
nt	Nucleotide
O	
OKT-3	Muronomab-CD3
OX40	TNFRSF4
P	
p	Phosphorylation
P/S	Penicillin/Streptomycin
p38	p38 mitogen activated kinase
p53	Tumor protein p53
PAGE	Polyacrylamide gel electrophoresis
PBMC	Peripheral blood mononuclear cell
PBS	Phosphate buffer saline
PCR	Polymerase chain reaction
PD-1	Programmed death 1
PDAC	Pancreatic ductal adenocarcinoma
PD-L1	Programmed death ligand 1
PE	Phycoerythrin
pH	Latin "poteintia hydrogenii"
PIP2	phosphatidyl 4,5-bisphosphate
PI3K	Phosphatidylinositol-4,5-bisphosphate 3-kinase
PKC	Protein kinase C
PLC	phospholipase C
PLK1	polo-like kinase 1
PMA	Phorbol 12-myristate 13-acetate
PO	Pacific orange
Q	
qPCR	Quantitative PCR
R	
RCI	Regensburg Center for Interventional Immunology - Regensburg
REP	Rapid expansion protocol
rHu	Recombinant human
RLU	Relative luminescence Unit
RNA	Ribonucleic acid
RNAi	RNA interference
RT	Room temperature
S	
scr	scramble, non-coding siRNA sequence
SD	standard deviation
SDS	Sodium dodecyl sulfate
SEM	Standard error of the mean
SHP-2	SH2-domain containing tyrosine phosphatase 2
shRNA	Short hairpin RNA
siCD	"Cell Death" siRNA cocktail
siRNA	small interfering RNA
SIK3	Salt-inducible kinase 3
siRNA	small interfering RNA
STAT	Signal transducer and activator of transcription
T	
TAA	Tumor-associated antigen
TAE	Tris-Acetate-EDTA
TAM	Tumor associated macrophage
TAP	Transporter associated with antigen processing
TBS	Tris buffer saline
TBS-T	Tris-buffered saline with Tween 20
TCGA	The cancer genome atlas
Tcm	Central memory T cell
TCR	T cell receptor
TCs	T cells
Tem	Effector memory T cell
TGF-β	Transforming growth factor beta
Th	T helper
TIGIT	T cell immunoreceptor with Ig and ITIM domains
TILs	Tumor infiltrating lymphocytes
TIM-3	T cell immunoglobulin mucin 3
TKI	Tyrosine kinase inhibitor
TLR4	Toll-like receptor 4
™	Trademark
TME	Tumor microenvironment
TNFRSF	TNF receptor superfamily members
TNF	Tumor necrosis factor

TRADD	TNFR-I-associated death domain protein
TRAF2	TNF receptor associated factor 2
TRAIL	TNF-related apoptosis inducing ligand
T_{reg}	Regulatory T cells
Trp	Tryptophan
TSAs	Tumor specific antigens

U

U	Unit
UBC	Ubiquitin C
UV	Ultraviolet

V

V	Volt
VEGF	vascular endothelial growth factor
VEGFR2	Vascular endothelial growth factor receptor 2

W

WB	Western blot

X

X	X-fold
XIAP	X-linked inhibitor of apoptosis

Other

α	Alpha
β	Beta
β2m	β-2 microglobulin
γ	Gamma
δ	delta
κ	Kappa
%	Percentage
°C	Degree celsius
µg	microgram
µl	micorliter
µm	micrometer
4-1BB	TNFRSF9